

Basic Studies for Sterile Filtration Processing of Therapeutic Protein Formulations

Von der Naturwissenschaftlichen Fakultät der
Gottfried Wilhelm Leibniz Universität Hannover

zur Erlangung des Grades

Doktorin der Naturwissenschaften (Dr. rer. nat.)

genehmigte Dissertation

von

Susanne Maria Hilda Haindl, M.Sc.

[2020]

Referent: Prof. Dr. Thomas Scheper

Korreferent: PD Dr. Sascha Beutel

Tag der Promotion: 06.02.2020

Abstract

The central aim of this study is the investigation of the sterile filtration of therapeutic protein formulations. Filtration studies were performed with standardized protein formulations based on BSA and γ -globulin with a drug like composition and protein concentration. Formulation, manufacturing and characterization methods for these test solutions were developed at the beginning of this work.

With these formulations filtration trials were carried out with different sterilizing-grade filters (PES, Hydrosart, CN, among others). According to the results, filter fouling depends strongly on the filtration process conditions, on the composition of the protein formulation and on the sterile filter used. To achieve low filter fouling filtration with a constant flow rate through filters with hydrophilic surface and an open pore size distribution can be recommended. Constant pressure filtration exacerbates filter fouling. Surfactants, such as polysorbate 80 (PS80), have a huge impact on the colloidal stability of the protein formulation and the aggregation degree, on protein adsorption towards the membrane filter and filter fouling.

Protein adsorption to membrane filters during filtration was studied by inverse liquid chromatography. The results show that protein adsorption can be controlled by the surfactant concentration. PS80 containing protein formulations with a surfactant concentration above the critical micelle concentration exhibit low and reversible protein adsorption independent on the surface properties of the membrane filter used. In this case, the isotherm for adsorption of BSA and γ -globulin on CN- and Hydrosart membranes was measured. Protein adsorption during filtration of surfactant free protein formulations depends on the surface properties of the membrane filter. Hydrophobic cellulose nitrate membrane filters show strong and irreversible protein adsorption, whereas low and reversible adsorption was found in case of hydrophilic Hydrosart filters.

For scale-up of filtration trials to process level a new approach was developed in this work. The approach utilizes a resistance-in-series model based on the Darcy equation. Main parameters are the filtration flow rate, filter fouling and the active filter area of filtration devices. It was shown that tube constrictions of the filter device have a restrictive impact on the filtration flow rate, and can be calculated as an additional resistance. Several scaling trials were conducted, with good agreement of experimental and calculated data.

Further investigations were carried out to study the influence of salts and surfactants on bacteria retention and the filterability of liposomal solutions.

Zusammenfassung

Gegenstand dieser Arbeit sind Untersuchungen zur Filtrierbarkeit biopharmazeutischer Proteinformulierungen. Zusammensetzung, Herstellungsverfahren und Charakterisierungsmethoden entsprechender Testlösungen aus BSA und γ -Globulin wurden im Rahmen der Arbeit entwickelt.

Die Filtrationsuntersuchungen wurden mit Sterilfiltern aus verschiedenen Materialien (u.a. PESU, Hydrosart, CN) durchgeführt. Im Ergebnis der Untersuchungen konnte gezeigt werden, dass die Filtrierbarkeit von Proteinformulierungen abhängig ist von den Filtrationsbedingungen, der Zusammensetzung der Proteinformulierung und vom verwendeten Sterilfilter. Eine geringere Foulingrate wird insbesondere bei Filtration mit konstantem Volumenstrom durch Filter mit hydrophilen Oberflächeneigenschaften und offener Porenradienverteilung erreicht. Filtrationen mit konstantem Druck verstärken Filterfouling. Der Gehalt von Tensiden, wie Polysorbat 80 (PS80), in der Proteinformulierung hat einen starken Einfluss auf die kolloidale Stabilität der Lösung und die Proteinaggregation, auf die Adsorption von Proteinen an die Membranoberfläche und das Filterfouling.

Die Adsorption von Proteinen an die Membranoberfläche während des Filtrationsprozesses wurde mittels inverser Flüssigkeitschromatographie untersucht. Dabei konnte gezeigt werden, dass die Adsorption von Proteinen durch PS80 gesteuert werden kann. Bei hydrophilen Membranen, sowie bei hydrophoben Membranen und einer Tensidkonzentration oberhalb der kritischen Mizellkonzentration ist die Proteinadsorption vergleichsweise niedrig und reversibel. Bei Filtration PS80-freier Formulierungen führt die Filtration durch hydrophobe Membranen zu einer stärkeren und irreversiblen Proteinadsorption. Die Adsorptionsisothermen für BSA und γ -Globulin wurden oberhalb der kritischen Mizellkonzentration von PS80 gemessen und berechnet.

Berechnungsgrundlagen und experimentelle Methoden zur Durchführung von Untersuchungen zur Skalierung von Filtrationsprozessen wurden im Rahmen der Arbeit weiterentwickelt. Grundlage der Berechnungen ist ein Modell mit in Serie geschalteten Widerständen zur Beschreibung von Filtrationsdevices ausgehend von der Darcy-Gleichung. Wichtige Prozessparameter sind die Filtrationsflussrate, das Filterfouling und die aktive Filtrationsfläche der verwendeten Filterprodukte. Es wird gezeigt, dass Rohrverengungen einen restriktiven Einfluss auf den Filtrationsfluss haben und als zusätzlicher Widerstand eingerechnet werden können, der linear vom Filtrationsfluss abhängt. Verschiedene Skalierungsuntersuchungen zur Filtration von partikularen Lösungen und Proteinformulierungen wurden mit guter Übereinstimmung zwischen experimentellen und berechneten Daten durchgeführt.

Weitere Arbeitspakete im Rahmen dieser Arbeit sind die Untersuchung des Bakterienrückhaltes in Abhängigkeit von Salz- und Tensidgehalt der Proteinformulierung sowie Untersuchungen zur Filtrierbarkeit von liposomalen Lösungen.

Schlagworte

Proteinfiltration

Prozessfiltration

Filterfouling

List of abbreviations

BCT	Bacteria challenge test
BET	Brunauer, Emmett and Teller
BSA	Bovine serum albumin
CA	Cellulose acetate
CLS	Confocal laser scanning microscope
CMC	Critical micelle concentration
CN	Cellulose nitrate
CSA	Cross-section area
DLS	Dynamic light scattering
DLVO	Derjaguin-Landau-Verwey-Overbeck
FDA	Food & Drug Administration
ILC	Inverse liquid chromatography
IT test	Integrity test
MFP	Mean flow pore size
PA	Polyamide
PDA	Parenteral Drug Association
PES	Polyether sulfone
pI	Isoelectric point
PVDF _{hyd}	Hydrophilized polyvinylidene fluoride
QID	Quality information documents
RSA	Random sequential adsorption model
SEC	Size exclusion chromatography
SOP	Standard operating procedure
SSB	Sartorius Stedim Biotech GmbH
UV-Vis	Ultraviolet and visible light spectroscopy

List of Symbols

Symbol	Description	Unit
A_C	Constant for calculation of Coulomb interactions	C/m ²
A_{mem}	Membrane area	m ²
A_{mem_LS}	Membrane area for the large-scale device	m ²
A_{mem_SS}	Membrane area for the small-scale device	m ²
$A_{SS-connector}$	CSA of a SS-connector	m ²
A_{pore}	Cross-section of a pore	m ²
B	Constant for calculation of Van-der-Waals interactions	J·m
c	Protein concentration	g/l
d	Particle diameter	m
d_i	Inner tube diameter	m
I	Ionic strength	mol/l
J	Filtration flow rate	l/min
J_{LS}	Filtration flow rate for the large-scale device	l/min
J_{SS}	Filtration flow rate for the small-scale-device	l/min
J°	Filtration flux	ml/(min·cm ²)
J°_0	Initial filtration flux	ml/(min·cm ²)
k_{ad}	Adsorption rate constant	s ⁻¹
k_{de}	Desorption rate constant	s ⁻¹
k_i	Constant for description of device resistance	10 ¹³ min/m ⁶
k_{LS}	Constant for description of device resistance of the large-scale device	10 ¹³ min/m ⁶
k_{SS}	Constant for description of device resistance of the small-scale device	10 ¹³ min/m ⁶
k_x	Blocking constant for one of the four blocking mechanisms	see k_c , k_l , k_s or k_v
k_1^{ad}	Adsorption rate constant for state 1	s ⁻¹
k_2^{ad}	Adsorption rate constant for state 2	s ⁻¹
k_1^{de}	Desorption rate constant for state 1	s ⁻¹
k_2^{de}	Desorption rate constant for state 2	s ⁻¹
$k_{1\rightarrow 2}^{trans}$	Rate constant for transformation of state 1 to state 2	s ⁻¹
$k_{2\rightarrow 1}^{trans}$	Rate constant for transformation of state 2 to state 1	s ⁻¹
K	Adsorption equilibrium constant	-
m	Cumulative weight	g

m_{ads}	Adsorbed amount of protein	$\mu\text{g}/\text{cm}^2$
$m_{ads_h@40\text{ml}}$	Adsorbed amount of protein to the membrane housing after 40 ml of test solution in an ILC experiment	$\mu\text{g}/\text{cm}^2$
$m_{ads_m@40\text{ ml}}$	Adsorbed amount of protein to the membrane sample after 40 ml of test solution in an ILC experiment	$\mu\text{g} / \text{cm}^2$
m_{eq}	Equilibrium coverage	$\mu\text{g}/\text{cm}^2$
n	Exponent for determination of blocking mechanism	-
N	Number of pores per square centimeter	cm^{-2}
P	Measured filtration pressure	bar
ΔP_{tot}	Applied pressure difference across a filtration device	bar
P_0	Initial filtration pressure in constant flow filtration	bar
r_D	Thickness of electrical double layer	m
r_N	Radius of nucleus	m
Re	Reynolds number	-
$R_{housing}$	Resistance of the housing of a filtration device	10^{10} m^{-3}
$R_{J=0}$	Extrapolated intercept in a $R_{tot}(P)$ -plot	10^{10} m^{-3}
$R_{J=0,LS}$	Extrapolated intercept in a $R_{tot_LS}(P)$ -plot	10^{10} m^{-3}
$R_{J=0,SS}$	Extrapolated intercept in a $R_{tot_SS}(P)$ -plot	10^{10} m^{-3}
R_{mem}	Membrane resistance, divided by membrane area	10^{10} m^{-3}
R_{mem_LS}	Membrane resistance of the large-scale device	10^{10} m^{-3}
R_{mem_SS}	Membrane resistance of the small-scale device	10^{10} m^{-3}
R_{tot}	Total resistance of a filtration device, divided by membrane area	10^{10} m^{-3}
R°_{tot}	Total resistance of a filtration device	10^{10} m^{-1}
R_{tot_LS}	Total resistance of a large-scale filtration device	10^{10} m^{-3}
R_{tot_SS}	Total resistance of a small-scale filtration device	10^{10} m^{-3}
R°_0	Initial filtration resistance	10^{10} m^{-1}
$R^{\circ}_{1.5\text{g protein}/\text{cm}^2}$	Filtration resistance after filtration of 1.5g protein/cm ²	10^{10} m^{-1}
$R^{\circ}_{25\%}$	Membrane resistance when 25% of the membrane is blocked	10^{10} m^{-1}
$R^{\circ}_{50\%}$	Filtration resistance when 50% of the membrane is blocked	10^{10} m^{-1}
s	Distance of surfaces of two particles	m
S	Scale-up factor	-
SF	Safety factor for scale-up	-
t	Time	s
Δt	Time difference between two adjacent data points	s
T	Solution temperature	K, °C

$t_{25\%}$	Filtration time when 25% of the membrane is blocked	s
$t_{50\%}$	Filtration time when 50% of the membrane is blocked	s
u	Interaction potential	J
ΔV_{CNG}	Free energy of nucleus	J
V	Filtrate volume	l
\tilde{V}	Filtration throughput	ml/cm ²
V_{batch}	Batch size to be filtered	l
V_{final}	Maximum filterable amount of fluid in a small-scale trial	ml
$\tilde{V}_{25\%}$	Filtration throughput when 25% of the membrane is blocked	ml/cm ²
$\tilde{V}_{50\%}$	Filtration throughput when 50% of the membrane is blocked	ml/cm ²
$V_{Coulomb}$	Intermolecular electrostatic interactions	J
ΔV	Volume difference between two adjacent data points	l
V_{LS}	Filtrate volume of the large-scale device	l
V_{SS}	Filtrate volume of the small-scale device	l
V_{VdW}	Van-der-Waals interactions	J

Greek symbols

γ	Surface tension	N/m
$\dot{\gamma}$	Shear rate	s ⁻¹
ϵ_S	Solvent permittivity	-
ζ	ζ -Potential	mV
η	Solution viscosity	mPa·s
θ	Complete surface coverage	-, %
θ_1	Surface coverage with protein molecules in state 1	-, %
θ_2	Surface coverage with protein molecules in state 2	-, %
θ_j	Maximum surface coverage described by the RSA model	-, %
$\Delta\mu$	Chemical potential of nucleating phase	J
ρ	Solution density	g/ml
ρ_n	Number density	l ⁻¹
Φ	Surface coverage function as described in the RSA model	-

Constants

Symbol	Physical quantity	Value	Unit
F	Faraday constant	9.64853·10 ⁴	C/mol
R_g	Gas constant	8.31447	J/(mol·K)
ϵ_0	Vacuum permittivity	8.85419·10 ⁻¹²	C ² /(J·m)

Table of Contents

1	Introduction	1
2	Main Focus of this Study	3
3	Theoretical Background	4
3.1	Proteins and Protein Formulations	4
3.1.1	Protein Structure and Conformational Characteristics	4
3.1.2	Therapeutic Protein Formulations	6
3.1.3	Protein Solutions	9
3.1.4	Properties of Bovine Serum Albumin and Bovine γ -Globulin	15
3.2	Sterile Filtration in Biopharma Production	17
3.2.1	Filtration as a Part of the Biopharmaceutical Process	17
3.2.2	Description of Filtration Process and Monitoring of Filter Fouling	19
3.2.3	Filter Products	20
3.3	Scale-Up of Microfiltration from Lab-Scale to Process-Scale Filtration	30
3.4	Validation of Sterile Filtration with <i>Brevundimonas diminuta</i>	34
3.5	Protein Adsorption	36
3.5.1	Physicochemical Basics of Protein Adsorption	36
3.5.2	Adsorption Kinetics in Protein Filtration	36
3.6	Therapeutic Liposome Formulation	39
3.6.1	Chemical and Physical Aspects of Liposomes	39
3.6.2	Application of Liposome Formulation	41
4	Materials and Methods	42
4.1	Materials and Formulations for Filtration Trials	42
4.2	Characterization of Formulations	44
4.2.1	BSA and γ -Globulin Formulations	44
4.2.2	Characterization of the Liposomal Formulation	45
4.3	Overview of Membrane Materials	46
4.4	Characterization of Membrane Materials	47

4.4.1 Porometry	47
4.4.2 SEM	47
4.4.3 BET	48
4.5 Execution and Evaluation of Filtration Trials	49
4.5.1 Description of Filtration Setups	49
4.5.2 Evaluation of Filtration Experiments	51
4.5.3 General Information on Scaling Experiments with Protein Formulations.....	52
4.6 Confocal Laser Scanning Microscopy (CLS).....	53
4.7 ILC for Adsorption Measurements.....	54
4.8 Bacterial Challenge Tests	58
5 Results and Discussion	60
5.1 Formulation, Manufacturing and Characterization of Standardized Protein Formulations for Filtration Studies	60
5.1.1 Formulation Development for γ -Globulin by SEC.....	60
5.1.2 Preparation and Characterization of Standardized Protein Solutions in kg Scale	63
5.1.3 Characterization of Protein Formulations	64
5.1.4 Summary	66
5.2 Filtration of Protein Formulations	67
5.2.1 Evaluation of Filtration Data – Monitoring of Filter Fouling.....	67
5.2.2 Impact of Process Conditions on Filtration of Protein Formulations	70
5.2.3 Influence of Membrane Structure and Material on Fouling.....	87
5.2.4 Localization of Fouling Layer Within the Membrane Material	91
5.2.5 Pre-Filter and Main Filter Combinations.....	93
5.2.6 Summary	97
5.3 Development of Scale-Up Concept for Biopharmaceutical Process Filtration	98
5.3.1 Resistances and Active Filter Areas of Filtration Devices	98
5.3.2 Scale-Up of Filtration Processes: Experimental Approach and Calculation Basis.....	103
5.3.3 Case Studies – Up-Scaling Studies for Filtration of Protein Formulations	105

5.3.4 Summary	118
5.4 Protein Adsorption during Filtration Process.....	119
5.4.1 Protein Adsorption to Membrane Housings.....	119
5.4.2 Influence of Surfactant (PS80) on Protein Adsorption	121
5.4.3 Influence of Protein Concentration – Adsorption Isotherm.....	123
5.4.4 Influence of Filtration Flow Rate on Protein Adsorption.....	124
5.4.5 Protein Adsorption and Desorption – Multiple Measurement Cycles	125
5.4.6 Calculation of Monolayer Coverage	128
5.4.7 Summary	131
5.5 Influence of Formulation Ingredients on Retention of <i>Brevundimonas diminuta</i>	133
5.6 Filtration of Liposome Solutions	135
5.6.1 Characterization of Liposomal Formulations.....	135
5.6.2 Filtration Trials of Liposomal Formulations	136
5.6.3 Summary	147
6 Summary and Conclusions	148
7 Literature.....	153

1 Introduction

Therapeutic protein formulations are drugs containing proteins as active ingredients, e.g., monoclonal antibodies (48% of approved therapeutics), coagulation factors (19%), enzymes (11%), plasma proteins, growth factors, hormones, or fusion proteins. The drugs are usually classified as large molecule drugs or biologics, because large proteins or fusion proteins often exceed a molecular weight of 100 kDa. Due to the size and molecular weight of proteins the physical behavior of their aqueous solution is similar to that of classical colloids, which are thermodynamically unstable. The surface of classical colloids is charged evenly, in contrast to proteins. Proteins are biopolymers essentially made of different amino acids as building blocks, folded in a specific conformation connected to their mode of action; due to these different amino acids their surfaces are charged heterogeneously. In the case of multidomain proteins, such as immunoglobulins (IgGs), strong intramolecular interactions additionally occur. Highly concentrated protein formulations tend to aggregate. [3,5,6] This distinguishes them from small molecule drugs, which contain small organic components with therapeutic activity. [1] Protein therapeutics are also used as vaccines, e.g., against hepatitis B, or as therapeutic anticancer vaccines [2].

Protein drugs are administered either intravenously at the hospital or subcutaneously, which can be done by the patient himself without any medical assistance and is therefore often the preferred route. Due to two reasons for subcutaneous injection a high protein concentration of up to 200 g/l is needed: only 2 ml injection volume can be applied this way, and to reach a therapeutic effect usually 2 mg protein per kg of patient body mass is needed. These drug formulations have high viscosities, up to ca. 100 mPa·s. [3,4]

Biopharmaceutical production processes are generally divided in the cell cultivation process and the protein purification process. Purification encompasses protein A chromatography, cation exchange, anion exchange, virus inactivation, viral clearance, concentration, diafiltration, and formulation. [1,7] The formulation step is the last process step before the Fill and Finish process. [5,8,9] Protein formulations usually contain further ingredients or excipients, e.g., a buffer, surfactants and additional stabilizers to prevent side reactions. A sophisticated way to stabilize proteins is to encapsulate them in liposomes.

Development and drug production are highly regulated by government authorities [10,11]. Throughout the production process, sterile filtration is used to remove insoluble aggregates and to reduce the bioburden, but the most critical sterile filtration step is the Fill and Finish process, the last one before the filling line [12]. In this case, the PDA requires manufacturers to provide evidence for the effectiveness of a membrane filter. Additionally, it has to be proven that the filter does not cause particulate

1 Introduction

contamination, release leachables or change the concentration of formulation ingredients by adsorption [10].

Because of the complex production process, the development of protein pharmaceuticals is quite expensive. Development costs are in the range of one billion dollars from preclinical development to market approval. In 2017, more than 300 monoclonal antibodies were in a clinical stage. [7]

2 Main Focus of this Study

The scope of this study is to examine issues related to sterile microfiltration of therapeutic protein formulations, especially the Fill and Finish process. The main work packages were the following:

1. Development of standardized, stable drug-like model protein formulations based on γ -globulin and BSA, which were used for the further investigations. This included the formulation, characterization and the manufacturing procedure in the scale of up to 20 liters.

2. Filtration trials with the model protein formulation at different operating conditions (constant flow, constant pressure, different filtration temperatures) and with different membrane filters (material, membrane structure, and surface chemistry) to identify optimum filtration conditions.

3. Development of a scale-up approach from lab scale filtration to process filtration, which includes the complete modeling of a filtration process. Central aspects of this concept were the analysis of the influence of a filtration setup and the determination of the resistance and the effective membrane area of the filter devices used. Case studies were performed with a standardized particulate test solution and the model protein formulations.

4. Examination of the influence of the formulation on bacteria retention by performing bacteria challenge tests (BCT) using different surfactants and salt concentrations as well as of the influence of cation valence and ionic strength.

5. Study of protein adsorption during filtration using an inverse liquid chromatography system (ILC) and the development of the measurement procedure and the evaluation methods. Here the influences of the membrane and of formulation ingredients on protein adsorption were investigated.

6. Filtration of liposomal formulations and study of the influence of composition and process conditions on filter fouling.

3 Theoretical Background

3.1 Proteins and Protein Formulations

Proteins are biological polymers essentially made up of different amino acids as building blocks. Most natural proteins contain between 50 and 2 000 amino acids, linked by peptide bonds. These amino acids can be distinguished by their side chains, which can be hydrophilic, hydrophobic, aromatic, or acidic/alkaline. Proteins are part of essentially all biological processes, e.g., catalysis, molecular transport and storage, immune protection, and nerve transmission. [6]

3.1.1 Protein Structure and Conformational Characteristics

The three-dimensional protein structure has repetitive subunits at smaller scales. They are usually described as primary, secondary, tertiary, and quaternary structure. The primary structure encompasses all the covalent bonds; i.e., the amino acid sequence and the disulfide linkages of cysteine residues and determines the chemical stability and the protein net charge. The secondary structure describes parts of the amino acid sequence that are folded in a regular structure and stabilized by hydrogen bonds. The most prominent examples here are α -helices and β -sheets, helical structures contrary to the rather straight parts within a protein. The tertiary structure describes the folding of one complete polypeptide chain. If a protein is made up of several polypeptide chains, their arrangement is depicted by the quaternary structure. The biologically active structure of a protein is called the native structure. [6] The primary, secondary and quaternary structure are depicted in figure 1. The structure of an immunoglobulin is chosen as an example; this protein is made up of four chains.

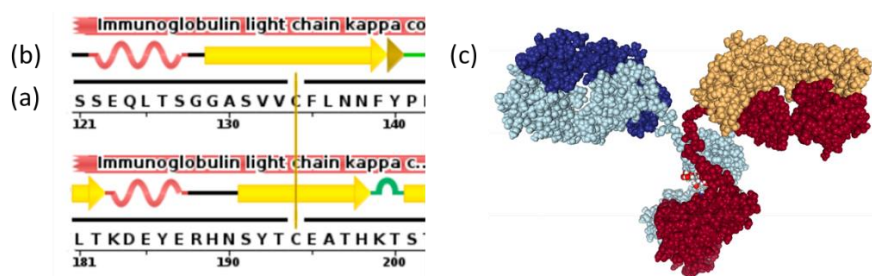


Figure 1: Schematic representation of the protein structure of an immunoglobulin: (a) excerpt of the amino acid sequence including disulfide linkages, shown with yellow lines; (b) the corresponding secondary structure with helical parts in red, β -sheets in yellow and turns in green; (c) the quaternary structure, showing each of the four chains in separate colors. (PDB-file 1IGT) [13–15].

The physical structure of a protein is stabilized by hydrogen bonds, ionic effects and van-der-Waals interactions. In an aqueous solution, side chains of hydrophobic amino acids are preferably directed into the interior of a protein, while hydrophilic side chains are at the surface. For proteins embedded within biological membranes this arrangement of hydrophilic and hydrophobic side chains is usually reversed.

3 Theoretical Background

Proteins are not rigid molecules. Rather, they constantly rearrange in solution. Local conformational changes take place within nanoseconds. [16] Due to their structural complexity, flexibility and chemical properties proteins react in solution to any changes in environment or physical stress (e.g., shearing) by local conformational rearrangements, which can cause refolding or aggregation. If proteins are folded in a way that a refolding in the native structure is unlikely, the process is called denaturation. [6] Such denaturation can be induced by shearing, exposure to heat or changes in pH, to name a few [17]. The associated conformational changes can take several minutes [18].

Proteins adsorb to surfaces depending on their orientation and the surface charge, and usually change their conformation. Examples of these conformational changes are given in literature, for example, the denaturation of the β -sheets of lysozyme on a hydrophobic surface (figure 2). [19] It can take hours to complete all conformational changes associated with an adsorption process [16,20].

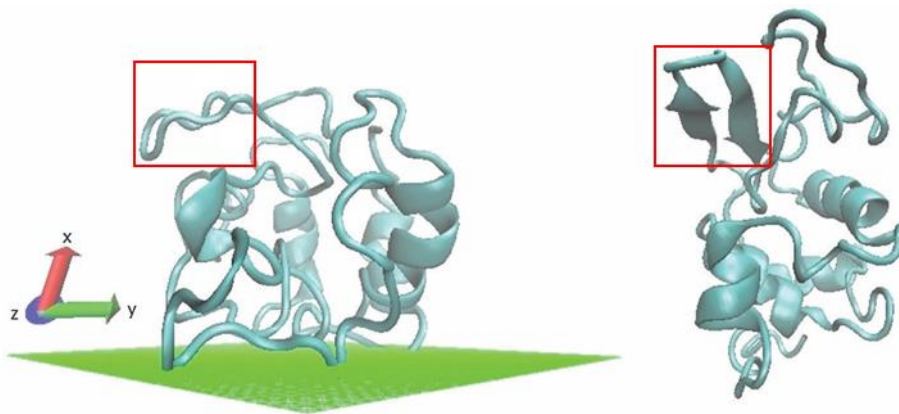


Figure 2: Conformational changes of lysozyme upon adsorption to a hydrophobic surface, obtained by simulation. Adsorbed structure shown to the left, native structure depicted on the right [19]. The red box highlights β -sheets that defold upon adsorption.

The stability of the protein molecules for the necessary shelf-life of protein therapeutics (18-24 months [21]) is a challenge. Protein drugs contain excipients to stabilize the protein for storage, transportation and administration to patients, as well as and to prevent physical and chemical destabilization related to the complexity of protein structure and their chain dynamics. Chemical stability refers to chemical modifications of the primary structure, such as site-directed mutagenesis (exchange of a single amino acid) while physical stability describes changes in the conformation and aggregation. [5] Chapters 3.1.3 and 3.2 provide an overview on formulation trends and the physical stability of protein formulations.

3.1.2 Therapeutic Protein Formulations

The aim of the formulation of a protein drug is to provide the drug in a therapeutic active form, stabilize it and adjust it for administration. Current development trends for drug formulations are summarized in the next section and in the reference literature [22,23].

Excipients - Basic Formulation Ingredients

In protein therapeutics, formulation ingredients, the excipients, are used to prevent aggregation and chemical degradation of proteins, and to reduce the drug solution viscosity. Only substances allowed by the pharmacopeias can be used as drug excipients. These ingredients are usually divided into several classes such as buffers, surfactants, sugars, preservatives and other substances. An overview of excipients and their use is shown in table 1.

Table 1: Overview of excipients for protein formulations and their function [24–26].

Class	Example	Function
Buffer	Phosphate	pH stability
Surfactants	Polysorbate 20, Polysorbate 80	Prevention of aggregation and adsorption by protection of surfaces
Sugars	Sucrose, trehalose	Cryoprotectant
Other excipients	Amino acids: histidine, glycine, arginine	Buffer, antioxidant, aggregation prevention, viscosity reduction
	Preservatives (<i>m</i> -cresol)	Prevention of microbial growth

The most critical formulation step governing the solubility and stability of a protein is usually the choice of pH and buffer system. The physical and chemical background is described in chapter 3.1.3. Popular protein buffers are phosphate, acetate and citrate. [22,27]

Surfactants, e.g., Polysorbate 80 (PS80) prevent adsorption to solid surfaces and suppress aggregation during agitation, shaking, freeze-drying and freeze-thawing processes. The disadvantage is the tendency of PS80 to auto-oxidate at moderate temperatures, and to hydrolyze at higher temperatures. [28] Therefore, the concentration range usually applied is between 0.001% and 1% [24].

Sugars are usually used as cryoprotectants and lyoprotectants. They stabilize proteins against denaturation and aggregation during freezing and lyophilization. To achieve this stabilizing effect, a molar ratio of 360 : 1 (sugars to antibody) is required. Sugars inhibit dehydration-induced unfolding by donating hydrogen bonds to the protein. [29]

Amino acids employed in protein formulations are arginine, histidine and proline. Arginine suppresses aggregation during refolding of a protein, increases the solubility of aggregation-prone

3 Theoretical Background

molecules and suppresses heat-induced aggregation. Moreover, it suppresses protein-protein interactions, thus reducing the solution viscosity for formulations of monoclonal antibodies, but not of globular proteins, such as albumine. Histidine also suppresses aggregation induced by heat, lyophilization or storage in a dried state. It can directly bind to a protein and preserve intramolecular β -sheets, thus preventing protein unfolding. Additionally, histidine captures iron and singlet oxygen, thus preventing oxidation. Proline also suppresses aggregation during refolding. It is the most soluble amino acid, but has hydrophobic parts that shield the hydrophobic parts of a protein. [22,30,31]

Preservatives are required to prevent microbial growth for use of protein formulations in multi-use pens, minipumps and for multi-dose drugs. About one third of the protein formulations are multi-dose drugs. The drawback of preservatives is that most of them induce protein aggregation. [21,32]

Current Trends for Drug Dosage

Biopharmaceuticals are available as ready-to-use solutions, freeze-dried powders that have to be reconstituted just before administration, and ready-to-use suspensions. They can be administered intravenously, as intravenous infusions, subcutaneously, intralesionally or intramuscularly. [9] The dosage form depends on the type of medicine; drugs that should be taken regularly are administered subcutaneously with a limited volume of maximum 2 ml for patient convenience. Usually, 2 mg/kg of patient body mass are needed to reach therapeutic doses. The high concentrations of up to 200 g/l consequently needed cause stability issues. Depending on the shelf-life of a protein drug, it is available either as a solution (for preparation of an IV infusion), as an IV solution or as lyophilized powder. It can be seen in figure 3 that formulations above 50 mg/ml are all intended for patient administration at home and are therefore available as solutions for injection or as lyophilized powders. [3,24,33]

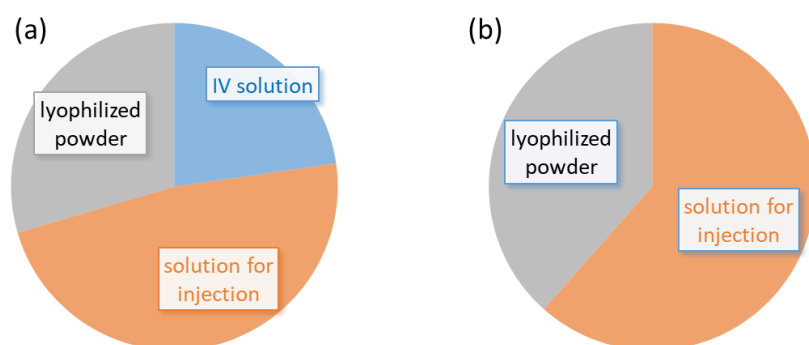


Figure 3: Overview of shares of dosage forms of protein pharmaceuticals; (a) all formulations independent of protein concentration; (b) formulations with concentration above 50 mg/ml [24].

3 Theoretical Background

High protein concentrations lead to increased viscosity and protein aggregation due to intermolecular interactions, as is explained in chapter 3.1.3. These effects can be reduced by formulation and choice of excipients as presented earlier in this section.

Trends for Buffers Used in Protein Formulations

Currently, most parenteral drugs are phosphate-, acetate-, citrate- or histidine-buffered (figure 4). Almost all buffers have drawbacks: the pH of phosphate shifts on freezing to pH 3.6, citrate can reach a pH of 3; therefore destabilization of the protein is likely. Citrate induces more pain upon subcutaneous injection compared with phosphate and histidine, and acetate is volatile; thus, the pH of the latter buffer increases on lyophilization.

Histidine is becoming increasingly common in new formulations, which are provided in lyophilized form; it actually protects proteins against stress during lyophilization in liquid and lyophilized state due to direct binding of histidine to the protein molecules. Histidine has three ionization sites on the molecule, and can be used as a buffer between pH 5.5-6.5. Additionally, it has antioxidant properties due to its affinity to iron. The problem with histidine is that it undergoes a change of color under elevated temperatures, and histidine is known to extract iron from stainless steel under acidic conditions. [5,22,29]

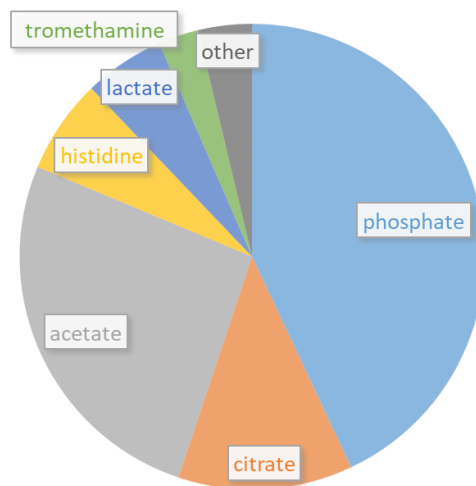


Figure 4: Overview of buffers currently in use for protein drugs administered subcutaneously. [24]

Protein Pharmaceuticals as Vaccines

The term “therapeutic vaccine” can describe either a traditional vaccine that protects the patient from infection by a disease. However, therapeutic vaccines are also biopharmaceuticals that are given to cancer patients to fight a tumor.

3 Theoretical Background

In vaccines the active ingredient is usually a weakened live, inactivated or killed virus; the active ingredient can be conjugated to a protein; sometimes human albumin is used as a stabilizing agent. In contrast to therapeutic protein formulations with high concentrations, vaccines contain only low concentrations of active ingredient, usually below one milligram per dose, so adsorption is an important issue here. The additional formulation ingredients of a vaccine can be separated into adjuvants (substances that enhance the effectiveness of the respective vaccine) and excipients (stabilizers). [34]

Excipients are comparable to protein formulations, buffers, surfactants, preservatives and other stabilizers, e.g., albumin. The oldest adjuvants are aluminum salts, which have been in use for over 80 years. Modern formulation development shows a trend to squalene-based emulsions. [34,35]

A trend for therapeutic vaccines in cancer treatment is the use of liposomes to reduce side effects and enhance the effectiveness of a vaccine. Liposomes deliver the encapsulated antigen directly into the cytosol (the liquid components of a cell). The therapeutic effectiveness of liposomes depends on their composition, size, the chirality of the lipids and the type of antigens. [36] An overview on liposomes is presented in chapter 3.6.

3.1.3 Protein Solutions

Colloidal Solutions

Protein solutions can be regarded as an ensemble of colloidal particles suspended in an aqueous environment [5]. Colloidal solutions or dispersions contain particles, of 1 nm up to 1 μm in a solvent [37]. They are thermodynamically unstable; due to their large surface-volume ratio, the particles tend to attract one other. The colloidal stability of protein solutions depends on the protein-protein interactions and has an impact on solution characteristics such as solubility, viscosity, crystallization and aggregation. The nature of interaction between proteins (attractive or repulsive) influences the aggregation rate and the size of aggregates.

In the case of highly concentrated protein formulations, e.g., protein drugs, the particles are in close proximity to one other; intermolecular distances can be even smaller than the protein diameters [4]. Figure 5 shows a Brownian dynamics simulation of hen egg white lysozyme, here it can be seen that at a concentration of 169 g/l the protein molecules are already close to one another, and at 254 g/l they are even more crowded together. This causes significant challenges; the long-term stability is affected by self-association and aggregation. Processing, manufacturing and administration of drugs are complicated due to high viscosities: Most analytical methods cannot be directly used for these formulations. [33]

3 Theoretical Background

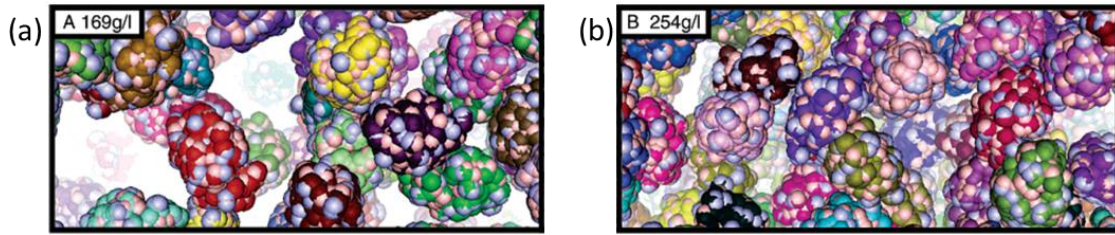


Figure 5: Brownian dynamics simulation of protein dispersion in solutions with different protein concentration; hen egg white lysozyme at 169 g/l (a) and at 254 g/l (b) [38]. Reprinted with permission from (S.R. McGuffee, A.H. Elcock, Atomically detailed simulations of concentrated protein solutions: The effects of salt, pH, point mutations, and protein concentration in simulations of 1000-molecule systems, *J. Am. Chem. Soc.* 128 (2006) 12098–12110). Copyright (2006) American Chemical Society.

Rheology of Protein Formulations

Viscosity of a liquid is caused by intermolecular interactions [39]. In water, molecular interactions occur on a timescale of 10^{-12} s at 25 °C. For proteins, segmental motions and conformation rearrangements occur on a timescale of 10^{-7} - 10^{-9} s. Here, the time scales are influenced by the protein properties and further formulation ingredients. [40]

Viscosity can exhibit non-Newtonian behavior due to the protein-protein interactions within a protein formulation. Shear-thinning behavior (figure 6) or viscoelastic properties can be observed. [39,41]

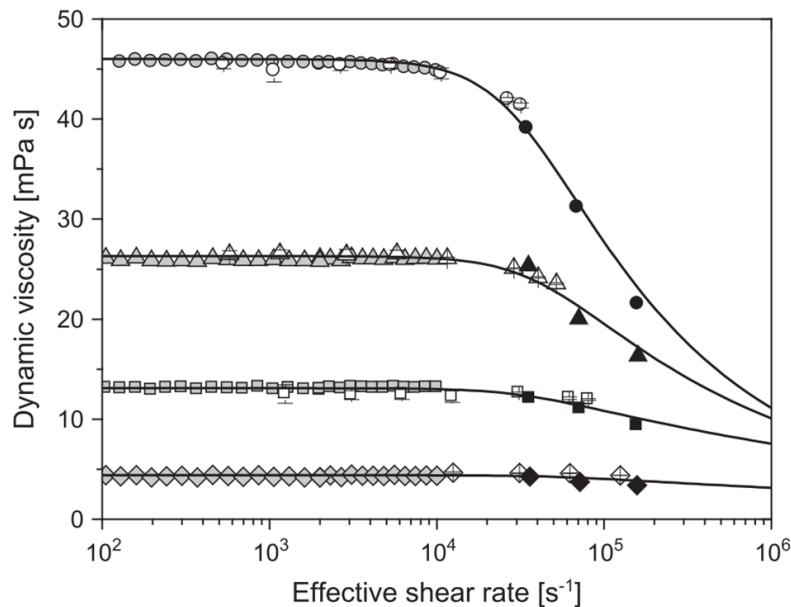


Figure 6: Shear-thinning behavior of a monoclonal antibody with 120 g/l (diamonds), 170 g/l (squares), 210 g/l (triangles) and 225 g/l (circles) protein [41].

Aggregation can be induced during processing by the process conditions, for example due to temperature changes (cold denaturation). The influence of shear sensitivity is dependent on the pro-

3 Theoretical Background

tein; some proteins lose their activity at a shear rate of $2 \cdot 10^4 \text{ s}^{-1}$, while others show no sign of destabilization at $2 \cdot 10^5 \text{ s}^{-1}$. For mixing and filtration the problems are quite similar: shearing and exposure to interfaces are a problem, as protein unfolding and, therefore, loss of activity might occur. [4,42]

Thermodynamic Stability of Colloidal Solutions

The stability of colloidal formulations can be generally rated in terms of the Derjaguin-Landau-Verwey-Overbeck (DLVO) theory and is described by the sum of electrostatic repulsive interactions and attractive Van-der-Waals interactions. Coulombic interactions can occur due to an electric double layer surrounding the proteins. These interactions can be calculated depending on the thickness of the double layer in comparison to the particle size. According to the Debye-Hückel-theory double layer thickness r_D can be estimated depending on the ionic strength I , solution temperature T , solution density ρ and the gas constant R_g as given in equation 1: [43]

$$r_D = \sqrt{\frac{\varepsilon_0 \varepsilon_s R_g T}{2 \cdot F^2 I}} \quad (1)$$

The constants here are the vacuum permittivity ε_0 , the solvent permittivity ε_s and the Faraday-constant F . [44] For a phosphate buffer of 100 mM NaH_2PO_4 and 100 mM Na_2SO_4 solution ($I = 0.9 \text{ mol/l}$) at room temperature (293 K) in water (solvent permittivity of 80.1 at 20 °C [45]), this double layer thickness is approximately 0.3 nm and therefore small in comparison to the BSA diameter of approximately 7 nm. Because of the relationship between particle size and double layer thickness, electrostatic interactions $V_{Coulomb}$ can be calculated by equation 2. The Van-der-Waals interactions V_{vdW} are described by equation 3.

$$V_{Coulomb} = \frac{A_C d \zeta}{4} \cdot \ln(1 + e^{-s/r_D}) \quad (2)$$

$$V_{vdW} = -\frac{B}{s} \quad (3)$$

Here A_C is a constant, d the diameter of the particles, ζ the ζ -Potential, s the distance of the particle surfaces, and B is a constant. The energy profiles and the total of both energies are shown in figure 7. For dilute solutions, intermolecular distances are quite large; however, such distances shrink as the concentration of the solution increases. A secondary minimum can occur; here flocculation of the solution occurs and small aggregates are formed. This flocculation is reversible, as aggregates dissociate upon dilution again. In case of even higher concentrations particles need to take up smaller distances. At really short distances the energy plot (figure 7) shows a primary minimum. For a higher ionic strength the double layer thickness is decreased (equation 1) and the repulsive coulombic interaction is lowered (equation 2) according to the theory, which results in a lower energy barrier.

3 Theoretical Background

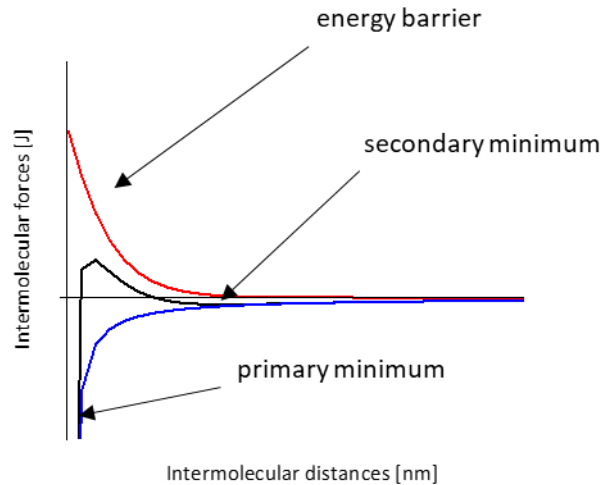


Figure 7: Presentation of intermolecular forces between spherical particles according to the DLVO-theory: Attractive Van-der-Waals-interactions (blue), repulsive electrostatic interactions (red) and sum of both intermolecular forces (black) (own representation).

According to the DLVO theory it can be expected for filtration of protein formulations that with different protein concentrations (and therefore different intermolecular distances), filter fouling will occur at different fouling rates; for low concentrated protein formulations, no aggregates or only small aggregates are present in the formulation; therefore only protein monomers can block the membrane. As the concentration increases, soluble aggregates are formed, which should accelerate membrane blockage.

The reality might be more complicated. DLVO uses the Poisson-Boltzmann-equation for the calculation of the repulsive electrical double-layer force and can hence be applied only for diluted salt concentrations of up to approximately 0.01 mol/l. Ions are treated as point charges; actually, the influence of a salt varies depending on its anions and cations. Ion-specific effects are described in the Hofmeister series. Here ions are separated into kosmotropes (SO_4^{2-} and H_2PO_4^-), which stabilize protein structures, and chaotropes (I^- , ClO_4^-) that are known to destabilize folded proteins. [46]

Critical Nucleus Growth Theory

The critical nucleus growth theory explains the formation of large aggregates in colloids. Aggregate formation is hindered by an energy barrier – until a critical nucleus is formed. Then the growth of an aggregate is thermodynamically favored. To represent this mathematically, the free energy of the nucleus with radius r_N is described as the sum of a bulk term and a surface term.

$$\Delta V_{CNG} = -\frac{4}{3} \cdot \pi \cdot r_N^3 \cdot \rho_n \cdot \Delta\mu + 4 \cdot \pi \cdot r_N^2 \cdot \gamma \quad (4)$$

3 Theoretical Background

The number density ρ_n and the chemical potential $\Delta\mu$ of the nucleating phase are part of the bulk term, the surface tension γ determines the surface term [47]. The resulting function is illustrated in figure 8.

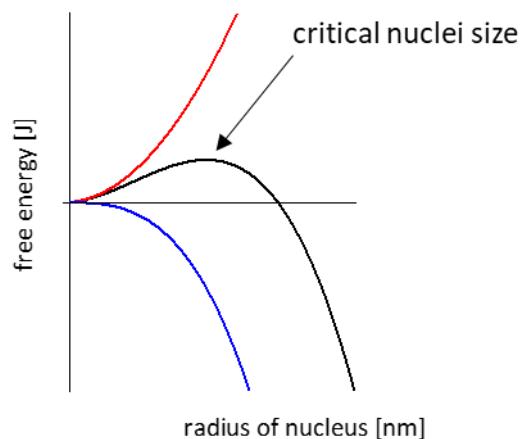


Figure 8: Diagram of the free energy of nuclei formation. Aggregate formation driving bulk term (blue), disruptive surface free energy (red) and the sum of both energies (black) (own representation).

The critical nucleus growth theory complements the DLVO theory. It explains the fact that the formation of small aggregates is reversible. Once the critical nucleus size is reached aggregate growth is thermodynamically favored. The critical nucleus is not necessarily made up of the same material, heterogeneous nucleation is much more common. [47] Besides proteins, particles can also serve as aggregation nuclei, for example, particles shed due to abrasion in a process [17,48]. Surface charges are not considered in this theory.

Properties of Proteins in Aqueous Solution

Proteins have a heterogeneous, charged surface. At the pH of the isoelectric point (pI) the net charge is zero; in more acidic conditions the net charge is positive, whereas in more basic conditions it is negative. The pI is a value that is specific for each protein, and can be calculated for known primary structures. The net charge causes an electrical double layer to be formed around a protein. The interactions between different proteins depend on the protein charge and the formulation ionic strength and determine solution properties such as viscosity. For example, as the pI is approached, an increase in the viscosity of the formulation can be observed for highly concentrated BSA and mAb formulations. [6,33]

The type of intermolecular interactions changes with different protein concentrations. In dilute solutions long-range protein interactions are dominant. As the protein concentration increases, the proteins move ever closer to one another and short-range interactions are therefore more dominant.

3 Theoretical Background

As explained by the DLVO theory earlier in this section, repulsive charge-charge interactions contribute most to protein interactions for longer distances, whereas attractive forces play a stronger role in short-range interactions. Additionally, monoclonal antibodies interact through self-association, forming transient networks. Consequently, the radius measured by dynamic light scattering (DLS) is usually somewhat larger than the actual hydrodynamic radius. Knowing the intermolecular interactions at low concentrations enables the pH of maximum viscosity to be predicted for highly concentrated solutions. [33]

A protein structure and its surface are not uniform; therefore, interaction and adsorption to a surface occur, depending on the orientation of a molecule. Furthermore, as explained in chapter 3.1.1 proteins are not rigid molecules, rather they rearrange in a time span of only a few nanoseconds. Such rearrangements are usually slight, yet complete denaturation can take up to a few minutes. [16, 18]

Physical Stability of Proteins in Solution – Protein Aggregation

Aggregation describes self-association of proteins in a conformation that deviates from the native quaternary structure. It is diverse in terms of linkage (covalent or non-covalent), size (nm up to more than 100 μm), order (ordered/random configurations), protein conformation (native/denatured), reversibility, and solubility. Limits of aggregates are defined only for insoluble proteins in the pharmacopoeias, whereas for soluble aggregates the required limits need to be validated for every single case. Aggregation always changes the activity of a protein drug. An example here is hexamer-formation of insulin. Monomeric insulin takes effect fast within 10 minutes, in contrast to hexamer, which remains effective for up to 8 hours. [49] Another issue is that protein aggregates can cause an immune response in the human body; this immune response, in turn, can destroy the pharmacologically active proteins [17]. Protein drugs are usually stabilized by formulation ingredients as described in chapter 3.1.2 to prevent proteins from aggregating.

Aggregation Mechanism

Protein aggregation can generally be separated into three different steps: initiation, propagation and termination. The timescale of aggregation is protein-specific: aggregation can occur within seconds or over weeks. [50,51] Each protein has its own aggregation pathway; the same protein can even aggregate with several mechanisms to form different products [17,52]. Three general pathways for oligomer or aggregate formation are shown in figure 9.

The difference between the pathways lies in the reversibility of the steps, denaturation and the intermediates in forming large aggregates. Figure 9 does not include heterogeneous nucleation as a source of aggregation; in this case the process is more complex.

3 Theoretical Background

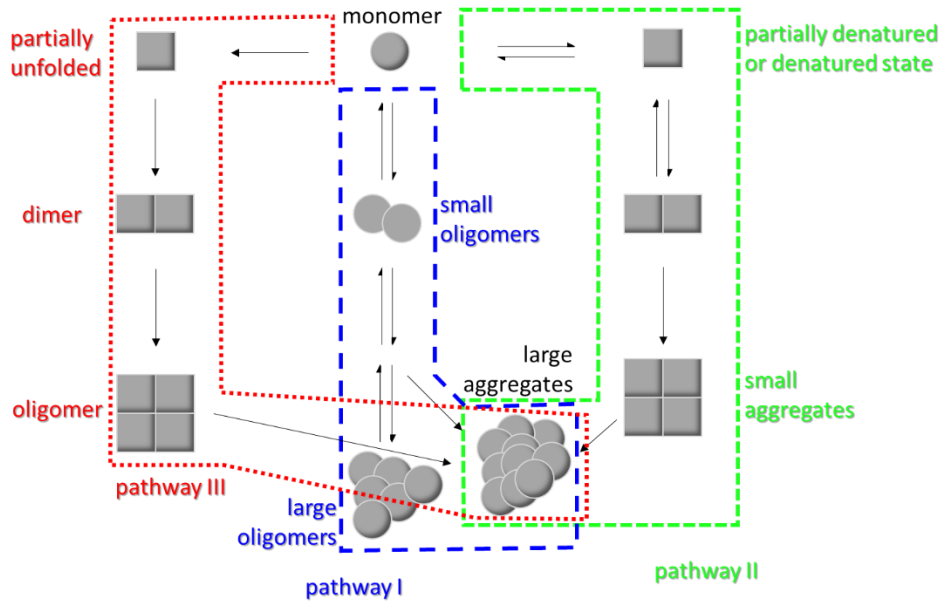


Figure 9: Schematic representation of different protein aggregation mechanisms (own representation) [24,52].

3.1.4 Properties of Bovine Serum Albumin and Bovine γ -Globulin

A central work package of this thesis is the development of and the examination of filtration trials with standardized protein formulations for filtration studies based on BSA and γ -globulin. This chapter and table 2 give an overview about the characteristic features of both proteins.

Serum albumin is a protein that makes up 50 % of the proteins in human blood plasma, γ -globulin is a smaller fraction. Serum albumin and immunoglobulin are gaining importance as human serum proteins. At the beginning of this century, 20 million liters of human plasma were used for the production of 500 000 kg human serum albumin and 40 000 kg immunoglobulin. [53,54]

Table 2: Overview of properties of BSA and γ -globulin [13–15,55–63].

	BSA	γ -globulin
Molecular weight [kDa]	67	150
Diameter [nm]	7	10-12
pI	4.7	6.55
Secondary structure	74% helical	6% helical, 49% beta sheets
PDB file	3V03	1IGT
Chains	2 identical chains	2 identical light and 2 identical heavy chains
Adsorption tendency	High	High
Monolayer coverage [ng/cm ²]	150-200	150-180

3 Theoretical Background

The albumin protein blood fraction is responsible for transporting molecules within the blood. BSA proteins have a molecular weight of 67 kDa and a diameter of 7 nm [58, 64]. Their typical shape is shown in figure 10. Serum albumin makes up 60% of the blood plasma fraction [65].

Gamma-globulin is the general term for the blood fraction containing antibodies that can be divided into five classes: IgG, IgA, IgM, IgD and IgE. Each protein is made of two identical heavy chains and two identical light chains, connected by disulfide bonds. The typical Y-shaped structure (figure 10b) is common for IgGs. Antibodies weigh approximately 150 kDa and are 10-12 nm in diameter. The IgG depicted in figure 10 has a pI of 6.55. [60,61]

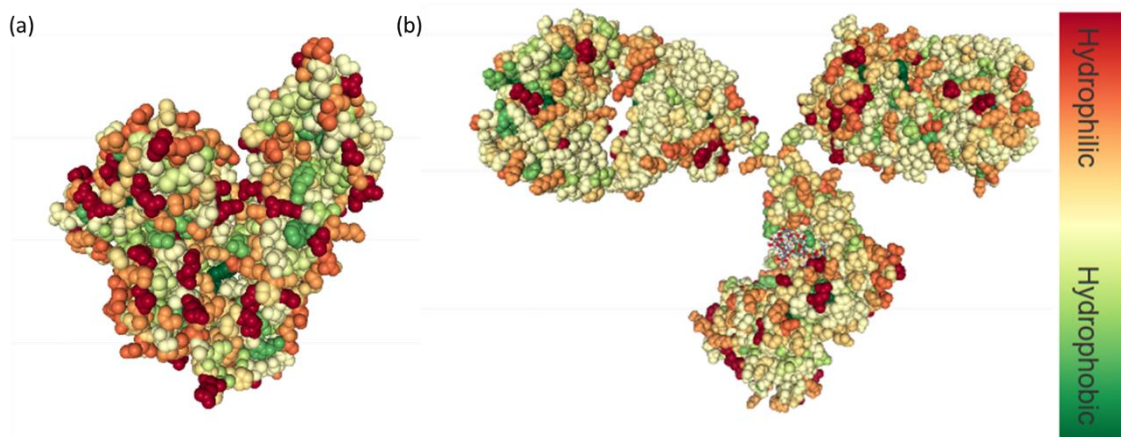


Figure 10: Images of BSA (a) and an Immunoglobulin (b) (PDB-files 3V03 and 1IGT) [13–15,57].

Both proteins are so-called “soft” proteins, i.e. they adsorb on nearly every surface and change their conformation due to a conformational entropy gain. Therefore, desorbed proteins re-adsorb at a higher adsorption rate. [63]

3.2 Sterile Filtration in Biopharma Production

3.2.1 Filtration as a Part of the Biopharmaceutical Process

The manufacturing process of therapeutic proteins is subdivided into an upstream part, comprising the cell culture process and harvest and into a downstream part, designed to purify the target protein and formulate a protein drug [66]. The manufacturing process is concluded by the Fill and Finish process, final sterile filtration and filling of a protein drug [67]. An overview of the overall process is shown in figure 11.

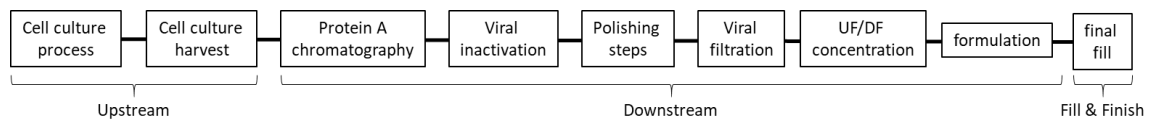


Figure 11: Biopharma process chain for production of monoclonal antibodies [68–70].

Throughout this process, filtration steps are included for removal of host cells, removal of viruses, concentration and for buffer exchange. Additionally, the FDA requires prior sterilization of all media to be used throughout the process— e.g., cell culture media, column elution buffer or final protein buffer. [71,72] Typical filtration steps are summarized in table 3 [9,69,73]. During purification of a protein in its downstream processing composition, the pH and viscosity of the protein formulation will change in the course of the biopharma process, resulting in a different degree of filter fouling.

3 Theoretical Background

Table 3: Overview of filtration steps in biopharma production [4,9,74,75].

Process stage	Purpose of filtration	Typical type of filter used/nominal pore size
Filtration of cell culture medium	Sterile filtration	Pre-filter/main filter combination with final 0.1 µm sterile filters for mycoplasma retention
Buffer filtration	Sterile filtration	0.2 µm sterile filters
Cell culture harvest	Removal of cells and cell debris	Filter train containing different depth filters and a pre-filter/main filter combination with final 0.2 µm membrane
Protein A eluate filtration	Bioburden reduction	Pre-filter/main filter combination with final 0.2 µm membrane
Column guard filtration	Protection of polishing column/ bioburden reduction	Pre-filter/main filter combination with final 0.2 µm membrane
Virus filtration	Removal of viruses	Virus filters
Ultrafiltration/ diafiltration	Concentration of protein solution/ buffer exchange	Crossflow ultrafilters
Fill and Finish	Sterile filtration	Pre-filter/main filter combination or single filter with 0.2 µm membrane

Filtration steps in biopharma production must fulfill regulatory requirements. Biopharma production needs to satisfy the FDAs “Good Manufacturing Praxis”. Consequently, process filters used in biopharma production must meet defined user requirements, e.g., guidance issued by the FDA on aseptic processing or the PDA (Parenteral Drug Association) Technical Report No. 26, “Sterilizing filtration of Liquids”. [10,71] Validation of filter products by both the manufacturer and the customer entails the following, in particular:

- Demonstrating that the filter meets all requirements of biopharma production; e.g., for example, costumers require proof of scalability for filters used in final filling
- Corroboration that the filter can be sterilized effectively and that the sterilization method does not compromise the filter
- Proof that the filter removes bacteria from the product stream effectively (ASTM 838-05) [76]
- Integrity testing before and after use
- Proving that the filter does not affect and is not affected by the biopharma process stream, e.g., solvent compatibility
- Evidence that the filter has low adsorptive properties and does not bind or remove product or critical excipients, e.g., surfactant from the process stream
- Proof that the filter does not affect the biopharma process stream by release of leachables

3 Theoretical Background

Biopharma production is very expensive due to the complex production process and the high regulatory requirements. As a result, process development activities and filtration trials have to be carried out using a minimum of materials.

3.2.2 Description of Filtration Process and Monitoring of Filter Fouling

In a filtration experiment, a minimum of two parameters have to be monitored; first, the transmembrane pressure of the system; and second, either the cumulative weight m , which is measured by a balance, or the filtrate mass flow m or flow rate J have to be measured. Given then solution density ρ , m can be converted to volume V :

$$V = \frac{m}{\rho} \quad (6)$$

The flow rate J can be calculated by the first derivation of filtration volume:

$$J = \frac{dV}{dt} \quad (7)$$

For comparing different membrane areas A_{mem} , V and J can be normalized using the membrane area, resulting in throughput \tilde{V} and filtration flux J° :

$$\tilde{V} = \frac{V}{A_{mem}} \quad (8)$$

$$J^\circ = \frac{J}{A_{mem}} \quad (9)$$

The flow rate of a fluid through a porous membrane filter can be described with the Darcy-equation, usually written in the following form for filtration:

$$J = \frac{P \cdot A_{mem}}{\eta \cdot R_{tot}^\circ} \quad (10)$$

The Darcy equation is an empirical equation that was later explained as a solution of the Navier-Stokes equation. In the case of low Reynolds-numbers the Darcy equation can be applied and the resistance of the described component is a constant. [77] The viscosity of the filtration media is a required parameter of the model that needs to be measured. For highly concentrated protein filtrations, viscosity is usually above 1 mPa·s. According to Darcy's law membrane resistance R_{tot}° can be calculated using the transmembrane pressure P and the solution viscosity η :

$$R_{tot}^\circ = \frac{P \cdot A_{mem}}{\eta \cdot J} \quad (11)$$

The initial resistance is a filter-specific value, as it is normed by the process parameters (filtration pressure P , filtration flux J), the media properties (viscosity η) and the membrane area A_{mem} . membrane fouling occurs during filtration. Such fouling can be observed as a decline in flux in constant

3 Theoretical Background

pressure filtration and as increase in pressure during constant flow filtration. The membrane resistance rises in both cases due to formation of a fouling layer. Therefore, resistance versus throughput plots ($R_{tot}^o(\tilde{V})$) are well suited for comparing of different membrane areas or process parameters.

3.2.3 Filter Products

Filtration Devices

There is a general trend towards employing single-use equipment, especially single-use filtration units, in biopharma production. This has resulted in an increased usage of filter capsules that can be easily handled and do not require any cleaning or sterilization steps unlike reusable filter housing. [78]

Process filters are usually cartridges containing single or multiple membrane layers and non-woven materials in pleated form. A typical 10" element has a membrane area between 0.6 m – 1 m², depending on the type of pleating and the choice of material (e.g., standard pleating with pre-filter/main filter combination, figure 12a). For mechanical stability, the pleated membrane is incorporated between a core and an outer sleeve (figure 12b), both made of polypropylene and having slightly different structures (figure 12c). The direction of the filtrate flow in a filter cartridge is from the outside of the filter element to the inside.

Cartridges need to be used either in combination with a stainless steel reusable housing or as single-use devices (MaxiCaps® or T-Style MaxiCaps®). 20" and 30" devices are made by stacking 10" elements. Large-scale single-use systems (MaxiCaps® MR) are available as preconfigured and pre-assembled devices in the form of multiple 30" MaxiCaps®, each containing a total membrane area of up to 27 m². [79–81]

3 Theoretical Background

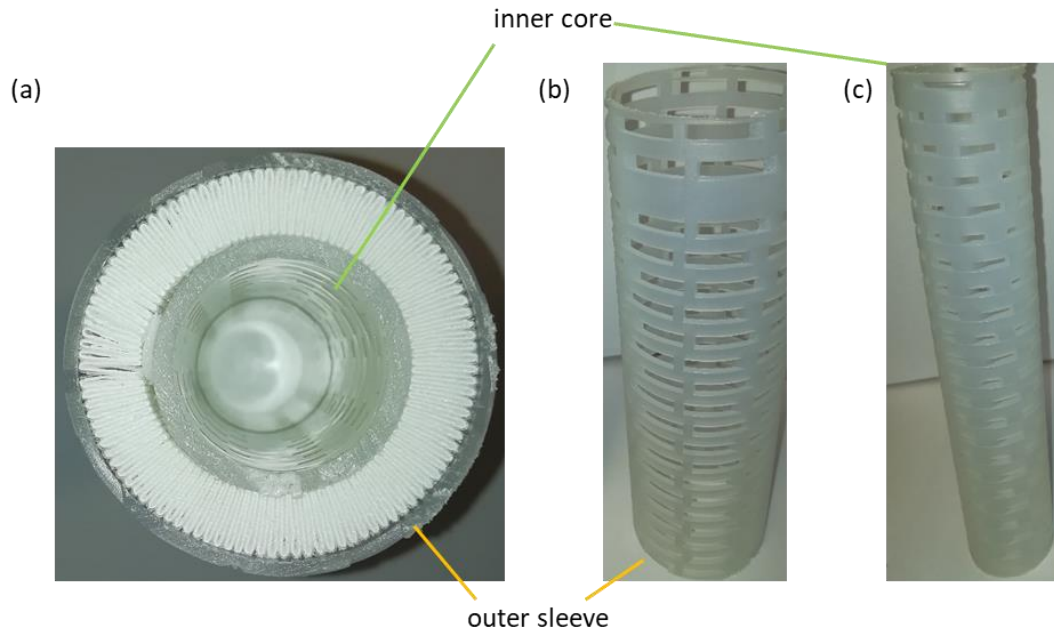


Figure 12: Construction of a cartridge: membrane pleating (a), outer sleeve (b) and inner core (c).

Depending on the setup, different devices with different configurations are manufactured. Filter cartridges are available with various connectors (figure 13). The choice of connector has impact on the fluid resistance of a device as described in section 5.3.1.

For this study, Sartoscales, size 4 capsules, MidiCaps®, MaxiCaps®, T-Style MaxiCaps® and cartridges are used for scaling experiments. Prefiltration for the scaling experiments was performed with MidiCaps®. The various products are shown in figure 13.

3 Theoretical Background

Unparalleled Flexibility

Independently whether you run your filtration process on re-usable stainless steel equipment or a fully single use manufacturing process, Sartorius Stedim Biotech provides you with the right choice of filter designs and configurations for each process requirement. Standard filter cartridges and Mini Cartridges are available in different sizes and with multiple adapter geometries to fit into stainless steel housings. MaxiCaps® in T-Style or "in-line" format and MidiCaps® feature a broad variety of special adapter combinations and filter sizes to allow for a flexible integration into single use filtration systems and to adapt to changing process volumes.

Sartorius Stedim Biotech's filter products for liquids and gases are available starting with SartoScale devices with 17 cm² filtration area up to 3 m² filtration area in Sartopore® Platinum 30" cartridges and MaxiCaps® allowing for reliable Scale-up with consistent materials and design parameters from R&D to commercial manufacturing.

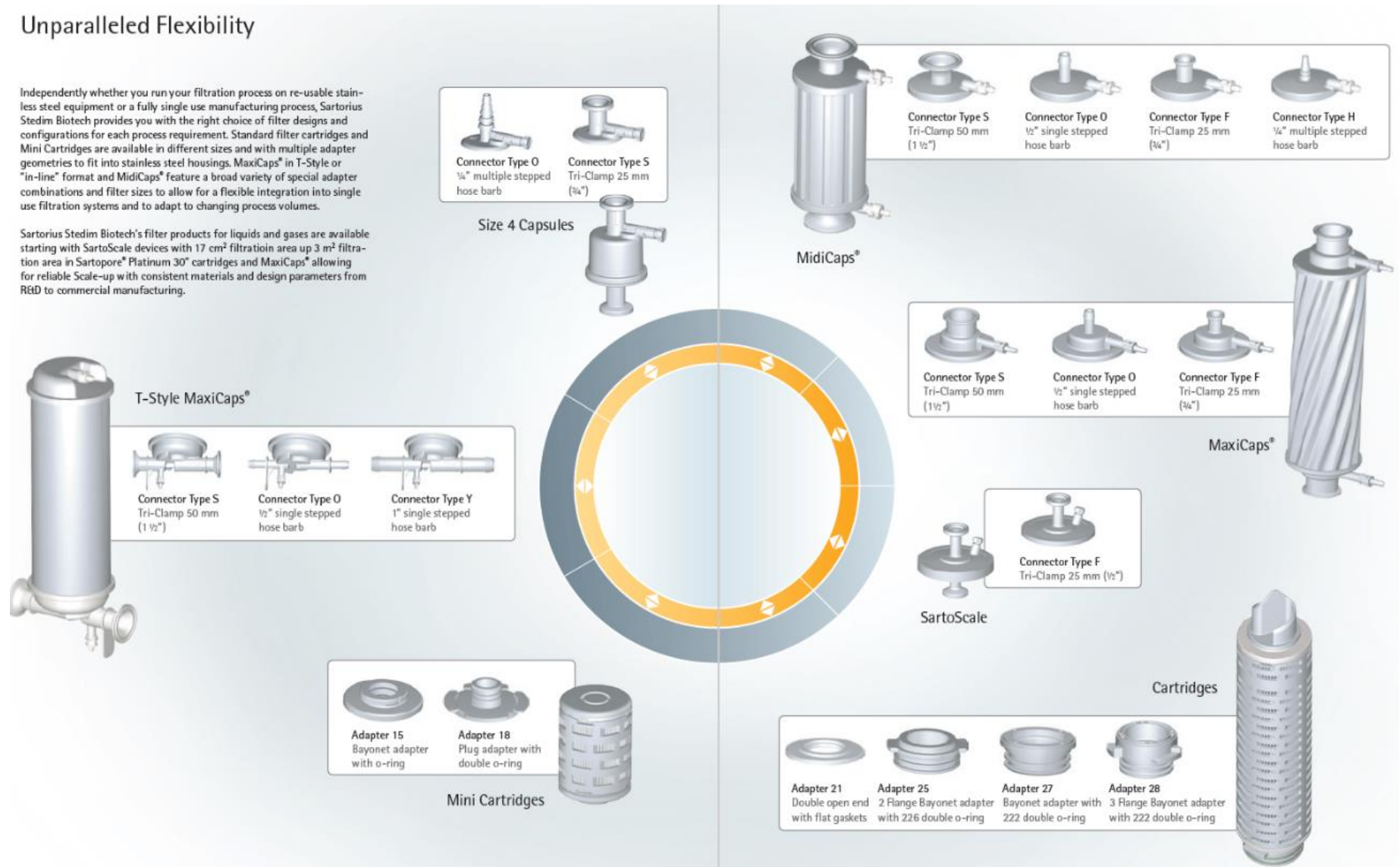


Figure 13: Portfolio of membrane devices manufactured by SSB [82].

Microfilter Membranes – Structure and Performance

Most commercial filter products are membranes with hydrophilic surfaces made of polyether sulfone (PES), polyamide (PA), hydrophilized polyvinylidene fluoride (PVDF_{hyd}) or cellulose acetate (CA). Hydrophobic cellulose nitrate microfilters are also available for diagnostics and microbial applications. These filters have limited wettability. Filters with hydrophilized membrane surfaces, that show better wettability than the untreated materials are also provided, e.g., the Durapore® product line supplied by Millipore, which contains surface-hydrophilized PVDF_{hyd} and Sartopore Platinum® manufactured by SSB with a surface modified PES membrane. Cellulose-based products are available from Asahi (hollow fibers) and from SSB (Hydrosart® membranes). All these membranes carry a negative surface charge in filtration with common biopharma media. [83]

Microfilter membranes are usually produced by phase inversion processes and therefore have sponge-like structures (figure 14a). As a result, pores are not uniform. Usually, a nominal pore size is defined by size specification in the range of 0.1 µm to 0.2 µm for sterile filters. The nominal pore size is large enough to enable most proteins to pass through. However, in reality a pore size distribution can be measured for all of these membrane filters (figure 15). [9,83]

Consequently, fluid flow through a membrane is not uniform either (figure 14b). However, fluid flow through microfilter structures can be satisfactorily modeled by describing the membrane structure as an assembly of cylindrical pores. A pore density of $3 \cdot 10^8$ pores per cm² was used for 0.2 µm membranes in this study for further calculation.

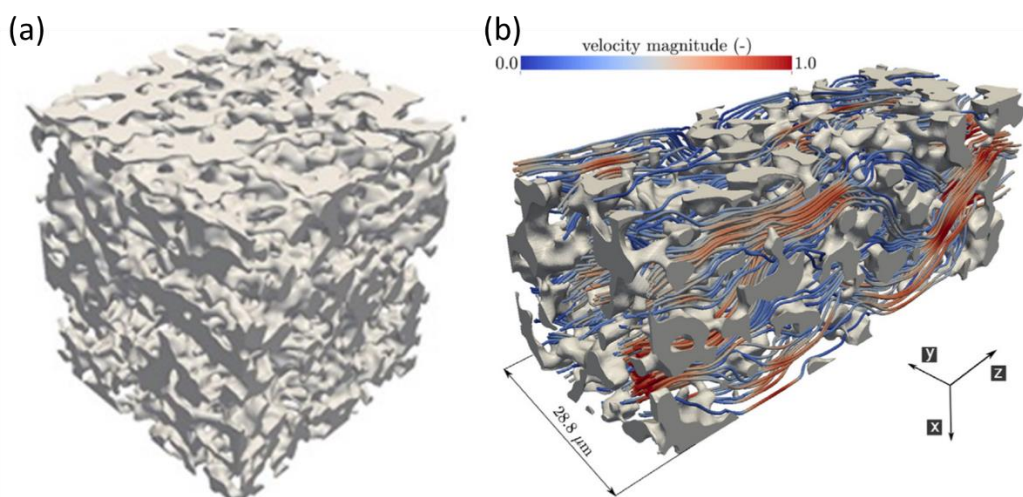


Figure 14: Mathematic modeling of (a) structure of a diagnostic CN membrane and (b) the flow simulation through a membrane [84].

3 Theoretical Background

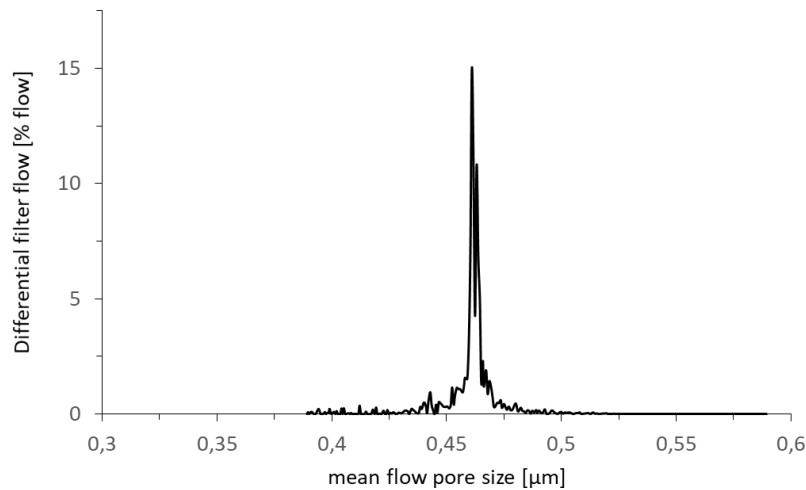


Figure 15: Pore size distribution of a Hydrosart membrane measured by capillary flow porometry (own representation).

Sterile filter membranes, which are used to separate microorganisms from fluid flow are usually specified by a nominal pore size of 0.2 μm . The sterile filtration limit for bacteria retention depends on the pore size of the membrane and also on media properties and experimental conditions. Therefore, this limit needs to be verified by bacteria challenge testing as described later in chapter 3.4.

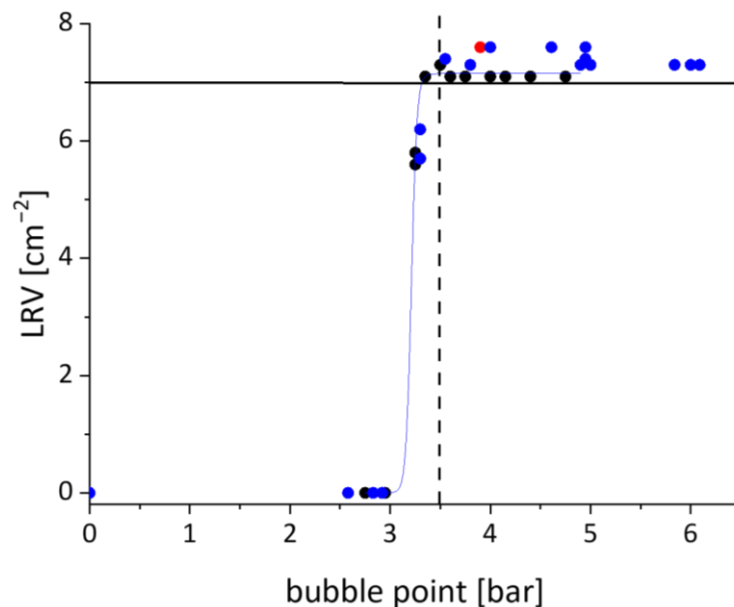


Figure 16: Measurements of bacteria retention due to filtration depending on the bubble point of the membrane; LRV for *Brevundimonas diminuta* for membranes based on cellulose (green), CA (black) and PVDF_{hyd} (red) [83].

Important for filtration performance in general is the permeability of the membrane, which is determined by its total porosity, thickness and effective pore size. Figure 17 shows the typical correlation between the water flow rate and the bubble point of microfilter membranes.

3 Theoretical Background

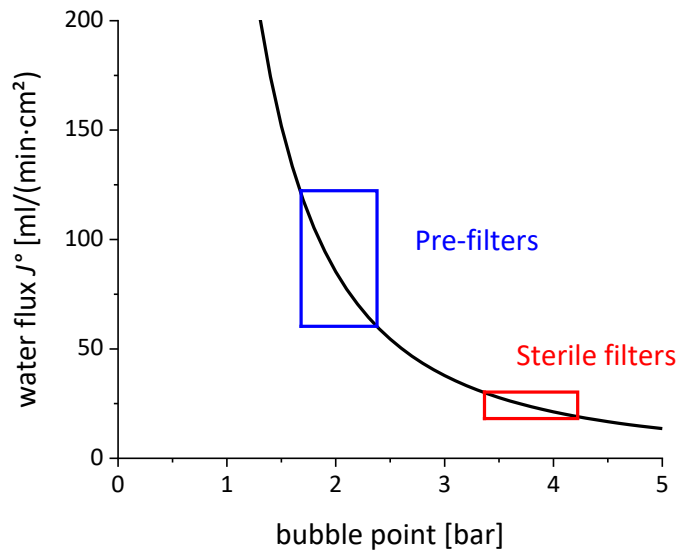


Figure 17: Correlation of water flux at 1 bar and bubble point of typical microfilters (own representation).

A typical 0.2 μm sterile filter membrane has a water flux of approximately 18-25 $\text{ml}/(\text{min}\cdot\text{cm}^2\cdot\text{bar})$. The Reynolds number for the water flux through a membrane can be estimated under the assumption that membrane pores are regarded as straight tubes with an inner diameter d_i and a cross-section area (CSA), using the following equation: [85]

$$Re = \frac{J^\circ \cdot \rho \cdot d_i}{A_{pore} \cdot N \cdot \eta} = \frac{21 \frac{\text{ml}}{\text{min} \cdot \text{cm}^2} \cdot 1 \frac{\text{kg}}{\text{l}} \cdot 0.2 \mu\text{m}}{3 \cdot 10^8 \text{cm}^{-2} \cdot \pi \cdot 0.1^2 \mu\text{m}^2 \cdot 1 \text{mPa} \cdot \text{s}} = 7 \cdot 10^{-3} \ll 1 \quad (12)$$

As can be seen in equation 12 the Reynolds number for fluid flow through membrane pores is quite low, therefore it is laminar.

Membrane characteristics that can have an impact on filter fouling are geometrical aspects (pore size, porosity, and surface topography) and material properties (hydrophilicity and surface charge). For example cellulose is known to have a hydrophilic surface and low adsorption properties, whereas adsorption is stronger for hydrophobic surfaces. [17,86]

Filtration of Protein Formulations in Production Scale – Special Aspects

Filtration steps play an important role in the proper removal of microorganisms and particulate contaminants, having crucial impact on the smooth progress of the entire biopharma process, the product yield and quality [71,87,88]. Biopharma process engineering must ensure maximum product yield and process consistency by the correct choice of operating conditions and equipment. To this end, the FDA has strengthened regulatory measures to improve biopharma process consistency. [71] As biopharma formulations are quite expensive, filtration equipment and processes need to be properly sized to avoid product loss.

3 Theoretical Background

Challenges concerning the filtration of protein formulations are related to their solution properties. As described in chapter 3.1.2, protein formulations are colloidal solutions with limited thermodynamic stability. Changes in formulation that involve pH, salt concentration, and surfactant content might affect aggregation and filter fouling. A good example of this is the pH, which is a process parameter that needs to be as far as possible from the isoelectric point of the protein without the risk of damaging the protein. [89]

The viscosity of protein formulations can vary between 1 mPa·s for diluted systems and 100 mPa·s for full therapeutic formulations in final fill filtration. The viscosity of the formulation has impact on the filtration flow across the filter. Highly concentrated protein solutions are fluids with non-Newtonian behavior and show shear-thinning behavior. [4,90]

In designing a biopharma process, the overall process needs to be considered, not just an isolated filtration step. A filtration process is always part of a sequential arrangement, which determines the necessary process parameters. Flow rates, for example, have to be high enough to keep up with filling machines, [91] to provide buffer for column chromatography or to evade enzymatic degradation [92]. Furthermore, it is well known that process conditions have an impact on filter fouling or product quality.

Most biopharma filtration steps are designed for constant flow mode, as this mode perfectly matches the general biopharma process flow [88,93,94]. Filter fouling is usually lower for constant flow filtration [95]. However, there are also production processes that use the constant pressure mode or intermittent-flow mode [9].

Temperature, transmembrane pressure and thus the shear rate within the membrane pores can be adjusted [94]. A high flow rate can cause protein aggregation due to shear stress. The shear rate is especially important if non-Newtonian behavior occurs, a common phenomenon in monoclonal antibody formulations. [96] The critical values for shear rates are dependent on the protein, as described in section 3.1.3. A very low flow rate can possibly increase filter fouling due to a long interaction time between protein and membrane surface [4]. Thermal labile products are usually manufactured between 2 °C and 8 °C [97].

Typical filtration flow rates depend on the filtration step. For bioburden reduction and sterile filtration typical filtration rates are 3 000-8 000 l/(m²·h). Concentrated bulk drug substance is filtered at 250-1 000 l/(m²·h), and sterile filtration is performed with a filtration rate between 60 and 200 l/(m²·h), depending on the filling line. Process design must also consider additional processes revolving around filtration, such as sterilization, sterile connection and integrity testing.

Final Fill Filtration

The last steps for manufacturing a biopharmaceutical product are formulation of the drug, filling in a primary packaging and, in some cases, lyophilization, depending on the properties of the active compounds and the administration route [67]. Sterile filtration for final fill is typically performed in an isolator with two sterile filters connected in series to provide microbial retention and, ultimately, additional safety. The filtration flux is between 60 l/(m²·h) and 200 l/(m²·h), as determined by the filling machine. Of crucial importance in this sterilization step is the reliability of bacteria retention and the impact of the process on product quality. [98] FDA regulations strongly suggest redundant sterile filtration for additional safety [71].

The constant flow mode works best in the Fill and Finish process for the filtration of protein formulations. It can be combined directly in a process with a filling line. The advantage is that no sterile holding tank needs to be used between the filter and the filling needles. In this mode of operation it is important that the complete production batch is filtered continuously and the line is not interrupted. The constant pressure mode is used in combination with a sterile holding tank, from which liquid is drawn for the filling operation. The intermittent-flow mode is also used in combination with a holding tank. In this case, filtration is switched on and off, as needed. [9]

Several preconfigured setups are available for filtration and filling of a biopharmaceutical drug. These include Pharmatec Filtration (Bosch Packaging Technology GmbH) equipment for up to 10 000 l/h [99]. Filling lines are supplied by e.g., Bosch Automotive Solutions (FLC 3000, up to 36 000 units/h [100]) and Snowbell Machines [101] (up to 18 000 vials/h [102]). Figure 18 depicts a typical Fill and Finish process. Here, a holding tank is used to supply the filling needles.

3 Theoretical Background

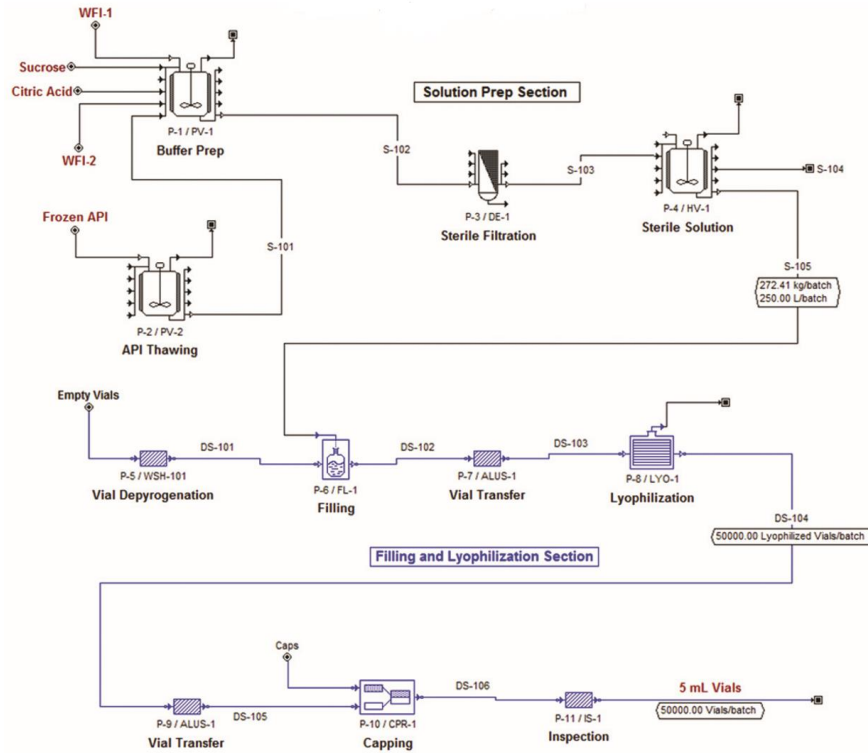


Figure 18: Process flow diagram of a Fill and Finish process for production of a lyophilized intermediate [67].

Filter Fouling in Protein Filtration

Filter fouling in protein filtration was carefully studied in recent years. The findings of these studies show that filter fouling depends on the location of the production step in the downstream process. Filter fouling is usually not an issue for diluted solutions, but a severe problem for clarification by filtration, filtration of bulk drug substance and final fill filtration, depending on concentration of solution, particle load and process conditions. [88,103,104]

According to most reports in the literature available, filter fouling usually occurs in several successive steps at different rates; the first fouling phase is characterized by a slow increase of the transmembrane pressure (in constant flow filtration), whereas in the second phase, fouling is more rapid [89,94,105]. A study on fouling of a microfiltration membrane, measured in constant flux mode revealed three fouling stages during filtration of a bovine serum albumin (BSA) formulation (figure 19). The mechanism of fouling suggested by the study is that in the first stage, the membrane retains aggregates by its sieving effect. As a result, monomers deposit on the aggregates as revealed by washing the membranes. Still, transmembrane pressure is higher than the initial value; this difference can be attributed to irreversible fouling with aggregates. The protein fouling layer was visualized at the membrane surface (figure 20), which supports this aggregate theory.

3 Theoretical Background

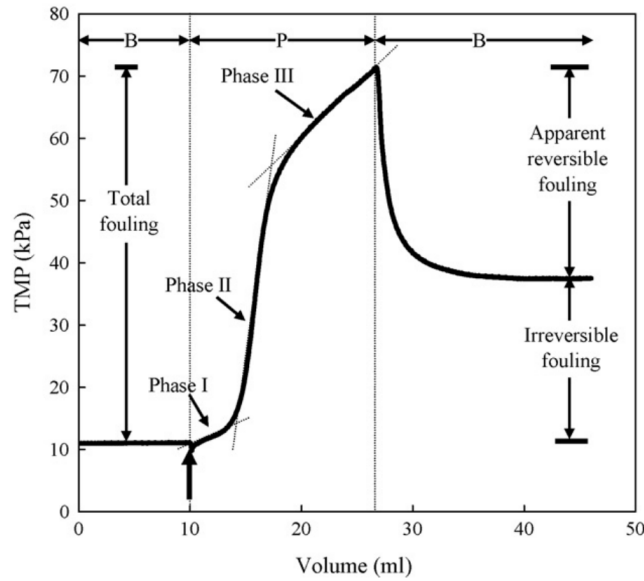


Figure 19: Presentation of pressure increase versus throughput during constant flow filtration of a BSA formulation (10 g/l) through a CA membrane (0.45 μm nominal pore size) at a flow rate of 5 ml/(min \cdot cm 2) [94].

Confocal scanning laser microscopy can be used to visualize the fouling layer. Figure 20 shows an image of a cross section of a membrane after filtration of a BSA formulation. It can be concluded that membrane fouling does not occur evenly across the whole membrane; instead, a thin layer is formed within the first 10 μm . [94]

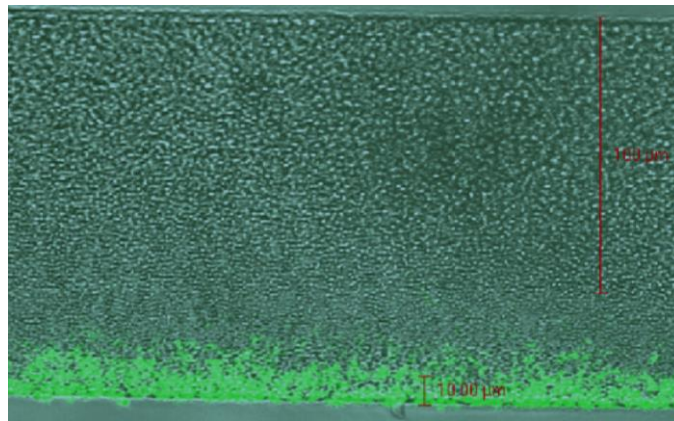


Figure 20: Fluorescent image of a membrane cross-section as measured by confocal laser scanning microscopy (CLS) after filtration of a BSA-formulation; upstream side with BSA fouling layer on the bottom [94].

3.3 Scale-Up of Microfiltration from Lab-Scale to Process-Scale Filtration

Scale-up is an engineering approach in process filtration for the selection of suitable process filtration equipment and filter devices as well as of operating conditions for filtration of a given fluid volume. For filtration scale-up, small-scale test filtration runs are conducted to evaluate the required membrane material, membrane area and the best process conditions. The necessary membrane area is determined by the ratio of optimal membrane area to volume, without the risk of filter blockage or negative impacts on the quality of the drug. [97]

Experimentally, the filter capacity for filtration of a given fluid phase is determined by small-scale filtration trials with the area A_{mem_SS} , usually on the basis of constant pressure filtration trials. [106] For these small-scale experiments, scaling devices with a minimal membrane area are available, such as Sartoscale 25 manufactured by SSB, [107] Optiscales® provided by Merck KGaA [106] or the Mini Kleenpak™ products supplied by Pall Corporation [108].

In a lab-scale filtration, the pressure, filtrate volume and time are recorded. Resulting experimental data are displayed usually in a volume-versus-time plot. For scale-up, the filtrate volume until complete filter blocking V_{final} is calculated. The necessary membrane area A_{mem_LS} for filtration of a batch size of the volume V_{batch} can be calculated by the following equation using V_{final} and A_{mem_SS} :

$$A_{mem_LS} = SF \cdot \frac{V_{batch}}{V_{final}} \cdot A_{mem_SS} \quad (13)$$

Usually the risk of underestimating the filter area is minimized by the introduction of a safety factor, SF . The safety factor is necessary to compensate for the uncertainty usually related to scale-up processes. For example, membranes show a variability of properties, and the filtration device has a variance in its geometric dimensions. This is especially the case for small scaling devices with a filter area of some square centimeters. Also, there might be a variability of process conditions [104,109]. Safety factors are given with 0.75-0.9 [110], 1.1-2.5 [111], 1.3-2 [34], 1.5 [72] or 2 [95], depending on the process (constant flow or constant pressure) [110,112] or on the blocking mechanism. [110] The importance of safety factors for biopharma process development is reported by Lutz et al. [111].

Customers in the biopharmaceutical industry usually require up-scaling trials with a minimum amount of media as the respective formulations are quite expensive and thermodynamically unstable. Therefore, small-scale trials must be reliable, because they are used to evaluate the impact on product quality, and they are the basis for a large-scale filtration process. Modeling of filtration processes can help to minimize the number of necessary scaling experiments.

3 Theoretical Background

Modeling of filtration curves usually is performed on the basis of pore blocking models. V_{final} can be extrapolated by fitting a pore blocking model to the experimental filtration data [113]. Modeling of filter fouling based on pore blocking models has a history in filtration technology that began in the 1930s. Usually four blocking models are employed to describe filter fouling: complete blocking, standard blocking, intermediate blocking, and cake filtration. Schematic drawings of the blocking models are shown in figure 21.

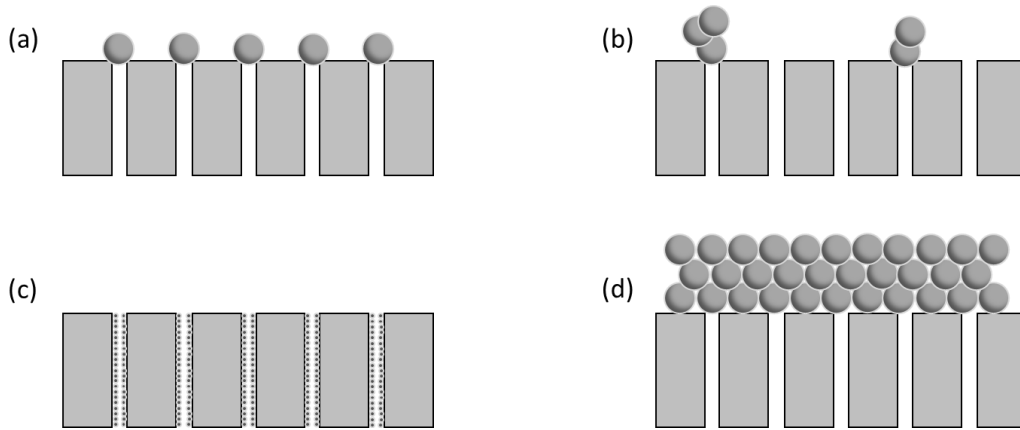


Figure 21: Schematic diagrams of blocking models. Complete pore blocking (a), intermediate blocking (b), standard blocking (c) and cake filtration (d) [113].

The general blocking law for all four cases is:

$$\frac{d^2t}{dV^2} = k_x \cdot \left(\frac{dt}{dV}\right)^n \quad (14)$$

This blocking law uses different exponents n for the type of filter blockage: $n = 2$ for complete blocking, $n = 1.5$ for standard blocking, $n = 1$ for intermediate blocking and $n = 0$ for cake filtration. All models assume that membranes have cylindrical pores with equal pore diameters and pore lengths. The complete pore blocking and intermediate blocking model assume that particle diameters are larger than the pore diameters. In the complete pore blocking model, every single particle blocks one pore. The intermediate blocking law considers that particles block pores or deposit on other particles. Therefore the blocking rate is proportional to the number of open pores. The standard blocking law was developed for membrane fouling caused by particles smaller than the pore size. In this case, particles deposit on the pore walls; hence, the pore diameter gradually decreases. For simplicity, it is assumed that the pore volume decreases proportionally to the filtrate volume. In the case of cake filtration, particle diameters are larger than the pore diameters and, during filtration, particles deposit on the membrane surface, leading to the build-up of a cake. This cake can be regarded as a granular bed and causes an additional resistance. [113]

The theoretical background of and the basis for the calculation of the blocking models are described in a review article by Iritani *et al.* [113]. The blocking models were developed for ideal fluids

3 Theoretical Background

with a narrow particle size distribution flowing through ideal membranes with cylindrical pores. Neither membranes nor fluids fulfill these model requirements in industrial process filtration. Microfilter membranes exhibit a sponge like porous structure rather than cylindrical pores [72,113]. Most industrial process media, especially biopharma formulations, are colloidal solutions with limited thermodynamic stability as described above [5,38,114]. Dispersed particles are not necessarily spherical and undergo interactions between one other and with the membrane surface. Moreover, the blocking mechanism can change during filtration; e.g., at the beginning, small particles deposit within the membrane pores until the pores become so tight that they are plugged by a single particle. Therefore, the predictability of the use of single blocking models for up-scaling and filter sizing is limited and up-scaling results based on these models deviate significantly. [110,112,115] The predictability can be improved by a certain degree by combining several blocking models. The combination of blocking models extends the quantity of parameters that can be modified, resulting in generated data that are closer to actual experimental measurements. [116,117]

An example of the approach mentioned for up-scaling of filtration processes, and a set of experiments and working methods is given by Rajniak *et al.* [110] for redundant sterilizing filtration of an active pharmaceutical ingredient solution using a PVDF_{hyd} membrane filter with scaling from a 47 mm filter disc to pilot and production scale [118]. Different blocking models and combinations were applied for curve fitting. The calculated capacities were usually lower than the experimentally determined values and were consequently regarded as worst-case scenario. An extra safety factor of 2 was included due to large batch-to-batch-variation. Furthermore, the article gives an overview about resistances of filtration equipment in dependence on scale and details of construction (table 4). Finally, it was stated that sterilizing filtration is not a linearly scalable unit operation because the pressure-normalized initial flux differs among the scaling devices used. The initial flux decreases as the filter area increases due to the occurrence of additional flow resistances related to device construction, tubing and fittings [110]. Other reviews about experimental procedure, theoretical approaches, and aspects to consider for conducting microfiltration up-scaling studies are given in the literature [109,110,119,120]. The need to avoid setup restrictions is even mentioned in regulatory guidelines [10].

Giglia's scaling approach for process setups calculates filters-in-series, combines multiple blocking models and considers batch-to-batch variations of the membrane material [104,119,120]. To improve the predictability and to avoid the use of blocking laws, it is generally recommended to perform calculations based on small-scale filtration trials runs until nearly complete membrane blockage occurs. This is a problem if only a limited amount of test solution is available.

3 Theoretical Background

For up-scaling, it has to be considered that biopharma formulations usually show process-dependent filter fouling. Therefore the small-scale trials should be performed in the same mode as the process trials, usually at a constant flow rate.

There is a strong trend in recent literature to use flow rate and resistance to monitor filtration processes and filter fouling, as the filtration flow rate can be restricted by the filtration setup. Resistances of components of a filtration setup are given in table 4. [110,113]

Table 4: Resistances of typical components of a filtration setup [110].

Part	Inner diameter [mm]	Resistance [10^{10} m^{-1}]	CSA [m^2]	Resistance/CSA [10^{-12} m^{-3}]
Filter disc	-	6.18	0.0013	35.35
Millipak 20 hose barb	6 (hose barb)	7.00	0.01	7.00
Millipak 60 hose barb	6 (hose barb)	8.29	0.03	2.76
Millipak 60 Sanitary Flange	19	6.87	0.03	2.29
1 m straight tube	6	-	-	0.031
1 m straight tube	19	-	-	0.0003

The resistance can be calculated by the Darcy equation (section 3.2.2). The viscosity of a filtration fluid is the only additional value required to calculate the membrane resistance on top of the parameter set encompassing the filtration time, flux (or volume) and differential pressure. The approach has many advantages: Monitoring of flow rate and resistance versus throughput (filtrate volume per effective membrane area) relates both change of flow rate and the occurrence of fouling processes to the passage of contaminants through the filter. Moreover, it provides insights into the process dependency of filter fouling, which is quite strong for biopharma process filtration. The change in the initial water flux with device size can be visualized. The magnitude of the resistance of the membrane and the filter housing can be quantified, which enables experimental issues to be identified, e.g., reduction of effective filter area by insufficient wetting or inclusion of air within a system. Finally, filter fouling can be modeled without the use of blocking laws.

3.4 Validation of Sterile Filtration with *Brevundimonas diminuta*

The validation of sterile filtration is described in the corresponding ASTM Standard F838-05 and the PDA Technical Report No. 26. Sterile filters have a rated pore size of 0.2 μm . For validation *Brevundimonas diminuta* (ATCC 19146) is used as a model organism due to its small size (0.3 μm mean diameter). [71,76]

Membrane manufacturers qualify their pore sizes according to this ASTM Standard as well. To validate sterile filtration, it has to be shown that *B. diminuta* is viable in the process media, the membrane can retain a challenge concentration of at least 10^7 organisms/ cm^2 and the filtrate is sterile (bacteria challenge test, BCT). As a positive control, a filtration run with a 0.45 μm membrane has to be performed, in this case, bacteria breakthrough must be observed.

For a validated process, an IT test (integrity test) has to be performed before and after the sterile filtration step in order to confirm the integrity of the filter device. Here the first step is wetting the membrane. An IT is usually performed before assembly of the devices. After assembly, they are IT tested again, but this time with the filtration product and no more flushing is required. To avoid flushing the membrane after the process, an IT test is performed with product solution as well. The measured bubble points usually subside with product solution as the membrane bubble point correlates to the surface tension of the test medium; for biopharma media, the surface tension of the medium is lower compared to water due to surfactants or proteins. [121]

According to the PDA Report [10] a BCT has to be performed under worst-case process conditions (filtration time, filtration flow rate, process temperature, device bubble point, etc.). For every given process the worst-case conditions need to be defined, but there is no general definition of a high-challenge BCT.

Organisms can be retained by sieve retention or adsorption. Therefore changes in the bacteria size or a change in the bacteria-membrane-interactions will affect bacteria retention. This retention efficiency is largely influenced by the formulation composition and its pH. For example, when non-ionic surfactants attach to the membrane and bacteria, mutual repulsion occurs and adsorption declines. High salt concentrations cause an osmotic pressure difference. Bacteria lose their cell water through their membrane and shrink. Divalent cations additionally have an effect on the binding capacity of the cell surface. As the concentration of divalent cations increases, the negative charge density at the cell surface, and, therefore, bacteria retention, decreases. Assimilable carbon also has an impact on bacteria size. Without sufficient nutrient levels, bacteria enlarge their surface by reduction of cell size. This is a disadvantage for sieve retention, but beneficial for adsorption. [122,123]

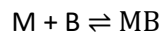
3 Theoretical Background

On the process side the influences of filtration pressure, filtrate flow and process temperature have to be regarded. A higher filtration pressure results in higher filtration fluxes; therefore, process time is shorter. However, in the case of adsorptive retention this fact is not beneficial; a high flow rate is therefore seen as worst-case condition. The influence of temperature is not linear. A rise in temperature lowers the viscosity; hence, filtration flow increases. Additionally, bacteria reproduces more easily. Yet if temperatures are too high bacteria such as *B. diminuta* lose their viability. A higher viscosity lowers Brownian motion; but it also reduces filtrate flow. So the process influence on bacterial retention can only be regarded as a combination of temperature, pressure and filtrate flow. [10,122,123]

3.5 Protein Adsorption

3.5.1 Physicochemical Basics of Protein Adsorption

Adsorption processes of protein molecules are usually described using the Langmuir adsorption model [124,125]. The Langmuir adsorption isotherm was originally described for adsorption of gases. The theory assumes that only a monomolecular layer adsorbs reversibly to a homogeneous and smooth surface with equivalent binding sites (B). The molecules (M) do not interact with each other. [125]



The surface coverage θ can be described by the partial pressure of the respective gas, in an aqueous solution by the solute concentration c , and a constant K .

$$\theta = \frac{K \cdot c}{1 + K \cdot c} \quad (15)$$

The constant K is defined by the rate constant k_{ad} for the adsorption and the rate constant k_{de} for the desorption step:

$$K = \frac{k_{ad}}{k_{de}} \quad (16)$$

In reality, proteins do not fulfill the assumptions of the Langmuir theory: they are large macromolecules that interact with one other, can aggregate, interact with multiple binding sites on the surface, and change their conformation; therefore, the Langmuir model has to be expanded. [125] In literature on proteins, the term adsorption and the Langmuir isotherm are used for all kinds of surface reactions, even those with irreversibly bound protein [56,126–128].

For adsorption processes in aqueous solution, it is important to know the transport rate from the bulk solution to the interface. Important mechanisms for this transport are diffusion, described by the Brownian equation, thermal convection, convective transport, and coupled transport mechanisms. [129] Due to adsorption, protein concentration in the boundary layer decreases and a concentration gradient is generated. The concentration gradient drives the diffusion towards the interface as is stated in Fick's law of diffusion. [43] Normally, the diffusion-controlled boundary layer has a thickness of a few microns, but the pore diameter of sterilizing-grade membrane is in the submicron range, so diffusion can be neglected.

3.5.2 Adsorption Kinetics in Protein Filtration

For the description of protein adsorption kinetics, many different models are available [20,129]. Most models expand the classical Langmuir model by one or more reactions that can

3 Theoretical Background

occur at the interface (conformational changes or flocculation). This can be summarized with the two state model that can be used to describe adsorption processes including conformational changes, dimerization processes or denaturation (figure 22, for conformational changes). [130]

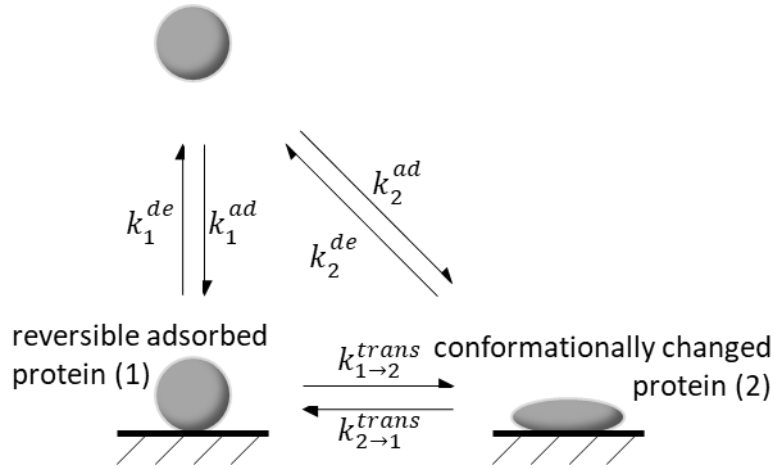


Figure 22: Schematic presentation of the two-state model for protein adsorption [130].

To describe the equilibrium at the interface, an equation for each state is needed.

$$\frac{d\theta_1}{dt} = k_1^{ad} \cdot c \cdot \Phi(\theta) - k_1^{de} \cdot \theta_1 - k_{1 \rightarrow 2}^{trans} \cdot \theta_1 + k_{2 \rightarrow 1}^{trans} \cdot \theta_2 \quad (17)$$

$$\frac{d\theta_2}{dt} = k_2^{ad} \cdot c \cdot \Phi(\theta) - k_2^{de} \cdot \theta_2 - k_{2 \rightarrow 1}^{trans} \cdot \theta_2 + k_{1 \rightarrow 2}^{trans} \cdot \theta_1 \quad (18)$$

The surface coverage of the respective state are calculated by the adsorption and desorption rate k_n^{ad} and k_n^{de} of state 1 and 2, the concentration in the bulk solution and the respective surface coverages θ_n of state 1 and 2. The transition of state 1 and 2 and of state 2 to state 1 are included by the rate constants $k_{1 \rightarrow 2}^{trans}$ and $k_{2 \rightarrow 1}^{trans}$. $\Phi(\theta)$ is called the available surface function and part of the Random Sequential Adsorption (RSA) model (equation 19). [20]

$$\Phi(\theta) = \frac{\left(1 - \frac{\theta}{\theta_j}\right)^3}{1 - 0.812 \cdot \left(\frac{\theta}{\theta_j}\right) + 0.2336 \cdot \left(\frac{\theta}{\theta_j}\right)^2 + 0.0845 \cdot \left(\frac{\theta}{\theta_j}\right)^3} \quad (19)$$

It accounts to the fact that proteins can only adsorb to surface sites that are not occupied by another protein. If a protein approaches a site that is (partially) occupied by another protein, it is rejected and does not adsorb. Adsorption is assumed to be an irreversible process, and the molecules cannot diffuse on the surface. [131] In case of protein-protein adsorption this function might have to be replaced.

For a complete mechanistic understanding, all the different adsorption processes with their different adsorption and desorption rates should be considered (e.g., monomers, oligomers, different

3 Theoretical Background

orientation). However, this is not possible with the available equipment; therefore it was decided for this study that only the macroscopic effect is to be described and not the single elementary reactions. All the adsorption and desorption reactions are described by their total; furthermore it is examined how much protein is irreversibly bound to the interface due to multiple side adsorption or conformational changes. By turning state 2 to an irreversible adsorbed protein as presented in figure 23, equations 17 and 18 are simplified:

$$\frac{d\theta_1}{dt} = k_1^{ad} \cdot c \cdot \Phi_1(\theta) - k_1^{de} \cdot \theta_1 - k_{1 \rightarrow 2}^{trans} \cdot \theta_1 \quad (20)$$

$$\frac{d\theta_2}{dt} = k_2^{ad} \cdot c \cdot \Phi_2(\theta) + k_{1 \rightarrow 2}^{trans} \cdot \theta_1 \quad (21)$$

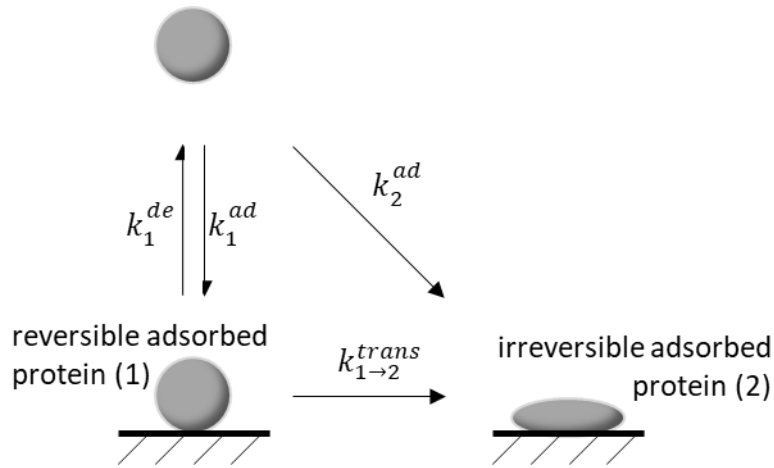


Figure 23: Schematic protein adsorption model: reversible adsorption and irreversible adsorption due to conformational changes.

3.6 Therapeutic Liposome Formulation

3.6.1 Chemical and Physical Aspects of Liposomes

Liposomes are spherical vesicles formed by lipid molecules. Lipids are amphiphilic molecules with a hydrophilic head group and a hydrophobic tail. The hydrophilic part can be anionic, cationic or neutral. In contrast to common surfactants, the hydrophobic part of the molecule is sterically larger; as a consequence no micelles but more complex structures are formed. [132]

The simplest liposome in a solvent is a hollow sphere made out of double layers with the solvent molecules on the inside of the sphere as well. In aqueous solution the hydrophilic part of the molecules are directed to the surfaces, in non-polar solvent the hydrophobic tails. Liposomes are classified in terms of their size and the number of double layers, called lamellarity. Small (20-100 nm), large (0.1-1 μm) and giant vesicles (up to 50 μm) are differentiated; the vesicles can be either uni-lamellar or multi-lamellar as presented in figure 24. [8,133,134]

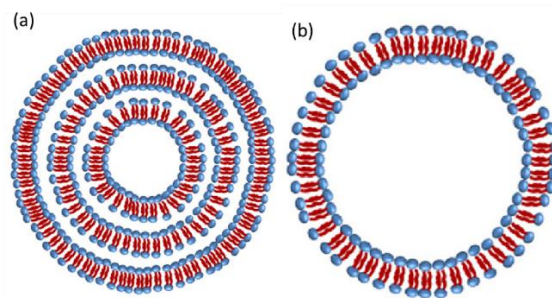


Figure 24: Lamellarity of liposomes. Multi-lamellar liposome (a) and uni-lamellar liposome (b) [132].

Liposome are typically mixtures of phosphatidylcholines or ethanolamines, e.g., DSPC (Distearylphosphatidylcholine), DOPC (Dioleoylphosphatidylcholine), DOPE (Dioleoylphosphatidylethanolamine) and cholesterol (figure 25) [135].

3 Theoretical Background

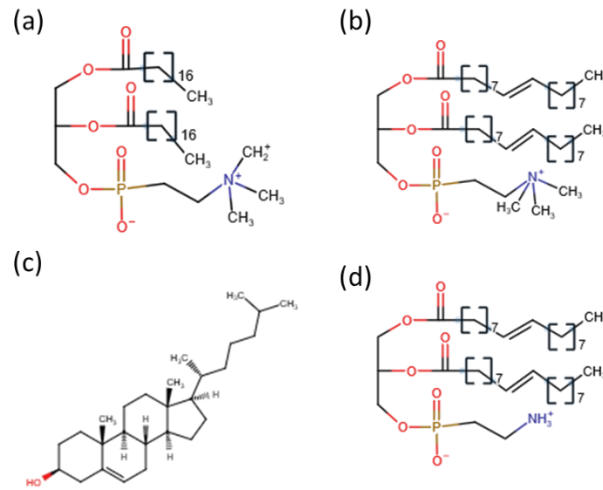


Figure 25: Chemical structures of DSPC (a), DOPC (b), cholesterol (c), and DOPE (d) [135,136].

On heating, lipids undergo one or more intermediate liquid-crystalline or mesomorphic changes, for example the gel to liquid-crystalline phase transition of DSPC. It can be shown that DPPC undergoes several endothermic transitions on heating, which have an effect on the mobility of the polar head groups (subtransition and pretransition of the gel to liquid-crystalline phase transition) or the order of the hydrocarbon chains (gel to liquid-crystalline phase transition, figure 26). These transitions can be measured by DSC. [137,138]

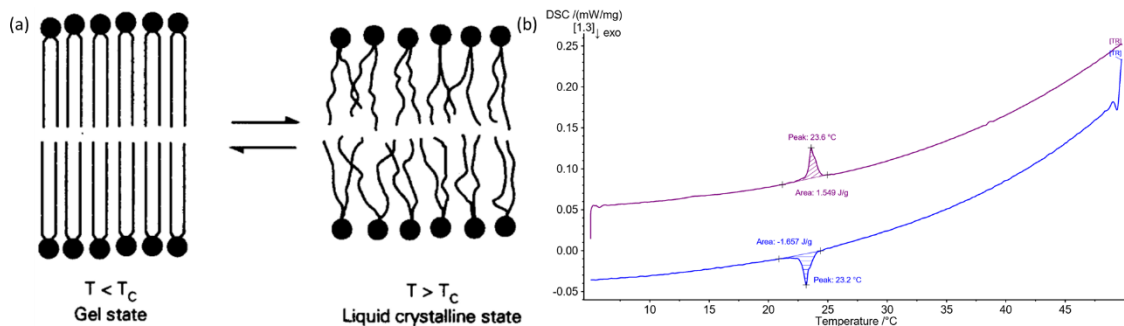


Figure 26: Liposomal solutions: (a) schematic presentation of the difference between gel state and liquid crystalline state [139]; (b) DSC thermogram of the thermal transition of 1,2-dimyristoyl-*sn*-glycero-3-phosphocholine in water. Heating curve (red), cooling curve (blue) (own representation).

For sterile filtration of liposomes it is essential to keep the temperature above the transition temperature of a liposome [138,140–142]. The transition temperature can be lowered by shorter alkyl chains, unsaturated alkyl chains or by adding cholesterol to a lipid composition [137,138]. Sterile filtration of liposomes can be challenging in terms of bacterial retention. Here usually either narrow 0.2 μm or 0.1 μm membranes are necessary to ensure complete bacterial retention. A higher throughput is achieved by applying a high pressure (at least 2 bar) or a pressure ramp, which is more difficult to control. [123]

3.6.2 Application of Liposome Formulation

In 2017 15 Liposome drugs are used in the market for antifungal and antitumor purposes, Hepatitis A and Influenza. The entrapment of drugs (for example proteins) in liposomes is used to enhance the antibacterial activity, pharmacokinetic properties and to reduce toxic side effects. Hydrophilic drugs can be entrapped within the encapsulated water compartment, hydrophobic drugs within the liposome bilayer. Proteins, such as γ -globulin, can be used to modify the surface of liposomes; that way they can be directed to specific targets (immunoliposomes). [8,140,143–145]

Typically liposomal formulations are made of several lipids and cholesterol, encapsulating the active ingredient in a buffer formulation. The liposome content varies, for example vials with 50 mg active ingredient Depocyt® contain 60 mg liposomes, DanuoXome® 870 mg liposomes. [145,146]

4 Materials and Methods

4.1 Materials and Formulations for Filtration Trials

Table 5 gives an overview of the chemicals used for the filtration trials. PS80 has been used for the adsorption measurements, Tween® 80 (PS80 containing by-products) for the filtration trials. Table 6 summarizes the composition of standardized protein formulations used for filtration trials.

Table 5: Overview of chemicals used for the experiments

Chemical	Supplier	Order number
BSA	Kraeber & Co Kg	04180 10900
γ-Globulin	Merck KGaA	G5009
Alexa Fluor™ 488 NHS-Ester	Thermo Scientific	A20100
Alexa Fluor™ 594 Cadaverine	Thermo Scientific	A30678
PS80	NOF Corporation	Polysorbate 80 (HX2)™
Tween® 80	AppliChem GmbH	A4743
Latex-Beads	Agilent Technologies, Inc.	PL6001

Table 6: Composition of protein formulations

#	Protein	Target concentration [g/l]	Concentration UV [g/l]	Buffer	pH	Additives	Surfactant	Viscosity [cP]
1	BSA	250	225	100 mM NaH ₂ PO ₄ 100 mM Na ₂ SO ₄	6.9	1 w/w% Trehalose 0.1 w/w% NaCl	0.5 % Tween® 80	4
2		75	-	Formulation as above, diluted with 65% glycerol				40
3	γ-globulin	100	98	75 mM His	6.4	-	0.5 % Tween® 80	2

The protein formulations are prepared according to internal SOPs by SSB (standard operating procedure, hereafter called “QID”, quality information documents). QID 2461655 describes the preparation of the protein formulations, the compositions of the formulations are given in the QIDs

4 Materials and Methods

2461916 (formulation 1) [147], 2461918 (formulation 2) [148] and 2461920 (formulation 3) [149]. The particulate formulation, containing a 0.1 w/w% mixture of Caro-Kaffee and Ovomaltine, is prepared according to the QID 2284143 [150].

The preparation of protein formulations can be separated in buffer preparation (dissolving of the buffer salts, pH adjustment and addition of all excipients except glycerol), addition of the lyophilized protein by stirring with a ViscoJet® and for formulation 2 finally the addition of glycerol. In order to remove aggregates every formulation was pre-filtered each day with a Sartoclean CA (0.45 µm) before use. A more detailed description is given in section 5.1.2.

For filtration of liposomal solutions two formulations were provided. One formulation was purchased from Polymun, a supplier for the biopharma industry (liposomal formulation 1). This formulation is according to the manufacturer a challenge for sterile filtration and was used for the filtration trials diluted with buffer to 10 g/l. Another formulation was prepared by SSB R&D (liposomal formulation 2). For comparison with spherical, uncharged particles Latex-beads with a particle size distribution around 100 nm were purchased from Agilent. All formulations are summarized in table 7.

Table 7: Overview of liposomal formulations

Name	Supplier	Formulation	Particle size distribution	Transition temperature (according to filtration trials)	Viscosity [mPa·s]
Liposomal formulation 1	Polymun	47.6 g/l HSPC 2.6 g/l cholesterol 10 mM HEPES 9% sucrose	≈ 100 nm	20 °C-40 °C	4.8
Liposomal formulation 2	SSB R&D-formulation	114 g/l solid content	≈ 100 nm	< 20 °C	1.2
Formulation 3	Agilent	10 g/l Latex-beads	≈ 100 nm	N/A	1

4.2 Characterization of Formulations

4.2.1 BSA and γ -Globulin Formulations

UV-Vis

The concentration of the proteins in the respective formulation was measured with a SoloVPE UV/Vis-Spectrometer by C Technologies according to QID 2461651 [151]. Highly concentrated BSA is measured without dilution at 290 nm, background correction is performed by separate measurement of the buffer. Measurements were performed three times, the results were averaged. The absorption of γ -globulin was measured at 280 nm, measurements were performed three times as well without buffer correction. Due to scattering, a dual wave length correction had to be carried out, thus the absorption of the sample was measured at 320 and 350 nm as well. After linear regression to both wavelengths, the scattering at 280 nm was extrapolated and omitted as blank from the measurement.

Rheology

Viscosity was determined according to QID 2461649 [152] with a Haake Mars 60 and a plate-plate geometry with 35 mm in diameter at a gap of 0.5 mm. RheoWin Job Manager (Version 4.63) was used for data acquisition. Shear rate range was adjusted as needed, but usually encompassed the range of 10 s^{-1} to 1000 s^{-1} . Every data point was measured for four seconds, and recorded data points are calculated by integrating 3 seconds. 20 data points were measured in logarithmic scale. The first measurement points were usually influenced by surface tension of the formulation and the measured viscosity was too high, whereas the last few measurement points sometimes were influenced by heating of the sample due to shear stress (viscosity lower than expected) or air bubbles due to surfactants (sudden increase of viscosity). As the used formulations showed Newtonian behavior, for calculation of the respective viscosities the data points were averaged except for the above mentioned outliers.

Size Exclusion Chromatography (SEC)

SEC measurements were carried out with a SECcurity GPC System 1260 Infinity (Agilent Technologies, Santa Clara, CA), equipped with a Yarra 3 μm SEC-3000 300x7.8 mm column and a GFC-3000 4x3.00 mm guard column, is used. The standard injection volume was 5 μl and the flow rate was 1 ml/min. As running buffer the protein buffer (table 6) is used without the addition of Tween[®] 80. For the protein detection a RI detector and an UV-detector at 220 nm for the phosphate buffered formulations were used.

In case of the histidine-buffered formulations (chapter 5.1.1) the wavelength for protein detection had to be evaluated first. Two wavelengths (220 nm and 280 nm) were tested for detection of

proteins. 230 nm was ruled out at the beginning as histidine itself shows high UV adsorption at this wavelength. Reliable detection was ensured at 280 nm as presented in chapter 5.1.1.

Dynamic Light Scattering (DLS)

For the measurement of the protein size distribution according to QID 2461631 [153], samples were diluted with RO-water to 5 g/l (BSA) or 0.5 g/l (γ -globulin). Measurements were performed with a Malvern Zetasizer ZS at 20 °C and the acquired data was evaluated by the Zetasizer software (version 7.12).

4.2.2 Characterization of the Liposomal Formulation

Cryo TEM

Cryo TEM measurements were performed by the University of Hamburg with a Tecnai G2 Spirit TWIN (FEI Company). Samples were quick-frozen in liquid ethane with a Vitrobot (FEI Company).

Rheology and DLS

The same above mentioned methods were applied to the liposomal formulation, except for a dilution factor of 50 for DLS measurements.

4.3 Overview of Membrane Materials

For this work, several different membranes were studied as summarized in table 8. If not indicated otherwise, Hydrosart 1 was used for the trials. For the sake of better comparison with CN membrane, temperature trials and adsorption studies were performed with Hydrosart 2. For scale-up studies with γ -globulin Hydrosart 3 was used. For the γ -globulin adsorption trials the membrane CN (2) was used. All other measurements were performed with CN (1).

Table 8: Overview of properties of microfilter membranes used for experiments.

Material	Water flux [ml/(min·cm ² ·bar)]	Resistance [10 ¹⁰ m ⁻¹]	Bubble Point [bar]	Mean flow pore size (MFP) [μ m]	BET-surface [m ² /g]
Hydrosart 1	12.9	4.7	4.3	0.40	4.2
Hydrosart 2	18.4	3.3	3.4	0.52	4.2
Hydrosart 3	15.3	3.9	4.2	0.47	5.4
CA	18.0	3.3	4.2	0.50	6.5
PES	20.9	2.9	4.2	0.28	13.2
PA	15.3	3.9	4.1	0.48	13.0
PVDF _{hyd}	12.2	4.9	4.0	0.595	4.9
CN (1)	20.4	2.9	4.4	0.44	11.1
CN (2)	28.1	2.1	4.1	0.46	10.9

4.4 Characterization of Membrane Materials

4.4.1 Porometry

Pore size distributions of the membrane filters were measured by a Porolux™ 500. Filter discs of 2.75 cm² membrane area were wetted with water and the membrane was assembled in a membrane housing. Pressure was increased and the flow of the gas through the membrane was measured until the membrane was completely dry (wet curve). Afterwards the flow of the gas through the membrane was measured for the dry membrane as well (dry curve). The dry curve was divided by half to generate the half dry curve. The bubble point equals the applied pressure for which the onset of air diffusion was detected, and the meeting point of dry curve and wet curve equals the smallest membrane pore. The mean flow pore size (MFP) is the intersection point of the half dry curve and the wet curve. All of those values are visualized in figure 27.

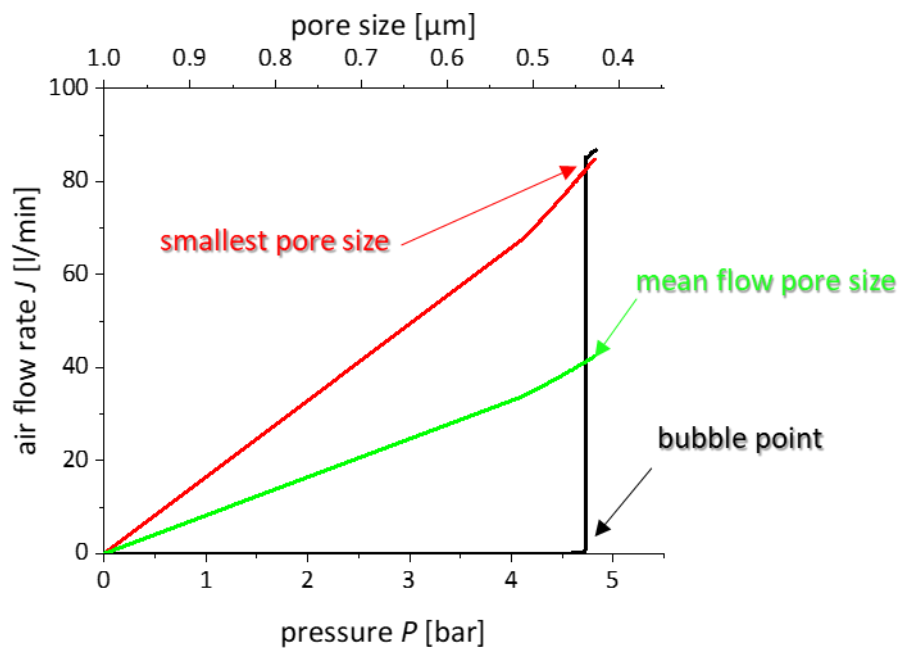


Figure 27: Presentation of bubble point, mean flow pore size and smallest pore size as measured by a capillary flow porometer; data for porometry measurement of a CN membrane with water as wetting fluid; wet curve (black), half dry curve (green) and dry curve (red) are shown.

4.4.2 SEM

For the determination of the pore size distribution and the porosity distribution established methods were used [154,155]. First the membrane material is embedded in epoxy resin, afterwards the membrane cross-section is polished with a Buehler EcoMet250. The obtained sample was measured with a FEI Quanta 200.

For further analysis, raw images were binarized and processed afterwards with MATLAB R2014b. The threshold for the binarization was adjusted automatically and governed by the average

4 Materials and Methods

porosity, which was determined by measurement of the membrane volume and the weight of a membrane sample. In order to give reliable pore size distributions also the size of the original image had to be known.

For further visualization the membrane cross-section was sub-divided into ten layers with an averaged number of consecutive pixels. Based on these limits the pore size distribution and the distribution of the porosity could be calculated for each layer. For visualization of the membrane surfaces samples were coated with gold with a K550 Emitech Sputter Coater and recorded with a JEOL JCM-6000Plus NeoScope™.

4.4.3 BET

BET measurements were performed according to DIN-ISO 9277 at Quantachrome with a Quantachrome Quadrasorb Evo using nitrogen at 77 K as test medium. The samples were prepared by keeping them at 90 °C in vacuum for 5 hours.

4.5 Execution and Evaluation of Filtration Trials

4.5.1 Description of Filtration Setups

The execution of filtration trials is described in QID 2462507, for focus on protein formulations in QID 2461652 [156,157]. For all measurements the filtrate weight was monitored by a balance. The density of the filtration medium was used to calculate the filtrate volume. Pressure was monitored at all times, the temperature was monitored for constant pressure measurements only due to setup restrictions. Filter discs were pre-wetted with the respective protein buffer, devices were pre-wetted with RO-water. Filter discs were installed in membrane holders with identical support, cartridges were installed in stainless steel housings. In the filtration systems incorporating filter discs the system was flushed with the test solution to remove air. Membranes were installed and air was removed again by venting the system. Membrane housings for 2.75 cm² filter discs do not possess a vent, so that the air could not be removed after the assembly.

For constant flow measurements, either a syringe driver with 80 ml volume or a peristaltic pump (SciLog Tandem 1081 or 1082) for higher filtrate volumes was used. For the constant flow setup only 2.75 cm² membrane housings were used. A schematic representation is shown in figure 28. Each membrane holder was equipped with a separate pressure sensor and pump head. According to the required flow rate pump speed, tubing size, pump head and motor was chosen, respectively.

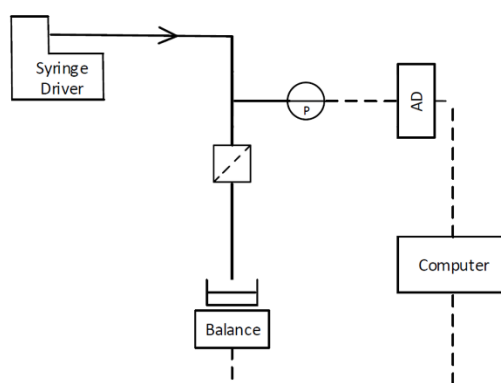


Figure 28: Experimental setup for constant flow filtration measurements.

Constant pressure trials were performed with a pressure vessel of 5 l, 6 l with double wall for temperature control, 20 l or 80 l as needed. The system was used for 2.75 cm², 14.1 cm², 136 cm² filter discs, and size 4 capsules. In case of 136 cm² filter discs and size 4 capsules only one of these elements was installed during a trial in the setup, for smaller membrane areas up to four measurements were

performed simultaneously. All membrane holders for filter discs were equipped with the same membrane support. Usually the 2.75 cm² membrane housing was used, except for the particulate test solution (14.1 cm²) and for the scaling experiments (section 5.3). The setup is presented in figure 29.

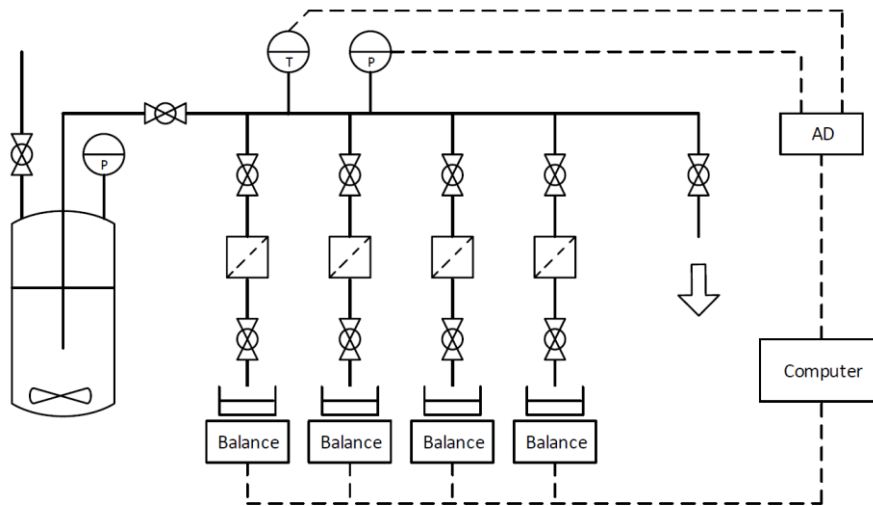


Figure 29: Filtration setup for constant pressure filtration measurements.

For measurements of water flow rates of MaxiCaps[®] setup 3 was used (figure 30). The water was recirculated in a loop using a rotary pump (Koch). The water temperature was maintained at 20 ± 0.5 °C using a heat exchanger. A 300 L water tank (Heider) served as a water reservoir to assure a constant water flux during the whole measurement. Before each measurement, the filtration device was installed into the setup and wetting was done by adjusting a constant differential pressure of 0.3 bar between cartridge inlet and outlet for 300 seconds. The differential pressure was recorded using two pressure sensors from Wika (Pressure Transmitter S11) and maintained by an automation, controlling the pump speed. At the beginning of each wetting cycle, the MaxiCap[®] was vented by opening the valve until no further air bubbles appeared. Subsequently to the wetting, the pump was adjusted to a water flux leading to a differential pressure between the MaxiCaps[®] inlet and outlet of 2.0 bar, 1.5 bar, 1.0 bar, 0.5 bar, 0.3 bar, 0.2 bar and 0.1 bar, respectively. At each pressure step, the water flux was recorded for 300 s using the flow meter Process master 300 from Danfos.

4 Materials and Methods

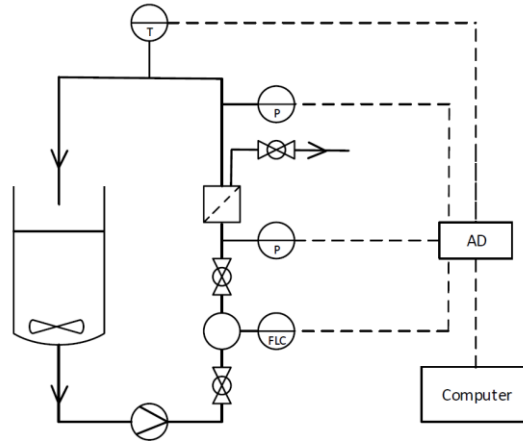


Figure 30: Experimental setup for water flow rate measurement of In-line MaxiCaps® and T-Style MaxiCaps®.

4.5.2 Evaluation of Filtration Experiments

The evaluation of filtration experiments is described in QID 2461652 [157]. In a first step, the recorded data was smoothed by the Savitzky-Golay-algorithm, which requires equidistant data points. To achieve this, the timescale had to be modified. The data points were collected nearly equidistant, every 0.4-0.6 seconds. The length of an experiment was divided by the number of data points, this interval is assumed to be the polling rate throughout the experiment. Figure 31 illustrates the calculated measurement time and the actual measurement time for a filtration trial of 90 minutes. It can be seen that no deviation between both timescales can be observed.

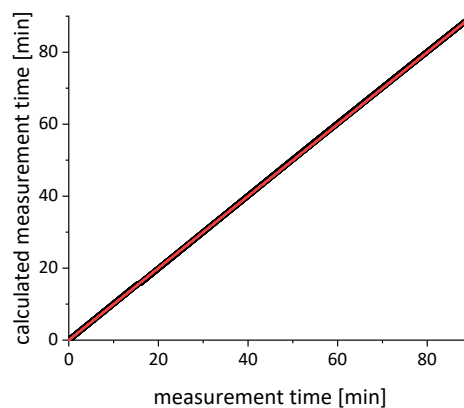


Figure 31: Comparison of the calculated measurement time and the actual measurement time (black) and the bisecting line (red).

The Savitzky-Golay algorithm was used with the order of 1 and the number of data points was chosen separately for each measurement, depending on the filtration flow rate. For constant flow rate measurements the pressure data were smoothed by the Savitzky-Golay-algorithm as well. With the obtained data, filtration flux J° , membrane resistance R°_{tot} and throughput \tilde{V} were calculated according

4 Materials and Methods

to chapter 3.2.2. Afterwards the plots of $\tilde{V}(t)$, $J^\circ(t)$, $R^\circ_{tot}(t)$, $J^\circ(\tilde{V})$ and $R^\circ_{tot}(\tilde{V})$ were plotted. In case of constant flow rate measurements, additionally $P(t)$ or $P(\tilde{V})$ were plotted.

Furthermore, typical filtration parameters are determined: both the initial flux and the initial resistance were calculated by linear regression to $J^\circ(t)$ and $R^\circ_{tot}(t)$, respectively. To obtain $t_{50\%}$ (filtration time at 50% filter blocking) an experimental decay was fitted to the $J(t)$ plot (OriginLab) and the x-value at 50% J_0 was determined. To ensure data consistency the resistance $R^\circ_{50\%}$ (resistance at 50% membrane blocking) was calculated by an exponential regression to the $R^\circ_{tot}(t)$ plot. Ideally $R^\circ_{50\%}$ should be equal to $2 \cdot R^\circ_{tot}(t=0)$. For constant flow filtration the initial resistance $R^\circ_{tot}(t=0)$ was calculated by modelling an exponential growth of the first few minutes of the trial. The initial pressure $P(t=0)$ was calculated by linear extrapolation at the beginning of the pressure curve. In order to ensure reproducibility, all measurements are performed in triplicates except for constant flow and scaling experiments. In case of low filter fouling, instead of filtration parameters for 50% filter blocking filtration parameters for 25% filter blocking were calculated ($R^\circ_{25\%}$ and $t_{25\%}$).

4.5.3 General Information on Scaling Experiments with Protein Formulations

For every scaling experiments pre-trials have been performed to estimate the necessary filtration volumes and pressures. According to that the respective pumps, tubing, and valves were selected. As pumps usually tandem pumps (1081 and 1082 with 160 rpm or 600 rpm, as needed) were used, only for size 1 cartridges and the concentrated BSA formulation (formulation 1) a Quattroflow SU 5050 was needed. Pressure sensors were installed directly with a T-piece close to the device, and the setup was vented at the highest point of the setup. Venting was performed either by a vent installed at the top of the setup or by removing the pressure sensor on flushing. An example for MidiCaps and size 4 capsules is presented in figure 32.

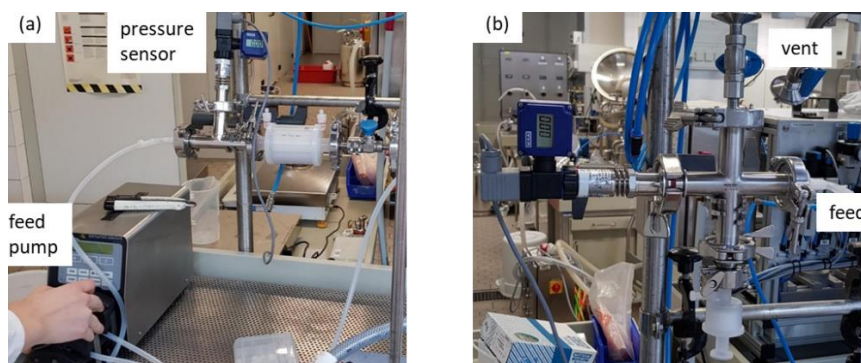


Figure 32: Filtration setup for MidiCaps (a) and size 4 capsules (b).

For small elements (Sartoscales and Sartoscales 25) the pressure is increased up to 300 mbar and released by a vent, until no further air bubbles are observed. During the venting process the valve below the device is closed.

4.6 Confocal Laser Scanning Microscopy (CLS)

For these trials an established method [158] was modified. Protein fouling layers are visualized within the membrane material by fluorescence staining. 25 mm filter discs of Hydrosart membrane were gently shaken in NaIO_4 -solution (2 wt%) for 16 hours. After this period the membranes were flushed with RO-water for 15 minutes and dried for 15 minutes. Alexa Fluor 594 cadaverine (0.3 mg) was diluted in KPI-buffer (12 ml). 2 ml of the staining solution was added to each membrane and the membranes were shaken for 6 more hours. Excess dye was washed out and the filter discs are dried and stored protected from light.

The KPI-buffer for dissolving the fluorescent dye was prepared by mixing two solutions of K_2HPO_4 (208.5 g) and KH_2PO_4 (117 g) in RO-water (541 g and 383 g, respectively) until a pH of 7 is obtained. The stock solution was slowly added to RO-water (2 l) until a conductivity of 1.75 mS/cm was reached.

Filtration trials were performed with protein concentrations of 2.5 g/l and 200 g/l in formulation 1. Experiments were performed in constant flow and constant pressure mode. Filtration trials were performed until complete membrane blocking, for the constant flow experiments until a filtration pressure of 2 bar and for constant pressure experiments until no flux could be observed anymore.

After the filtration trials the membranes were dried for 4 hours at 70 °C. For staining of the proteins AlexaFluor488 NHS-ester (5 mg) are dissolved in KPI-buffer (5 ml). A 1x1 cm² rectangle was prepared from each membrane sample and staining solution (1 ml) was added. The membranes were shaken overnight in the dark and rinsed with RO-water for 15 minutes, and dried at 70 °C.

Measurements are performed with a TCS SP-8 confocal laser scanning microscope by Leica Microsystems™, fitted with a HC PL APO-20x/1.40 IMM-CS2 20x oil objective. The software LAS X (Version 2.0.0.14332) was used for image acquisition.

4.7 ILC for Adsorption Measurements

The Inverse Liquid Chromatography (ILC, setup shown in figure 33) is a chromatographic method used for the examination of protein adsorption by measurement of breakthrough curves. The setup presented in figure 33 was configured by SSB and Knauer in collaboration. All tubing of the setup was made from stainless steel, with identical lengths for minimum adsorption.

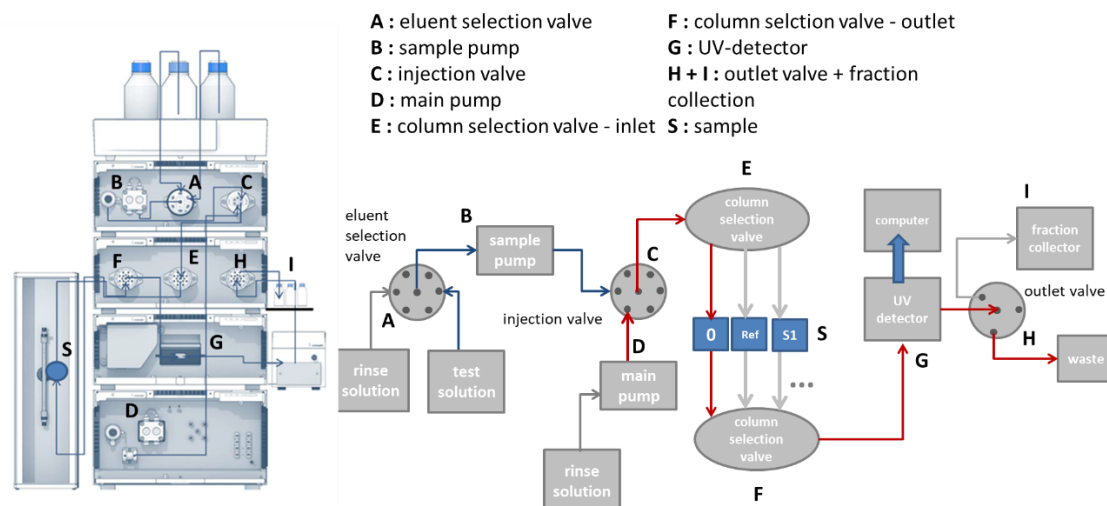


Figure 33: Setup of Inverse Liquid Chromatography (configured by SSB and Knauer; picture reprinted with permission from Knauer)

Adsorption and desorption processes were studied by injection of 40 ml of test fluid followed by the respective buffer solution. For 5 measurement cycles the setup was flushed with 30 ml buffer solution between each cycle.

The detector allowed the collection of data at four different UV wavelengths simultaneously every 0.001 minutes. 280 nm was used for data evaluation; signals at 195 nm, 230 nm, and 240 nm were measured as well, however BSA concentration was not linear with the signal intensity in the measured concentration range.

Two different types of blank measurements were necessary. The first type is the system blank measurement, for this measurement runs were performed for the whole setup except for the membrane housing. System blank measurements were included in every run. The second blank is the measurement of protein adsorption to empty membrane housings; those were performed in a separate trial for several membrane housings. The adsorbed amount of protein to the membrane housing was determined by averaging the results of more than 6 housing measurements. After several material tests, Cyrolite® (figure 34) was chosen as membrane housing due to the low protein adsorption. Single layer

4 Materials and Methods

30 mm filter discs (5.52 cm² effective membrane area) were installed in the membrane housings for the measurements. As membrane material, Hydrosart 2 and CN (table 8 in section 4.3) are compared.



Figure 34: Cyrolite® membrane housing for ILC measurements.

The Hydrosart membrane is wetted spontaneously and swells upon water contact, therefore this membrane was installed in dry state. The CN membrane was pre-wetted before assembly with the respective buffer solution. After assembly, the system was flushed with water to remove air, followed by preconditioning with protein buffer. After the respective measurement position was flushed with buffer, the sample valve was switched to the test solution and 40 ml of the test fluid were injected. Afterwards, the sample valve was switched to the buffer solution again and desorption could be monitored. Between the measurement trials the setup was flushed with a cleaning solution (1 wt% SDS and 0.1 M sodium hydroxide) for complete protein removal.

After data reduction, the starting point of each measurement was calculated manually by determination of the breakthrough point of the buffer solution when the injection of test solution is finished. This method was established in order to eliminate errors due to a 100% adsorption at the beginning of each measurement. In literature usually the first initial rise of the UV-signal is taken [126].

With a distance of –10 data points to the determined breakthrough point the intensity values of 10 data points were averaged; this intensity was assumed to correlate with the initial sample concentration. According to Beer's law a linear relationship of the intensity signal and the protein concentration was assumed, allowing the calculation of concentration curves.

The adsorption curves for the membrane housing were determined by integrating the area between the calculated system blank concentration curve and the concentration curve of an empty membrane housing. The adsorption curves for the empty membrane housing were calculated. The adsorbed amount of protein was taken for each membrane housing at 40 ml.

The adsorption curves for membranes were calculated as presented in figure 35. First, the adsorption curves were calculated with the system blank measurement as a reference. After determination of the raw adsorption curve it had to be compressed by a correction factor, which refers to the amount of protein that was determined to adsorb to the membrane housing (equation 22). For this

purpose the adsorbed amount of protein on the membrane housing after 40 ml $m_{ads_h@40ml}$ and the adsorbed amount of protein that is adsorbed on the membrane $m_{ads_m@40ml}$ after 40 ml is determined.

$$correction\ factor = \frac{m_{ads_m@40\ ml} - m_{ads_h@40\ ml}}{m_{ads_m@40\ ml}} \quad (22)$$

With the adsorbed amounts of protein m_{ads} the adsorption rate was calculated by the following equation:

$$adsorption\ rate = \frac{dm_{ads}}{dt} \quad (23)$$

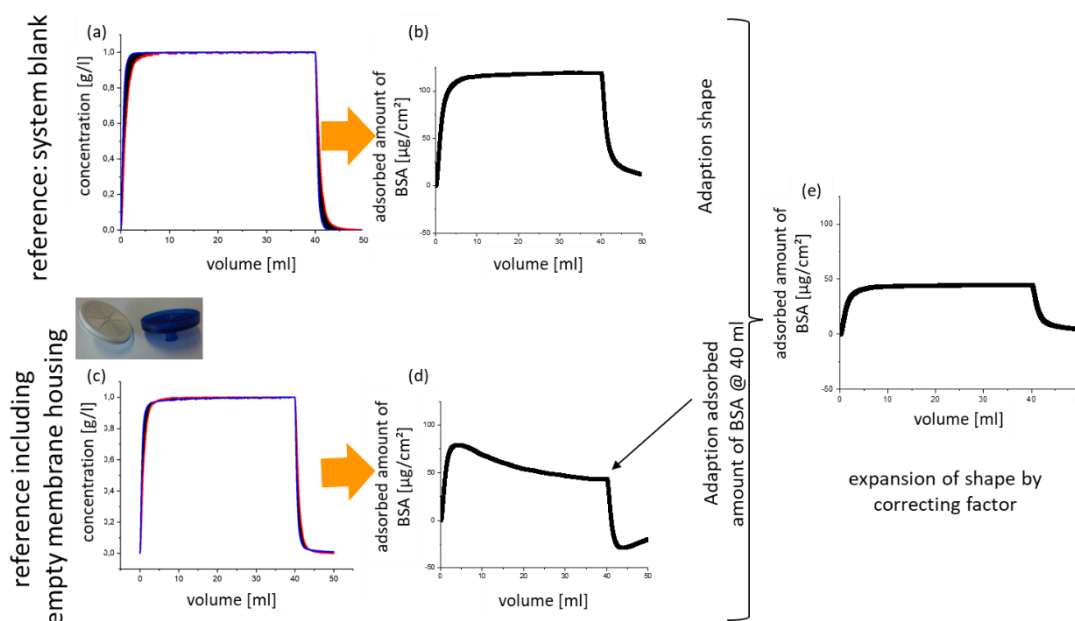


Figure 35: Schematic overview of the data evaluation of ILC experiments. (a) The area (black) between the system blank concentration (black) and the protein concentration with the membrane (red) is integrated to give plot (b). The same is done with the housing measurement as reference (c) to give plot (d). By expansion of curve (b) with the adsorbed amount of BSA at 40 ml in curve (d) the result (e) is obtained.

Solutions were prepared according to chapter 5.1.2. All solutions (reverse osmosis water, buffer, test solution and cleaning solution) were pre-filtered with a 0.2 µm Sartolab PES filter and de-gassed before use. The composition of the test solution was varied between trials as presented in table 9 to observe formulation influences and impact of filtration conditions on protein adsorption.

4 Materials and Methods

Table 9: Compositions of different test solutions for ILC trials.

Trial	BSA-concentration [g/l]	Buffer	PS 80-concentration [%]	Additives	Flow rate $\left[\frac{\text{ml}}{\text{min}\cdot\text{cm}^2}\right]$	
Standard composition A	1	100 mM NaH ₂ PO ₄ , 100 mM Na ₂ SO ₄ , pH 6.9	0.01	0.01% NaCl, 0.002% NaN ₃	0.90	
PS 80 test series			0, 0.00016, 0.01, 0.5			
Variation of protein concentration			0.1, 0.5, 1.0, 2.0, 5.0			0.01
Flow rate series			1			0, 0.01%
Multiple cycles			1			0, 0.01%
Trial	γ-Globulin concentration [g/l]	Buffer	PS 80-concentration [%]	Additives	Flow rate $\left[\frac{\text{ml}}{\text{min}\cdot\text{cm}^2}\right]$	
Standard composition B	1	75 mM histidine, pH 6.4	0.01	0.002% NaN ₃	0.90	
PS 80 test series			0%, 0.01%			
Variation of protein concentration			0.1, 0.5, 1.0, 2.0, 5.0			0.01
Flow rate series			1			0%
Multiple cycles			1			0%

4.8 Bacterial Challenge Tests

Tryptic soy agar plates were pre-incubated to eliminate the risk of bacterial contamination. All equipment was autoclaved before use and all transfers were done under aseptic conditions.

Viabank™ beads loaded with *B. diminuta* were kept at $-80\text{ }^{\circ}\text{C}$. One bead was immersed in 10 ml of tryptic soy broth and kept at $30\text{ }^{\circ}\text{C}$ for 24 h. 1 ml of the solution was diluted in 100 ml of saline lactose broth (9.7 ml of 0.9 wt% NaCl-solution and 30 ml lactose broth for 1 l). The solution was incubated at $30\text{ }^{\circ}\text{C}$ for 16 hours at 200 rpm. 2 l of the respective test solution (table 10) was prepared and 6 ml of bacteria solution was added. The challenge level is determined parallel by filtering the diluted bacteria suspension by vacuum on a 14.1 cm^2 analytical filter, incubation for three days and colony counting. The target challenge level was 10^7 cfu/cm^2 .

The components with the test membrane filters installed inside (filter discs with 136 cm^2 membrane area) were autoclaved at $121\text{ }^{\circ}\text{C}$ for 40 minutes, the test rig was steam-sterilized for 30 minutes at 2 bar. The setup (figure 36) was assembled and preflushed with the test solution. It was filtered at 2 bar for 60 minutes in recirculation mode. Afterwards the rig was flushed with 13.5 l sterile RO-water and remaining water from the analytical filters (11106-142 CA) was sucked out under reduced pressure.

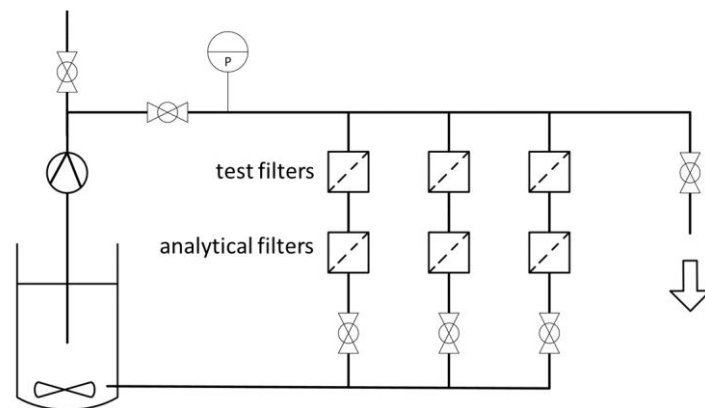


Figure 36: Experimental setup used for the bacterial challenge tests.

The analytical filters were incubated on tryptic soy agar plates at $30\text{ }^{\circ}\text{C}$ for three days. After this period, bacteria colonies on the analytical filters were counted. The different test media are listed in table 10, the membranes used for the BC tests are listed in table 11.

4 Materials and Methods

Table 10: Overview of test media used for bacteria challenge tests

Test media	Concentration
NaCl	0.3%, 0.6%, 0.9%, 4.5 %, 8 %
NaH ₂ PO ₄ /Na ₂ SO ₄	200 mmol, 500 mmol, 800 mmol
MgCl ₂	0.49%, 2.45%, 4.4%
CaCl ₂	0.57%, 2.85%, 5.1%
Tween® 80	0.1%, 1%, 2%
Pluronic F-127	2.7%

Table 11: Overview of characteristic parameter of PES-membranes used for bacteria challenge tests

Membrane	BP [bar]	Water flux [ml/(min·cm²·bar)]
PES1	2.34	51.5
PES2	2.51	46.9
PES3	2.76	40.5
PES4	3.00	35.5
PES5	3.28	34.3
PES6	3.47	30.1
PES7	3.70	26.0
PES8	3.89	24.8
PES9	4.05	23.0

5 Results and Discussion

The central aim of this study is to examine issues connected with microfiltration of stable therapeutic protein formulations. First of all protein formulations had to be developed for use in filtration trials. Formulation development and characterization methods are described in chapter 5.1. Chapter 5.2 gives an overview about results of filtration trials and suitable filtration conditions for these protein formulations. The development of an up-scaling approach from lab filtration to process filtration is presented in chapter 5.3. The chapter summarizes the experimental approach and the calculation basis for modeling of filtration processes based on filtration trials and parameters as resistance and effective membrane area of the studied filter devices. Based on this up-scaling approach filtration case studies were performed with the standardized protein formulations described in chapter 5.1 and various experimental and commercial filter products, which are summarized in chapter 5.3.2. Chapter 5.4 gives an overview about the results of a study of protein adsorption on the membrane surface during filtration by inverse liquid chromatography (ILC). The impact of protein formulation and excipients on bacteria retention is described in chapter 5.5. Finally, some orienting investigations on filtration of liposomal solutions are reported in chapter 5.6.

5.1 Formulation, Manufacturing and Characterization of Standardized Protein Formulations for Filtration Studies

Aim of this section was the development of formulation and preparation of stable drug-like protein formulations based on BSA and γ -globulin for filtration studies in kg scale. Formulations were defined according to current biopharma trends summarized for example by Uchiyama *et al* [24] and described in chapter 3. Experimental details are presented in chapter 4.2.

The phosphate-buffered BSA formulation with 250 g/l (formulation 1) was already developed in a previous work for a smaller batch size [83]. In result of this work two further formulations were defined, a viscous BSA formulation (formulation 2, $\eta = 40$ mPa·s) and a histidine buffered γ -globulin formulation (formulation 3). All formulation details, e.g., composition, pH, viscosity are summarized in table 6 in section 4.1. The formulation development for the histidine buffered γ -globulin formulation and the up-scaling of the production process are described in the following chapter.

5.1.1 Formulation Development for γ -Globulin by SEC

Aim of this work was the adjustment and definition of basic aspects of formulation 3, e.g., the necessary protein concentration, the protein buffer, pH, surfactant and further excipients. The targeted formulation should have a high concentration of 100 g/l. It should be possible to lyophilize the

formulation, hence the formulation should be histidine buffered and stabilized with 0.5% Tween® 80. The formulation development was based on SEC investigations

SEC Investigations - Determination of Measurement Wavelength

A UV detector was used for detection of protein monomers and aggregates for characterization of γ -globulin and BSA formulations. At the beginning of the measurements the necessary wavelength had to be determined. UV wavelengths of 220 nm and 280 nm were tested.

In result the wavelength of 280 nm was chosen for further experimental investigations. It can be seen in figure 37 that for the same samples no linear relationship can be observed for the detected amount of γ -globulin at 220 nm, but at 280 nm. Despite the lower sensitivity at 280 nm dimers and oligomers can be detected better at this wavelength. Those results were also observed for measurements of formulations with up to 75 mM histidine and 10 g/l γ -globulin, and for BSA-formulations. Furthermore the sample loop of the SEC was tested by injecting 5, 10, 15 and 20 μ l, here linearity could be observed.

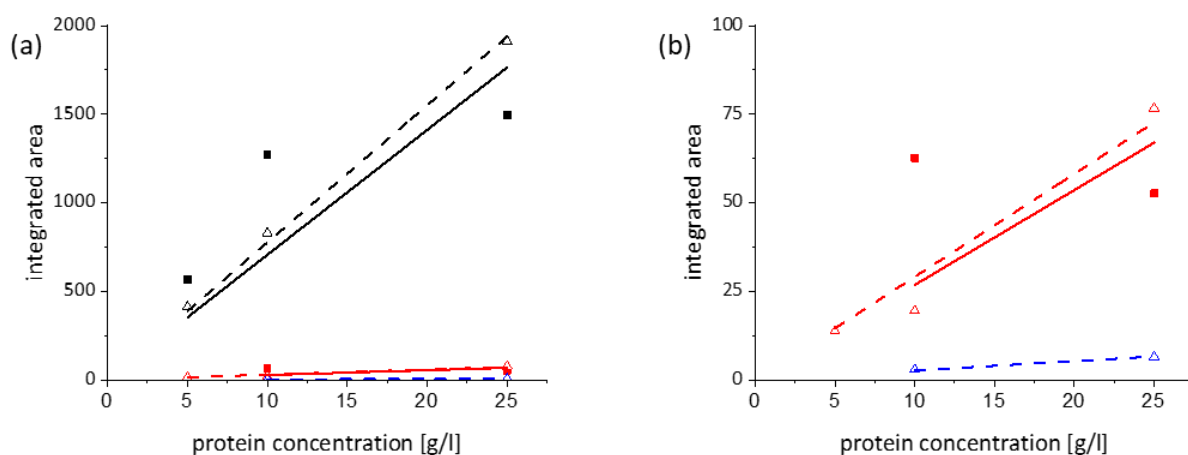


Figure 37: Evaluation of UV wavelengths for SEC measurements of protein formulations; presentation of peak area of UV signals at a wavelength of 220 nm (closed symbols) and 280 nm (open symbols) plotted versus protein concentration; monomers (black), dimers (red) and oligomers (blue) for measurement of γ -globulin formulation in 25 mM histidine, and 0.5% PS 80 at pH 6.4; fit with linear regression (220 nm, straight lines and 280 nm, dashed lines). SEC measurement parameters: injection volume 5 μ l, flow rate 1 ml/min.

Determination of Formulation pH

The pH of the formulation was defined in result of SEC measurements with γ -globulin formulations (25 mM histidine and 0.5% Tween® 80) of different pH: 5.4, 6.4 and 6.9. According to the result presented in figure 38 the formulation pH was fixed to pH = 6.4. With a more acidic pH hardly any protein could be detected; probably aggregates are formed that are retained at the safety column. With a more basic pH obviously dimers are formed.

5 Results and Discussion

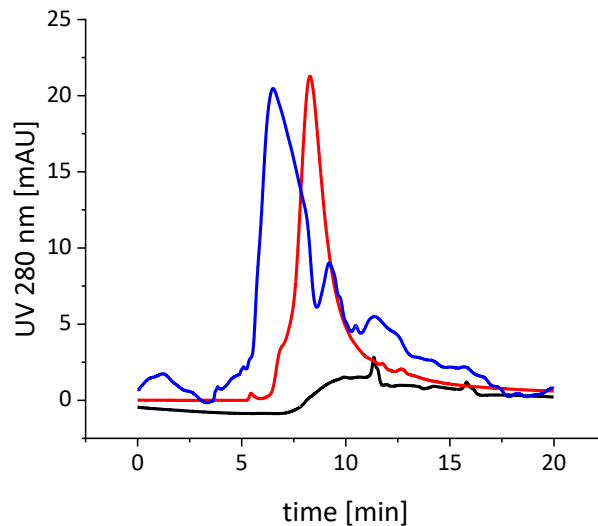


Figure 38: SEC chromatograms for testing the influence of the pH value on the aggregation of a γ -globulin formulation (25 g/l γ -globulin, 25 mM histidine and 0.5% Tween® 80), SEC measurement. Measurements at pH 5.4 (black), pH 6.4 (red) and pH 6.9 (blue). SEC measurement parameters: injection volume 5 μ l, flow rate 1 ml/min.

Selection of Formulation Excipients

Influence of sucrose and sodium chloride on protein aggregation was again studied by SEC measurement. Sucrose was tested because of its use as stabilizer in lyophilized formulations and sodium chloride to change the ionic strength. The results are presented in figure 39.

On adding 200 mM Sucrose (a) to the formulation no change in the SEC-signal could be observed. With NaCl (b) the peaks increase in intensity. With regard to the fact, that for lyophilization salts are detrimental for protein stability an addition of salt content was not further considered, instead the influence of the histidine concentration on the protein stability is tested.

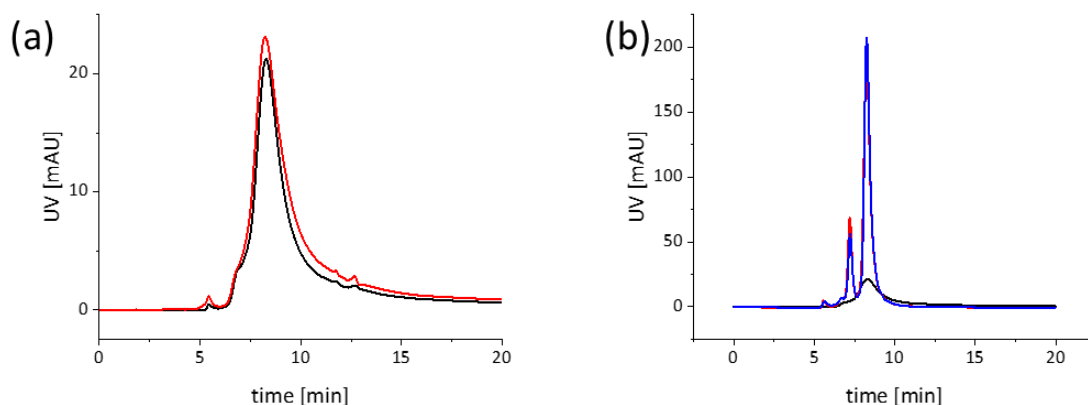


Figure 39: SEC chromatograms for testing the influence of additives on the stability of a γ -globulin formulation: 25 g/l γ -globulin in 25 mM histidine-formulation at pH 6.4; (a) signal intensity (280 nm) for sucrose containing formulations: black lines without sucrose, red lines with 200 mM sucrose and (b) signal intensity (280 nm) for NaCl containing formulations: black lines without NaCl, red lines with 0.25 mM and blue lines with 0.5 mM NaCl; SEC measurement parameters: injection volume 5 μ l, flow rate 1 ml/min.

5 Results and Discussion

The influence of the concentration of histidine on protein stability can be seen in figure 40. The protein concentration is lowered for the tests to 10 g/l due to the high histidine concentrations. SEC chromatograms show a distinct increase in peak intensity on rising histidine concentration; peak areas for 10 g/l protein are 829 (25 mM histidine), 2062 (50 mM histidine), and 2276 (75 mM histidine). Finally, the histidine concentration was fixed to 75 mM. The peak intensity reached with 75 mM histidine is also higher than in case of a 0.5 M NaCl containing formulation of the same protein concentration (1781). In result of these measurements formulation 3 was finally defined with 100 g/l γ -globulin, 75 mM histidine and 0.5% Tween[®] 80.

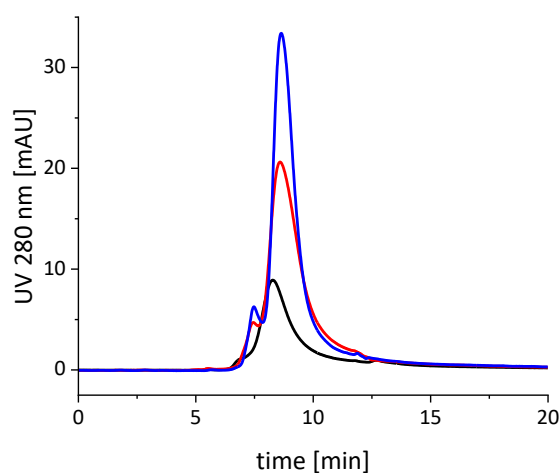


Figure 40: SEC chromatogram for testing the influence of the histidine concentration on the stability of a protein formulation of 10 g/l γ -globulin at pH 6.4. 25 mM histidine (black lines), 50 mM histidine (red lines) and 75 mM histidine (blue lines).

5.1.2 Preparation and Characterization of Standardized Protein Solutions in kg Scale

Critical issues for up-scaling of the formulation preparation were the quality of the product, the order of the steps and the preparation time. Most technical problems could be solved using the ViscoJet[®] stirring technology for manufacturing of the formulations.

ViscoJet[®] stirrers for lab purposes are available with two cones (60 mm stirrer diameter) and three cones (80 mm and 120 mm stirrer diameter) as presented in figure 41. The stirring setup has to be adjusted depending on the amount of solution to be prepared. Ideally the filling level is equal to the vessel diameter; the stirrer diameter equates to 0.4 – 0.6 times the vessel diameter, and the distance between the vessel bottom and the stirrer is 1/3rd of the stirrer diameter. The ViscoJet[®] combines efficient mixing, good solid entrainment, low shearing and a degassing effect and is therefore quite suitable for the preparation of protein formulations. Production procedure of the protein formulations is described in QID 2461655 [159].

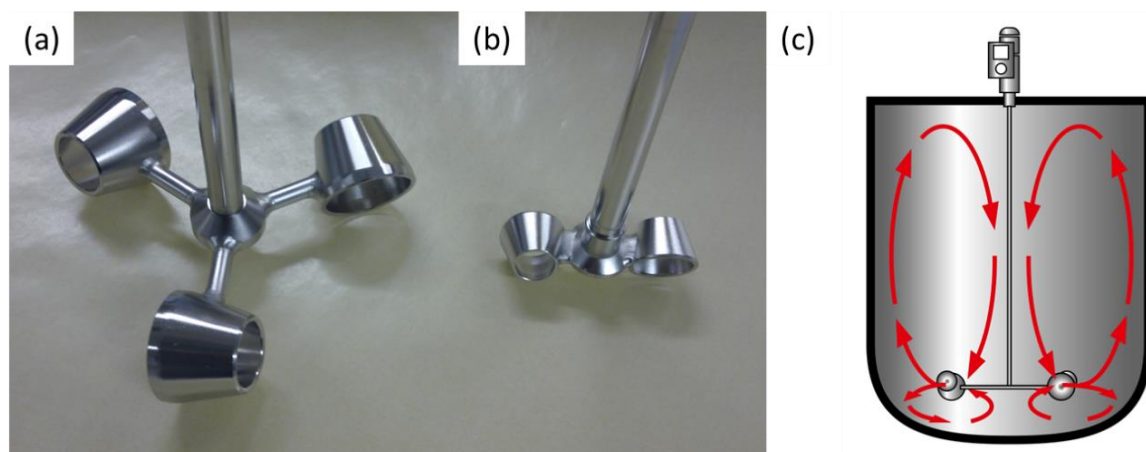


Figure 41: (a) ViscoJet stirrers with 120 mm stirrer diameter, (b) 60 mm stirrer diameter; (c) schematic presentation of flow distribution in a vessel stirred by a ViscoJet® stirrer [160].

5.1.3 Characterization of Protein Formulations

Best method to qualify test formulations for further investigations is a test filtration with a standardized membrane. Typical filtration curves for all formulations are presented in section 5.2.

Typical results of viscosity measurements by rotational viscometer are presented in figure 42. For Formulation 1 a viscosity of 4 mPa·s, for formulation 2 a viscosity of 37 mPa·s and for formulation 3 a viscosity of 2 mPa·s was measured.

The viscosity measurement with a rotational rheometer faces some challenges at low shear rates as can be seen in figure 42. The measurement principle of a rotational viscometer is the evaluation of the necessary force for spinning the measurement geometry. In case of low shear rates and low viscosities this force is quite small and the measurements become inaccurate (observed for formulation 3 below $\dot{\gamma}=20 \text{ s}^{-1}$); surface tension can increase this force as well. In case of high shear stress the temperature of the sample solution is prone to rise slightly and the viscosity can decrease. Furthermore, the liquid-air-interface is critical for surfactant containing formulations. Air bubbles can enter the test solutions at high spinning rates, which causes a viscosity increase. Turbulences can occur within the test solution as well, which can be another error source at high shear rates. This can be observed for formulation 1 and formulation 3 above 1000 s^{-1} . Thus, the expected shear thinning behavior known for protein formulations cannot be observed.

5 Results and Discussion

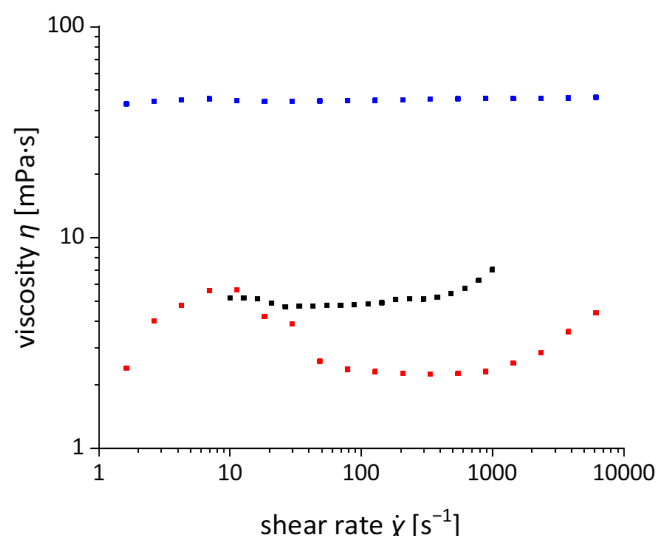


Figure 42: Viscosity measurements of protein formulations (table 6) by rotational viscometer at 20 °C: Formulation 1 (black), formulation 2 (blue) and formulation 3 (red).

The aggregation degree of protein formulations was characterized by SEC and DLS measurements. Methods and equipment are described in chapter 4.2.1. SEC measurements (figure 43a) show a monomer content of above 90% for formulation 3 and more than 80% for formulations 1 and 2. DLS measurements (figure 43b) confirm the presence of large aggregates, which cannot be detected by GPC.

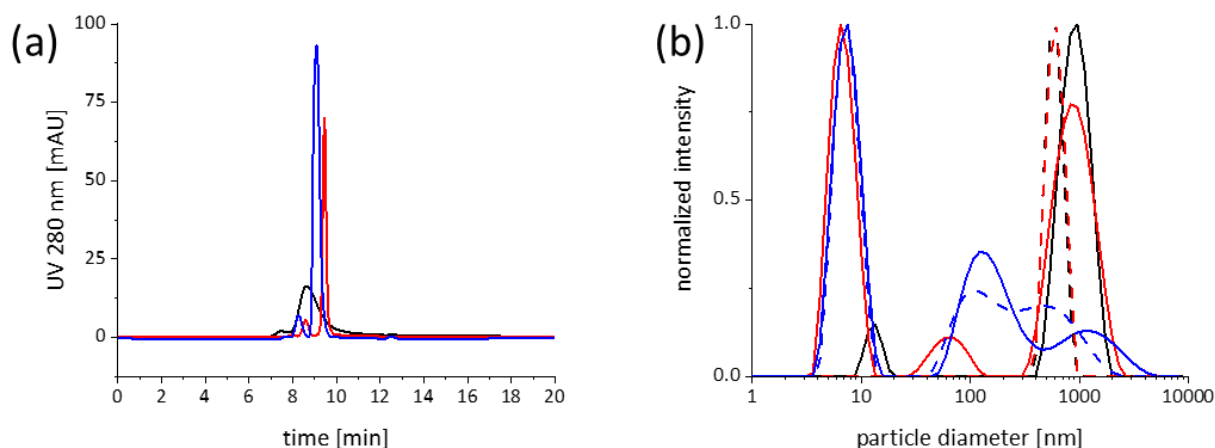


Figure 43: Protein aggregation in studied protein formulations (table 6): formulation 1 (red), formulation 2 (blue), and formulation 3 (black); (a) SEC-measurement of formulation 1 and formulation 3, both diluted by buffer to 5 g/l and formulation 2 diluted with RO-water to 25 g/l; (b) DLS measurement; protein formulations, diluted to 5 g/l (formulation 1 and 2) and to 0.5 g/l (formulation 3). DLS detection at 173° (straight lines) and 12.8° (dashed lines).

5.1.4 Summary

Three stabilized drug like protein formulations were developed on basis of BSA and γ -globulin for filtration test trials. The term “stabilized” refers to a high chemical and physical stability of the protein and a high colloidal stability of the formulation with a low degree of aggregation. Formulations are summarized in table 6 in chapter 4.1, this chapter also gives experimental procedures for production and characterization of the formulations. Formulations can be prepared in kg scale using ViscoJet® stirring technology and can be used in the course of some days for filtration trials after pre-filtration with a 0.45 μm pre-filter.

5.2 Filtration of Protein Formulations

5.2.1 Evaluation of Filtration Data – Monitoring of Filter Fouling

Filtration processes are usually monitored by filtrate volume V versus time t plots. However, in this work consequently filtration flux J° and membrane resistance R°_{tot} were calculated and plotted versus time t and throughput \tilde{V} . Furthermore, characteristic filtration parameters as initial flux J°_0 , initial resistance R°_0 and throughput at 50% filter blocking $\tilde{V}_{50\%}$ were always summarized in tabular form. The data collection and evaluation are both described in section 4.5.

Figure 44 presents in an exemplary way typical filtration plots and characteristic filtration parameter for filtration of a standardized particulate test solution at different membrane areas and different filtration pressures through a 0.2 μm PES membrane with initial resistance of ca. $3 \cdot 10^{10} \text{ m}^{-1}$. At all conditions the same blocking rate is achieved (figure 44e) and nearly 9 ml/cm^2 of solution can be filtered until 50% blocking (table 12).

If filtration trials can be performed at any process condition (temperature or filtration pressure), and the same amount of filtrate at identical blocking rates is achieved ($R^\circ_{tot}(\tilde{V})$ -plot), there is no influence of the filtration process on membrane fouling. This behavior is typical for the particulate test solution shown in figure 44. The influence of the filtration pressure on filtrate flow can be observed in plot (b) and (d). The initial filtration flux is higher for 1 bar, but the decline of the filtration flow is accelerated as well. Resistance-plots $R^\circ_{tot}(\tilde{V})$ or $R^\circ_{tot}(t)$ are always scaled identically with a maximum value at $50 \cdot 10^{10} \text{ m}^{-1}$ on the y-axis. Higher resistance values do not have process relevance.

5 Results and Discussion

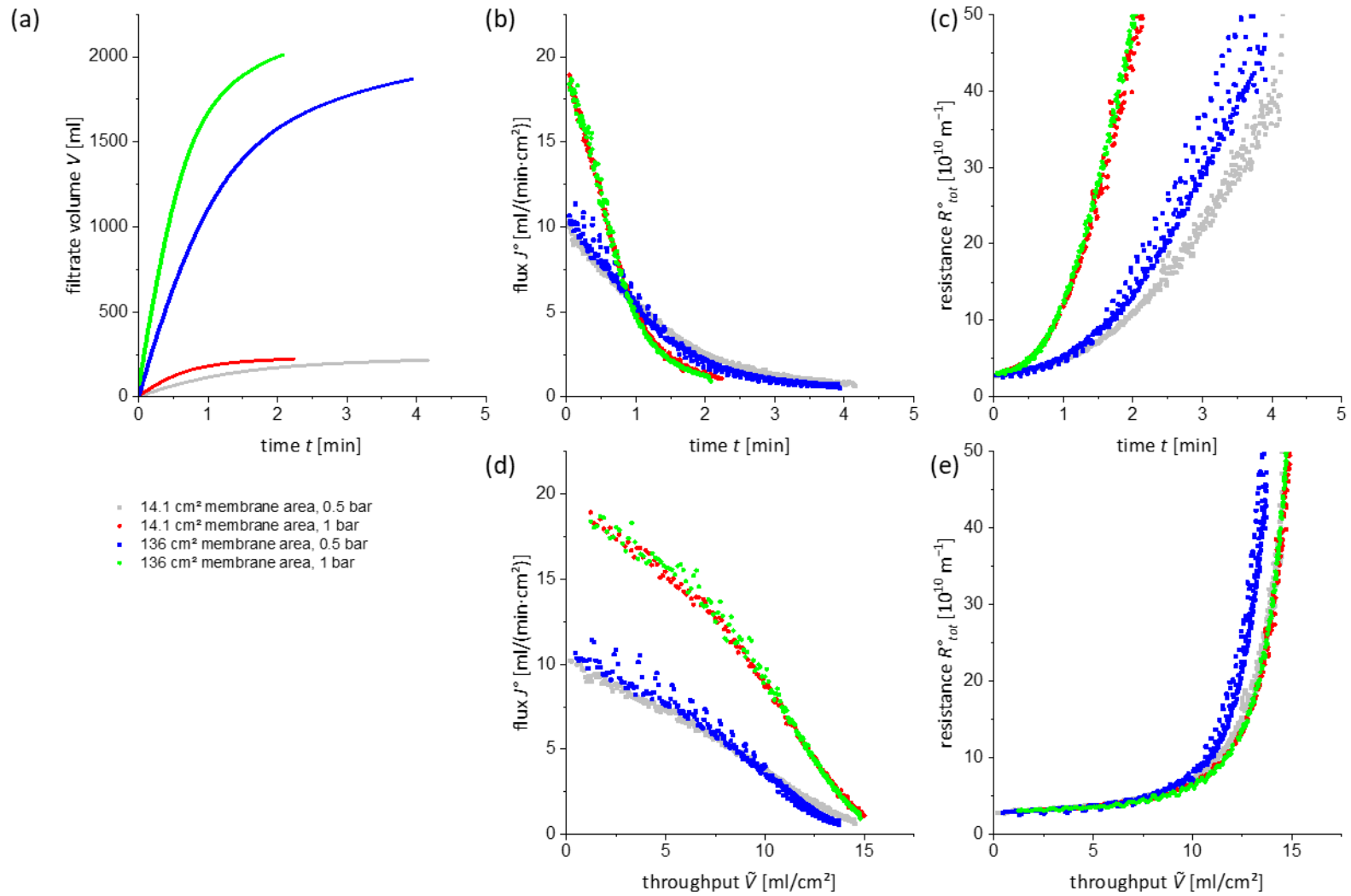


Figure 44: Results of constant pressure filtration of a particulate test solution through a 0.2 μm PES membrane with different filter area: Filtration with filter discs of 14.1 cm² (grey) and 136 cm² filter discs (blue) at 0.5 bar and 1 bar (red and green). Filtration curve (a), flux curve J° (b), resistance R_{tot}° -plot (c) and flux J° and resistance R_{tot}° versus throughput \tilde{V} (d and e).

5 Results and Discussion

Table 12: Filtration parameter for results presented in figure 44, filtration of a particulate solution at different membrane areas and different filtration pressures.

Membrane area A_{mem} [cm²]	Pressure P [bar]	Initial flux J_0^o [ml/(min·cm²)]	Time at 50% blocking $t_{50\%}$ [min]	Initial resistance R_0^o [10¹⁰ m⁻¹]	Throughput $\tilde{V}_{50\%}$ at $t_{50\%}$ [ml/cm²]
14.1	0.5	10.0	1.1	2.8	8.4
14.1	1	19.0	0.6	2.9	9.6
136	0.5	10.8	1.0	2.8	8.3
136	1	19.3	0.6	3.0	9.7

5.2.2 Impact of Process Conditions on Filtration of Protein Formulations

Aim of this section is to identify process conditions for filtration of protein formulations, which lead to low filter fouling. Filtration trials were performed with standardized protein formulations as described in chapter 4.1. Data for the 250 g/l BSA formulation (formulation 1) are summarized in figure 45 and results for filtration of the 40 mPa·s BSA formulation (formulation 2) and the γ -globulin formulation (formulation 3) are shown in figure 46 and figure 47, respectively.

Formulation 1 (table 6) was filtered through 0.2 μm PES membranes under different process conditions (figure 45). It can be easily seen that membrane resistance in the $R_{tot}^{\circ}(\check{V})$ -plot is rising faster for constant pressure filtration, and that the fouling mechanisms are different (plot f) for the two operation modes (different progress of the filtration data). Changes of pressure or flow rate within the same filtration mode have low influence on membrane fouling.

In constant flow filtration a steep increase of filtration pressure (plot d) and of the membrane resistance (plot c and f) can be observed at the beginning of each measurement. In case of constant pressure filtration the sharp increase observed for constant flow filtration can be seen as well. But in contrast to constant flow filtration $R_{tot}^{\circ}(\check{V})$ -plot continues to rise fast. Even after filtration of 15 ml/cm² the pressure in constant flow filtration at 1 ml/(min·cm²) does not reach 1 bar, whereas the flow rate of a constant pressure filtration at 1 bar is already reduced below 1 ml/(min·cm²), so the reason for the different filter fouling is the process mode and not the total process pressure.

The difference between constant flow and constant pressure filtration is that for constant pressure filtration within the membrane pores the flow rate locally remains constant. But due to the constriction of pores or pore blocking the overall flow rate is reduced. In constant flow filtration the flux rises locally; the shear rate increases as well. The increasing shear rate or the consequently lowered residence time might be beneficial to reduce membrane fouling.

Figure 46 shows the results for filtration of the 40 mPa·s BSA formulation (formulation 2) through a 0.2 μm Hydrosart membrane. Due to the high viscosity (40 mPa·s) the initial filtration flux at constant pressure filtration is 10% of the initial filtration flux of formulation 1 and the time to reach a throughput of 15 ml/cm² is distinctly increased. Again it can be observed in plot (f) that the membrane fouling at constant pressure filtration is higher in comparison to the membrane fouling at constant flow filtration. The rise in membrane resistance, i.e. the fouling degree is lower compared with formulation 1. Glycerol has a stabilizing impact on protein formulations. Additionally, the protein concentration is lower, both effects can contribute to the results.

5 Results and Discussion

The γ -globulin formulation (formulation 3) was filtered through different 0.2 μm membranes (PES, Hydrosart and PVDF_{hyd}) at different process conditions. Results are shown in figure 47. Membrane fouling was generally low, independent on type of filtration process conditions. The resistance increases up to values of $10 \cdot 10^{10} \text{ m}^{-1}$ in maximum. Due to the lower viscosity (2 mPa·s) of this formulation higher initial flow rates were reached at constant pressure filtration and higher flow rates could be realized at constant flow filtration (table 15). It should be noted that the initial resistances of the PVDF_{hyd} and the Hydrosart membrane are twice as high as the initial resistance of the PES membrane.

As a conclusion for all filtration trials it can be said that the filtration flux for protein formulations is due to the relatively high viscosity values low. Filter fouling was usually low and constant flow filtration lead to less filter fouling than constant pressure filtration. Filter fouling connected with filtration of protein formulations is usually discussed based on the surface charge of a membrane; but this cannot be the whole explanation, as different filter fouling was observed for different process conditions for the same membrane material.

Comparing the three protein formulations, formulation 1 showed the highest degree of filter fouling. The reason might be instability due to the high protein concentration. On diluting the formulation with glycerol to increase the viscosity (formulation 2), the concentration is lowered, intermolecular and intramolecular diffusion are due to the higher viscosity slowed down, the stability of the formulation is increased and less filter fouling occurs. The optimization of the composition of the γ -globulin formulation (formulation 3, chapter 5.1.1) generated a stable protein formulation without pronounced membrane fouling; this is the only protein formulation without process dependent filter fouling in the tested range.

5 Results and Discussion

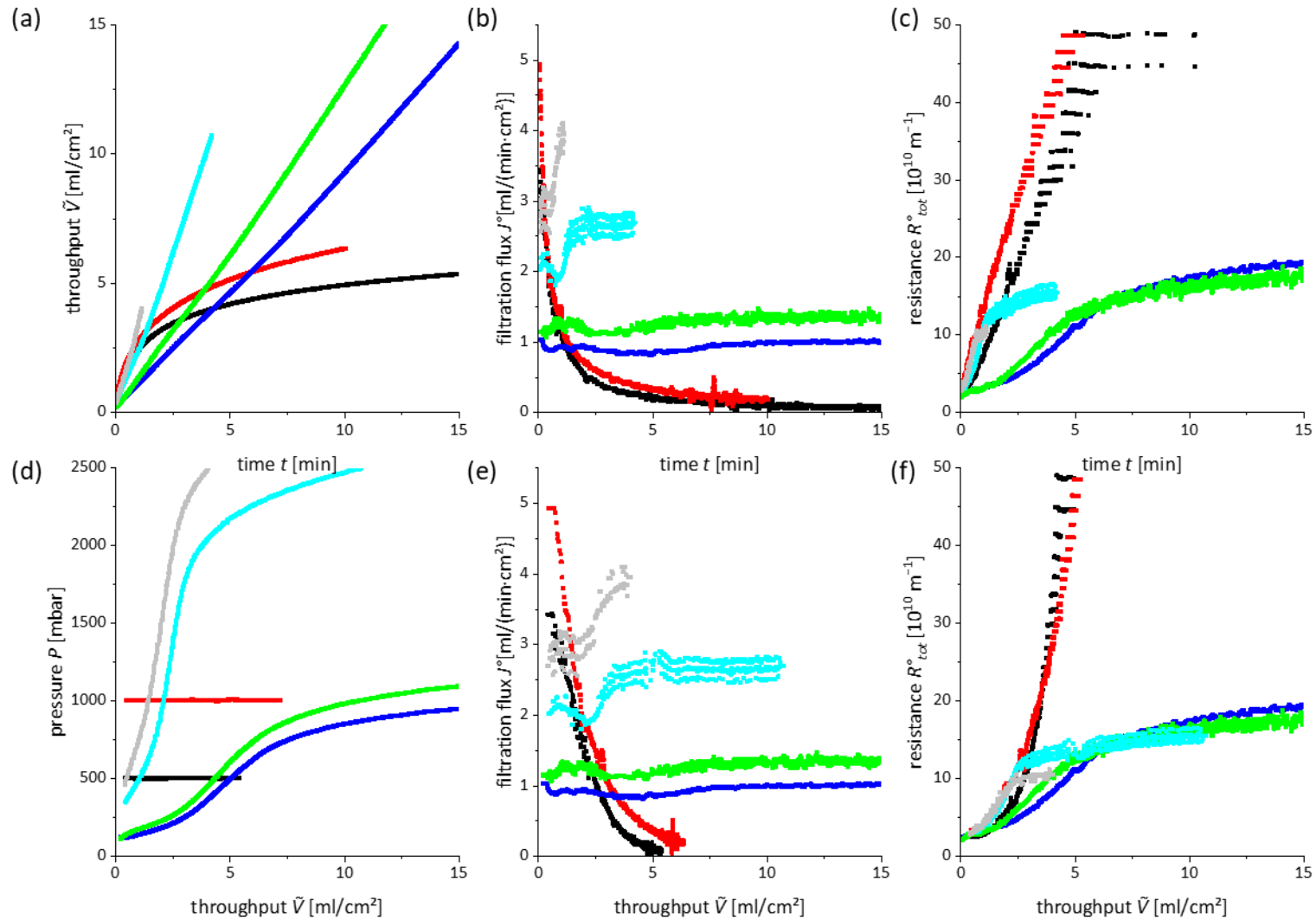


Figure 45: Results of filtration of the 250 g/l BSA formulation (formulation 1, table 6) through a 0.2 μm PES-membrane at different filtration conditions: filtration at constant pressure of 1 bar (red), 0.5 bar (black) and filtration at constant flux of 1 ml/(min·cm²) (blue), 1.3 ml/(min·cm²) (green), 2.5 ml/(min·cm²) (cyan) and 4 ml/(min·cm²) (grey).

5 Results and Discussion

Table 13: Filtration parameter for results presented in figure 45, filtration of the 250 g/l BSA formulation (formulation 1) through a PES-membrane at different process conditions.

Membrane area A_{mem} [cm²]	Pressure P [bar]	Initial flux J°_0 [ml/(min·cm²)]	Time at 50% blocking $t_{50\%}$ [min]	Initial resistance R°_0 [10¹⁰ m⁻¹]	Throughput $\tilde{V}_{50\%}$ at $t_{50\%}$ [ml/cm²]
2.75	0.5	3.4	0.6	2.3	1.9
2.75	1	5.1	0.3	3.1	1.8
Membrane area A_{mem} [cm²]	Flux J° [ml/(min·cm²)]	Initial pressure P_0 [bar]	Time at 50% blocking $t_{50\%}$ [min]	Initial resistance R°_0 [10¹⁰ m⁻¹]	Throughput $\tilde{V}_{50\%}$ at $t_{50\%}$ [ml/cm²]
2.75	1.0	0.13	1.5	2.5	1.3
2.75	1.3	0.11	0.5	2.3	0.4
2.75	2.5	0.34	0.5	2.7	1.3
2.75	4.0	0.45	0.2	2.3	1.1

5 Results and Discussion

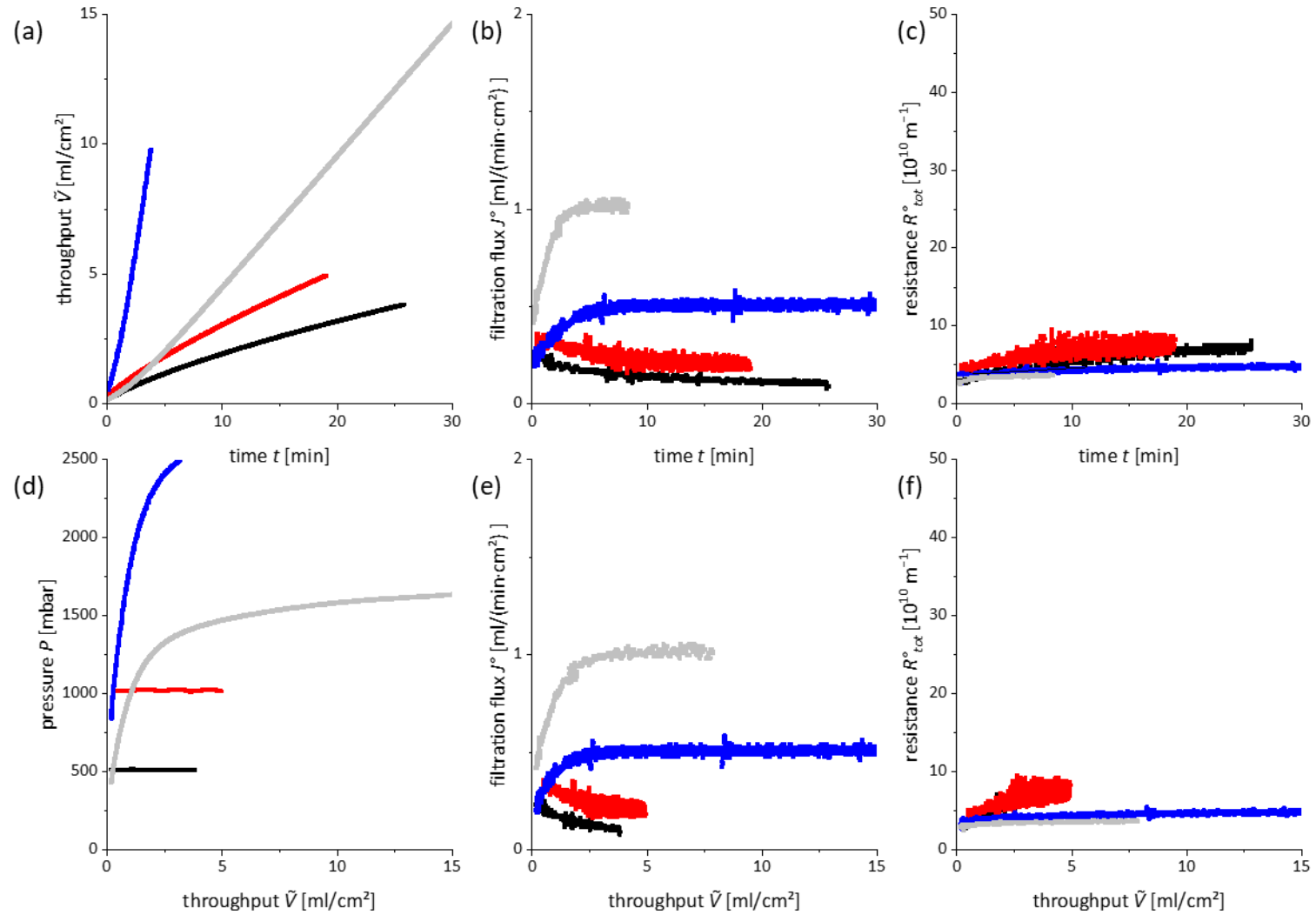


Figure 46: Results of filtration of the 40 mPa·s BSA formulation (formulation 2, table 6) through a 0.2 μm Hydosart membrane. Filtration at constant pressure of 1 bar (red) and 0.5 bar (black) and at constant flow rate of 0.5 ml/(min·cm²) (blue) and 1 ml/(min·cm²) (grey).

5 Results and Discussion

Table 14: Filtration parameter for results presented in figure 46, filtration of 40 mPa·s BSA formulation (formulation 2) through a Hydrosart membrane at different process conditions.

Membrane area A_{mem} [cm²]	Pressure P [bar]	Initial flux J°_0 [ml/(min·cm²)]	Time at 50% blocking $t_{50\%}$ [min]	Initial resistance R°_0 [10¹⁰ m⁻¹]	Throughput $\tilde{V}_{50\%}$ at $t_{50\%}$ [ml/cm²]
2.75	0.5	0.34	-	2.0	-
2.75	1	0.34	15.9	4.6	4.3
Membrane area A_{mem} [cm²]	Flux J° [ml/(min·cm²)]	Initial pressure P_0 [bar]	Time at 50% blocking $t_{50\%}$ [min]	Initial resistance R°_0 [10¹⁰ m⁻¹]	Throughput $\tilde{V}_{50\%}$ at $t_{50\%}$ [ml/cm²]
2.75	0.5	0.43	-	3.2	
2.75	1.0	0.80	-	3.0	-

5 Results and Discussion

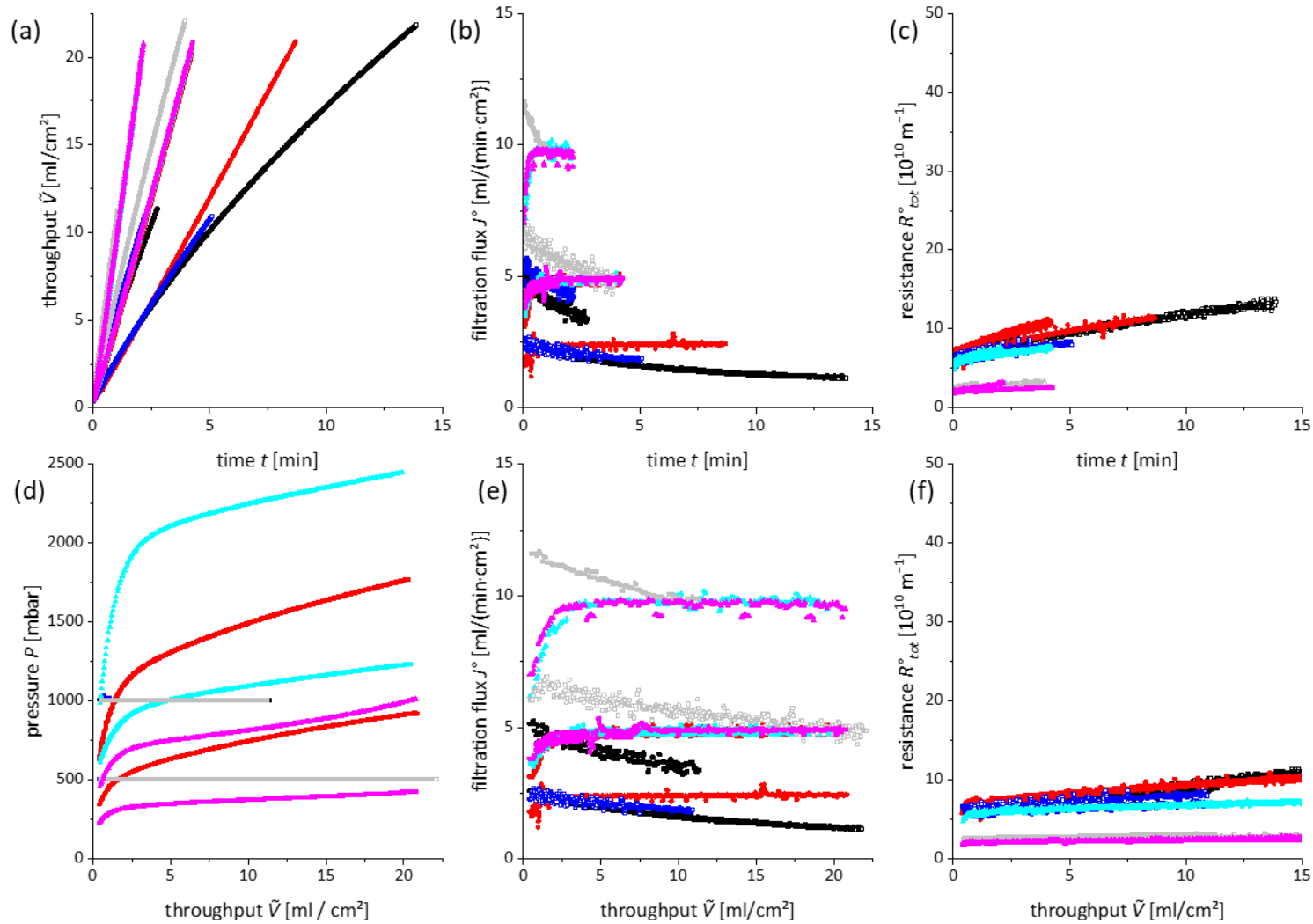


Figure 47: Results of filtration of the γ -globulin formulation (formulation 3, table 6) through different sterile filter membranes (0.2 μm nominal pore size) at different filtration conditions: constant pressure at 0.5 bar (open squares) and 1 bar (closed squares), constant flow filtrations at 2.5 ml/(min·cm²) and 5 ml/(min·cm²) (PVDF_{hyd}, circles and squares) and 5 ml/(min·cm²) and 10 ml/(min·cm²) (Hydrosart and PES, circles and squares). PES (grey, constant pressure and magenta, constant flow), Hydrosart (blue, constant pressure and cyan, constant flow) and PVDF_{hyd} (black, constant pressure and red, constant flow).

5 Results and Discussion

Table 15: Filtration parameter for results presented in figure 47, filtration of the γ -globulin formulation (formulation 3) through different sterile filter membranes; extrapolated data marked with *.

Membrane	Pressure P [bar]	Initial flux J° [ml/(min·cm ²)]	Time at 25% blocking $t_{25\%}$ [min]	Initial resistance R° [10^{10} m ⁻¹]	Throughput $\tilde{V}_{25\%}$ at $t_{25\%}$ [ml/cm ²]
PES	0.5	6.8	3.0	2.2	17.6
PES	1	11.8	4.6*	2.6	37.7*
Hydrosart	0.5	2.5	4.7	6.1	10.1
Hydrosart	1	5.5	3.1*	5.5	14.6*
PVDF _{hyd}	0.5	2.6	2.2	5.9	5.1
PVDF _{hyd}	1	5.2	1.5	5.8	6.8
Membrane	Flux J° [ml/(min·cm ²)]	Initial pressure P_0 [bar]	Time at 25% blocking $t_{25\%}$ [min]	Initial resistance R° [10^{10} m ⁻¹]	Throughput $\tilde{V}_{25\%}$ at $t_{25\%}$ [ml/cm ²]
PES	5	0.23	-	2.1	-
PES	10	0.45	1.7	2.2	16.7
Hydrosart	5	0.60	4.1*	5.6	19.9*
Hydrosart	10	0.95	-	6.0	-
PVDF _{hyd}	2.5	0.34	8.6	6.4	3.0
PVDF _{hyd}	5	0.63	2.2	7.0	10.5

Impact of Protein Concentration on Filter Fouling

For examination of the impact of the protein concentration filtration trials with different BSA concentrations (formulation 1) were performed in constant pressure mode. For this formulation 1 was prepared likewise to the preparation method described in chapter 5.1.2 with less BSA (5 g/l and 100 g/l). Hydrophilic Hydrosart and hydrophobic CN membranes were used for the filtration trials.

To obtain comparable initial flow rates the filtration pressure (table 16) is adjusted to the formulation viscosity. Throughout all the filtration trials filter fouling was really moderate and only a small increase in the membrane resistance can be observed after the filtration of 1.5 g BSA/cm². The filterability of stabilized protein formulations therefore is not dependent on the protein concentration.

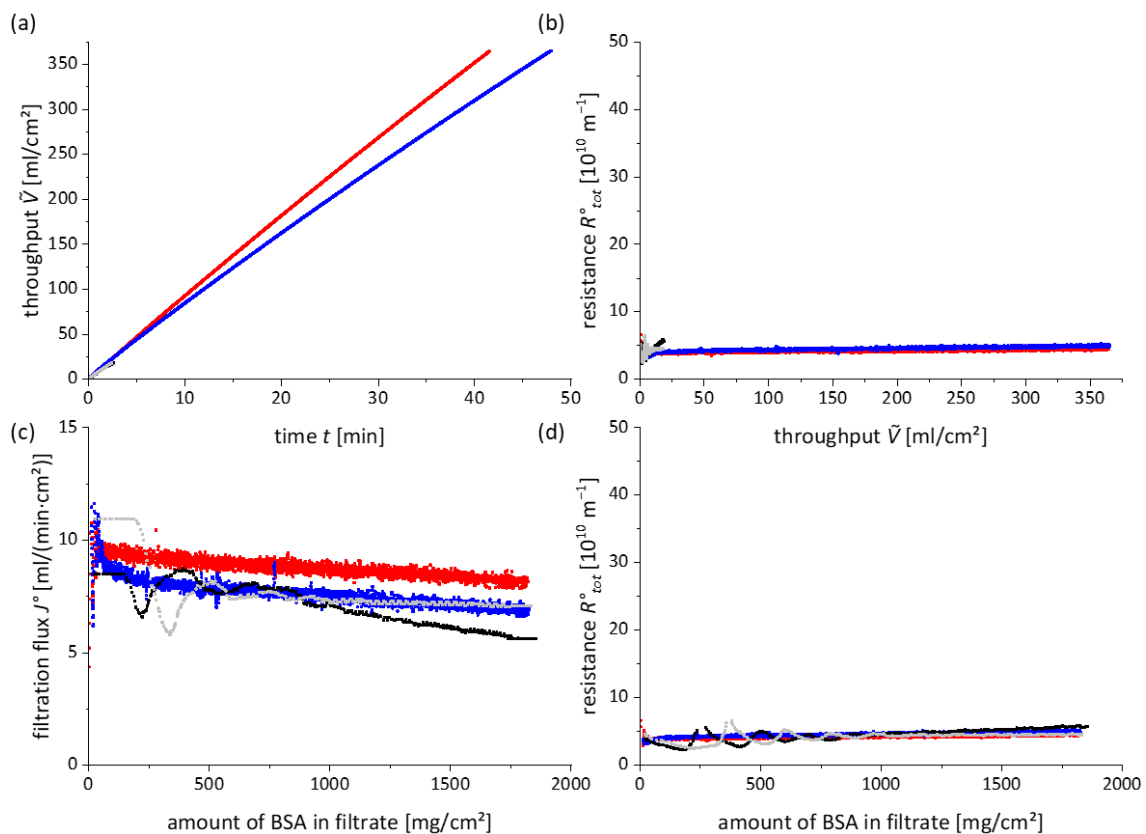


Figure 48: Results of constant pressure filtration of BSA formulation with different protein concentrations (formulation 1, table 6) through Hydrosart and CN membranes (0.2 μm nominal pore size); red: CN, 5 g/l; black: CN, 100 g/l; blue: Hydrosart, 5 g/l; light grey: Hydrosart, 100 g/l.

Table 16: Filtration parameters for results presented in figure 48, constant pressure filtration of BSA formulations with different concentration through CN and Hydrosart membranes.

Measurement	Pressure P [bar]	Initial flux J_0 [ml/(min·cm ²)]	Initial resistance R_0 [10 ¹⁰ m ⁻¹]	$R_{1.5\text{ g protein/cm}^2}^0$ [10 ¹⁰ m ⁻¹]
CN, 5 g/l	0.55	9.7	3.9	4.4
CN, 100 g/l	0.75	8.9	3.1	5.3
Hydrosart, 5 g/l	0.52	8.9	3.9	4.8
Hydrosart, 100 g/l	0.75	7.4	3.2	4.5

Impact of Filtration Time on Filter Fouling

Filtration trials are performed for several hours with diluted BSA formulations containing 2.5 g/l protein (buffer as in formulation 1). Filtration was performed with a flow rate of 6 ml/(min·cm²) through Hydrosart and CN-membranes. Figure 49 shows the filtration results. The results were inconsistent.

Both trials were performed on the same day. For the first filtration trial constant filter fouling could be observed and a steady increase in pressure. For the second trial hardly any pressure increase could be witnessed for a filtration time of two hours. Near the end of the measurement pressure increase by more than 1 bar occurred, combined with a sudden stop in filtration flux. Afterwards the pressure increase continued until the measurement was stopped. The measurements were repeated with addition of sodium azide to the formulation to eliminated bacterial growth as a reason for filter fouling, but still the results were inconsistent.

5 Results and Discussion

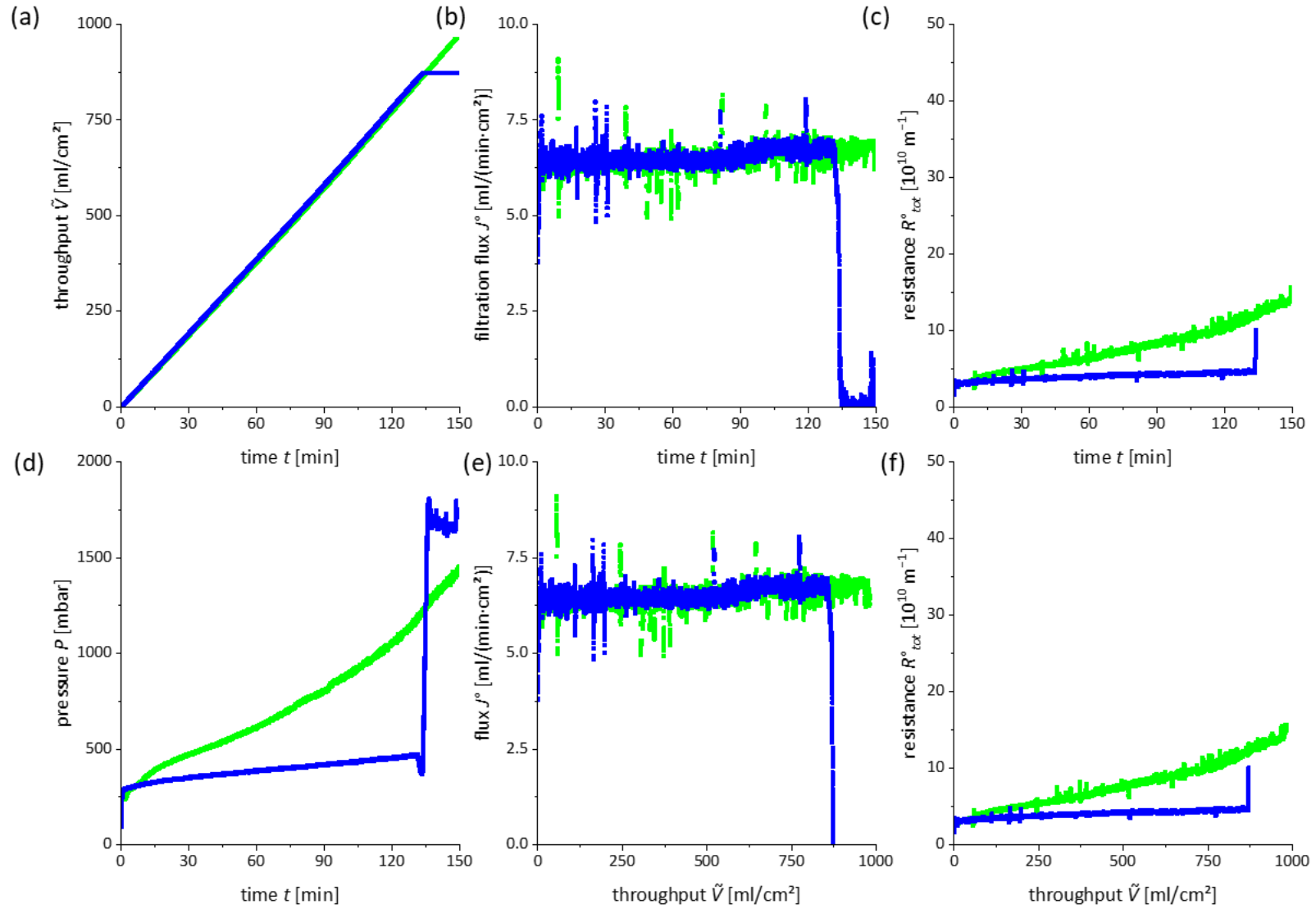


Figure 49: Results of filtration of a 2.5 g/l BSA formulation (diluted formulation 1 in table 6) through CN membranes (blue and green) at a flow rate of 6 ml/(min·cm²).

5 Results and Discussion

Table 17: Filtration parameters for constant flow filtration results as presented in figure 49: filtration of a diluted (2.5 g/l) BSA-formulation (formulation 1, table 6).

Membrane	Filtration flux J° [ml/(min·cm²)]	Initial pressure P_0 [bar]	Initial resistance R_0° [10¹⁰ m⁻¹]	$R^{\circ}_{1.5 \text{ g protein/cm}^2}$ [10¹⁰ m⁻¹]
Hydrosart	6.5	0.31	3.6	4.6
Hydrosart	6.2	0.19	4.1	18.3
CN	6.3	0.29	3.7	4.5
CN	6.5	0.22	3.8	9.1

Influence of Temperature on Filter Fouling

The effect of the filtration temperature on filter fouling was studied by filtration of 250 g/l BSA formulation (formulation 1) through CN and Hydrosart membranes at temperatures between 14 °C and 53 °C. The solution temperature were measured in-line throughout the filtration trials. The viscosity of the formulation changes with temperature. The relationship is shown in figure 50.

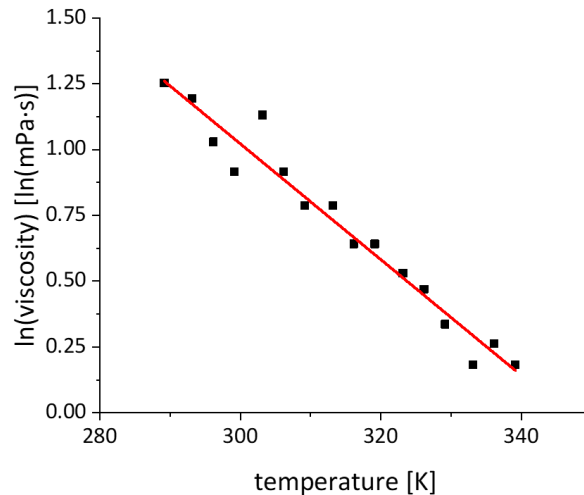


Figure 50: Viscosity of the 250 g/l formulation (formulation 1, table 6) in dependence on temperature; the linear regression has a slope of $-0.0220 \text{ ln(mPa}\cdot\text{s)/K}$ and a y-intercept of $7.62 \text{ ln(mPa}\cdot\text{s)}$.

The filtration results for the Hydrosart membrane are presented in figure 51 and for the CN membrane in figure 52. All filtrations are performed with a constant pressure of 1 bar.

The influence of the temperature on solution viscosity can be seen in both figures as well as in table 18 by the change of the initial flux, which is rising on increasing temperatures. For the hydrophilic Hydrosart membrane no temperature influence on filter fouling can be observed throughout the measurements (figure 51). For the CN membrane filter fouling increases in case of elevated temperatures (figure 52).

On elevated temperatures, two effects probably occur. First exchange reactions of the surfactant and the proteins are accelerated, second the conformational changes are speeded up and the physical stability of the protein molecules is decreased. These conformational changes might expose hydrophobic parts of the protein to the surface, and the protein adsorbs stronger on hydrophobic surfaces because the surface is less protected by the surfactant.

5 Results and Discussion

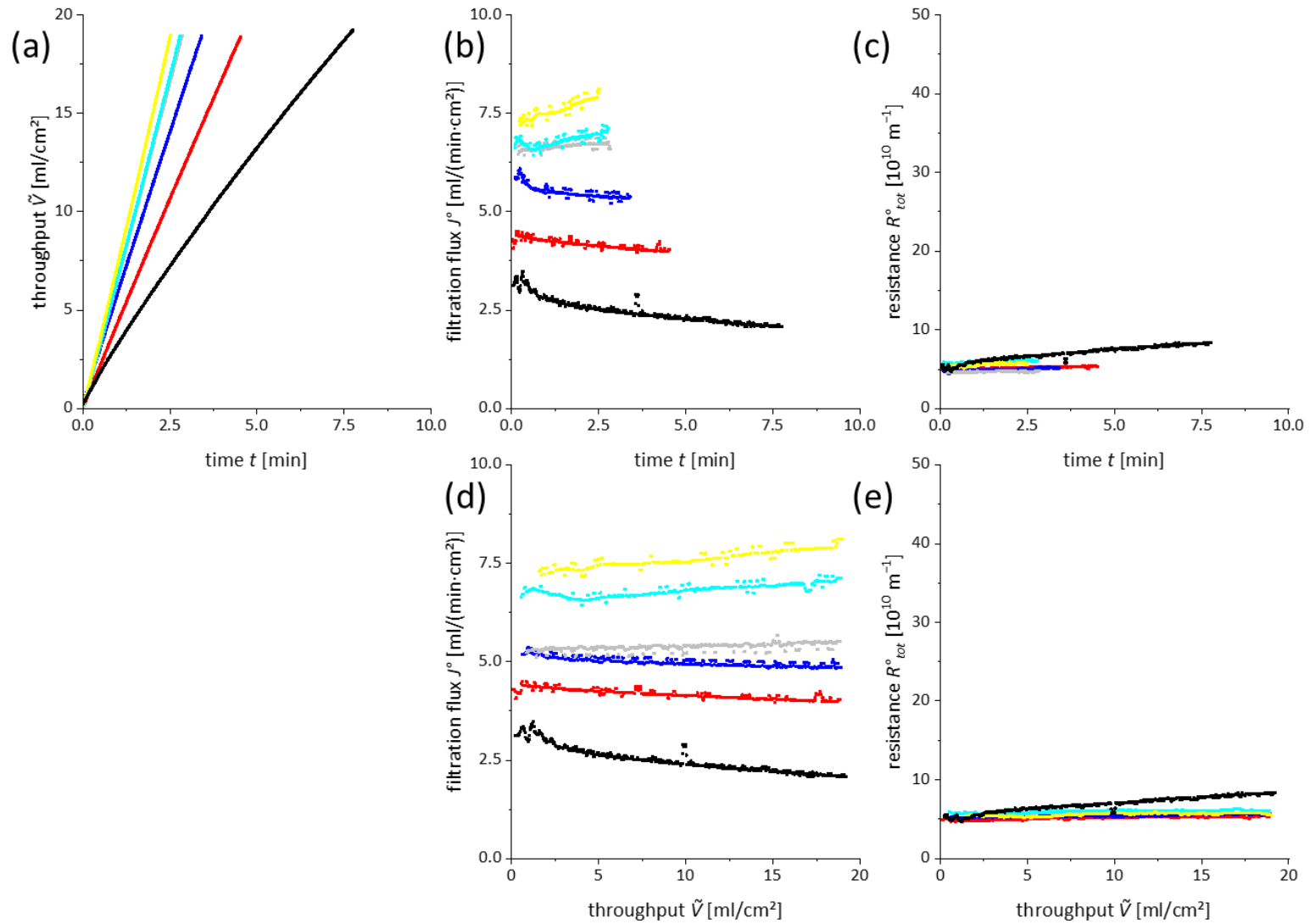


Figure 51: Filtration of the 250 g/l BSA formulation (formulation 1, table 6) at 1 bar through a Hydrosart membrane (0.2 μ m nominal pore size) at different temperatures; filtration temperatures of 14 °C (black), 17 °C (red), 29 °C (blue), 37 °C (grey), 47 °C (cyan), 53 °C (yellow).

5 Results and Discussion

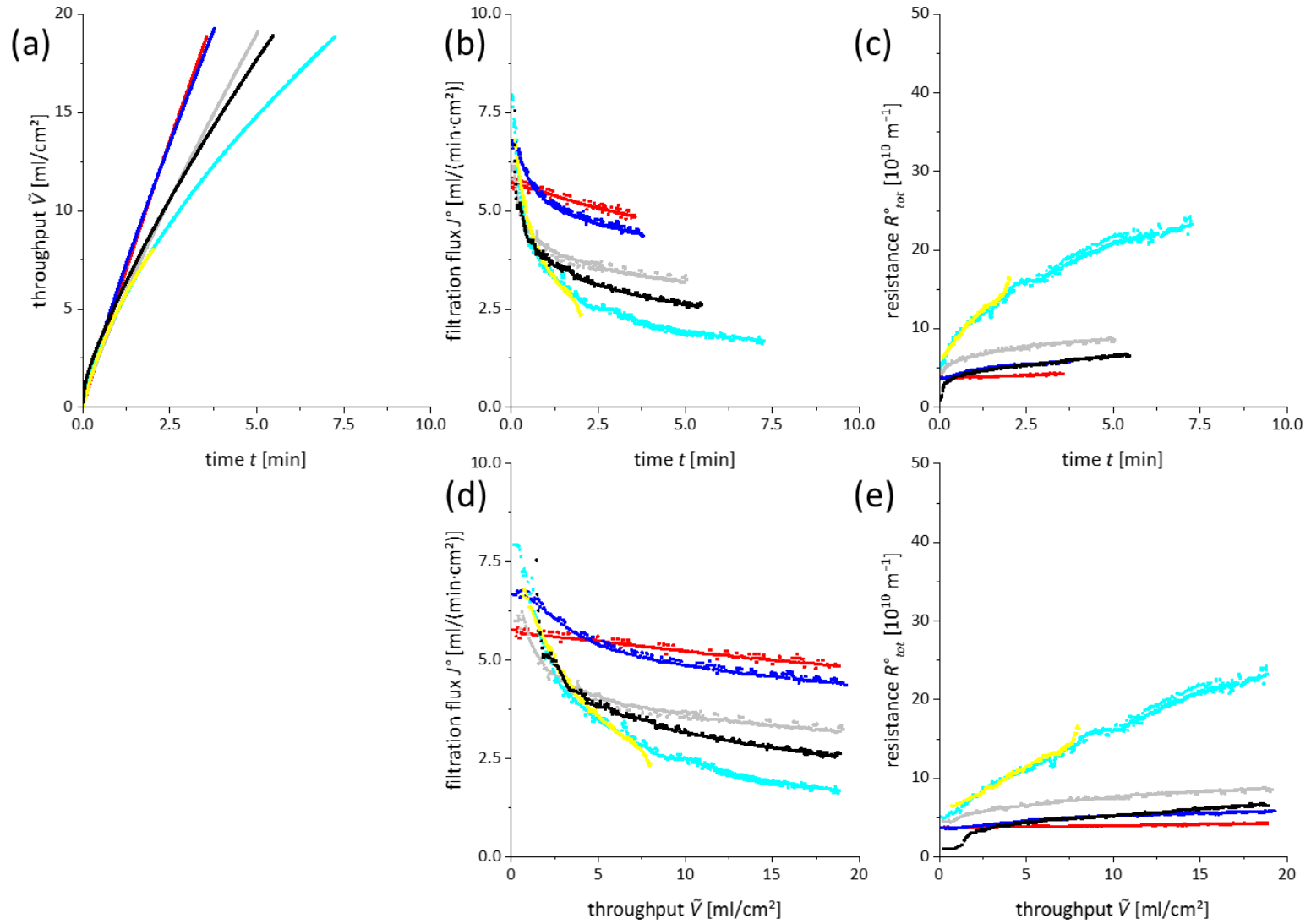


Figure 52: Filtration of the 250 g/l BSA formulation (formulation 1, table 6) at 1 bar through a CN membrane (0.2 μm nominal pore size) at different temperatures; filtration temperatures of 14 °C (black), 17 °C (red), 29 °C (blue), 37 °C (grey), 47 °C (cyan), 53 °C (yellow).

5 Results and Discussion

Table 18: Filtration parameters for results presented in figure 51 and figure 52; filtration of the 250 g/l BSA formulation (formulation 1) through Hydrosart and CN-membranes at different temperatures; extrapolated values marked with a *.

Membrane	Temperature [°C]	Viscosity η [mPa·s]	Initial flux J_0^o [ml/(min·cm ²)]	Time at 25% blocking $t_{25\%}$ [min]	Initial resistance R_0^o [10^{10} m^{-1}]	Throughput $\tilde{V}_{25\%}$ at $t_{25\%}$ [ml/cm ²]
Hydrosart	14	3.7	3.6	1.5	4.3	4.6
Hydrosart	17	3.5	4.0	18.9*	5.2	68*
Hydrosart	29	2.7	6.5	6.7*	4.1	39*
Hydrosart	36	2.3	7.1	-	4.3	-
Hydrosart	47	1.8	6.9	-	5.7	-
Hydrosart	53	1.6	7.4	-	4.8	-
CN	14	3.7	4.3	2.1	2.8	10.0
CN	18	3.4	5.7	6.1*	3.7	31
CN	28	2.7	7.1	1.0	3.5	6.2
CN	37	2.2	5.5	1.0	5.1	4.5
CN	48	1.7	8.0	0.2	6.7	1.6
CN	56	1.5	7.2	0.3	7.0	1.8

Characterization of Protein Formulation after Filtration

Protein formulations were characterized by rheology, DLS, and UV-measurements before and after filtration trials to examine the impact of the filtration on the quality of the protein formulation. Results were in all cases similar, so only a few examples are presented. Measured values showed some variation but were always in the expected range.

Figure 53 summarizes results for the analysis of the 250 g/l BSA formulation (formulation 1) before and after filtration with the membrane material given in the description. The UV-measurements (figure 53a) vary within a range of 2%, which is the specification of the instrument. The DLS measurements (figure 53b) show the same particle sizes before and after the measurements as well. The variation for the rheology measurements (figure 53c) can be accounted to an error on the measurement (not enough sample solution) as a consequence the measured viscosity after the pre-filtration and after filtration with the CA membrane is in this case too low.

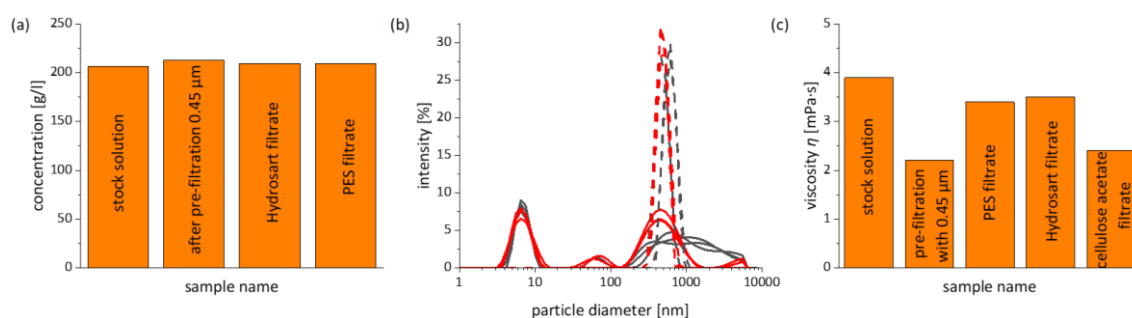


Figure 53: Characterization of the 250 g/l BSA formulation (formulation 1, table 6) after pre-filtration and filtration through different sterile filter membranes (0.2 µm nominal pore size): (a) protein concentration (UV-measurement); (b) particle size distribution: DLS-measurement after pre-filtration with 0.45 µm membrane (black) and after filtration with a PES 0.2 µm membrane (red) for 173° scatter angle (straight lines) and 12.8° scatter angle (dashed lines); (c) viscosity.

Figure 54 presents the results of the analysis of the 40 mPa·s BSA formulation (formulation 2) after filtration with the membranes given in the description. Here UV measurement of protein concentration is not possible due to experimental reasons, only DLS and rheology data were monitored.

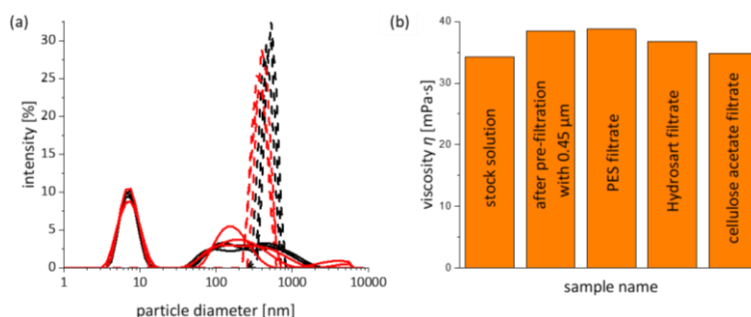


Figure 54: Characterization of the 40 mPa·s BSA formulation (formulation 2, table 6) after pre-filtration and filtration through different sterile filter membranes (0.2 µm nominal pore size): (a) particle size distribution: DLS-measurement after pre-filtration with 0.45 µm membrane (black) and after filtration with a PES 0.2 µm membrane (red) for 173° scatter angle (straight lines) and 12.8° scatter angle (dashed lines); (b) viscosity.

5 Results and Discussion

Figure 55 illustrates the results of the analysis of the γ -globulin formulation (formulation 3). After filtration the results for all measurements are within the expected range. Despite dilution to less than 0.5 g/l, multiple scattering still could be observed in the DLS-experiment. Therefore, the validity of these results cannot be entirely confirmed.

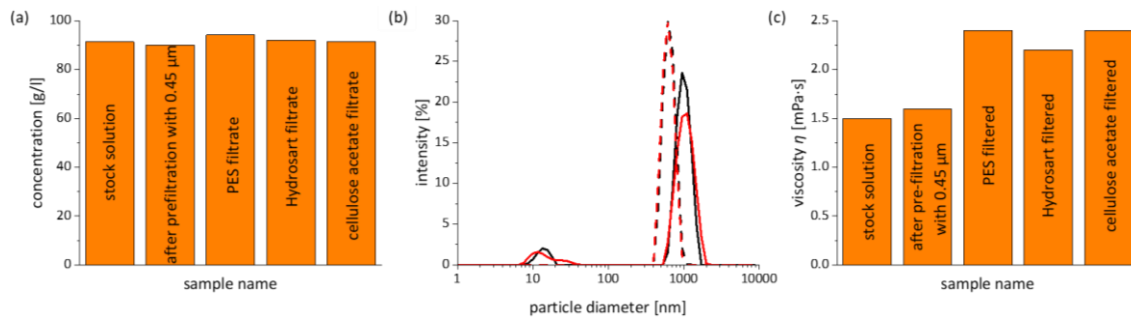


Figure 55: Characterization of the γ -globulin formulation (formulation 3, table 6) after pre-filtration and filtration through different sterile filter membranes (0.2 μm nominal pore size): (a) protein concentration (UV-measurement); (b) particle size distribution: DLS-measurement after pre-filtration with 0.45 μm membrane (black) and after filtration with a CA membrane (red) for 173° scatter angle (straight lines) and 12.8° scatter angle (dashed lines); issues with multiple scattering; (c) viscosity.

5.2.3 Influence of Membrane Structure and Material on Fouling

The influence of membrane structure and material was repeatedly studied with filtration trials in constant pressure and constant flow mode for all three protein formulations. In all trials the same trend is observed. Figure 56 presents the results in an exemplary way for constant pressure filtration of the 250 g/l BSA formulation (formulation 1) at 0.5 bar filtration through a selection of 0.2 μm membranes made of different polymeric materials.

It can be seen in figure 56d that the initial filtration fluxes measured for filtration through different membranes are decreasing in the order of PES, CA, CN, Hydrosart, PVDF_{hyd} and PA, which is more or less the same order as for the water flux measurements presented in table 8. Filter fouling as indicated by alteration of the resistance in course of filtration (figure 56e) changes in the same sequence with lowest values for the PES membrane with the highest flux and consequently the most open pore structure.

The resistance vs. throughput plots (figure 56e) show comparable behavior for PES-, Hydrosart, PVDF_{hyd} and PA membrane. The fouling process observed for filtration through the CA membrane is slowed down compared with the fouling rate of the PES membrane, probably due to the fleece-support embedded in the CA membrane. Contrary to this, the fouling process observed for filtration through the CN membrane seems to be accelerated, probably because of the hydrophobic membrane properties.

5 Results and Discussion

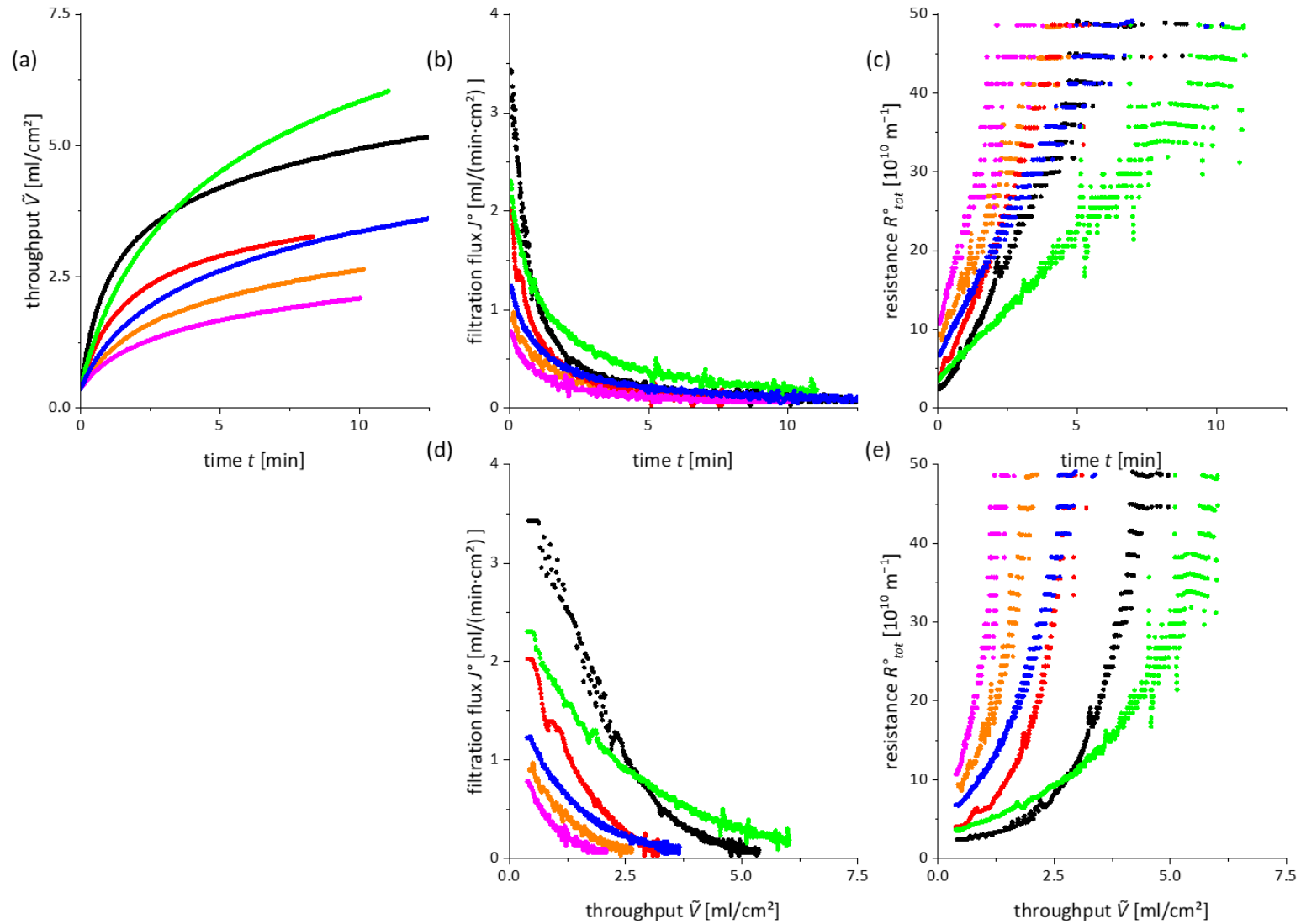


Figure 56: Results for filtration of the 250 g/l BSA formulation (formulation 1, table 6) through different sterile filter membranes (0.2 μm nominal pore size) at 0.5 bar; membranes: PES (black), CA (green), CN (red), Hydrosart (blue), PVDF_{hyd} (orange) and PA (magenta).

5 Results and Discussion

Table 19: Filtration parameters for results presented in figure 56, filtration of the 250 g/l BSA formulation (formulation 1) through different sterile filter membranes at 0.5 bar.

Membrane	Initial flux J_0 [ml/(min·cm²)]	Time at 50% block- ing $t_{50\%}$ [min]	Initial resistance R_0 [10¹⁰ m⁻¹]	Throughput $\tilde{V}_{50\%}$ at $t_{50\%}$ [ml/cm²]
PA	0.8	0.9	10.4	0.8
PVDF _{hyd}	1.1	0.8	9.3	0.9
Hydrosart	1.2	1.1	6.6	1.3
CN	2.1	0.7	3.9	1.3
CA	2.3	1.0	3.4	1.9
PES	3.4	0.6	2.3	1.9

Figure 57 summarizes data for filtration of all three protein formulations through different 0.2 μm membranes. Presented are the membrane resistances after the filtration of 500 mg protein/cm² at constant pressure of 0.5 and 1 bar and the water flux values. It can be seen that the fouling tendency is always stronger for membranes with lower water flux. Furthermore, the fouling rate of formulation 1 is quite stronger than the filter fouling observed for the two other protein formulations.

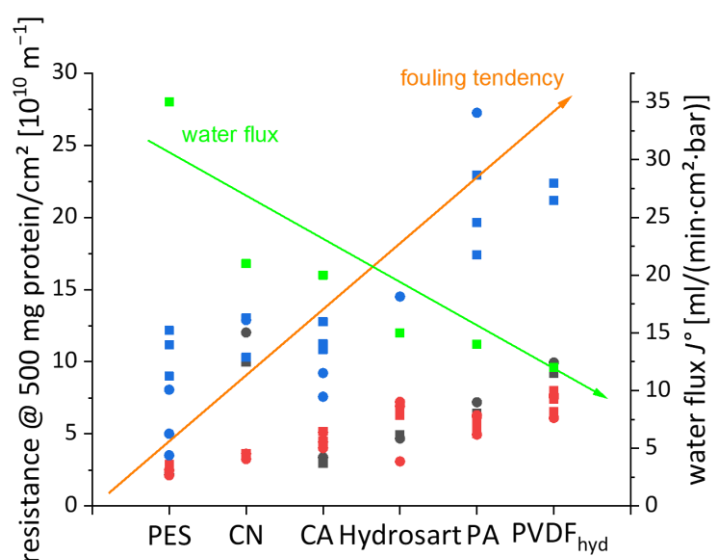


Figure 57: Membrane resistance related to passage of 500 mg protein through the filter during filtration of all three studied protein formulations (table 6) through various microfilter membranes at 0.5 bar (circles) and 1 bar (squares) compared with water flux of the studied membranes (0.2 μm nominal pore size): 250 g/l BSA (formulation 1, blue), 40 mPa-s BSA formulation (formulation 2, black), γ -globulin formulation (formulation 3, red); water flow rate (green).

In result of these investigations it can be concluded that filter fouling during filtration of stable and drug-like protein formulations is strongest for membranes with narrow pore sizes and consequently low water flow rates. The surface properties of the membranes were found to be of minor importance in this case. This result is quite contrary to the expectation of stronger filter fouling for hydrophobic membranes. More insight into that matter is given in result of adsorption measurements, described in chapter 5.4.

An explanation of the observed behavior is presented in figure 58. Here the correlation between the measured mean flow pore size (porometry measurement) and the membrane resistance (calculated by water flux) is shown to demonstrate the effect of the deposition of protein layers on the membrane surface on membrane resistance (fit to data collected by SSB). According to theory, protein deposit within the membrane pores due to adsorption. An adsorbed protein layer with BSA (7 nm in diameter) constricts the pores by 14 nm. Therefore the resistance increases, the whole dataset shifts in x-direction. To enlarge the effect, the shift is calculated for up to three protein layers. For a narrow

membrane type, the increase in resistance is much more pronounced than for a more open membrane. For this reason the fouling observed during filtration can be observed more clearly for membranes with narrow pore size distribution and lower initial filtration flow.

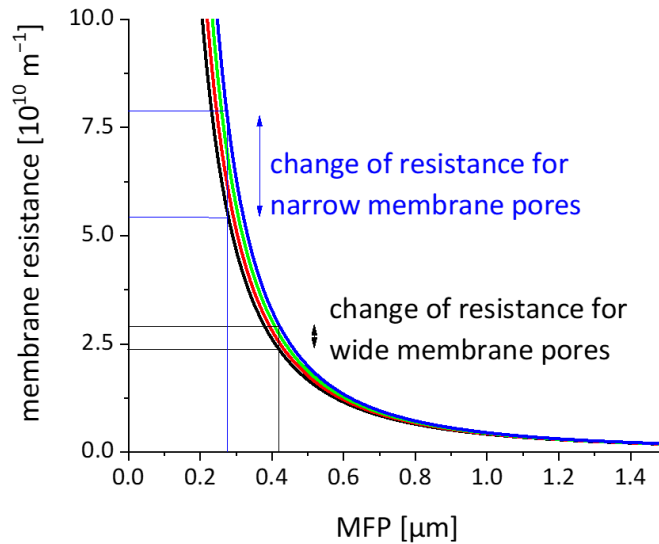


Figure 58: Resistance in dependence on MFP size for microfilter membranes with different protein (BSA) fouling layers: no fouling layer (black); protein monolayer (red), protein double layer (green); three protein layers (blue).

5.2.4 Localization of Fouling Layer Within the Membrane Material

In this section it is examined where in a membrane cross section filter fouling occurs on filtration with protein formulations. The protein fouling layer within a Hydrosart membrane is visualized after filtration with the BSA formulation (formulation 1) at 2.5 and 200 g/l and with different process conditions by staining both membrane and protein fouling layer with fluorescent dyes. The experimental details are presented in section 4.6.a

Figure 59 a) and b) visualize filter fouling with BSA formulations of different protein concentrations after constant flow and constant pressure filtration, respectively. In both cases similar fouling is observed. As figure 59 shows, fouling does not occur homogeneously on the surface of this membrane. Instead the fouling layer is located in a thin area of the membrane cross section. This part of the membrane cross section is characterized by a narrow pore size distribution as indicated by analysis of additional REM images, as can be seen in figure 60.

Images of the cross-sections of membranes after filtration of 2.5 g/l BSA formulation and 200 g/l BSA formulation are quite comparable. This shows once more that filterability of stabilized protein formulations does not depend on the protein concentration.

5 Results and Discussion

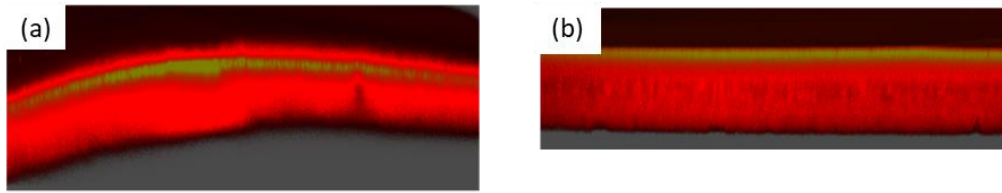


Figure 59: Fluorescence confocal microscopy image of protein fouling after filtration of BSA formulation (formulation 1, table 6) through a Hydrosart membrane ($0.2\ \mu\text{m}$ nominal pore size). (a) Filtration of $2.5\ \text{g/l}$ BSA at a flow rate of $7\ \text{ml}/(\text{min}\cdot\text{cm}^2)$ and (b) filtration of a $200\ \text{g/l}$ BSA formulation at constant pressure of $0.5\ \text{bar}$. Upstream side to the top

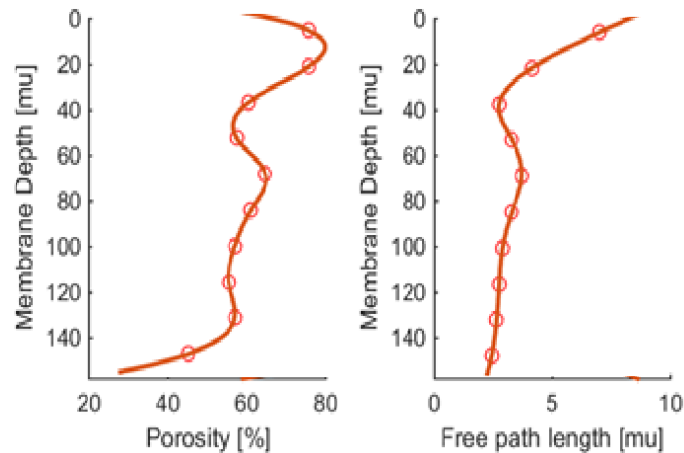


Figure 60: Pore size distribution and porosity within a cross-section of the Hydrosart membrane used for filtration in figure 59 and figure 61. Upstream side to the top.

Figure 61 a) and b) visualize fouling after filtration through two membrane layers, which were assembled in the same membrane housing; here it can be seen that fouling is concentrated in the upstream layer, whereas less protein can be detected in the second downstream membrane layer. But even there fouling is localized within a thin area of the membrane cross section. These results are in accordance to literature (figure 20, chapter 3.2.3). Here as well a thin layer near the membrane surface is reported where the protein fouling layer is localized, and no homogeneous distribution or a cake on top of the membrane was observed.

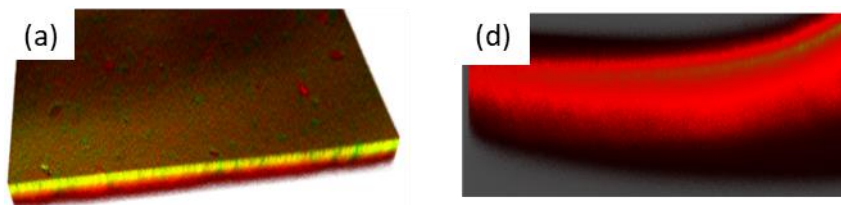


Figure 61: Fluorescence confocal microscopy image of protein fouling after filtration of BSA formulation (formulation 1, table 6) through a Hydrosart membrane ($0.2\ \mu\text{m}$ nominal pore size). Filtration of the $2.5\ \text{g/l}$ BSA formulation through two sheets of membrane embedded in one membrane housing at a flow rate of $19.6\ \text{ml}/(\text{min}\cdot\text{cm}^2)$: upper layer (a), second layer (b), upstream side to the top.

5.2.5 Pre-Filter and Main Filter Combinations

Pre-filter and main filter combinations were usually used to protect the main filter from fouling by particles or aggregates from the fluid stream. The protective role of the pre-filter is shown in an exemplary way in figure 62 for filtration of a particulate test solution through a PES pre-filter/main filter combination at 1 bar. The same behavior can also be demonstrated for pre-filter/main filter combinations made by PA or CA-membranes.

Figure 63 shows results for filtration of the 250 g/l BSA formulation (formulation 1) through the PES pre-filter/main filter combination. Here the pre-filter has no protective function, it only increases the total resistance of the membrane layers. The same behavior can again be demonstrated for PA or CA-membranes. Therefore, the use of pre-filters for filtration of protein solutions is only recommended if the fluid stream contains a particulate contamination, e.g., large aggregates, which is not the case for formulations 1 to 3 (table 6).

5 Results and Discussion

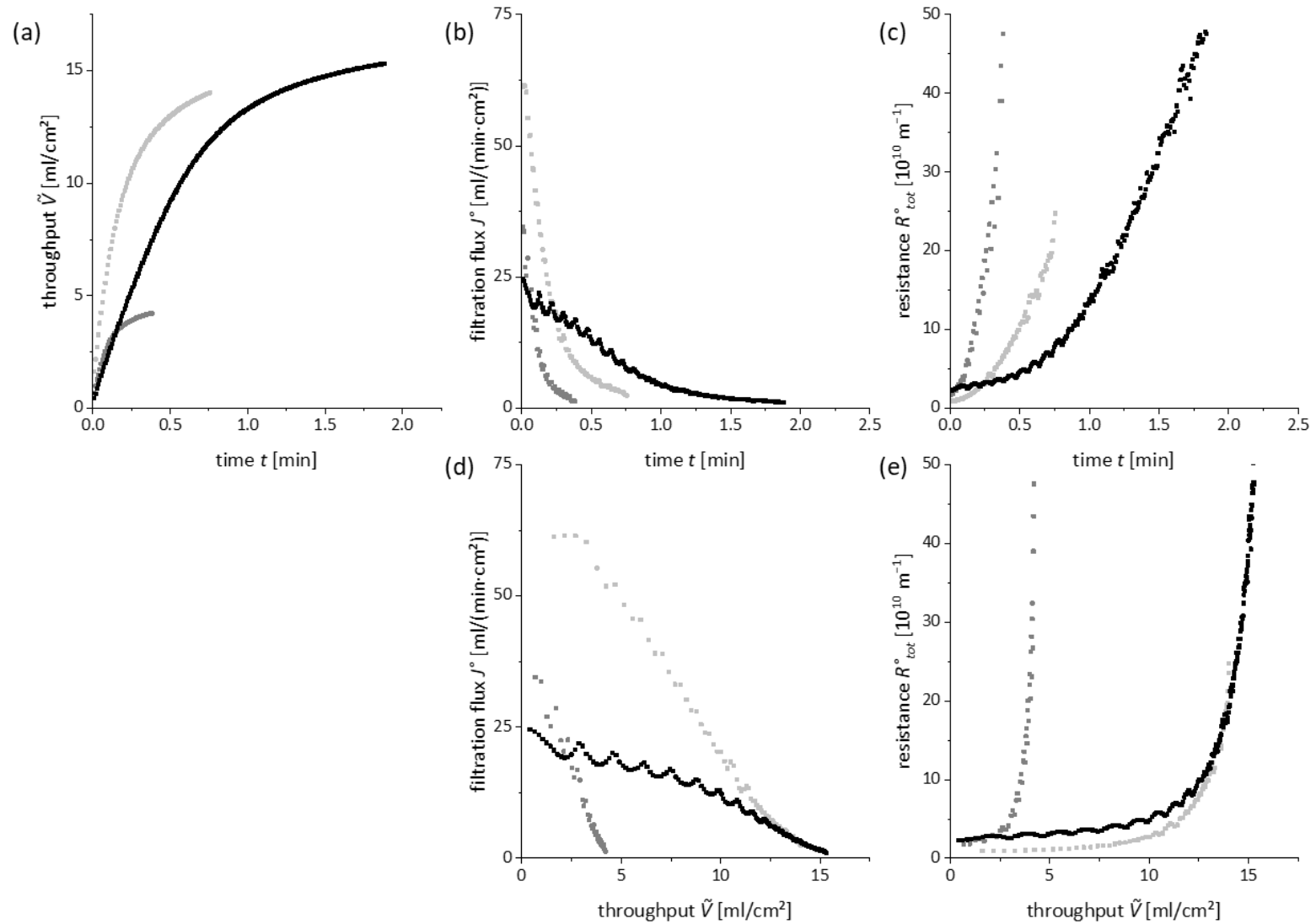


Figure 62: Results of filtration of a particulate test solution (chapter 4.1) with a PES pre-filter/main filter combination (0.45 μm /0.2 μm) at constant pressure of 1 bar. Pre-filter (light grey), main filter (dark grey) and the combination of both (black).

5 Results and Discussion

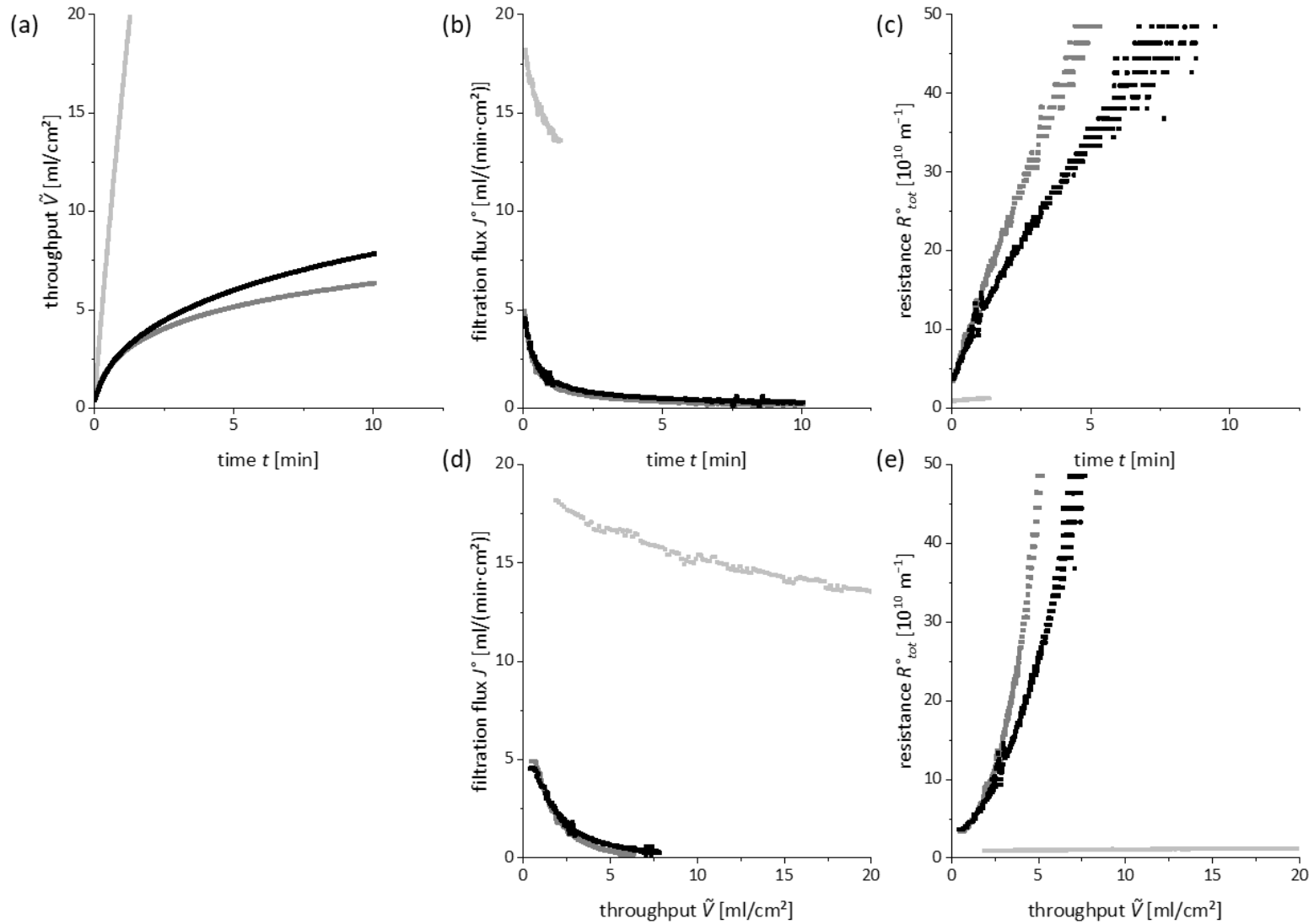


Figure 63: Results of filtration of the 250 g/l BSA formulation (formulation 1, table 6) with a PES pre-filter/main filter combination (0.45 μm /0.2 μm) at constant pressure of 1 bar; pre-filter (light grey), main filter (dark grey) and the combination of both (black).

5 Results and Discussion

Table 20: Characteristic filtration parameters for filtration of a particulate formulation and the 250 g/l BSA formulation (formulation 1, table 6) through PES membranes (pre-filter, main filter and combination) as presented in figure 62 and figure 63.

Particulate formulation					
Membrane	Nominal pore size [μm]	Initial flux J°_0 [ml/(min·cm ²)]	Time at 50% blocking $t_{50\%}$ [min]	Initial resistance R°_0 [10 ¹⁰ m ⁻¹]	Throughput $\tilde{V}_{50\%}$ at $t_{50\%}$ [ml/cm ²]
Pre-filter	0.45	68.3	0.1	0.8	7.6
Main filter	0.2	34.1	0.8	2.0	2.2
Combination	0.45 + 0.2	22.4	0.6	2.2	10.1
Formulation 1					
Pre-filter	0.45	19.1	0.9	0.9	14.8
Main filter	0.2	5.1	0.3	3.1	1.8
Combination	0.45 + 0.2	4.6	0.5	3.5	2.0

5.2.6 Summary

Filtration trials were performed with stabilized protein formulations comparable to therapeutic drug products. The respective filtration flux is low due to the viscosity of the respective formulations; therefore, shear rates are not critical. Constant flow filtration leads to less filter fouling than constant pressure filtration. Filter fouling is generally low for filtration of stabilized protein formulations, therefore, filter blocking is usually no issue for Fill and Finish filtration.

Filterability of stabilized protein formulations does not depend on the protein concentration. Protein formulations were characterized after filtration. No significant quality changes could be observed. Filter fouling does not homogeneously cover the whole membrane surface, but starts in the narrowest parts of the cross-section of a membrane.

Most important fouling mechanism is the gradual decrease of the pore diameters due to deposition of protein molecules. Therefore, membranes with open pore size distribution should be used for filtration of protein formulations. Pre-filters are unnecessary unless the protein formulation contains particulate impurities or larger aggregates.

Even stabilized protein formulations can be destabilized by process conditions. Therefore, filter fouling can occur spontaneously. The temperature is an important parameter for process filtration. For low temperatures the viscosity is increased and the filtration takes more time. Upon elevated temperatures conformational changes are accelerated and the hydrophobic interior of proteins can interact with surfaces, which causes additional fouling, especially on hydrophobic filter surfaces. Membranes with hydrophilic surface should be used for filtration because of lower fouling tendency even at challenging filtration conditions.

A particulate solution is no good surrogate for filtration trials with protein formulations due to different blocking mechanism. Further investigations are necessary to study the filterability of non-stabilized protein formulations, e.g., bulk drug substance filtration, which are probably more challenging.

5.3 Development of Scale-Up Concept for Biopharmaceutical Process Filtration

The aim of this section is the development of an approach that predicts filtration process parameters. This approach is based on a flow rate and resistances-in-series model built on Darcy's equation, and does not require knowledge of the blocking mechanism.

In chapter 5.3.1 it is described how basic system parameters, as the resistance of a filtration device and the active filtration area can be determined by water flow rate measurements. Furthermore, the influence of the types of connectors for the resistance of the filter devices is explained. Based on this, the development of the up-scaling model and the calculation basis are described. Then three scalability case studies with protein formulation are reported in chapter 5.3.2.

5.3.1 Resistances and Active Filter Areas of Filtration Devices

Water Flow Rate Measurements – Characterization of Devices

According to this approach, up-scaling studies begin with water flow rate measurements to determine the resistance and the active membrane area of the studied filtration devices. Water flow rates were measured with T-Style MaxiCaps® and In-line MaxiCaps® at 0.1, 0.2, 0.3, 0.5, 1, 1.5 and 2 bar. Measurements were performed using a rotary pump, with a limit of 180 l/min as described in section 4.5.1. For In-line MaxiCaps® with SS connectors and BB connectors at 1-2 bar these setup restrictions could be observed during the measurements.

An overview of the different connectors is presented in figure 64 and in table 21. It can be seen that the connectors differ distinctly concerning their inner diameters.

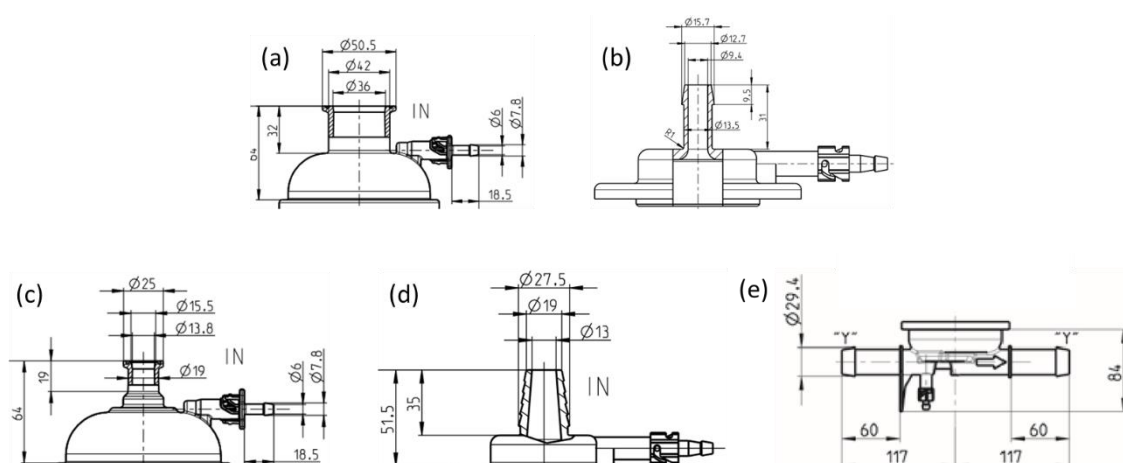


Figure 64: Drawings of connector types. S-connector (a) and O-connector (b) for In-line MaxiCaps® and T-Style MaxiCaps®, F-connector (c) and B-connector (d) for In-line MaxiCaps® and Y-connector (e) for T-Style MaxiCaps [161–165].

Table 21: Overview of connectors for MaxiCaps®.

Device	Connectors
In-line MaxiCaps®	S = 1 ½" tri-clamp (inner diameter of 36 mm), O = ½" single stepped hose barb (inner diameter of 9.4 mm) B = ¾ -1" multiple stepped hose barb (13 mm) F = ¾" tri-clamp (13.8 mm)
T-Style MaxiCaps®	S and O as for In-line MaxiCaps® Y = 1" single stepped hose barb (inner diameter of 19 mm)

Experimental results are summarized in figure 65. Connectors have a limiting influence on the flow rate, which is strongest for O-connectors (½" single stepped hose barb with an inner diameter of 9.4 mm). T-Style MaxiCaps® (a) and In-line MaxiCaps® (b) use partially different connectors. Using the same connectors (S and O), In-line MaxiCaps® achieve a higher flow rate compared to T-Style MaxiCaps®.

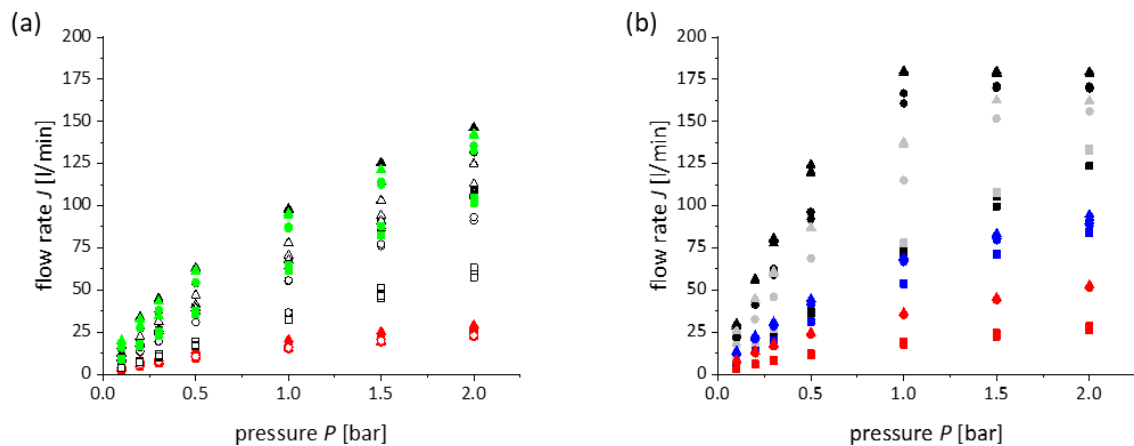


Figure 65: Results of water flow rate measurements of T-Style MaxiCaps® (a) and In-line MaxiCaps® (b) of Sartopore 2 at different filtration pressures. SS-connectors (black), OO-connectors (red), YY-connectors (green), BB-connectors (light grey) and FF-connectors (blue). Membrane area of 0.6 m² (squares), 1.2 m² (circles) and 1.8 m² (triangles) and membranes with a nominal pore size of 0.2 µm (closed symbols) and 0.1 µm (open symbols).

The resistance of a filter device R_{tot} is the sum of the resistance of the membrane housing and the resistance of the membrane:

$$R_{tot} = R_{housing} + R_{mem} \quad (24)$$

As can be seen in figure 65 with a wider pore size distribution (closed symbols compared to open symbols) a higher water flow rate can be obtained. Furthermore, with a higher membrane area a higher water flow rate can be observed as well. The connectors and their design have a huge impact. Therefore the description of the housing resistance is focused on the connectors of the devices, which were studied here and no further influences (pleating, non-woven, etc.) were considered.

5 Results and Discussion

The Darcy equation is a special solution of the Navier-Stokes equation and can be applied in case of low Reynolds numbers. For a device with SS-connectors (inner diameter of 36 mm) a Reynolds number of $7.8 \cdot 10^4$ is calculated according to equation 25, assuming a water flow rate of 132 l/min at 1 bar. This high Reynolds number clearly indicates turbulent behavior.

$$Re = \frac{J \cdot \rho \cdot d_i}{A_{SS-connector} \cdot \eta} = \frac{132 \frac{\text{l}}{\text{min}} \cdot 1 \frac{\text{kg}}{\text{l}} \cdot 36 \text{ mm}}{\pi \cdot 18^2 \text{ mm}^2 \cdot 1 \text{ mPa} \cdot \text{s}} = 7.8 \cdot 10^4 \quad (25)$$

Therefore, it can be assumed that the resistance of a filter device depends on the flow rate under condition of process filtration. For the membrane, it was demonstrated in chapter 3.2.2 that fluid flow through the membrane pores is laminar. Altogether, fluid flow through filter devices is determined by device design and tubing, and the porosity of the membrane used (figure 65). As the flow velocity through the tubing within a filter housing is large, the additional resistance occurs probably due to a force similar to friction, which would be linear to the velocity. To test this, first the total resistance of the devices is plotted against the water flow rate. The total resistance of a device is calculated by the Darcy-equation without consideration of the membrane area. The results are presented in figure 66. Here the total resistance R_{tot} in dependence on the water flow rate is shown. It can be seen that there truly is a linear relationship of the resistance of a filter device and the filtration flow rate.

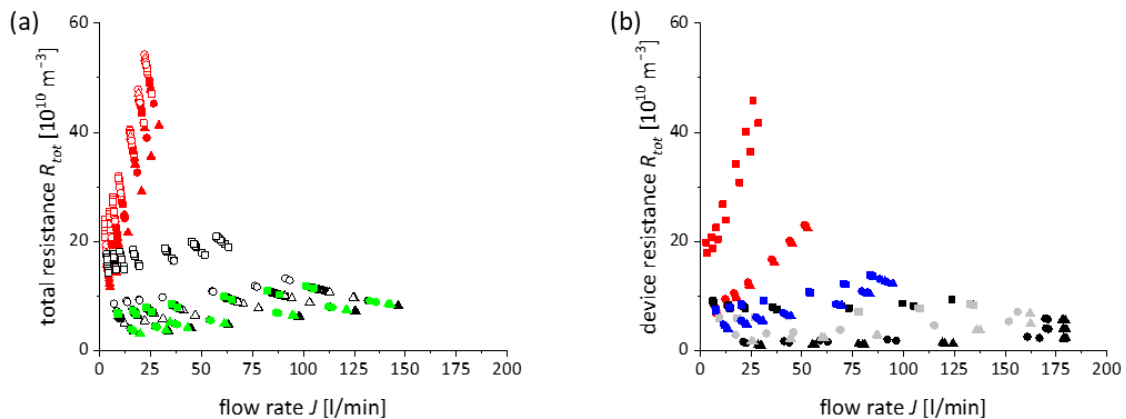


Figure 66: Total resistances R_{tot} for T-Style MaxiCaps® (a) and In-line MaxiCaps® (b); SS-connectors (black), OO-connectors (red), YY-connectors (green), BB-connectors (light grey) and FF-connectors (blue). Membrane area of 0.6 m² (squares), 1.2 m² (circles) and 1.8 m² (triangles) and membranes with a nominal pore size of 0.2 μm (closed symbols) and 0.1 μm (open symbols).

As a next step a linear regression to each dataset is performed and the housing resistance is calculated by subtracting the y-intercept according to equation 26 (figure 67). Taking Reynolds numbers into consideration it is assumed that only the resistance of the membrane material is flow rate independent.

5 Results and Discussion

$$R_{housing} = R_{tot} - R_{mem} = \frac{P}{\eta \cdot J} - R_{J=0} \quad (26)$$

Figure 67 summarizes plots of the resulting housing resistance in dependence on the flow rate for different devices. The part of the housing resistance that depends on the water flow rate due to the limiting effect of the connectors can be described by a constant k_i , the slope of the linear regression line according to equation 27. The calculated constants k_i are presented in table 22.

$$R_{housing}(J) = k_i \cdot J \quad (27)$$

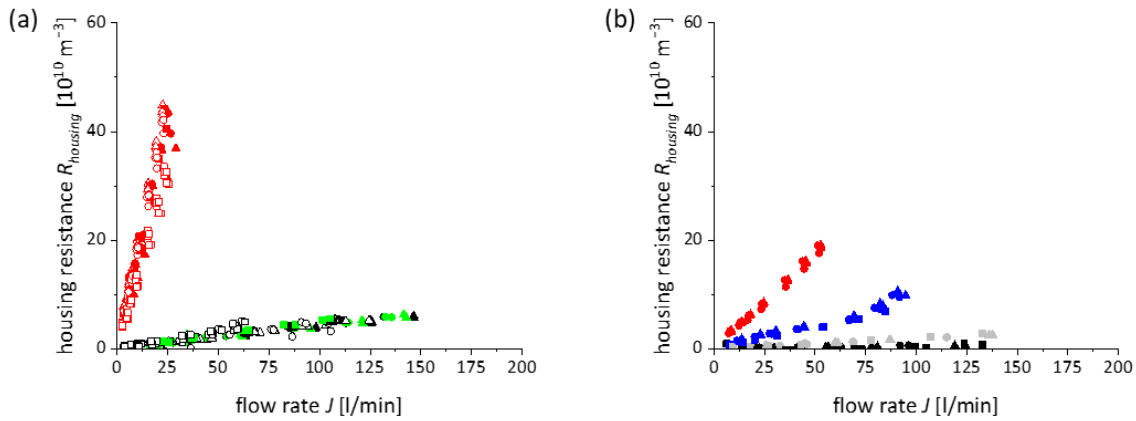


Figure 67: Flow rate-dependent housing resistance $R_{housing}$ of T-Style MaxiCaps® (a) and In-Line MaxiCaps® (b); SS-connectors (black), OO-connectors (red), YY-connectors (green), BB-connectors (light grey) and FF-connectors (blue). Membrane area of 0.6 m^2 (squares), 1.2 m^2 (circles) and 1.8 m^2 (triangles) and membranes with a nominal pore size of $0.2 \mu\text{m}$ (closed symbols) and $0.1 \mu\text{m}$ (open symbols).

A second variable is the previously subtracted intercept, which is assumed to consist primarily of the membrane resistance. Water flow rate measurements were performed with filter discs to determine the membrane resistance. $2.3 \cdot 10^{10} \text{ m}^{-1}$ was measured for the PES pre-filter/main filter combination. Therefore, the active membrane area can be calculated according to equation 28.

$$A_{mem} = \frac{2.3 \cdot 10^{10} \text{ m}^{-1}}{R_{mem}} \quad (28)$$

The calculated active membrane areas of MaxiCaps® are presented in table 22 together with the constants k_i . The calculated active membrane area is significantly smaller than the membrane area that is usually given in product specifications. Table 22 shows that the housing resistance for T-Style MaxiCaps® is higher than for the In-Line MaxiCaps® comparing the same connector types. A second trend can be observed regarding the devices: The higher the housing resistance the smaller the part of the embedded membrane area that contributes to the flow rate.

5 Results and Discussion

Table 22: Overview of parameters of T- Style MaxiCaps® and In-line MaxiCaps® of Sartopore 2 filter devices (of 0.2 µm nominal pore size) as determined by water flow rate measurements; values in italics are outliers and are not considered for the calculation of k_f .

Connector	MaxiCap®	Slope k_f [$10^{13} \text{ m}^{-6} \cdot \text{min}$]	Active membrane area A_{mem} [m^2]	Fraction of active membrane area A_{mem} [%]
SS	In-line size 1	0.0041 ± 0.0015	<i>0.27</i>	<i>45</i>
	In-line size 2		1.56	130
	In-line size 3		2.13	118
	T-Style size 1	0.0436 ± 0.0013	0.44	73
	T-Style size 2		0.83	69
	T-Style size 3		1.15	64
OO	In-line size 1	0.3502 ± 0.0061	0.17	28
	In-line size 2		0.42	39
	In-line size 3		0.59	33
	T-Style size 1	1.558 ± 0.043	0.31	59
	T-Style size 2		0.54	44
	T-Style size 3		0.64	35
BB	In-line size 1	0.0190 ± 0.0004	0.38	63
	In-line size 2		0.74	62
	In-line size 3		1.23	68
FF	In-line size 1	0.0940 ± 0.0039	0.32	53
	In-line size 2		0.62	52
	In-line size 3		0.84	47
YY	T-Style size 1	0.0431 ± 0.0015	0.44	73
	T-Style size 2		0.87	72
	T-Style size 3		1.11	62

The resistance of the whole filter device is a sum of the resistance of the setup (tubing) and the device itself (device construction, especially connectors, membrane, pleating, non-woven, etc.). As shown, the main contributions are the connectors and the membrane. Due to variations of different production lots the resistance of the membrane material is slightly different for the devices. The same goes for the calculation of the percentage of the active membrane area, here for 10" a membrane area of 0.6 m² is used for the calculation, but for technical reasons the embedded membrane area can vary a little. For these reasons an active membrane area of more than 100 % is calculated for In-line Maxi-Caps® with SS-connectors.

Influence of Viscosity on the Device Resistance

To examine the influence of the viscosity on the flow rate-dependency of filter devices, the flow rate of mixtures of RO-water and glycerol were measured. The mixtures of glycerol and RO-water varied between 27 mPa·s and 320 mPa·s. Trials are performed with three In-Line MaxiCaps®: size 1 with FF-connectors, size 2 with FF-connectors and size 2 with OO-connectors.

The results of the flow rate measurements with water glycerol mixtures and different viscosities are presented in figure 68. The results are presented on two different x-axis, because in figure 68b the dependency is unclear.

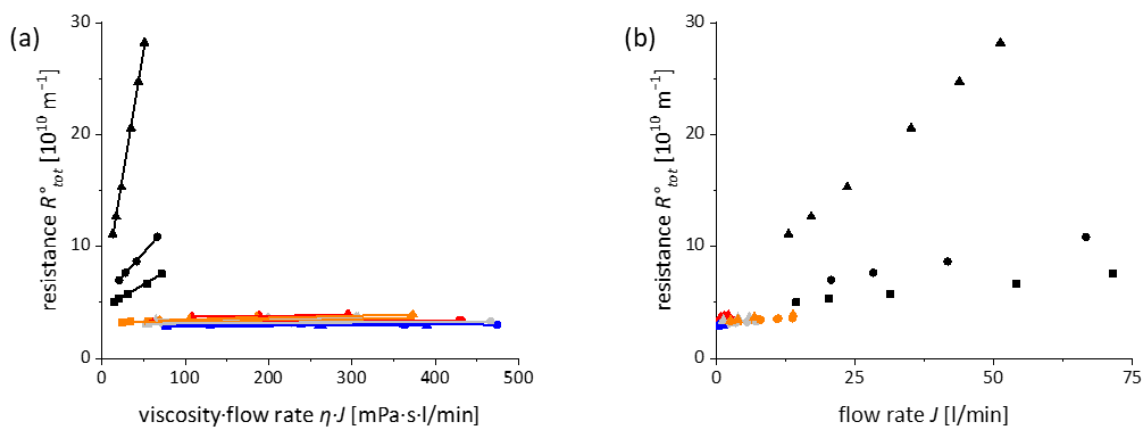


Figure 68: Presentation of influence of viscosity on resistance of a filter device during filtration of glycerol solutions of different viscosities through commercial process filter devices. Viscosity of 1 mPa·s (black), 27 mPa·s (orange), 65 mPa·s (grey), 136 mPa·s (red) and 321 mPa·s (blue); measurement values of size 1 In-Line MaxiCap® with FF-connectors (squares), size 2 In-Line MaxiCap® with FF-connectors (circles) and size 2 MaxiCap® with OO-connectors (triangles).

It can be concluded that on increasing viscosity the resistance dependency on the flow rate of the device cannot be observed any more. An explanation is again the Reynolds number. On multiplying the viscosity, first the flow rate is divided by that value and the Reynolds number is reduced. The viscosity itself is part of the Reynolds equation (equation 10) too, so the influence of the viscosity on the Reynolds number is squared. For a capsule of size 1 with SS-connectors a Reynolds number of $7.8 \cdot 10^4$ was calculated for water flow (1 mPa·s, 1 bar) in equation 25. A viscosity of 27 mPa·s would reduce the value of the Reynolds-number to 107 under the same experimental conditions, which is not turbulent any more.

5.3.2 Scale-Up of Filtration Processes: Experimental Approach and Calculation Basis

Prediction of the large-scale filtration process parameters can be made as presented in this section. Basic assumptions for this approach are the results and conclusions of the previous chapter: the assumption that resistances are additive, the active membrane area A_{mem} can be calculated by

5 Results and Discussion

water flow rate measurements, and the linear dependency of the housing resistance $R_{housing}$ for low viscosities.

Next step in the scale-up approach of filtration data is a test filtration in small-scale. Afterwards the resistance of the membrane and the fouling layer R_{mem_SS} is calculated by evaluating the test filtration in small-scale and subtracting the housing resistance $R_{housing}$.

$$R_{mem_SS}(\tilde{V}, J) = \frac{R_{tot_SS}(\tilde{V})}{A_{mem}} - k_{SS} \cdot J_{SS} \quad (29)$$

The scale-up factor S is determined by the ratio of the y-intercepts of the filtration setups in small-scale (SS) and in large-scale (LS) as determined by water flow rate measurements, which is assumed to be the ratio of the active membrane areas A_{mem} as well.

$$S = \frac{A_{mem_LS}}{A_{mem_SS}} = \frac{R_{J=0,SS}}{R_{J=0,LS}} \quad (30)$$

The volume V and the membrane and fouling layer resistances R_{mem_LS} are calculated by equations 31 and 32:

$$V_{LS} = S \cdot V_{SS} \quad (31)$$

$$R_{mem_LS}(\tilde{V}) = \frac{R_{mem_SS}(\tilde{V})}{S} \quad (32)$$

The large-scale device resistance R_{tot_LS} can be calculated by adding up the membrane and fouling layer resistance and the resistance of the membrane housing (equation 27) using the constant k_{LS} as determined by water flow measurements. The device resistance R_{tot_LS} can be expressed by Darcy.

$$R_{tot_LS} = k_{LS} \cdot J + R_{mem_LS}(\tilde{V}) = \frac{\Delta P_{tot}}{\eta \cdot J_{LS}} \quad (33)$$

This equation has to be solved for the filtration flow J_{LS} for constant pressure filtration, (equation 34) and for the filtration pressure ΔP_{tot} for constant flow filtration (equation 35):

$$J_{LS} = \frac{-R_{mem_LS} + \sqrt{R_{mem_LS}^2 + 4 \cdot k_{LS} \cdot \frac{\Delta P_{tot}}{\eta}}}{2 \cdot k_{LS}} \quad (34)$$

$$\Delta P_{tot} = k_{LS} \cdot J^2 \cdot \eta + R_{mem_LS} \quad (35)$$

For the obtained data points in a last step the filtration time t has to be calculated:

$$t = \sum_{i=0}^t \Delta t_i = \sum_{i=0}^t \frac{\Delta V_i}{J_i} \quad (36)$$

This approach was tested with a filtration trial with the particulate formulation presented in figure 44. The results of the calculations have been submitted for publishing [166].

5.3.3 Case Studies – Up-Scaling Studies for Filtration of Protein Formulations

With all three filtration trials an up-scaling study has been performed. To practice the higher filtration flow rates with the large-scale devices the studies are performed in the order of decreasing viscosity. For the first trial with the viscous BSA formulation (formulation 3, 40 mPa·s) an open membrane type is chosen (PES) to achieve a useful filtration flow rate even in small scale, for the 250 g/l BSA formulation (formulation 1) a narrow Hydrosart is chosen to limit the filtration flow rate. For the γ -globulin formulation (formulation 2) in the last trial the stack devices were examined, those are available with a Hydrosart membrane only.

Case Study 1: Up-Scaling Study with the 40 mPa·s BSA Formulation (Formulation 2) and with Pleated Filter Devices

The scale-up study presented in this chapter is applied to filtration of the viscous BSA formulation (formulation 2, table 6) in constant flow filtration mode for Sartopore 2® devices. This is a commercial filter containing a combination of PES pre-filter and main filter membrane combination of 0.45/0.2 μm nominal pore size. The membrane combination has a resistance of $2.8 \cdot 10^{10} \text{ m}^{-1}$ as determined by water flow rate measurements with a 14.1 cm^2 filter disc. The setups were adjusted as needed aligned with the filtration area, with the pressure sensor installed close to the device and the venting position to the top (section 4.5.3).

Table 23: Properties of filtration devices for up-scaling study with the 40 mPa·s BSA formulation (formulation 2).

Device	Official membrane area [cm^2]	Filtration flow rate [ml/min]
14.1 cm^2 filter disc	14.1	6.5
Size 4 capsule	150	73
Size 7 MidiCaps®	500	197
Size 8 MidiCaps®	1000	370
Size 9 MidiCaps®	2000	822
Size 1 cartridge	6000	2650

As in chapter 5.3.1 the effective membrane areas were determined by water flow rate measurements. Linear regressions were calculated for the $R_{tot}(J)$ -plot and the respective membrane areas for the large-scale devices were determined. The results are presented in table 24 and figure 69:

Table 24: Overview of parameters of filter devices used for up-scaling study with Sartopore 2 filter products as determined by water flow rate measurements.

Device	y-intercept [10^{10} m^{-3}]	Slope k_i [$10^{13} \text{ m}^{-6} \cdot \text{min}$]	Active membrane area A_{mem} [cm^2]
14.1 cm^2 filter disc	Reference	0	14.1 cm^2
Size 4 capsule	205	3.25	137
Size 7 MidiCaps®	59.1	0.275	474
Size 8 MidiCaps®	29.3	0.0478	955
Size 9 MidiCaps®	17.8	0.0296	1570
Size 1 cartridge	5.32	0.0124	5265

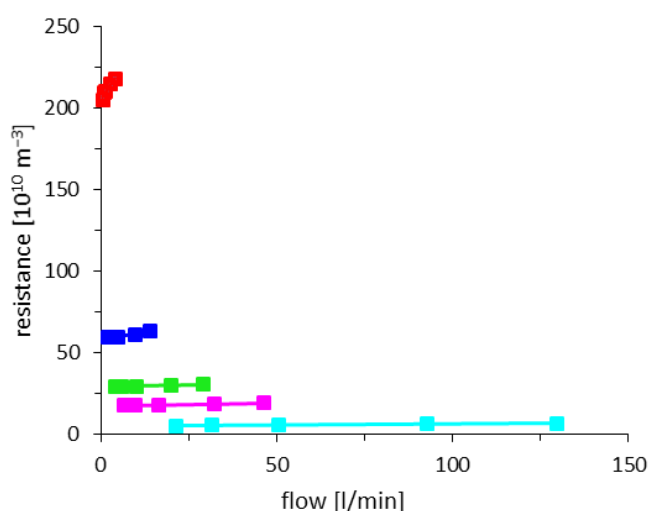


Figure 69: Results of water flow rate measurements of different devices of Sartopore 2: Size 4 capsule (red), size 7 MidiCaps® (blue), size 8 MidiCaps® (green), size 9 MidiCaps® (magenta) and size 1 cartridge (cyan).

In contrast to the results of the flow rate measurements of MaxiCaps® presented in chapter 5.3.1 it can be noted that for different sizes of the same product (MidiCaps®) the slope k_i is quite different. The up-scaling filtration trials are performed with the viscous BSA-formulation at constant flow of $0.5 \text{ ml}/(\text{min} \cdot \text{cm}^2)$. The measurement results are presented in figure 70.

The data acquired in the experiment for the size 4 capsules are used to predict theoretical filtration pressures for the other five devices, based on the actual measured flow rates for the respective device during the experiments. No k_i is included in the calculations, as it was shown in chapter 5.3.1 that with higher viscosities this parameter gets negligible. But the filtration areas obtained by the water flow measurements are used for the data evaluation presented in figure 70 and for the prediction of the filtration pressures. The predicted pressure curves in figure 71 show a good agreement with the experimental values. The largest deviations occur for size 8 MidiCaps® and size 1 cartridges, but that difference is for both cases less than 80 mbar (10%).

5 Results and Discussion

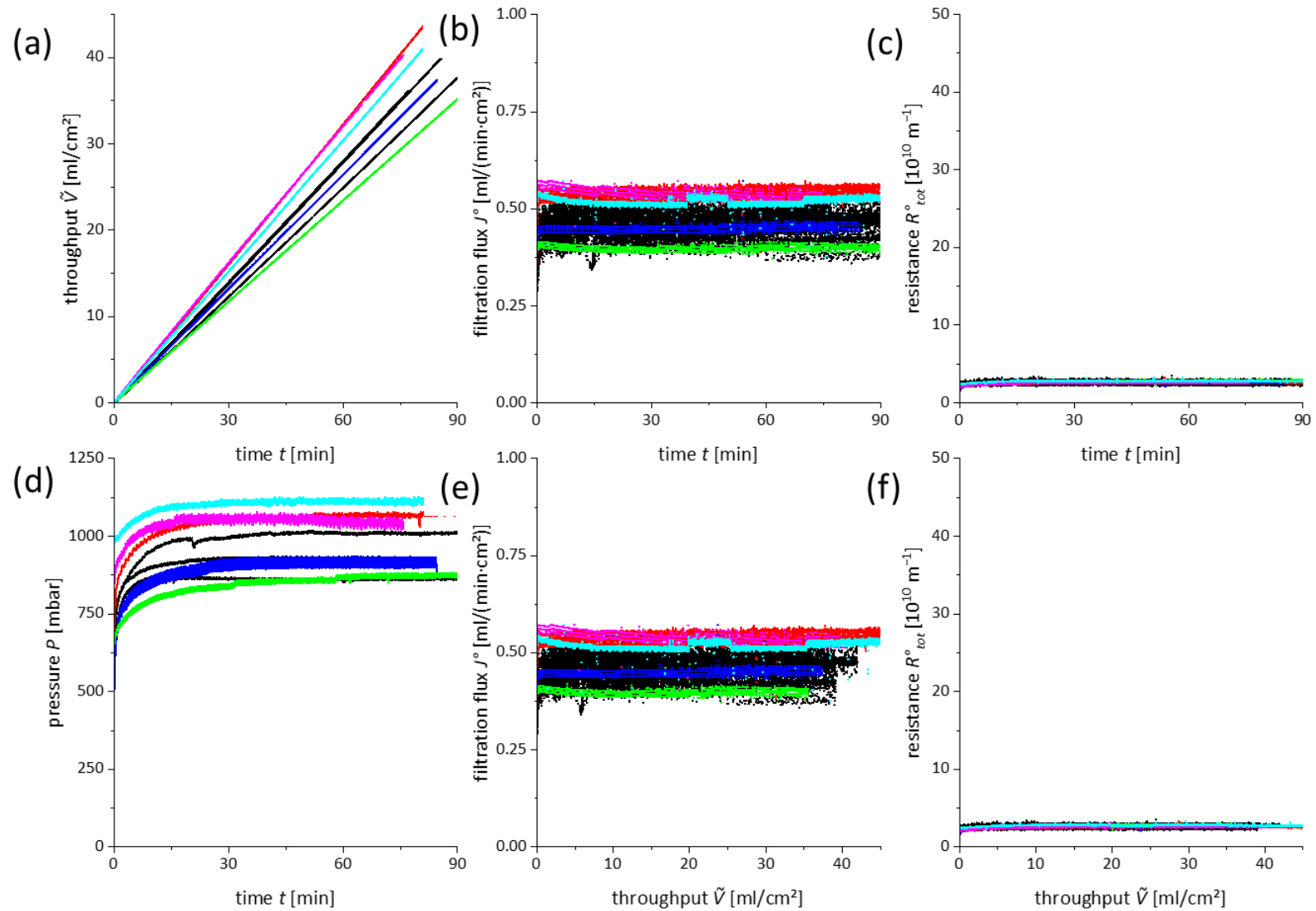


Figure 70: Results of scale-up trials for constant flow filtration of formulation 2 (table 6) with Sartopore filter products (devices described in table 24); 14.1 cm² filter discs (black), size 4 capsules (red), size 7 MidiCaps® (blue), size 8 MidiCaps® (green), size 9 MidiCaps® (magenta) and size 1 cartridge (cyan).

5 Results and Discussion

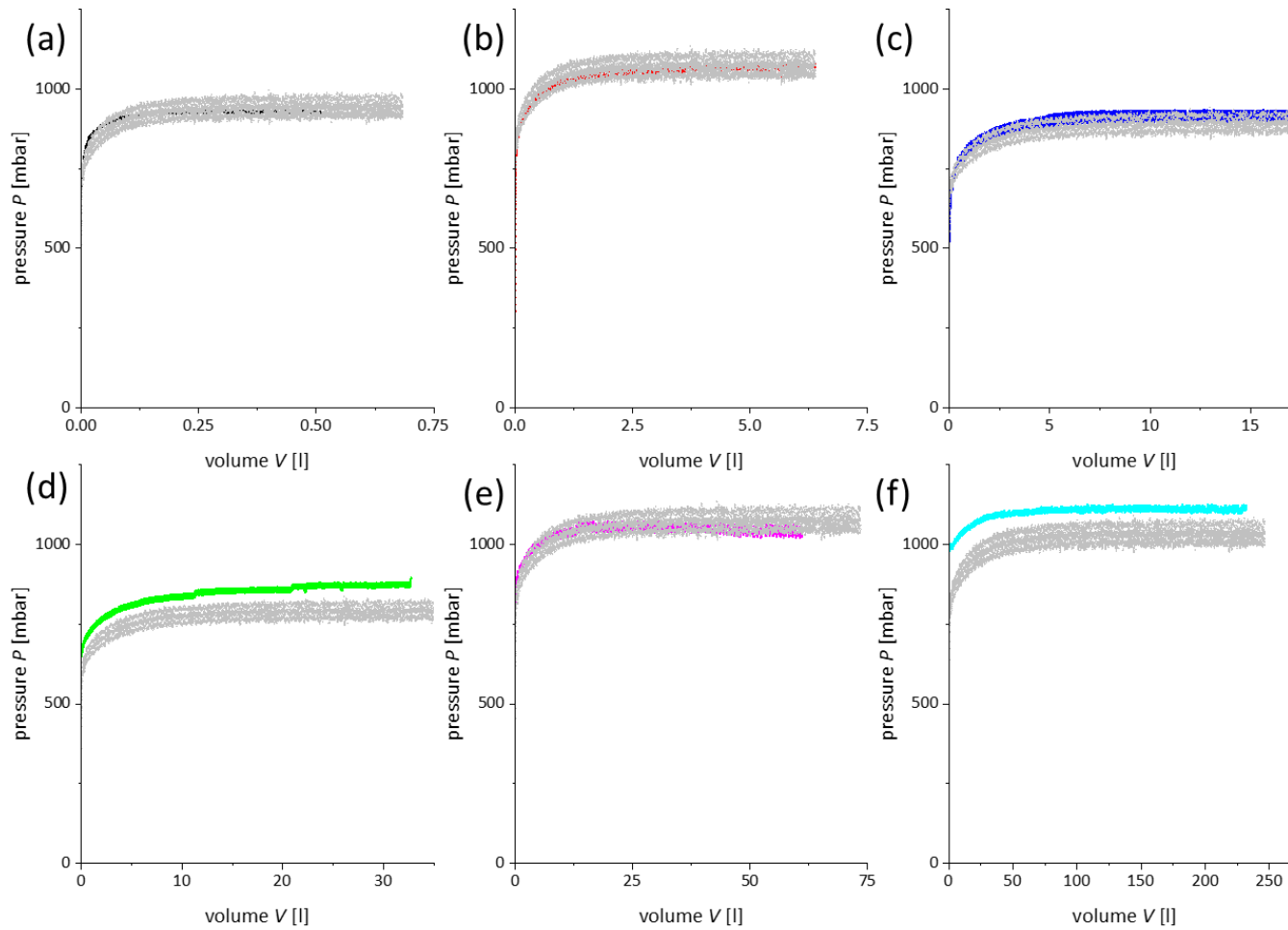


Figure 71: Prediction of filtration pressure on the basis of the up-scaling filtration trials presented in figure 70 for filtration of formulation 2 (table 6) through Sartopore filter products (devices described in table 24); 14.1 cm² filter disc (black, a), size 4 capsule (reference data, red, b), size 7 MidiCaps[®] (blue, c), size 8 MidiCaps[®] (green, d), size 9 MidiCaps[®] (magenta, e), and size 1 cartridge (cyan, f) and the respective calculated data in grey.

Case Study 2: Up-Scaling Study with Hydrosart Filter Products and the 250 g/l BSA Formulation (Formulation 1)

Up-scaling experiments with the 250 g/l BSA formulation (formulation 1) were performed with Hydrosart filter products at different scales of 4.5 cm² to 7073 cm² (Sartoscales, pleated devices and experimental stack devices). An overview of the devices is given in table 25. The experimental stack devices were connected by hose barbs and had narrow flow channels in the membrane support. A part of the membrane was sealed to the membrane support and does not contribute to the filtration process. According to color tests only 39% are still accessible, therefore this fraction of the actual embedded membrane area is given in table 25 as embedded area. Finally, the flow rates of the experiments were selected according to the embedded membrane area instead of the active membrane area. Water flow rate measurements were all performed at 0.5 bar. The results and the filtration flow rates for the scaling trials are given in table 25 as well.

Table 25: Overview of parameters of filter devices used for up-scaling study with the 250 g/l BSA formulation (formulation 1, table 6) filtered with the given filtration flow rate through prototypes of Hydrosart process filters, and the active membrane area as determined by water flow rate measurements.

Device	Filtration flow rate [ml/min]	Embedded membrane [cm ²]	Water flow rate at 0.5 bar [ml/min]	Active membrane area [cm ²]
Sartoscale 25	1.4	4.5	15.3	Ref
Sartoscale 47	5.2	17.3	58.8	17.3
Stack device 1	8	19.6	149	35.2
Stack device 2	75	234	1597	376
Stack device 3	150	485	3130	752
Size 4 Capsule	68	225	674	159
Size 8 MidiCap®	550	1834	5086	1198
Size 1 cartridge	2111	7037	27000	6360

Except for the size 1 cartridges the filtration setups were comparable to the previous case study; for the size 1 cartridge trials a T-piece had been included in the setup as presented in figure 72 for convenience because of the high filtration flow rates.

5 Results and Discussion

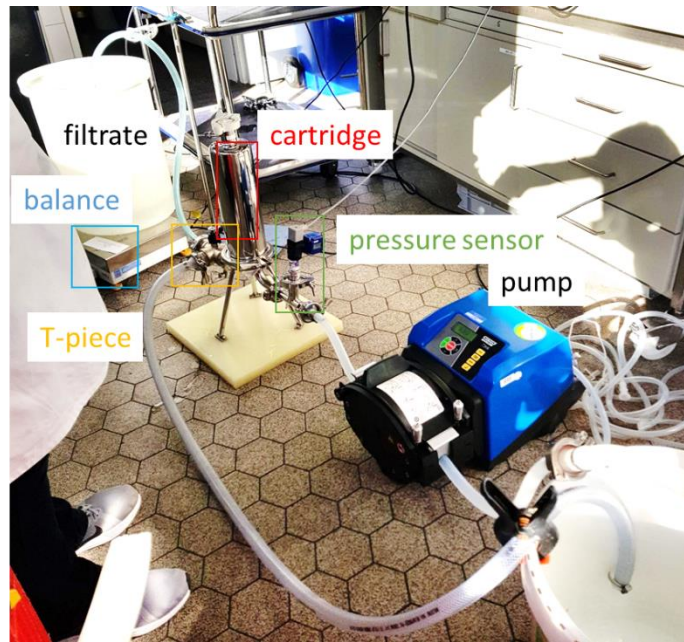


Figure 72: Filtration setup for size 1 cartridges for scale-up trial with the 250 g/l BSA formulation (formulation 1).

To economize on the media the formulation was repeatedly filtered. Pre-trials were performed in order to evaluate the influence of multiple filtrations on the quality of the protein formulation. The results of the pre-trials are presented in figure 74. Here it can be seen that filter fouling is going down for the first two filtrations and remains constant starting with the 3rd filtration. Therefore it was decided to do the filtration trials after pre-filtration with two Hydrosart devices. Protein formulations were characterized before and after filtration. Multiple filtration does not change the composition of the formulation as presented in figure 73.

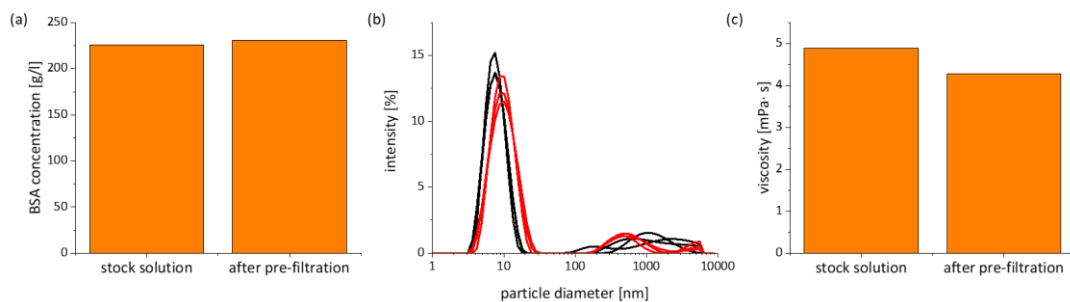


Figure 73: Influence of pre-filtration with a 0.45 μm CA and two Hydrosart devices on the quality of the concentrated BSA formulation (formulation 1). Results of UV-measurement (a), DLS (stock solution black, filtrate red, measurements in triplicates and at 173° scatter angle, (b) and formulation viscosity (c).

Figure 75 presents the filtration data of the scale-up trial. Of the multiple measurements, one representative trial is chosen for each device except for the Sartoscales 25. They were measured on two days, therefore one measurement for each day is selected here.

Filtration through the studied devices was scalable and the degree of filter fouling was generally low. However, some deviations in the performance of the single devices can be observed: in figure

(d) it can be seen that there is a variation in the initial filtration pressure. The reason here is that the filtration flow rate is adjusted to the embedded membrane area instead of the effective membrane area. Table 25 shows the differences of those membrane areas, which explains the discrepancies between the initial filtration pressures. The filtration flux (shown in (b) and (e)) shows a similar variation. The initial resistances (figure (c) and (f)) show three different groups: the lowest initial resistance for Sartoscales (25 and 47) and the large stack device, the second group formed by the smaller stack devices, the capsule and the Midicaps® and a high initial resistance for the size 1 cartridge.

In case of filtration through the stack device number 2 and one of the Sartoscale 25 a deviant and slightly stronger filter fouling was observed. The reason is that on the first day of the trials it could be observed that throughout the day filter fouling increased slightly, but steadily. Probably, the pre-filtrations produced a meta-stable formulation and during the trials aggregates formed again. Therefore, the trials performed in the morning produced less filter fouling than the ones in the afternoon (stack device 2, one of the Sartoscale 25).

The setup for the 10"-element contained a T-piece for convenience: the filtrate was pumped either at a balance to check the filtration flow (straight through the T-piece), or directly back in the formulation reservoir (at a 90° angle). The slight changes in the filtration pressure here can be attributed to changes of the resistance due to the flow direction of the T-piece.

Case Study 3: Up-Scaling Study with Stack Filter Devices and the γ -Globulin Formulation (Formulation 3)

A third scaling example was performed with the 100 g/l γ -globulin formulation (formulation 3) and stack filter devices. The filtration setup was chosen as presented in figure 32b in section 4.5.3. The case study was performed with two different Hydrosart devices, namely a Sartoscale 25 with 4.5 cm² membrane area and an experimental stack device as presented in the previous chapter, and two commercial filter devices containing a hydrophilic PVDF_{hyd} membrane. One was a small-scale device comparable to Sartoscale 25 with a membrane area of 3.5 cm², the other a stack device with narrow flow channels and F-connectors.

As in previous studies the effective membrane areas are determined by water flow rate measurements. Linear regressions are calculated for the $R_{tot}(J)$ -plot and the respective membrane areas for the large-scale devices are calculated. The results are presented in figure 76 and table 26.

5 Results and Discussion

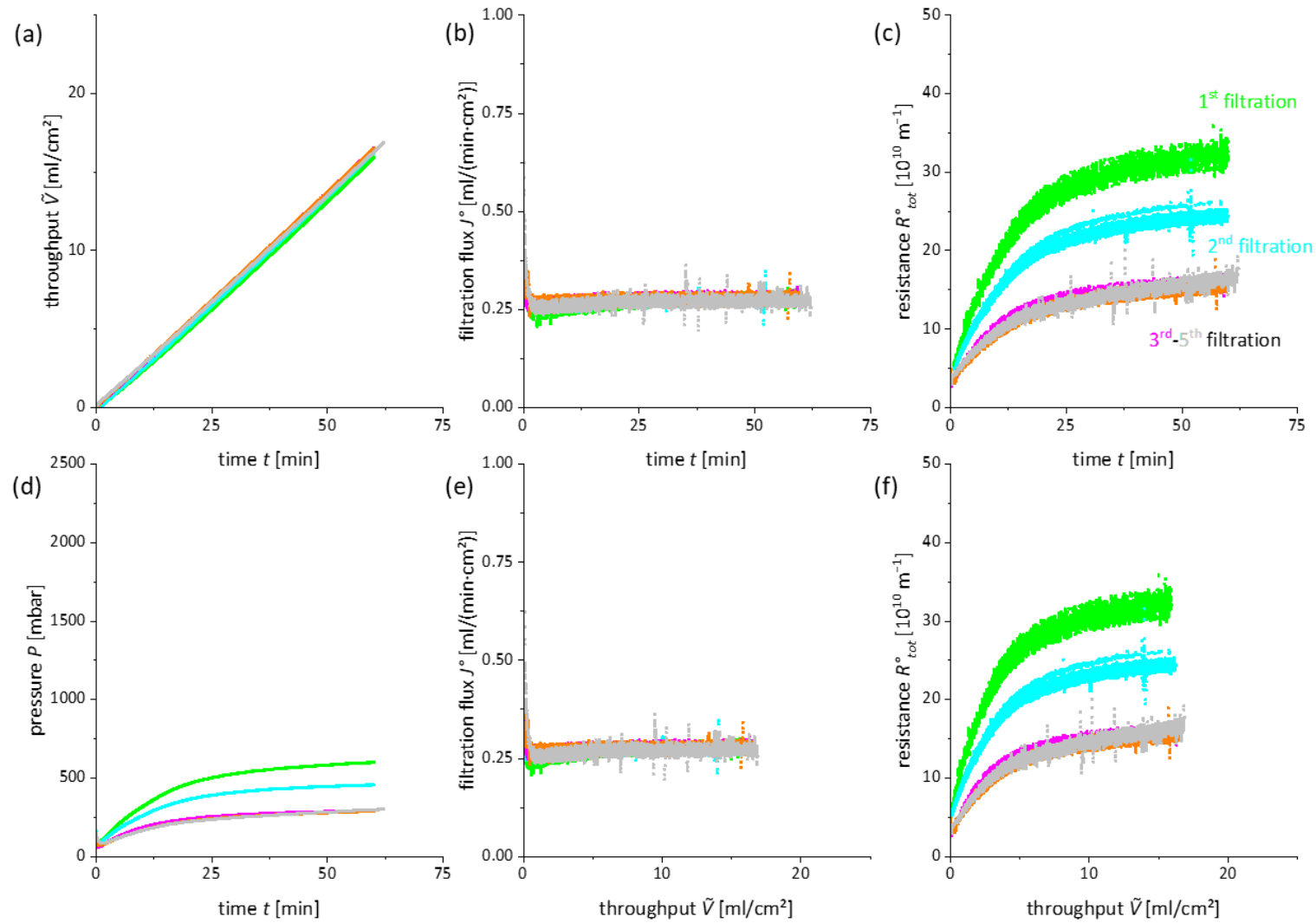


Figure 74: Results of filtration pre-trials with the 250 g/l BSA formulation (formulation 1, table 6) through a 14.1 cm² filter disc of Hydrosart membranes and evaluation of the influence of multiple filtrations at constant flow rate of 0.25 ml/(min·cm²); 1st filtration after pre-filtration with a 0.45 μm membrane (green), filtration of the filtrate of trial 1 (2nd filtration, cyan), filtration of the filtrate of trial 2 (3rd filtration, magenta), and two further filtrations of the filtrates of trial 3 and 4 (4th and 5th filtration, orange and grey).

5 Results and Discussion

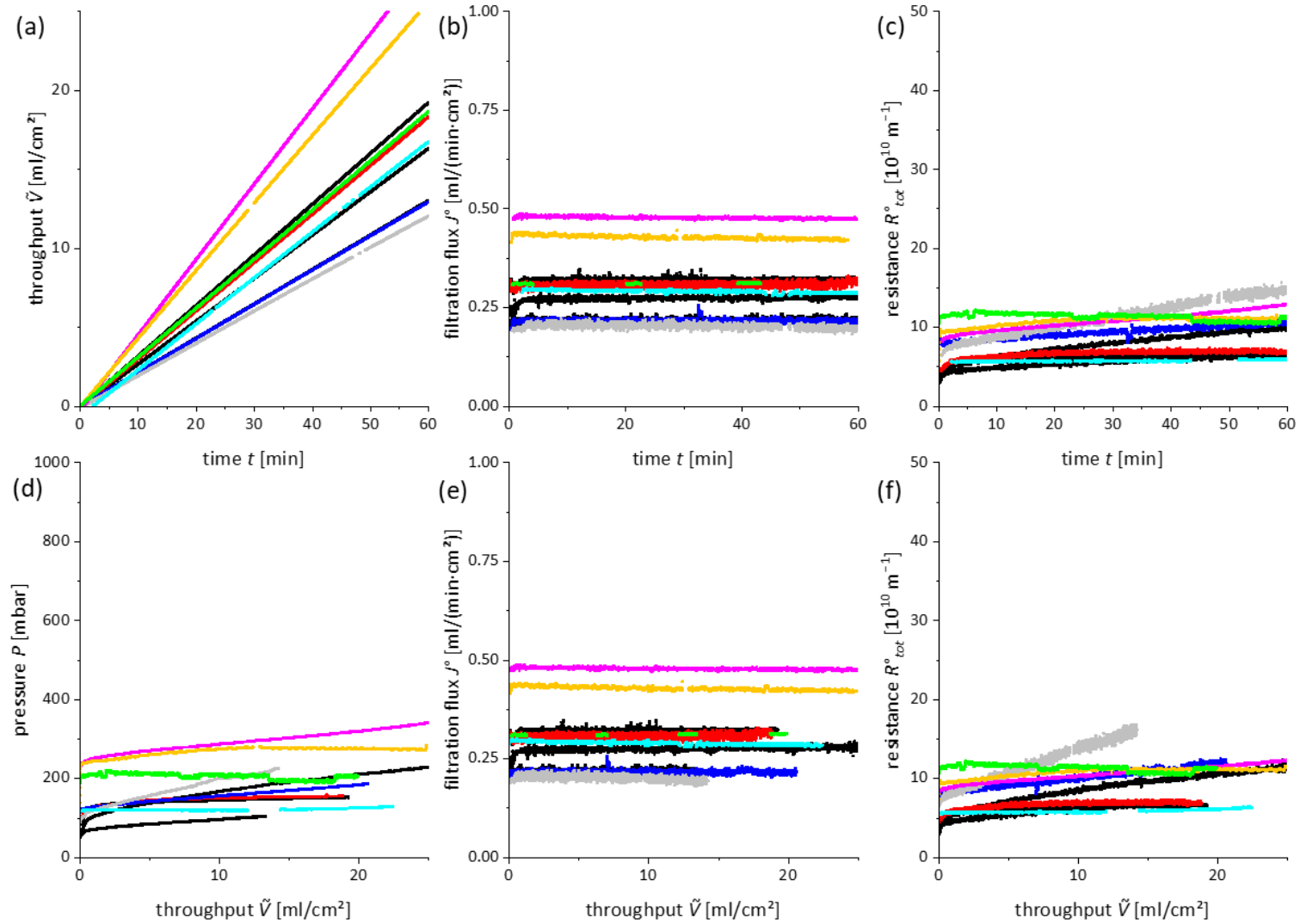


Figure 75: Results of scale-up trials for filtration of the 250 g/l BSA formulation (formulation 1, table 6) with devices described in table 25; constant flow filtration, flow rate adjusted to embedded membrane area; Sartoscale 25 (black), Sartoscale 47 (red), stack device 1 (blue), stack device 2 (grey), stack device 3 (cyan), size 4 capsule (magenta), size 8 Midicap® (orange) and size 1 cartridge (green).

5 Results and Discussion

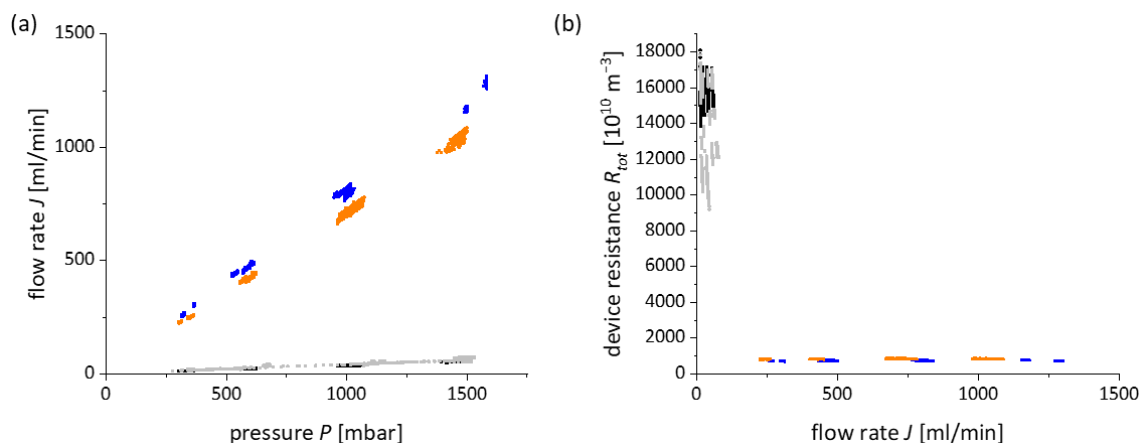


Figure 76: Results of water flow rate measurements of devices used for scale-up experiments with the γ -globulin formulation (formulation 3); small-scale device Hydrosart (light grey) and PVDF_{hyd} (black), large-scale device Hydrosart (orange) and PVDF_{hyd} (blue).

Table 26: Overview of parameters of filter devices used for up-scaling study with stack filter devices as determined by water flow rate measurements presented in figure 76.

Device	y-intercept [10^{10} m^{-3}]	Slope k_i [$10^{13} \text{ m}^{-6} \cdot \text{min}$]	scale-up factor	Active membrane area A_{mem} [cm^2]
Hydrosart small-scale	12183	1.00	15	4.5 (reference for large-scale device)
Hydrosart large-scale	820	0.23		66.9
PVDF _{hyd} small-scale	15178	0.47	21	3.5 (reference for large-scale device)
PVDF _{hyd} large-scale	721	0.02		73.6

Based on the active membrane areas determined by water flow-rate measurements the filtration flow rate has been fixed at 4.5 ml/min for the Sartoscale 25, 66.9 ml/min for the large-scale Hydrosart device, 3.5 ml/min for the small-scale PVDF_{hyd} device and 73.6 ml/min for the large-scale PVDF_{hyd}-device.

The stability of the formulation was tested in pre-trials. The influence of pre-filtration and the stability for 3 hours has been examined. The filtration results of the pre-trials are presented in figure 77. An influence of pre-filtration or waiting times could not be observed, the formulations were stable under the experimental conditions.

The results of the scale-up experiment are presented in figure 78. As in the pre-trials, filtration results for small-scale devices show no influence of waiting times or of reusing the filtrate for filtration trials.

Two filtrations were performed with PVDF_{hyd} large-scale devices. The results are different, depending on the type of pre-filter used. Filtration curves comparable with the results obtained for the

small-scale filtration trials were obtained after pre-filtration with a 0.2 μm filter. Contrary to this, filter fouling was found to be strongly increased after pre-filtration with a 0.45 μm membrane. The fouling mechanism is different as well, the resistance versus throughput plot shows a distinct bent after 40 minutes of filtration. Probably, small aggregates remain after pre-filtration with a 0.45 μm filter that block flow-channels within the device. Those aggregates are removed after filtration with a 0.2 μm membrane.

For all Hydrosart large-scale filtration trials the device resistance increased quite remarkably and stronger than expected by the small-scale filtration trials, indicating changes in the blocking mechanism. Resistance vs. throughput curves show already a stronger increase at the beginning of filtration compared with the small-scale filtration trials. As discussed for filtration of the protein solution through PVDF_{hyd} large-scale-devices, a distinct bent can be observed in the resistance vs. throughput curves after 20 minutes of filtration of a protein solution pre-filtered with a 0.45 μm filter, which does not occur after pre-filtration with a 0.2 μm filter. It must be concluded that the Hydrosart stack device is not scalable with the lab-scale device.

The Hydrosart stack devices were opened after the filtration trials to study the reason for the filter blocking. Ponceau S was used to dye and visualize bound protein. It was found that filter blocking obviously was caused by the device design and housing material. Protein was found in the exit area of the device. The channel surfaces within the device were covered by a thick protein layer, with different thickness in different areas of the device, indicating areas of different fluid flow within the device. The device was made by hydrophobic material (polypropylene), which is quite adsorptive for proteins as presented in section 5.4. Similar stacks with different filter area were used for the up-scaling study with the 250 g/l BSA formulation (formulation 1, case study 2). Here scalability was proven. Obviously filtration of the γ -globulin formulation is more challenging.

This result needs further investigation. However, it shows that optimization of fluid design and choice of housing material is of likewise importance as the selection of membrane for the performance of process filters for protein filtration.

5 Results and Discussion

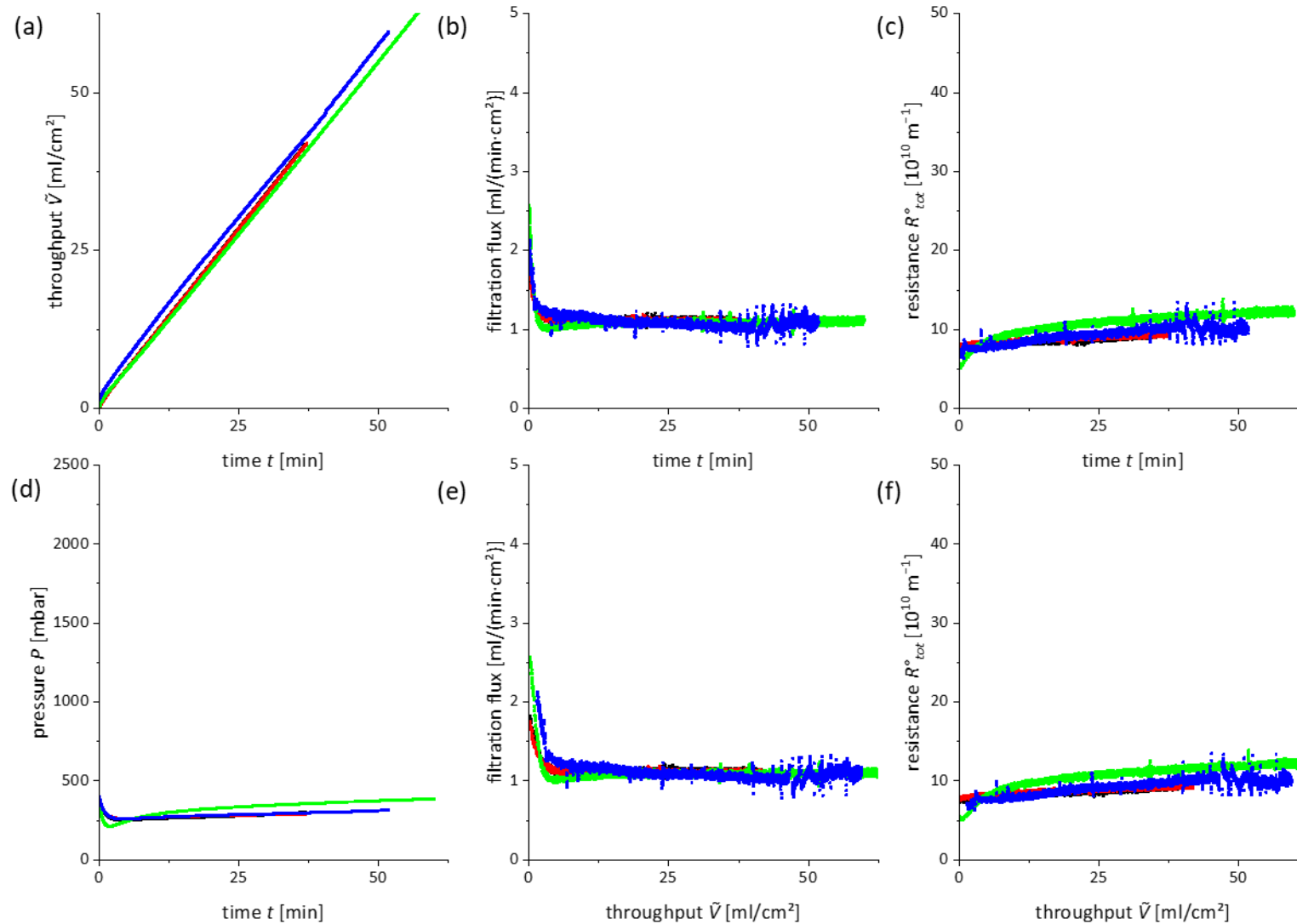


Figure 77: Filtration results of the pre-trials for the up-scaling experiment with the γ -globulin formulation (formulation 3, table 6). Filtration with 14.1 cm² Hydrosart filter discs right after preparation of the formulation (black), the filtration of the filtrate from trial 1 (red), filtration of the filtrate of trial 2 after 3 hours (green) and filtration of the filtrate from trial 3 (blue).

5 Results and Discussion

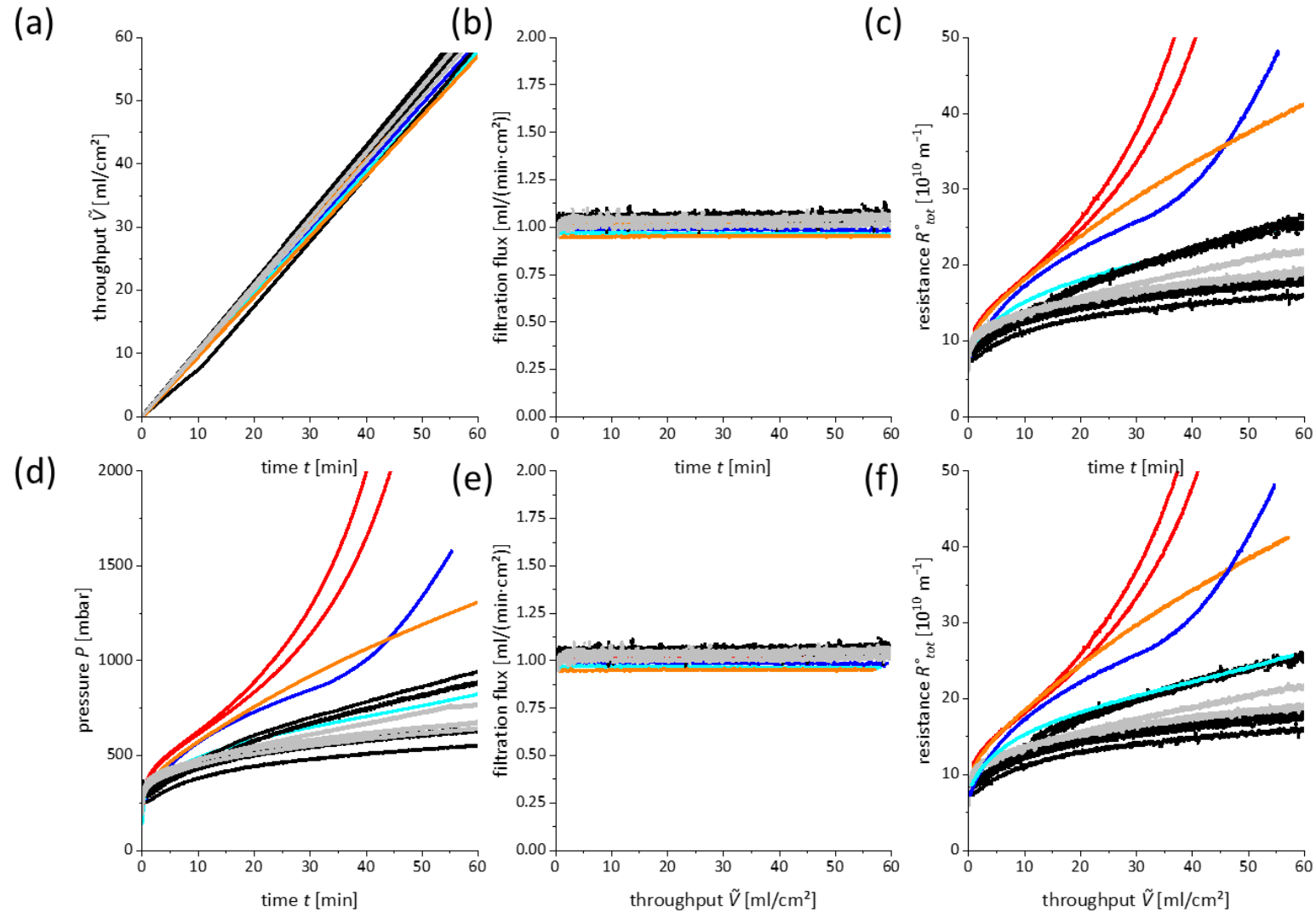


Figure 78: Results of scale-up trials for filtration of the γ -globulin formulation (formulation 3, table 6) with stack filter devices (described in table 26); constant flow filtration at 1 ml/(min·cm²); small-scale device Hydrosart (light grey) and PVDF_{hyd} (black), large-scale device Hydrosart (0.45 μ m pre-filtered: red, 0.2 μ m pre-filtered: orange) and PVDF_{hyd} (0.45 μ m pre-filtered: blue, 0.2 μ m pre-filtered: cyan).

5.3.4 Summary

A study was performed to show scalability of filtration devices for constant flow filtration of protein formulations. Case studies were performed involving all of the stabilized, drug-like protein formulations (table 6), which were introduced in this work for filtration trials.

The scalability studies were performed by means of a new, flow rate and resistance based up-scaling approach utilizing a resistance-in-series model based on the Darcy equation. This approach could be successfully applied to predict and visualize performance of filter products of different size and design for filtration trials with a particulate test solution [166].

For the up-scaling study with protein formulations, experimental setups and work methods were optimized to obtain reproducible results (pump, tubing, tube angles and valves), to provide and handle metastable protein formulation in process scale, to control flow rate adjusted to the active filter area and to evaluate filtration results. It was demonstrated how the filtration flow rate can be adjusted according to the active membrane area, which can be measured by water flow rate measurements and, which is distinctly smaller than the specified (embedded) membrane area of the filter product due to hydrodynamic reasons. This is especially the case for large process filters.

Furthermore, it was shown that the resistance of the filter product is strongly influenced by the choice of tubing. However, in case of protein filtration, fluid flow is often low and laminar due to the increased viscosity.

Generally, a low degree of filter fouling was observed for all studied protein solutions, due to their stable formulation. Scalability of the studied filter products could be demonstrated for filtration with BSA formulations. However, the case study for scalability of stack devices for filtration of a γ -globulin formulation surprisingly demonstrated that this cannot be taken for granted. Here, large-scale devices showed significantly stronger filter fouling than small-scale devices, which was probably caused by their fluid design and housing material.

5.4 Protein Adsorption during Filtration Process

As it is essential for Biopharma formulations that the composition is not changed during the filtration process because of e.g., adsorption, protein adsorption to membrane material is examined in this section by measurement of breakthrough curves in dead-end filtration mode with filter discs. ILC measurements are described in chapter 4.7. To evaluate the influence of the surface properties hydrophilic Hydrosart and hydrophobic CN membranes were chosen with comparable membrane resistances (table 8).

In pre-trials the measurement method was optimized. It was observed that membrane housings adsorb a large amount of protein, and the adsorbed amount of protein to membrane filter discs could not be multiplied with the number of membrane layers. Because of these results measurements were performed with experimental filter housings made from Cyrolite® with only one membrane layer.

Another issue is the fluid flow distribution, which is different in an empty membrane housing and a membrane housing with a membrane installed inside. Because of this difference the examined breakthrough curves show first a sharp increase of the adsorbed amount of protein and a decline afterwards. For this reason the evaluation approach presented in section 4.7 (figure 35) was used. A sample volume of 40 ml was chosen to obtain a compromise between measurement time and the measurement equilibrium as can be seen in figure 35 as well.

The aim of this section is to examine protein adsorption, and to evaluate influences of the formulation ingredients and process conditions. For the evaluation of thermodynamics different protein concentrations are examined, and adsorption/desorption measurement cycles are performed to evaluate the influence of an adsorbed protein layer. Based on those results the equilibrium membrane coverage is calculated. For the influence of the formulation ingredients different PS80 concentrations are tested. And for the evaluation of process conditions different filtration flow rates are used for the experiments.

5.4.1 Protein Adsorption to Membrane Housings

A high number of housing adsorption measurements were performed for all test solutions (at least 6 times for measurement of different flow rates, protein concentrations, and PS80 contents). For standard conditions (1 g/l protein) the deviation between several measurements is presented for the housing adsorption measurements in table 27. Outliers are eliminated.

5 Results and Discussion

Table 27: Protein adsorption values to Cyrolite® membrane housings during filtration protein formulations at standard conditions (table 9). Omitted values in italics.

Measurement run	Housing adsorption BSA [μg]	Housing adsorption γ -globulin [μg]
1	445	445
2	473	462
3	<i>340</i>	429
4	448	378
5	348	498
6	457	490
7	375	<i>361</i>
8	326	429
9	425	416

Table 28 presents the amount of protein adsorbed to Cyrolite® membrane housings at different filtration flow rates. It could be seen that within the measurement accuracy the same results were obtained; therefore, housing measurements were approximated mathematically together with the housing measurements of the different protein concentrations (presented in table 29). A linear regression was applied to those measurements in an adsorbed amount of protein vs. protein concentration plot ($R^2 > 0.99$ for both proteins). The linear regression is presented in figure 79.

Table 28: Results for protein adsorption of BSA and γ -globulin to Cyrolite® membrane housings during filtration of protein formulation (1 g/l) with different filtration flow rates.

Flow rate [ml/min]	Housing adsorption BSA [μg]	Housing adsorption γ -globulin [μg]
0.5	411	-
1	385	358
2.5	373	393
5	412	445
7.5	-	463

Table 29: Results for the adsorption measurements to Cyrolite® membrane housings during filtration of different protein formulations of BSA and γ -globulin at 5 ml/min.

Protein concentration [g/l]	Housing adsorption BSA [μg]	Housing Adsorption γ -globulin [μg]
0.1	28	42
0.5	163	191
1	412	445
2	628	907
5	2098	-

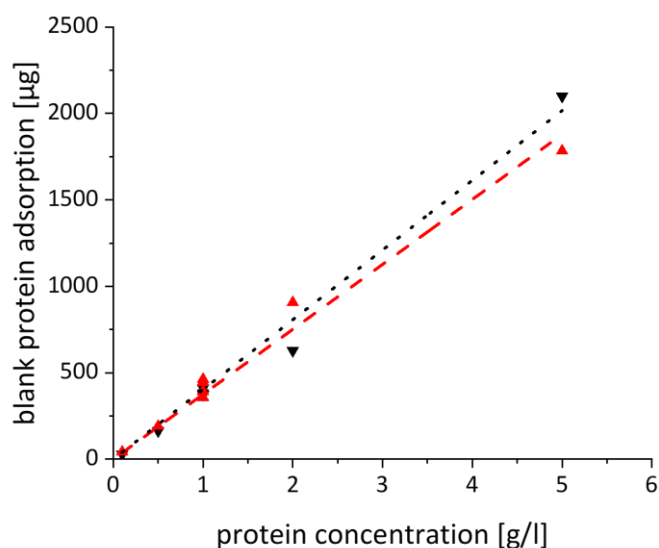


Figure 79: Housing adsorption measurements for different flow rates and protein concentrations for BSA (black, triangles down) and γ -globulin (red, triangles up) with linear regression and fixed y-intercept at 0 to the respective data sets.

The results obtained with the regression are listed in table 30 and used for the data evaluation in the following chapters. For BSA all 5 cycles without PS 80 were averaged, for γ -globulin only the 2nd to 5th cycle. All other adsorption measurements to Cyrolite[®] membrane housings are presented as measured without further approximation.

Table 30: Overview of adsorption measurements to Cyrolite[®] membrane housings for all adsorption measurements with the formulations described in table 9.

Formulation	Protein concentration [g/l]	BSA [μ g]	γ -globulin [μ g]
Standard	0.1	40	43
Standard	0.5	202	216
Standard, 1 st – 5 th cycle	1	404	-
Standard, 1 st cycle	1	404	433
Standard	2	807	865
Standard	5	2018	-
0% PS80, 1 st cycle	1	352	451
0% PS80, 2 nd – 5 th cycle	1	352	392
0.00016% PS80	1	366	-
0.5% PS80	1	421	-

5.4.2 Influence of Surfactant (PS80) on Protein Adsorption

Filtration trials were performed with formulations with protein concentration of 1 g/l at a flow rate of 0.9 ml/(min·cm²) to assess the influence of the surfactant PS80 on protein adsorption. The

5 Results and Discussion

surfactant concentration was varied between 0 and 0.5% PS80. PS80 has a critical micelle concentration (CMC) of 0.001% [167]. The results are presented in figure 80.

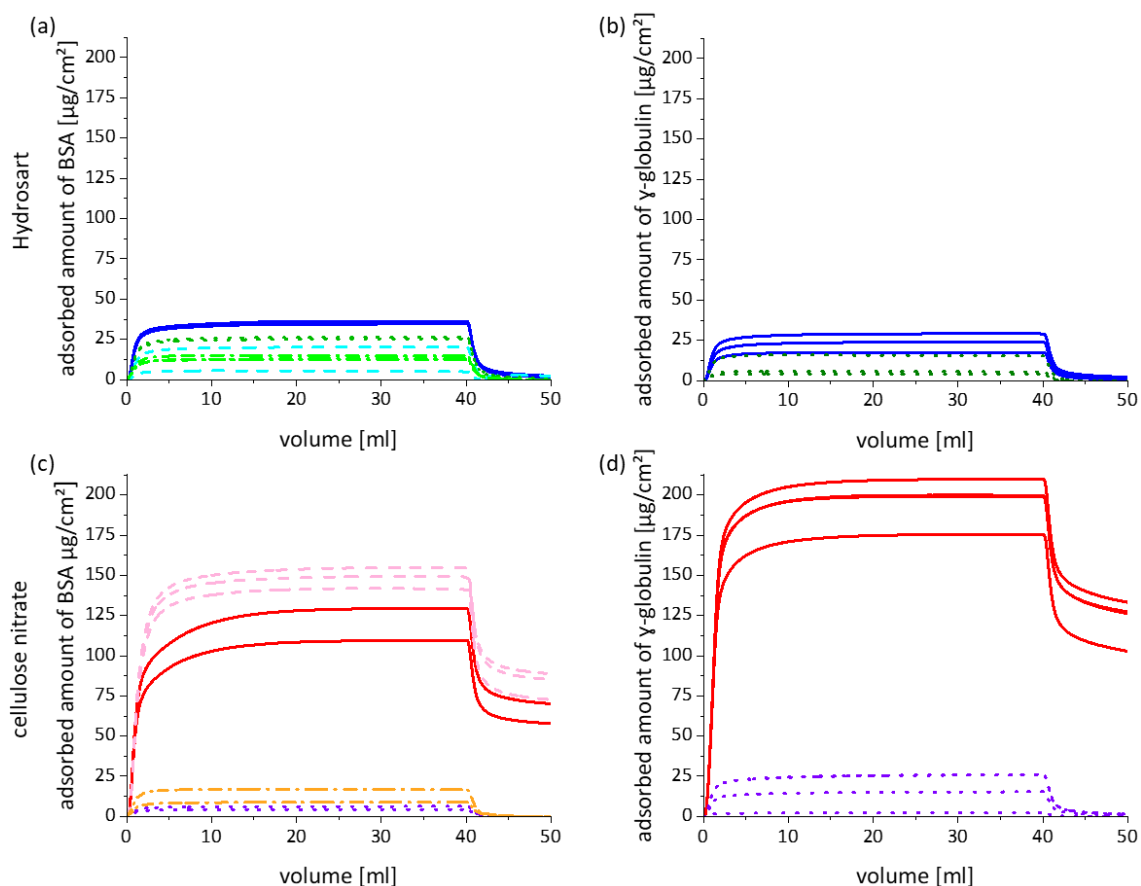


Figure 80: Adsorption of BSA and γ -globulin during filtration of protein formulations containing a different amount of PS80 through Hydrosart ((a) and (b)) and CN-membranes ((b) and (c)). Formulation and process conditions are given in table 9); 0% PS 80 (blue and red, straight lines), 0.00016% PS 80 (cyan and rose, dashed lines), 0.01% PS 80 (olive and lilac, dotted lines) and 0.5% PS 80 (green and orange, dotted and dashed lines).

The surfactant has low influence on protein adsorption on the surface of hydrophilic Hydrosart membranes. Adsorption was always minimal, in the range of $25 \mu\text{g}/\text{cm}^2$, independent of the surfactant concentration.

However, protein adsorption on hydrophobic CN membranes depends strongly on the surfactant concentration. For formulations with a PS80 concentration above the CMC (0.01% and 0.5% PS80), a behavior comparable with that described for protein adsorption on hydrophilic surfaces was observed.

For formulations with a PS80 concentration below the CMC a distinctly higher protein adsorption was observed. For BSA values around $100\text{-}150 \mu\text{g}/\text{cm}^2$ were measured and in case of γ -globulin $160\text{-}200 \mu\text{g}/\text{cm}^2$, respectively. Interestingly, less adsorption was obtained for the surfactant-free BSA formulation compared with a formulation containing 0.00016% PS80. Maybe, the presence of the surfactant enables the protein to pack more closely on the surface.

5.4.3 Influence of Protein Concentration – Adsorption Isotherm

Adsorption measurements were performed for formulations of BSA and γ -globulin with a protein concentration in the range of 0.1 g/l up to 5 g/l. All formulations contained 0.01% PS80. Formulations were filtered through Hydrosart and CN-membranes at a flow rate of 0.9 ml/(min·cm²).

For γ -globulin the UV-signal was linear only for a protein concentration up to 2 g/l. Therefore, no higher concentration could be measured. Results are presented in figure 81 and are similar for both proteins and membranes due to the presence of the surfactant.

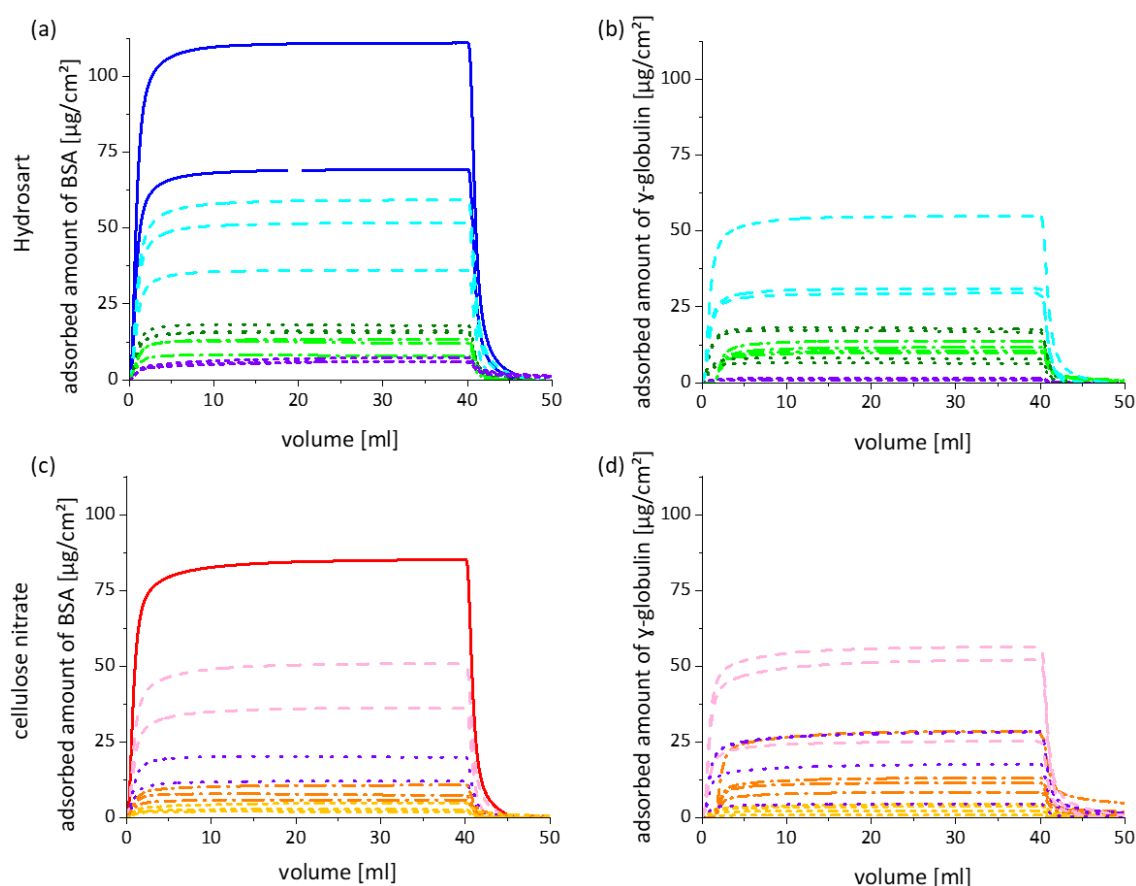


Figure 81: Adsorption of BSA and γ -globulin during filtration of protein formulations containing 0.01% PS80 with different protein concentrations (formulation and process conditions in table 9) during filtration through Hydrosart ((a) and (b)) and CN membranes ((c) and (d)); 5 g/l (blue and red, straight lines), 2 g/l (cyan and rose, dashed lines), 1 g/l (olive and lilac, dotted lines), 0.5 g/l (green and orange, dotted and dashed lines) and 0.1 g/l (yellow and lilac, short dashed lines).

Figure 82 shows Langmuir-plots of the measured results for BSA and γ -globulin adsorption. The Langmuir-isotherm was always found to be in the linear region in the measured concentration range up to 5 g/l, only a slight deviation from a linear plot can be observed at 5 g/l for BSA. Results are nearly independent of type of protein and type of membrane. Calculation of the monolayer coverage (figure 82) based on the Langmuir isotherm leads to unrealistic values of $4.8 \cdot 10^3$ for BSA and $6.7 \cdot 10^6$ for γ -globulin with standard deviations exceeding the actual calculated value. Finally, monolayer coverage was calculated as described in section 5.4.6.

5 Results and Discussion

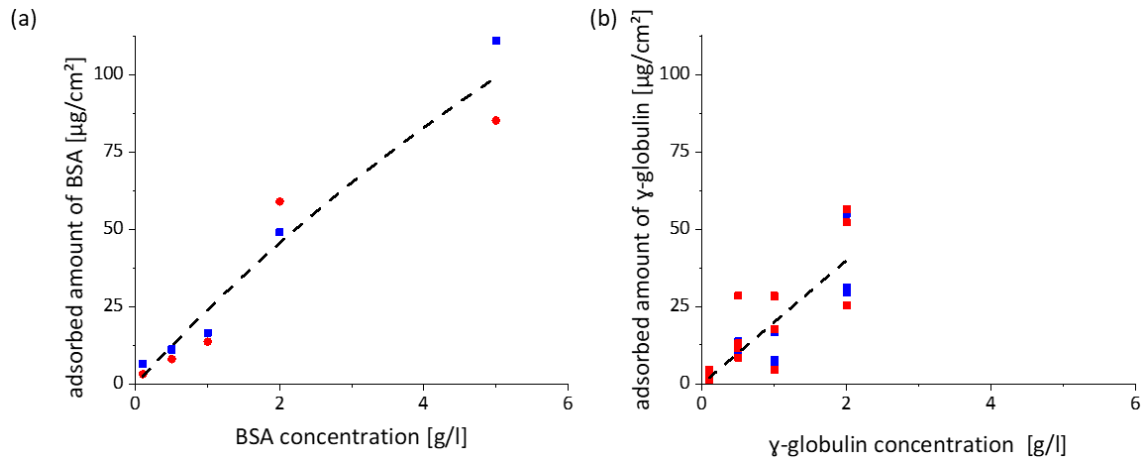


Figure 82: Adsorption isotherm according to adsorption data from figure 81 for adsorption of BSA and γ -globulin during filtration of protein formulations containing 0.01% PS80 through Hydrosart (blue) and CN (red) with Langmuir regression (black, dashed lines).

The issue with the evaluated adsorbed amount of proteins for stabilized formulations (protein formulations containing 0.01% PS80) is that the adsorbed amount of protein to the Cyrolite[®] membrane housings is clearly higher than the adsorbed amount of protein to the membrane material. This is presented in figure 83.

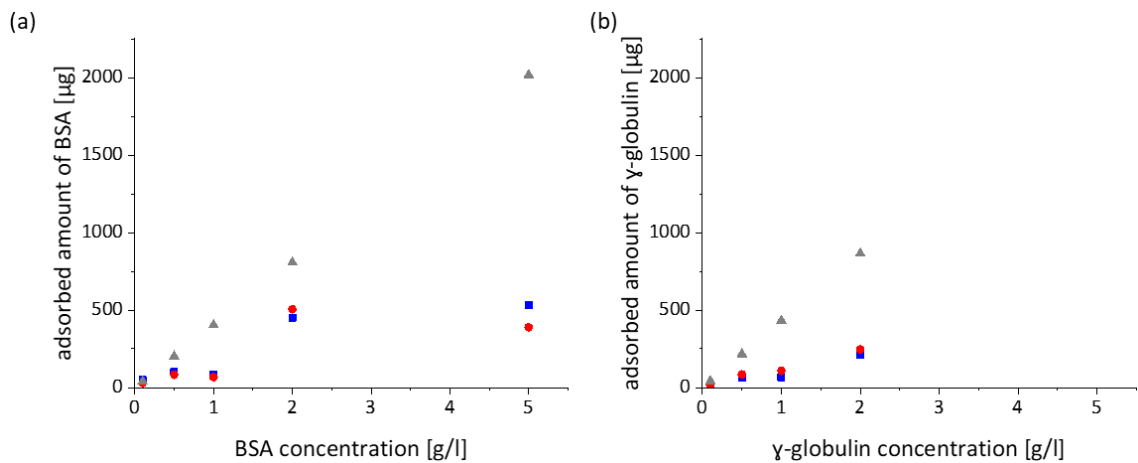


Figure 83: Comparison of protein adsorption of BSA (a) and γ -globulin (b) to Cyrolite[®] membrane housings (grey), Hydrosart (blue) and CN membrane material (red) at different protein concentrations. All formulations contain 0.01% PS80.

5.4.4 Influence of Filtration Flow Rate on Protein Adsorption

Measurements were performed for BSA and γ -globulin formulations containing 0.01% PS80. Flow rates were varied between 0.5 ml/min and 7.5 ml/min. The results are presented in figure 84. In case of the γ -globulin formulation no significant differences can be observed for protein adsorption in the measurement range of 1 ml/min to 7.5 ml/min. Adsorption measured for the BSA formulation shows a stronger variation but without clear trend. Therefore, it was concluded that protein adsorption

does not depend on flow rate under the experimental conditions. This result is in accordance with the Langmuir theory, in which protein adsorption depends on the protein concentration and the type of substrate only.

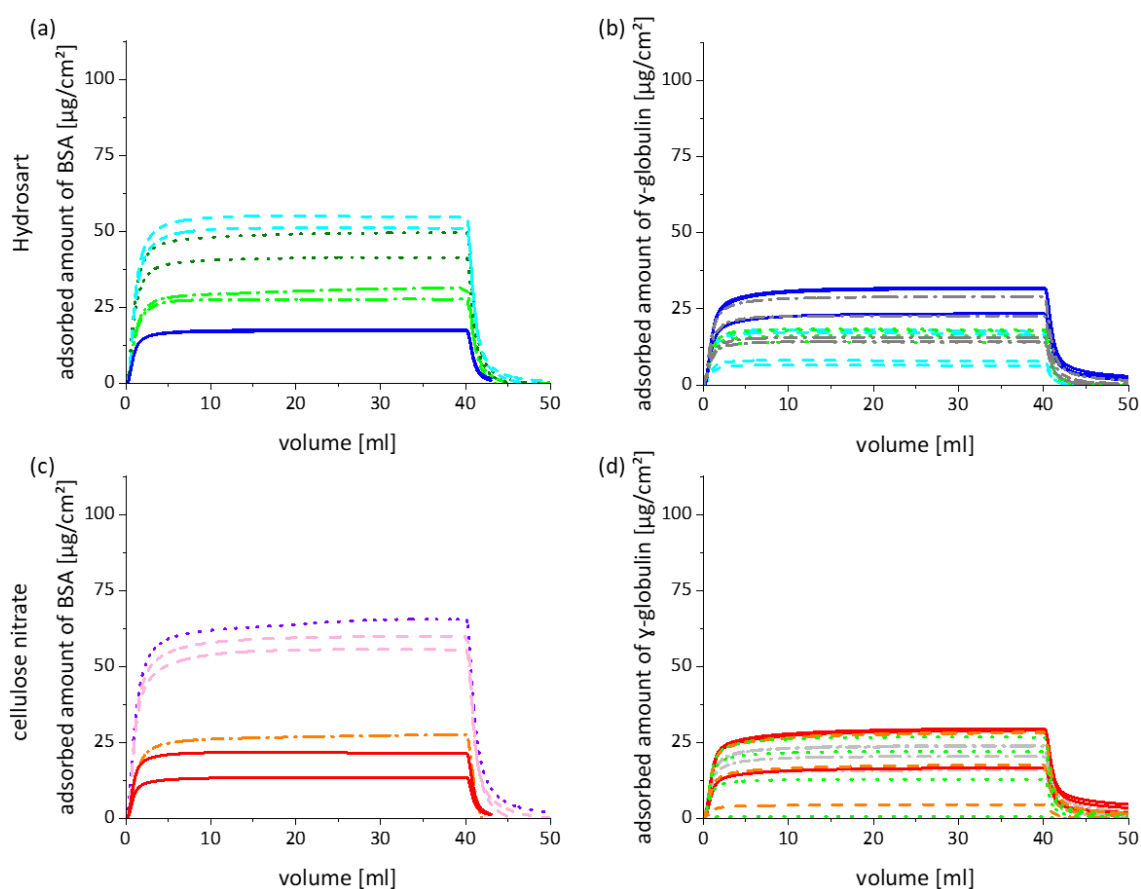


Figure 84: Adsorption of BSA ((a) and (c)) and γ -globulin ((b) and (d)) during filtration of protein formulations (formulation and process conditions as in table 9) on Hydrosart ((a) and (b)) and CN-membranes ((c) and (d)) at different filtration flow rates: 7.5 ml/min (dark and light grey, dotted and dashed lines, γ -globulin only), 5 ml/min (blue and red, straight lines), 2.5 ml (cyan and rose, dashed lines), 1 ml/min (olive and lilac, dotted lines), 0.5 ml/min (green and orange, dotted and dashed lines, BSA only).

5.4.5 Protein Adsorption and Desorption – Multiple Measurement Cycles

Multiple adsorption and desorption cycles were measured in order to examine the influence of pre-adsorbed protein molecules on the membrane surface on adsorption of further protein. Measurements were performed with surfactant free formulations and formulations containing 0.01% PS80, always with a protein concentration of 1 g/l and at a filtration flow rate of 0.9 ml/(min·cm²). Figure 85 presents results for the surfactant containing formulations. In accordance with the results described above, adsorption is always in the range of 10-25 $\mu\text{g}/\text{cm}^2$, independent of measurement cycle and type of membrane material. Adsorption is reversible.

5 Results and Discussion

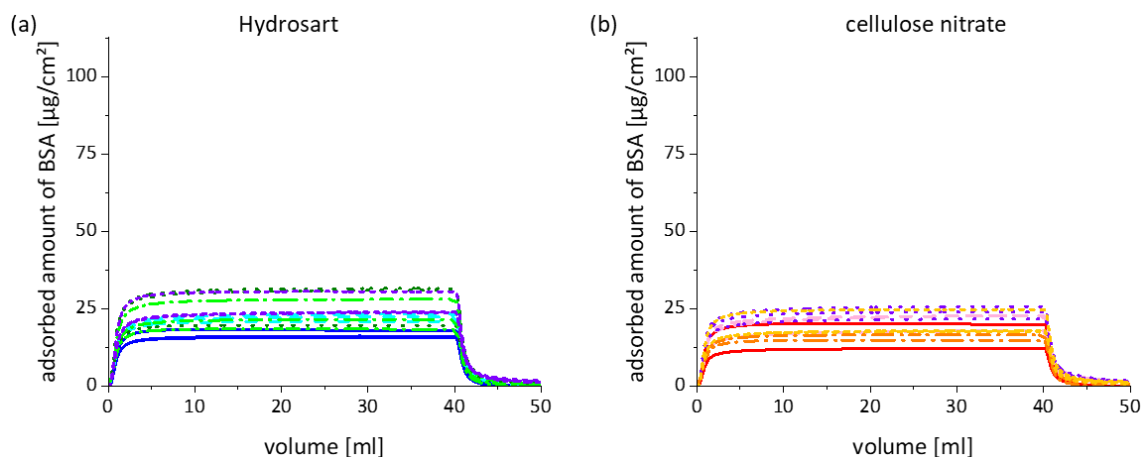


Figure 85: Adsorption of BSA during filtration of BSA formulations containing 0.01% PS80 (formulation and process conditions in table 9) in course of multiple adsorption and desorption cycles; a) Hydrosart and b) CN-membrane; 1st measurement cycle (blue and red, straight lines), 2nd measurement cycle (cyan and rose, dashed lines), 3rd measurement cycle (olive and lilac, dotted lines), 4th measurement cycle (green and orange, dotted and dashed lines) and 5th measurement cycle (lilac and yellow, short dashed lines).

Figure 86 presents the results for the surfactant free formulations. Adsorption on hydrophilic Hydrosart membranes is again in the range of 10-25 $\mu\text{g}/\text{cm}^2$ and reversible. A different behavior is observed for adsorption on hydrophobic CN membranes. Very strong adsorption was measured for the first measurement cycle for BSA (up to 100 $\mu\text{g}/\text{cm}^2$) and for γ -globulin (up to 200 $\mu\text{g}/\text{cm}^2$). In the following desorption process only parts of the adsorbed protein can be removed by flushing with the buffer solution, which clearly indicates that protein adsorption was partly irreversible. For all following adsorption and desorption processes again reversible behavior was observed with adsorption in the range of 10-25 $\mu\text{g}/\text{cm}^2$. The conclusion here is, that in the first cycle proteins stick irreversibly to the hydrophobic membrane surface, turning it hydrophilic and changing the adsorptive properties of the surface.

5 Results and Discussion

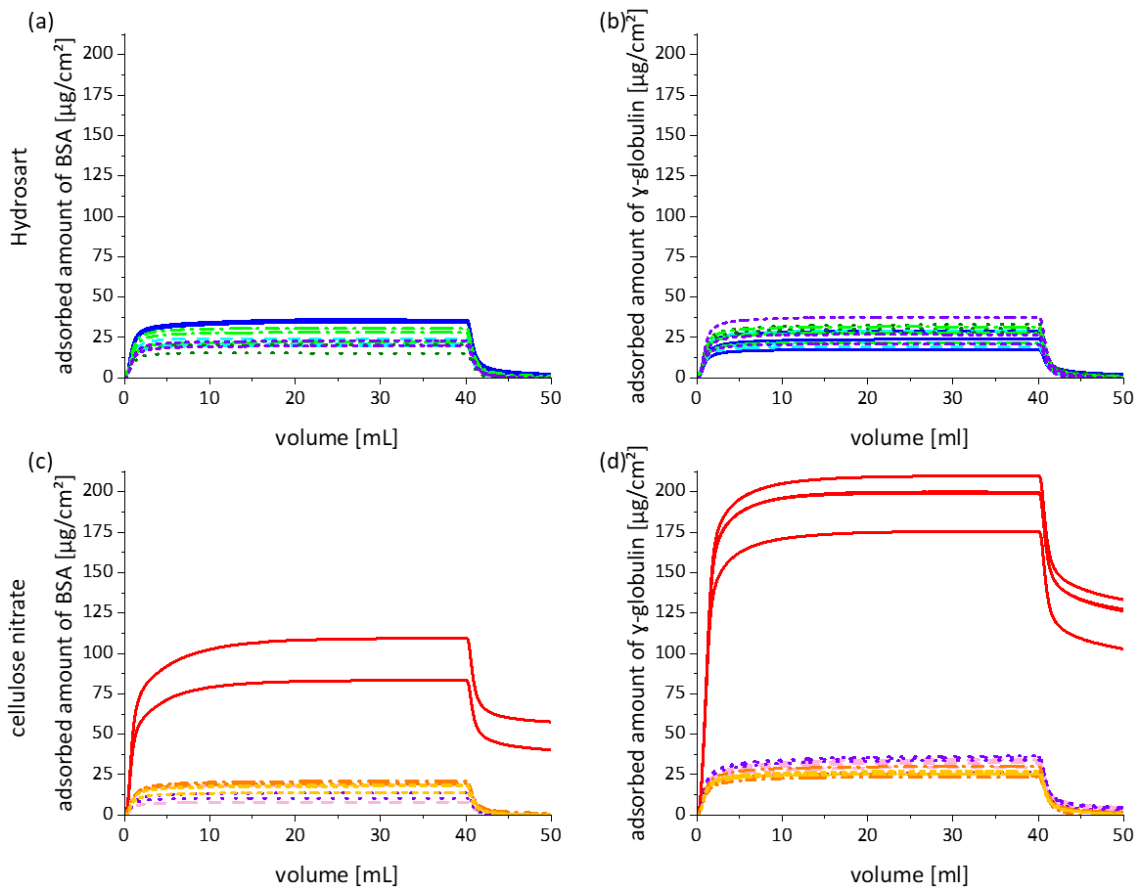


Figure 86: Adsorption of BSA and γ -globulin during filtration of protein formulations without PS80 (formulation and process conditions in table 9) in course of multiple adsorption and desorption cycles; (a) and (b) Hydrosart and (c) and (d) CN-membrane; 1st measurement cycle (blue and red, straight lines), 2nd measurement cycle (cyan and rose, dashed lines), 3rd measurement cycle (olive and lilac, dotted lines), 4th measurement cycle (green and orange, dotted and dashed lines) and 5th measurement cycle (lilac and yellow, short dashed lines).

Adsorption and desorption rates are calculated according to equation 23. The results are shown in figure 87. It can be seen that for Hydrosart hysteresis can be observed. Adsorption and desorption rates are comparable for all measurement cycles. For the CN membrane it can be seen that the adsorption rate for the first cycle is highly increased. For BSA the adsorption rate declines rather fast, whereas it stays on a high level for γ -globulin before the decline. The adsorption rates in the following measurement cycles are distinctly lower and on the same level as for the Hydrosart membrane material. Desorption rates are for CN in the first cycle elevated compared to the following cycles, but the difference is not as distinct as for the adsorption rate. Another effect that can be seen quite well is, that the protein desorption is not complete on CN in the first measurement cycle.

5 Results and Discussion

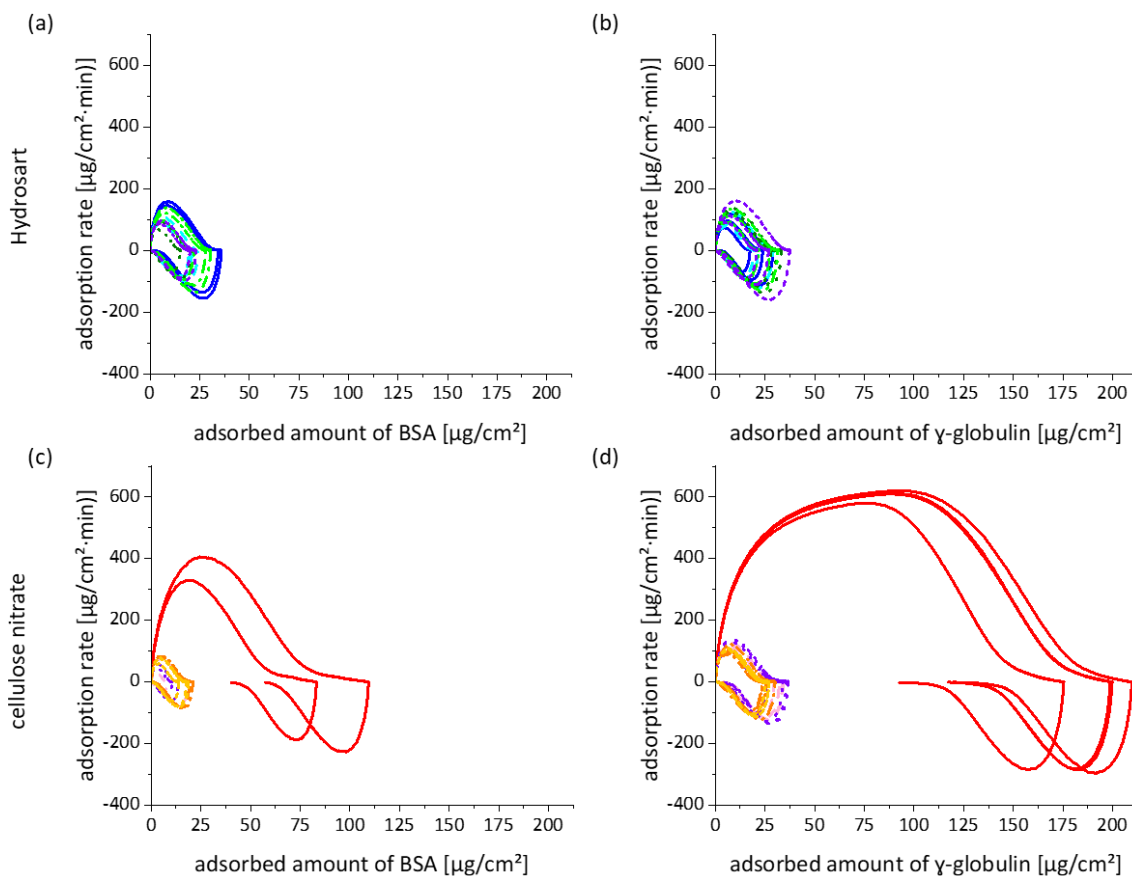


Figure 87: Adsorption and desorption rates for the multiple measurement cycles for BSA and γ -globulin presented in figure 86 in a formulation without PS80. Description as in figure 86.

The results show that in the first measurement cycle protein sticks to the hydrophobic CN material irreversibly, turning the surface hydrophilic for the following measurement cycles. Thus the adsorption level can be compared to Hydrosart after the first adsorption cycle.

5.4.6 Calculation of Monolayer Coverage

The coverage of the membrane surface can be calculated either based on the membrane properties or on the measured adsorption values presented in section 5.4.3. First the calculation based on the membrane properties is presented.

In literature the weight of a monolayer BSA on a surface is given with 150 ng/cm^2 - 200 ng/cm^2 [55]. The γ -globulin monolayer is given at saturation with $1.1 \pm 0.1 \text{ pmol/cm}^2$ surface area, [56] assuming a protein weight of 150 kDa (section 3.1.4) this equals $150\text{-}180 \text{ ng/cm}^2$. The surface of a membrane material can be calculated by measurement of the BET (Brunauer, Emmett and Teller) surface with nitrogen and the mass per unit area of a specific material. Those values are given in table 31. With this information the weight of the protein monolayers is calculated for Hydrosart and CN (table 31). But as the BET surface and the mass per unit area are both measured for the dry material it can

be assumed that in the wet state the surface of Hydrosart is significantly enlarged due to the swelling properties of cellulose and more protein is needed to obtain a monolayer coverage.

Table 31: Monolayer coverage calculated for adsorption of BSA on sterile filter membranes.

Membrane	Hydrosart	CN
BET-Surface [m ² /g]	4.2	11
Weight [g/m ²]	82	55
Membrane surface [cm ² /cm ²]	346	608
BSA monolayer [μg/cm ²]	52 – 69	91 – 122
γ-globulin monolayer [μg/cm ²]	52 – 62	91 – 109

For the calculation of the membrane coverage based on the adsorption measurement results presented in section 5.4.3 it cannot be assumed that the adsorption process leads to a homogeneous coverage of the membrane surface. Therefore instead of a monolayer an equilibrium coverage is calculated, but still based on the Langmuir equation (equation 15). The surface coverage θ is replaced by the adsorbed amount of protein m_{ads} (measured after filtration of 40 ml of protein solution) and the equilibrium coverage m_{eq} :

$$\frac{m_{ads}}{m_{eq}} = \frac{K \cdot c}{1 + K \cdot c} \quad 37$$

The adsorbed amount of protein m_{ads} can be measured, the protein concentration in the test solution is known, and the constant K can be calculated according to equation 38:

$$K = \frac{k_{ad}}{k_{de}} \quad 38$$

The parameters k_{ad} and k_{de} are the adsorption and the desorption rate. Both can be determined by evaluation of the adsorption measurements: at the beginning of the application of protein solution the whole surface is still available, here no desorption occurs. Therefore, it can be assumed that the measured adsorption rate is here equal to the adsorption rate constant. For calculation of the desorption rate a similar approach can be used for the desorption process: the maximum of the absolute value of the desorption rate at the beginning of the desorption process is equal to the desorption rate constant. With these values first the constant K , and with this the equilibrium mass m_{eq} is calculated. Adsorption and desorption rates in dependence on protein concentration are summarized in figure 88 for formulations containing 0.01% PS80.

5 Results and Discussion

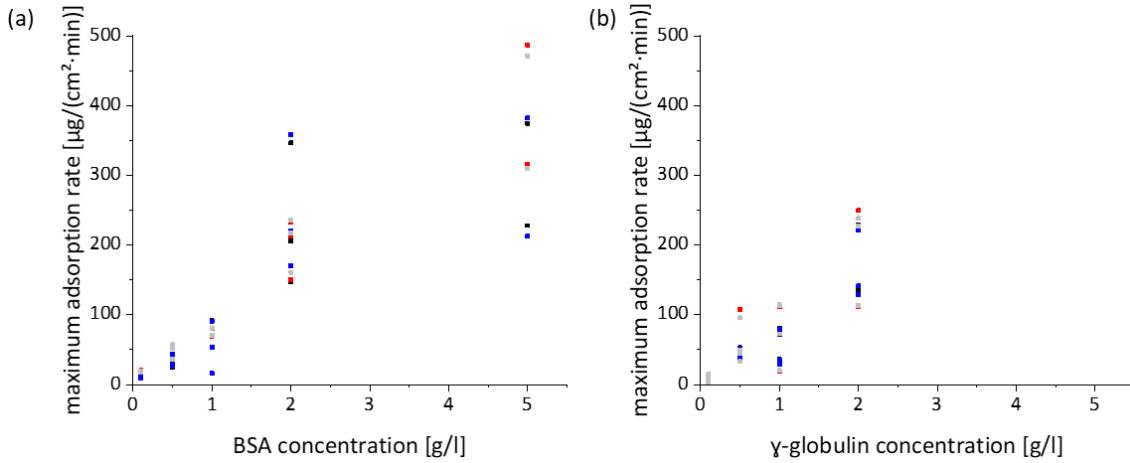


Figure 88: Maximum adsorption and desorption rates for BSA (a) and γ -globulin (b) during filtration of protein formulations through Hydrosart and CN-membranes (0.2 μm nominal pore size), calculated by deviation of the results given in figure 81. Adsorption and desorption rates on Hydrosart (black and blue) and on CN (red and grey).

In figure 88 it can be seen that for both membranes adsorption and desorption rate are quite similar. Therefore the constant K is averaged for both membrane types. For γ -globulin a constant $K_{\gamma\text{-globulin}}$ of 1.02 and for BSA a constant K_{BSA} of 0.98 is obtained.

$$m_{eq} = \frac{m_{ads}(1 + K \cdot c)}{K \cdot c} \quad 39$$

Now the equilibrium coverage can be calculated according to equation 39. Figure 89 summarizes the results in dependence on the protein concentrations.

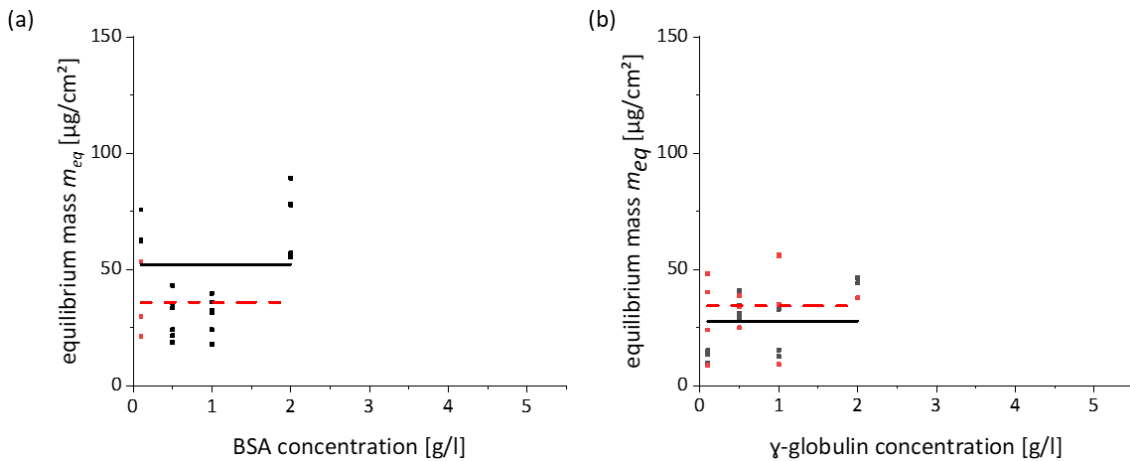


Figure 89: Calculated equilibrium mass m_{eq} according to equation 39 for adsorption of BSA and γ -globulin during filtration of protein formulations (table 9, adsorption data from figure 81) containing 0.01% PS80 through Hydrosart (black) and CN (red), both membranes with 0.2 μm nominal pore size; Hydrosart and CN outliers were eliminated.

The obtained equilibrium masses, m_{eq} according to equation 39, are compared with the theoretically estimated monolayers as given in table 31 in the following table:

Table 32: Comparison of calculated monolayer (table 30) and measured equilibrium coverage, m_{eq} as calculated according to equation 39 for adsorption of BSA and γ -globulin during filtration of protein formulations (table 9) containing 0.01% PS80 through Hydrosart and CN-membranes (0.2 μm nominal pore size).

Membrane	Hydrosart	CN
BSA monolayer [$\mu\text{g}/\text{cm}^2$]	52 – 69	91 – 122
γ -globulin monolayer [$\mu\text{g}/\text{cm}^2$]	52 – 62	91 – 109
BSA m_{eq} [$\mu\text{g}/\text{cm}^2$]	52 ± 6	36 ± 6
γ -globulin m_{eq} [$\mu\text{g}/\text{cm}^2$]	28 ± 4	34 ± 5

A good agreement was obtained for the calculated monolayer and the equilibrium mass m_{eq} for protein adsorption on hydrophilic Hydrosart membrane surface. In this study concentration dependency of protein adsorption was measured for surfactant containing protein formulation. Surfactants cover all surfaces and turn them hydrophilic. Therefore, m_{eq} values are well comparable and independent of the type of substrate.

An equilibrium coverage m_{eq} smaller than the monolayer coverage can be expected due to theoretical reasons (chapter 5.4.6, equation 19) and because not all parts of the membrane surface might be accessible during filtration. Additionally it was shown in figure 59 and figure 61 that fouling is not homogeneously distributed across the membrane material, therefore for protein adsorption this can be assumed as well. Higher adsorbed amounts of BSA were measured for protein concentrations above 2 g/l (figure 81). In this case, either the extent of the covered surface is enlarged, or multilayers are formed. In summary, modeling of protein adsorption on the basis of the Langmuir theory alone is not successful. Equilibrium coverage could be calculated in case of reversible protein adsorption as described above.

No further modeling of protein adsorption with the two state model (chapter 3.5.2) was undertaken because of the limited amount of data. Based on the results, it can be assumed that the transition of the reversibly to the irreversibly bound protein depends on the hydrophobicity of the substrate. The transition happens fast and the protein turns the surface hydrophilic in the process.

5.4.7 Summary

Protein adsorption occurs to every surface. This is an issue on studying protein adsorption, because usually the measurement system, especially the membrane housing, adsorbs more protein than the membrane itself. Protein adsorption on hydrophilic membranes during filtration is always minimal. Values in the range of 25 $\mu\text{g}/\text{cm}^2$ were measured for a protein concentration of 1 g/l BSA or γ -globulin at a flow rate of 0.9 ml/($\text{cm}^2 \cdot \text{min}$). The adsorption is reversible. The adsorbed amount of proteins increases with the protein concentration according to the Langmuir theory. No saturation

could be observed for both proteins in a Langmuir-plot for the studied concentration range up to 5 g/l. The filtration flow rate has no influence on the adsorption on the membrane surfaces under the studied experimental conditions.

Protein adsorption on hydrophobic surfaces depends on the composition of the formulation. For formulations containing a non-ionic surfactant (PS80) in a concentration above the CMC protein adsorption is comparable with the behavior described for hydrophilic surfaces or is in fact adsorption on a hydrophilic surface because of the surface activity of the surfactant covering the membrane surface. Therefore, the surface properties of the membranes are without influence.

For formulations with a surfactant concentration below the CMC of the respective surfactant a different behavior was observed. In this case additionally to the reversible adsorption an irreversible adsorption process occurs. This irreversible adsorbed protein layer can be thicker than a monolayer. It cannot be removed completely by rinsing with the formulation buffer. Remaining protein covers the surface and renders it hydrophilic, afterwards adsorption is minimized again and at the same level as in case of a surfactant containing formulation. The fact that non-ionic surfactants prevent adsorption is also described in the literature. Here it can be found as well that BSA adsorbs irreversibly to hydrophobic surfaces and prevent adsorption for other proteins. The results here are in agreement with that [168]. Other comparison with literature is not really possible, because for proteins the results of adsorption measurements are highly dependent of the formulation and the surface of interest as demonstrated, and no comparable experiments could be found.

Calculation of the equilibrium coverage, m_{eq} for protein adsorption of PS80 containing formulations was performed on the basis of a modified Langmuir equation using the quotient $\frac{m_{ads}}{m_{eq}}$ to describe the surface coverage θ and using experimental determined adsorption and desorption rates to describe K . Resulting values were in the range of $30 < m_{eq} < 50 \mu\text{g}/\text{cm}^2$ for both proteins studied independent on type of substrate, which is in good agreement with the expected monolayer coverage in case of protein adsorption on Hydrosart membranes.

Validation guide for qualification of filter products for filtration in biopharma production usually recommends to perform adsorption studies to assess the adsorptive properties of the membrane. Furthermore, the housing material of the filter and all the other single use plastic materials should be tested as well. All these materials are hydrophobic and often have a very rough surface, which facilitates protein adsorption.

5.5 Influence of Formulation Ingredients on Retention of *Brevundimonas diminuta*

As described in chapter 3.4 bacteria retention depends on the composition of the formulation, e.g., the salt concentration and the surfactant. Salt concentration or ionic strength of the formulation control osmotic phenomena with impact on the size of both membrane pores and bacteria. Here, formulation impact on microorganism shall be studied. Therefore the bacteria challenge tests have been performed with PES-membranes. PES membranes are highly hydrophobic and inert and no swelling or shrinking occurs on interaction with aqueous media. The experimental setup and the procedure are both described in section 4.8.

Three concentrations are measured for each salt and for Tween[®] 80, the concentrations of calcium chloride and magnesium chloride are adapted to the same ionic strength as the three highest sodium chloride concentrations. Pluronic F-127 is only measured at one concentration as reference for another surfactant. The selection of membranes listed in table 11 with graduated bubble point are used for the determination of the bacteria breakthrough bubble point. The viability tests are performed for each ingredient with the highest concentration twice. Within 1 hour 73% *B. diminuta* are viable in 5.1% CaCl₂, 85% in 4.4% MgCl₂, 98% in 9% saline, 91% in the phosphate buffer, 97% in Tween[®] 80 and 96% in Pluronic F-127. The results of the BCT measurements are presented in figure 90 in dependence on the bubble point of the PES membrane:

5 Results and Discussion

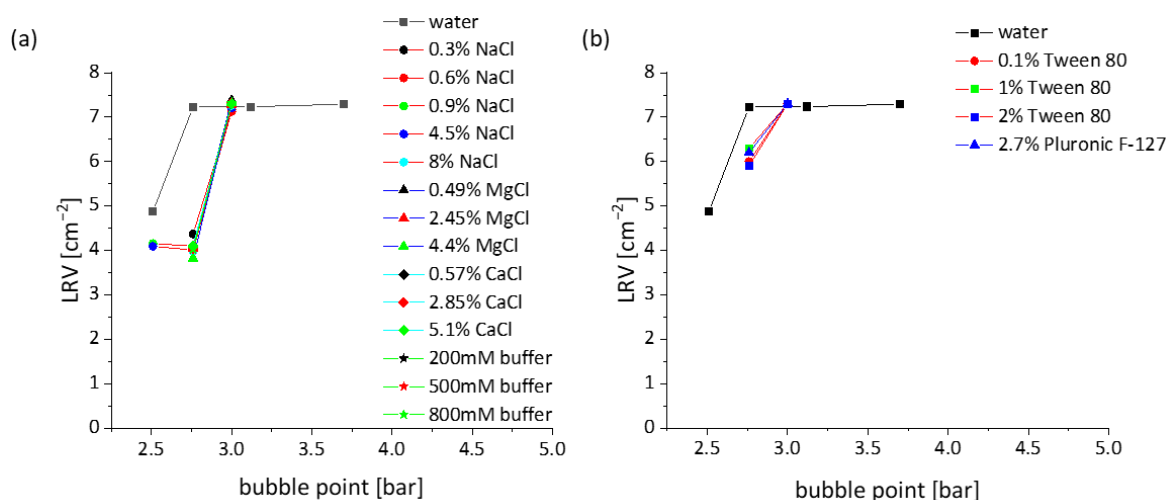


Figure 90: Results of bacteria retention of PES membranes for *Brevundimonas diminuta* with aqueous solutions containing different salts and surfactants and with different concentrations. Bubble point values measured independently. Description included in the figure, measurement setup and conditions described in section 4.8.

Bacteria breakthrough for aqueous solution in absence of salt or surfactant occurs between a bubble point of 2.5 and 2.8 bar. Upon addition of salt or surfactant the bacteria breakthrough shifts to a higher bubble point between 2.8 and 3.0 bar, regardless of the salt concentration or the type of cation, or the surfactant concentration. This result can be explained by shrinking of bacteria size due to osmotic effects for the salts, and a disruption of membrane-bacteria interactions due to the surfactants.

According to literature stronger effects were expected for increased salt concentration and at least a difference between monovalent and divalent cations. However, none of these effects could be confirmed. For the surfactants the LRV is in case of bacteria breakthrough higher compared to the salts (6 compared to 4). The influence of bacteria shrinkage seems to be more pronounced than the disruption of the interactions due to surfactants.

5.6 Filtration of Liposome Solutions

5.6.1 Characterization of Liposomal Formulations

An overview about the composition of the two studied liposomal formulations is given in table 7. The particle size distribution of the liposomal formulations was studied by DLS and Cryo-TEM microscopy. The results of the DLS measurements are presented in figure 91. The particle size distribution of both liposomal formulation is comparable and in the range of 100 to 200 nm.

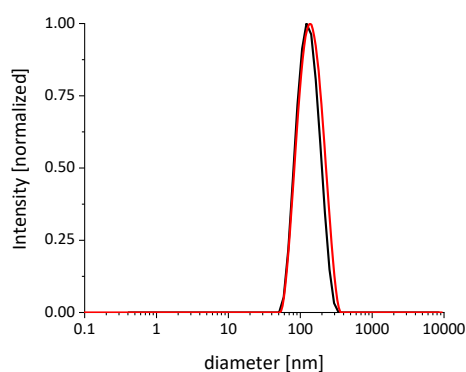


Figure 91: Particle size distribution of both liposomal formulations (table 7) measured by DLS. Liposomal Formulation 1 (by Polymun) in black, liposomal formulation 2 (R&D-formulation by SSB) in red.

The results of Cryo-TEM microscopy are presented in figure 92. The cryo-TEM images show liposomal particles with a mean particle diameter between 100 and 200 nm and a bilayer of 7 nm thickness in agreement with the DLS measurements; most liposome vesicles are unilamellar, some have liposome debris or complete liposomes inside. Emulsion droplets were detected in liposomal formulation 2 (figure 92b). The white corona around the emulsion droplets can be observed due to the hydrophobic properties; here the density is different as the water molecules are repelled.

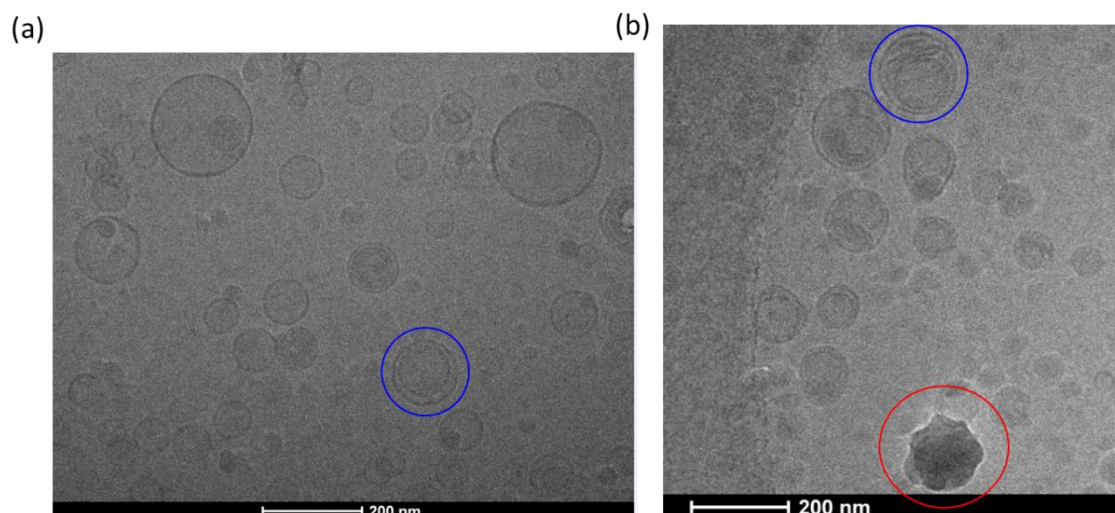


Figure 92: Cryo-TEM images of liposomal formulations (table 7): (a) liposomal formulation 1 (Polymun-formulation) and (b) liposomal formulation 2 (R&D-formulation by SSB). Both liposomal formulations diluted by factor 2; highlighted elements are multi-lamellar vesicles (blue) and emulsion droplets (red).

Both liposomal formulations are comparable concerning the particle size distribution. According to the Cryo-TEM results, liposomal formulation 1 contains a higher number of liposome vesicles, and the liposomes seem to be more circular and therefore more rigid compared with liposomal formulation 2.

5.6.2 Filtration Trials of Liposomal Formulations

Liposomal formulation 1 (Polymun-formulation) could not be filtered with 0.2 μm PES and Hydrosart membranes at room temperature. In all filtration trials immediate filter blocking was observed, independent on the filtration conditions. The filtration results for liposomal formulation 2 (R&D-formulation by SSB) are presented in figure 94 and figure 95 for filtration through Hydrosart and PES-membranes, respectively. Filtration parameters are summarized in table 33. Formulation 2 had a viscosity of ca. 1 mPa·s. Constant flow and constant pressure filtration was performed.

Lowest degree of filter blocking was usually observed for filtration at higher flow rate (more than 5 ml/(min·cm²) or highest pressure (above 1.5 bar), which is in agreement with the literature presented in section 3.6. Filtration through Hydrosart membranes showed a lower degree of filter fouling and Hydrosart enabled filtration of the liposomal formulation 1 at lower pressures and lower flow rates compared with PES membranes. Initial resistances were unusually high. The initial filtration resistances presented in table 33 are two times as high as the membrane resistance, for PES membranes the initial resistance is for 2 bar even at $25 \cdot 10^{10} \text{ m}^{-1}$ and for 1 ml/(min·cm²) at $30 \cdot 10^{10} \text{ m}^{-1}$, which is 10 times too high.

For filtration at elevated temperatures in a pre-trial the stability of the formulation was tested up to 55 °C by DLS-measurement. No change in the particle size distribution could be observed, so

5 Results and Discussion

filtration trials were performed at 40 °C. At this temperature liposomal formulation 1 could be filtered. The results are presented in figure 96 and table 34. Again, a high degree of filter fouling was observed with very high initial resistances. In case of filtration of liposomal formulations, filter fouling and initial resistance were usually correlated with decreasing values in the sequence: PVDF_{hyd}-membranes > Hydrosart > CA > PES. But in this trial CA has a distinctly higher resistance (table 34). Membranes with larger pore size are beneficial for this filtration case. The improved filterability of formulation 1 at 40 °C compared with room temperature can be explained with the temperature dependent properties of liposomes that are described in section 3.6.1.

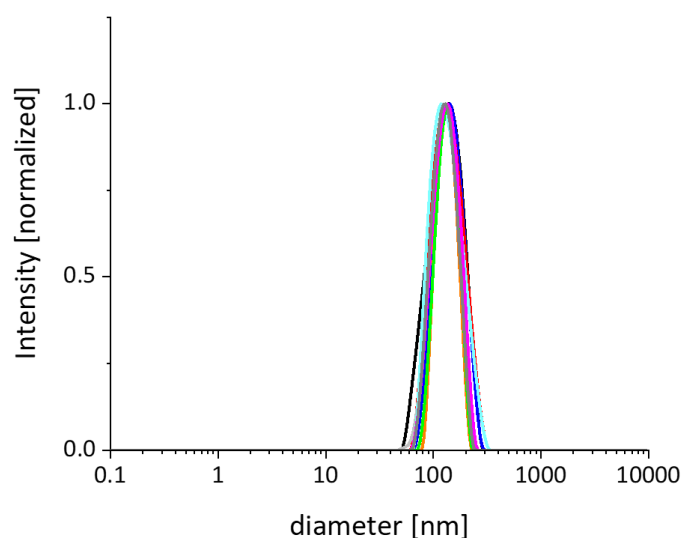


Figure 93: Particle size distribution of liposomal formulation 1 at different temperatures: 15 °C (black), 20 °C (blue), 25 °C (red), 30 °C (light grey), 35 °C (cyan), 40 °C (orange), 45 °C (green), 50 °C (magenta) and 55 °C (dark grey).

5 Results and Discussion

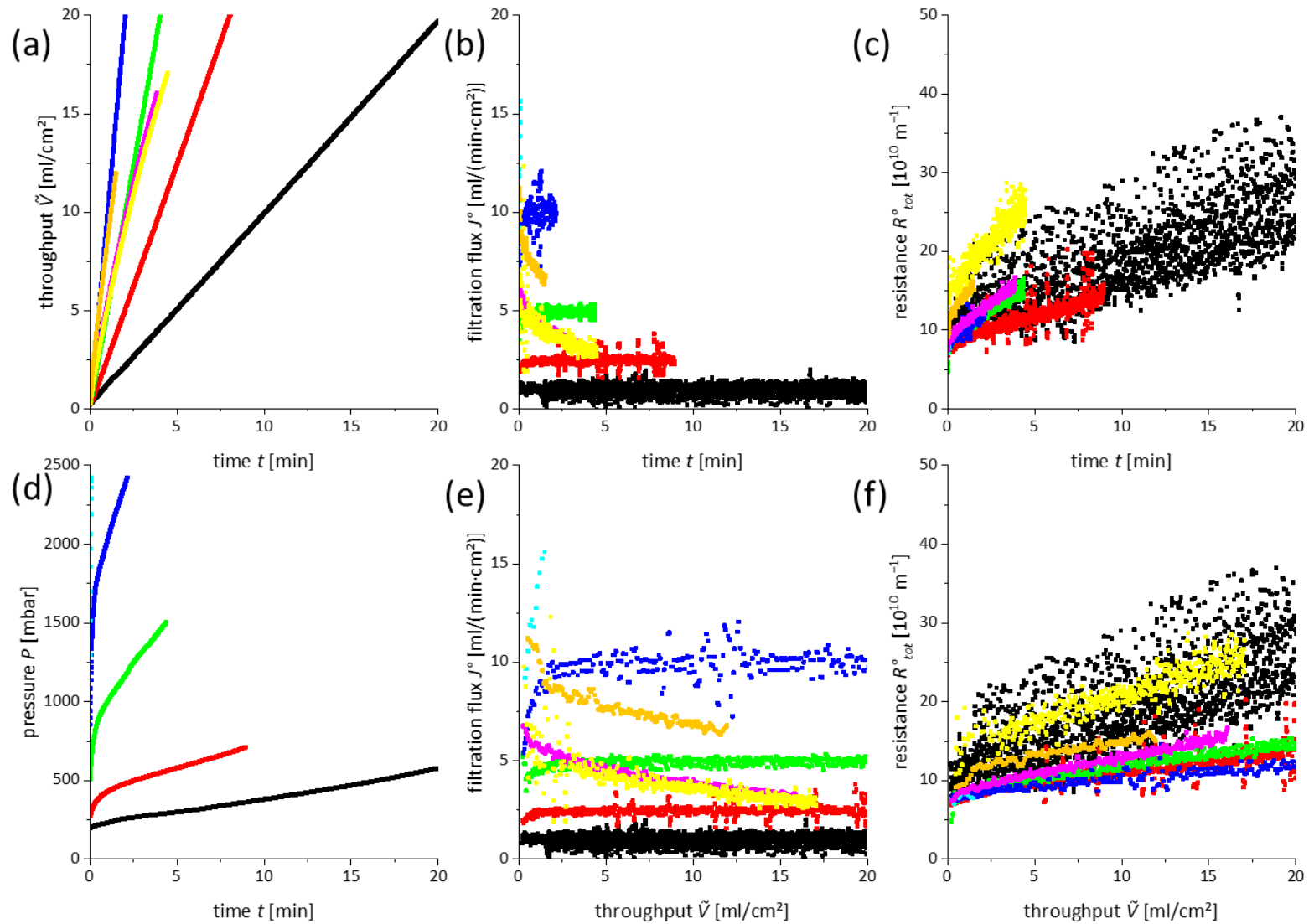


Figure 94: Summary of results for filtration of liposomal formulation 2 through Hydrosart membranes (0.2 μm nominal pore size). Filtration performed at constant flow: 1 ml/(min·cm²), black; 2.5 ml/(min·cm²), red; 5 ml/(min·cm²), green; 10 ml/(min·cm²), blue; 12.5 ml/(min·cm²), cyan. Filtration performed at constant pressure: 1 bar, magenta; 1.5 bar, yellow; 2 bar, orange.

5 Results and Discussion

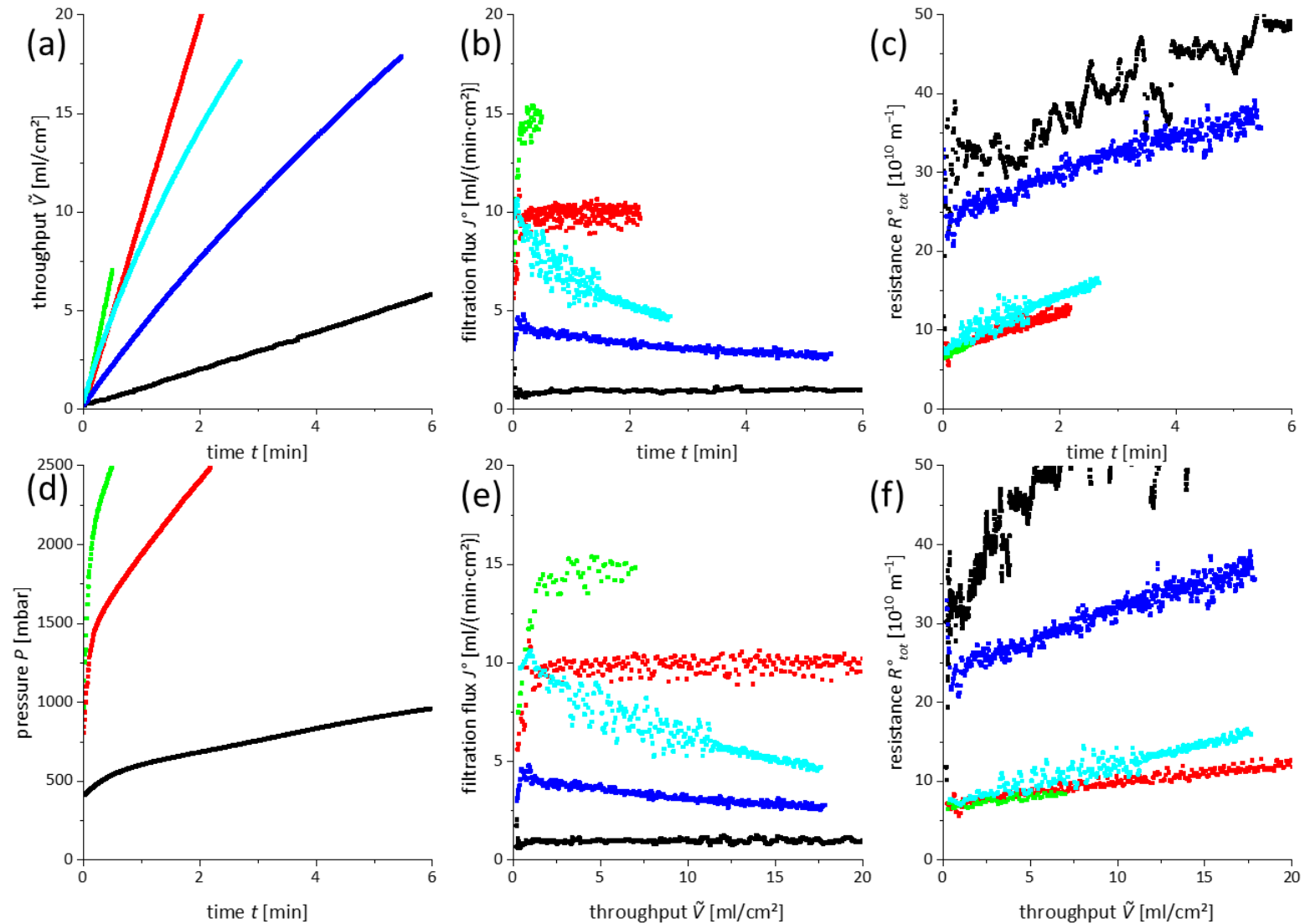


Figure 95: Summary of filtration results for filtration of liposomal formulation 2 through PES-membranes (0.2 μm nominal pore size). Filtrations performed with constant flow: 1 ml/(min·cm²), black; 10 ml/(min·cm²), red; 15 ml/(min·cm²), green. Filtration performed at constant pressure: 1.5 bar, cyan; 2 bar, blue.

5 Results and Discussion

Table 33: Characteristic parameters for constant pressure and constant flow filtration of liposomal formulation 2 through Hydrosart and PES membranes as presented in figure 94 and figure 95.

Membrane	Pressure P [bar]	Initial flux J° [ml/(min·cm²)]	Time at 50% blocking $t_{50\%}$ [min]	Initial resistance R° [10^{10} m⁻¹]	Throughput $\check{V}_{50\%}$ at $t_{50\%}$ [ml/cm²]
Hydrosart	1	6.9	3.1	7.2	13.5
Hydrosart	1.5	5.9	4.2	12.0	16.3
Hydrosart	2	11.7	2.1	9.0	15.5
PES	1.5	11.1	1.8	6.6	13.0
PES	2	4.6	-	21.6	-
Membrane	Flux J° [ml/(min·cm²)]	Initial pressure P_0 [bar]	Time at 50% blocking $t_{50\%}$ [min]	Initial resistance R° [10^{10} m⁻¹]	Throughput $\check{V}_{50\%}$ at $t_{50\%}$ [ml/cm²]
Hydrosart	1.0	0.2	14.5	13.3	14.3
Hydrosart	2.5	0.3	9.2	7.4	22.8
Hydrosart	4.9	0.5	-	8.4	-
Hydrosart	9.9	0.9	-	8.1	-
Hydrosart	12.5	1.6	-	6.8	-
PES	1.0	0.4	19.1	9.5	18.7
PES	9.9	0.8	-	7.2	-
PES	14.6	1.0	-	6.8	-

5 Results and Discussion

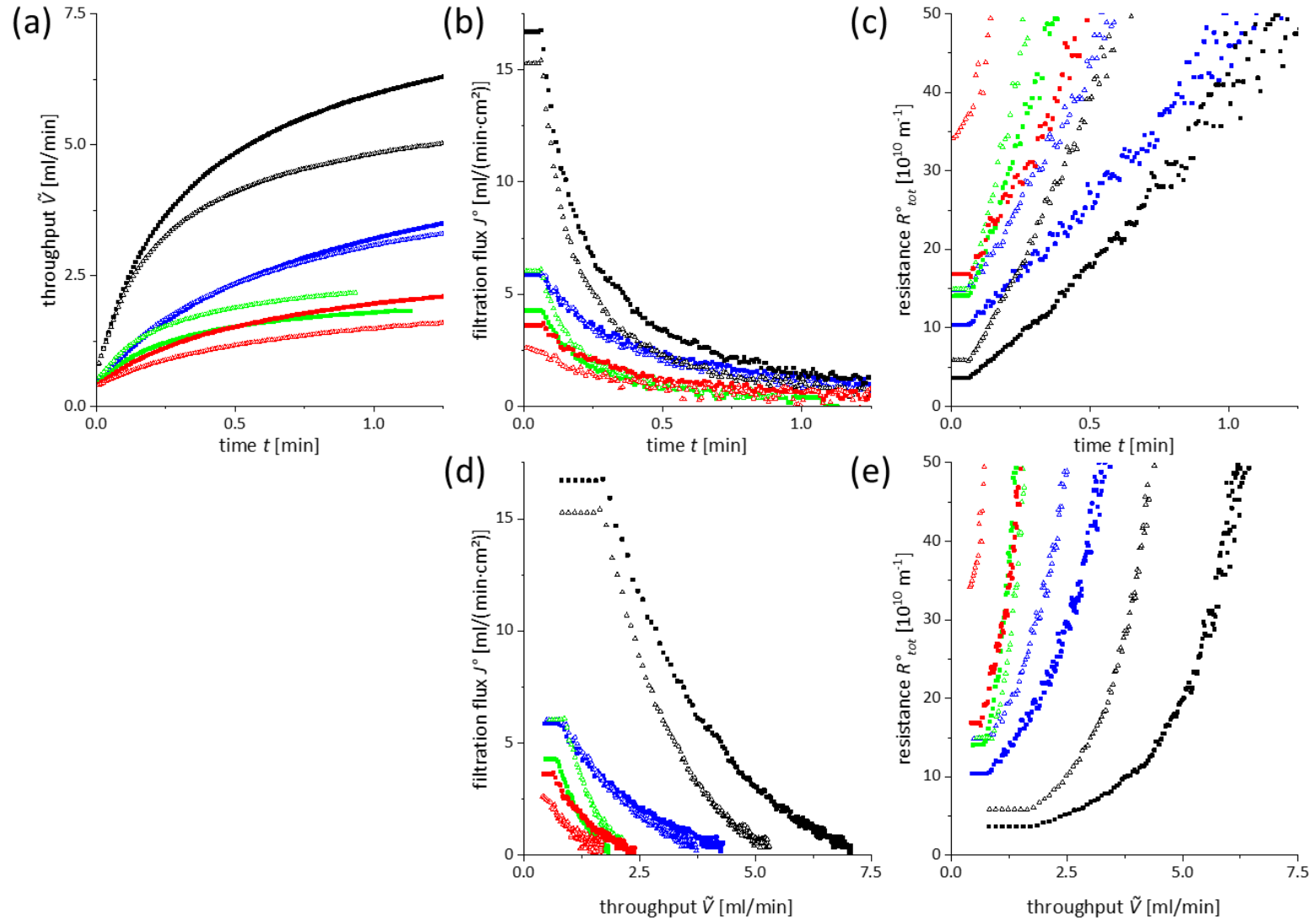


Figure 96: Summary of results for constant pressure filtration of liposomal formulation 1 at 40 °C; filtration at 1 bar (squares) and at 1.5 bar (triangles). Filtration membranes (0.2 μ m nominal pore size) are PES (black), Hydrosart (blue), CA (green) and PVDF_{hyd} (red).

5 Results and Discussion

Table 34: Characteristic parameters for constant pressure filtration of liposomal formulation 1 at 40 °C as presented in figure 96.

Membrane	Pressure p [bar]	Initial flux J_0 [ml/(min·cm ²)]	Time at 50% blocking $t_{50\%}$ [min]	Initial resistance R_0 [10 ¹⁰ m ⁻¹]	Throughput $\check{V}_{50\%}$ at $t_{50\%}$ [ml/cm ²]
PES	1	20.5	0.1	2.3	2.1
PES	1.5	20.6	0.1	2.3	2.1
Hydrosart	1	7.0	0.2	8.6	1.4
Hydrosart	1.5	7.0	0.2	12.3	1.3
CA	1	5.7	0.1	12.0	0.9
CA	1.5	7.7	0.1	11.8	1.1
PVDF _{hyd}	1	4.6	0.2	12.8	0.9
PVDF _{hyd}	1.5	2.8	0.3	27.8	0.9

5 Results and Discussion

The SEM images presented in figure 97 were recorded after the filtration trials for both formulations. It can be seen that the membrane pores are covered with a skin. In some cases not all of the surface is covered, but a network can be observed ((b) and (c)).

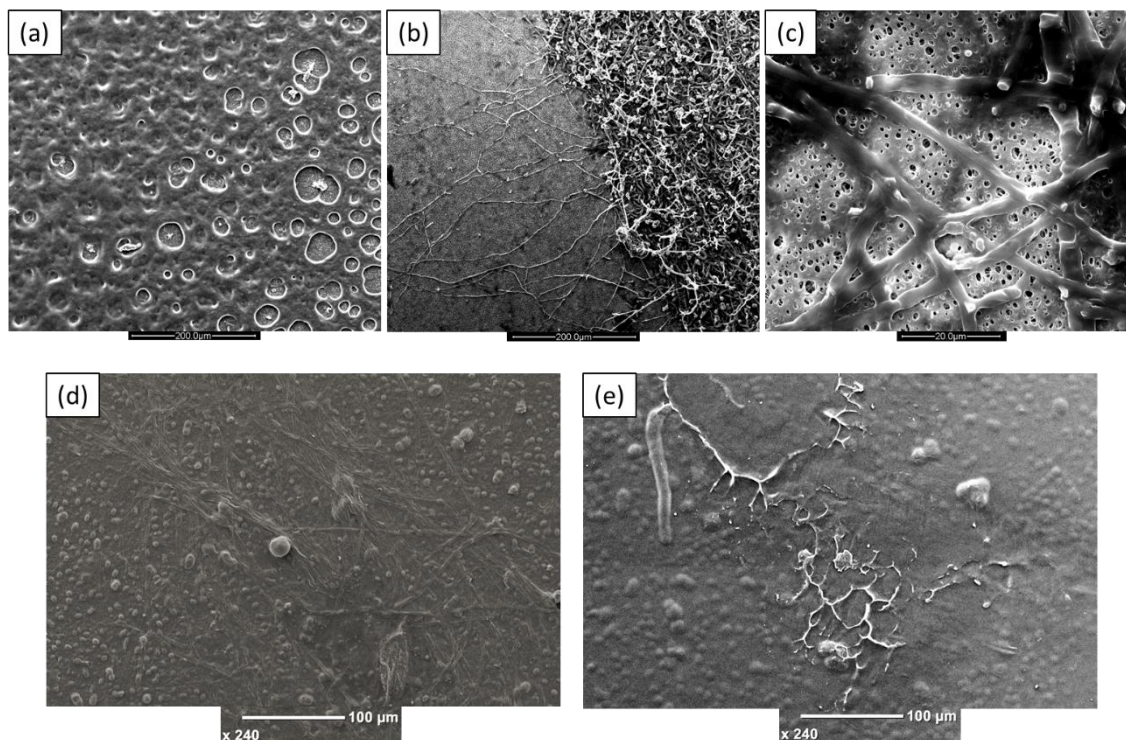


Figure 97: SEM images of membrane materials after filtration with liposomal filtration 1 (a-c) and liposomal formulation 2 (d, e) at elevated temperature at different magnifications. Membrane materials are Hydrosart (a,b,d) and PES (c,e).

In literature hardly any filtration studies can be found on the membrane performance, therefore hardly any reasons for membrane blocking are reported. It is assumed that components of the liposomes interact with the membrane and clog it because of their unique physical and chemical properties [134]. Those properties are caused by the surface activity of lipid molecules and either the liposome charge or the bilayer fluidity: negatively charged liposomes can exhibit repulsive interactions with each other and with the membrane material. The bilayer fluidity influences the rigidity of the liposome spheres. Probably both properties contribute to membrane blocking. [169]

To examine the high initial resistance further, filtration trials were performed with Latex bead formulations. The Latex beads have a spherical structure and are more rigid in their spherical structure, but do not carry any charged surface groups. Constant flow and constant pressure filtrations were performed through Hydrosart and PES membranes.

Figure 98 summarizes the results for constant pressure filtration. Again, strong filter fouling is observed along with high initial resistances, comparable with liposome filtration. Here, better filterability was observed for Hydrosart membranes and filtration at higher pressure. No results are reported

for constant flow filtration, because of immediate filter blocking and no filtrate could be obtained before the filtration pressure reached 2.5 bar.

These results show that the high initial resistance can be explained with the macroscopic particle structure. Despite the different surface chemistry, the latex beads and the liposomal formulations have high initial filtration resistances. The latex beads are more similar to the liposomal formulation 1 below the transition temperature of the liposome bilayer because of the rigidity of the vesicles. But in contrast to the Latex beads no filtration was possible in constant flow filtration.

Filter blocking leads to deposition of a fouling layer on top of the membrane. In case of the latex beads this can be observed directly by formation of a white cake. Fouling by liposome vesicles might be more complex. They are composed by individual lipid molecules, which self-assemble in a bilayer structure and might reorganize on interaction with the membrane surface. The stability of the liposomal vesicles depends on their chemical composition and temperature. Fouling can occur either by deposition of liposome particles or lipid molecules or both.

5 Results and Discussion

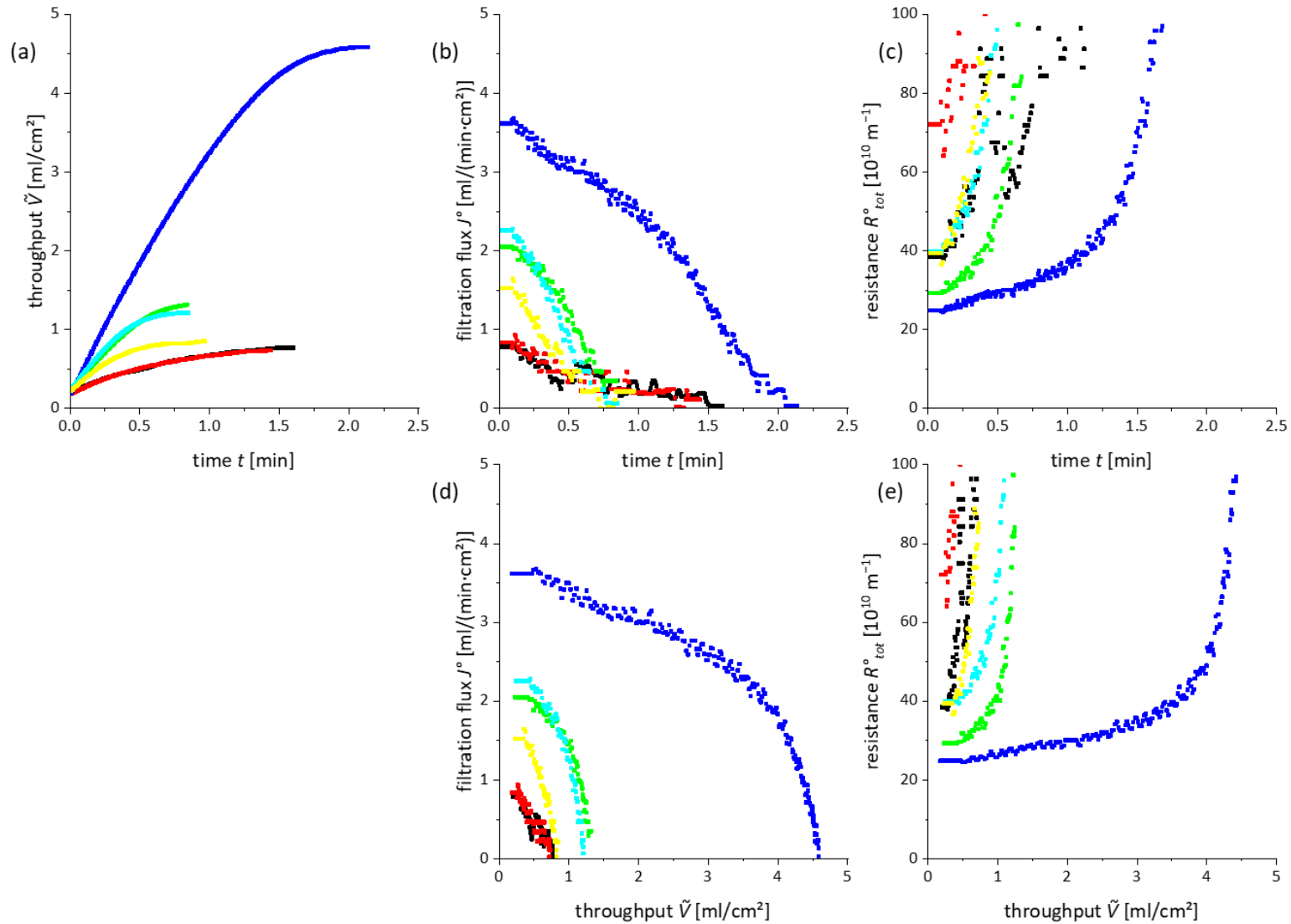


Figure 98: Results of constant pressure filtration trials with a solution of polystyrene beads (10 g/l) through Hydrosart and PES membranes (0.2 μ m nominal pore size). Hydrosart with differential pressure of 0.5 bar (black), 1 bar (red), 1.5 bar (blue) and PES with differential pressure of 1 bar (green) and 1.5 bar (cyan and yellow).

5 Results and Discussion

Table 35: Characteristic parameters for constant pressure filtration of polystyrene-beads as presented in figure 98.

Membrane	Pressure P [bar]	Initial flux J_0^o [ml/(min·cm ²)]	Time at 50% blocking $t_{50\%}$ [min]	Initial resistance R_0^o [10 ¹⁰ m ⁻¹]	Throughput at $t_{50\%}$ $= \tilde{V}_{50\%}$ [ml/cm ²]
Hydrosart	0.5	0.8	0.6	38	0.6
Hydrosart	1	0.8	0.6	72	0.5
Hydrosart	1.5	3.6	3.9	25	3.9
PES	1	2.1	0.5	29	1.1
PES	1.5	1.5	0.4	59	0.7
PES	1.5	2.3	0.4	40	1.0

5.6.3 Summary

Filterability of two liposomal formulations through sterile filter membranes was studied. According to the results, liposomal solutions should be filtered preferably by constant pressure filtration at differential pressure larger than 1.5 bar or constant flow filtration, the necessary filtration flow rate depends on the membrane material. Hydrophilic Hydrosart membranes had a larger operating window than the in comparison more hydrophobic PES membranes.

Filterability of liposomal solutions can be very different in dependence on the chemical nature of the lipids used for formulation. The viscosity of a liposomal solution can be increased compared with water, which leads to reduced flow rates. Furthermore, the rigidity of the liposome vesicles is an important factor for filterability of the formulation, which can be influenced by composition but also by filtration temperature. Filterability might be improved at higher temperature.

The degree of filter fouling was generally high, as indicated by high initial resistances, often much larger than the membrane resistance. SEM images of membrane surface after filtration show the formation of closed fouling layers rather than deposition of individual liposome vesicles. The strong fouling tendency can be explained by the chemical nature of liposomes. Liposome vesicles are composed by individual surface active lipid molecules, which can reorganize in contact with the membrane surface, when passing the membrane pores during filtration. Fouling can occur by deposition of entire liposomes or lipid molecules or both.

6 Summary and Conclusions

The central aim of this study is to investigate, which criteria must be considered in the sterile filtration of protein formulations, in particular the filtration of stabilized and drug-like protein formulations under Fill and Finish process conditions. The work included the development of standardized drug-like protein formulations, the study of the filterability of these test media, up-scaling studies and the investigation of protein adsorption as well as bacteria retention under challenging conditions. Furthermore, the filterability of liposomal formulations was tested. The results can be summarized as follows:

1. The filterability of protein formulations was tested with standardized test solutions. The test solutions were formulated according to the formulation criteria for antibody-based drugs as described by Uchiyama *et al.* [24] Three different formulations were provided based on γ -globulin and BSA, all containing 0.5% PS80: two phosphate-buffered BSA formulations, one with a protein concentration of 250 g/l and 4 mPa·s and one with 75 g/l and a viscosity of 40 mPa·s, and a histidine-buffered γ -globulin formulation with a protein concentration of 100 g/l.

Working procedures to prepare these formulations in liter scale were developed and documented [159]. The formulations were carefully adjusted concerning pH and excipients to achieve maximum stability. Protein test solutions with a reproducible low degree of aggregation can be produced by dispersing commercial lyophilized proteins in a buffer solution containing excipients according to the developed formulation recipe by means of a Viscojet® stirring technology and by filtration of the test solutions with pre-filters (0.45 μ m) before use. The low degree of aggregation has been proved by SEC and DLS measurements.

For all formulations, characteristic properties were described, i.e. concentration, viscosity, particle size distribution and filtration characteristics. Test procedures were developed and documented respectively [151–153].

2. The filterability of the protein test solutions of item 1 was studied under different process conditions and by using different sterile membrane filters (0.2 μ m nominal pore size: Hydrosart, CN, PVDF_{hyd}, PES).

Generally, a low degree of filter fouling was observed due to the high colloidal stability of the test solutions. According to the results, filtration performance and filter fouling are mainly influenced by the stability of the formulation, the filtration process conditions and the membrane properties.

The degree of filter fouling was not significantly influenced by the protein concentration in the studied concentration range between 5 and 200 g/l. Comparing the studied test solutions, the high

concentrated BSA formulation showed the highest fouling tendency and the γ -globulin formulation showed the lowest fouling tendency. Based on these results, filter fouling is not an issue during sterile filtration in the Fill and Finish process due to the high colloidal stability of protein drug formulations. However, sterile filtration of protein formulations, which are not well stabilized may be more challenging, e.g., filtration of the bulk drug substance in the course of downstream processing.

Filter fouling depends on the process conditions. The lowest degree of filter fouling was observed for constant flow filtration, which is preferable for process filtration. The filtration flow rate is usually low due to the increased viscosity. Typical values for filtration of the test solutions were 0.5-5 ml/(min·cm²) (300-3 000 l/(m²·h)) at an initial pressure of 0.5 bar.

The stability of the protein formulation is not solely assured by its composition and can be easily compromised by unsuitable process conditions, e.g., by inappropriate pumps and tubing, temperature increase, process interruption and interaction with air in filtration equipment resulting in an accelerated fouling rate. Therefore, fouling was found to be a spontaneous process in certain cases.

The main mechanism of filter fouling is the constriction of membrane pores due to the deposition of protein indicated by a slow and steady increase of the resistance versus throughput plot $R(\check{V})$. Fouling layers within the membrane material were visualized by confocal fluorescence microscopy. Based on these results, fouling starts in the narrow parts of the membrane structure and fouling layers are not homogeneously distributed across the membrane cross-section. Formation of aggregates in the formulation, e.g., by unsuitable process conditions, leads to an increase of the fouling rate. The curve in the resistance, R versus throughput \check{V} plot, turns into an exponential trend.

Hydrophilic membranes such as Hydrosart are most suitable for process filtration. Their fouling tendency is generally low, even for filtration of not well stabilized protein formulations and filtration under destabilizing process conditions, e.g., filtration at elevated temperature. Another important selection criteria of membranes for protein filtration is the pore size distribution. Membranes with a wide pore size distribution always showed less filter fouling regardless of their surface properties.

Filterability of stabilized protein formulations with a very low degree of aggregation cannot be improved by use of pre-filter/main filter combinations. The pre-filter only increases the filter resistance.

3. The adsorptive properties of membranes for proteins are an important selection criteria for membrane filters. Protein adsorption during filtration was studied with inverse liquid chromatography (ILC) by measuring and analyzing breakthrough curves.

Adsorption was examined for filtration of protein formulations through hydrophilic Hydrosart and hydrophobic CN membranes with a nominal pore size of 0.2 μm at a flow rate between 0.1 and 1.4 ml/(min·cm²). A phosphate buffered BSA formulation (pH 6.9) and a histidine buffered γ -globulin formulation (pH 6.4) with variable surfactant (PS80) content were studied in the concentration range between 0.1 and 5 mg/ml.

Pre-tests demonstrated that plastic parts of the filtration setup such as the filter housing or tubing show more protein adsorption than the membrane itself, which was especially high for parts with a rough surface. Consequently, filter holders made from low adsorptive Cyrolite® were used in the following adsorption studies.

The results showed that protein adsorption on membranes with hydrophilic surfaces (e.g., Hydrosart) is always minimal and reversible independent of the formulation. The amount of adsorbed protein depends on the protein concentration but not the filtration flow rate. For both proteins the adsorption isotherm did not reach saturation in the studied concentration range. The equilibrium protein coverage, m_{eq} was calculated on the basis of a modified Langmuir equation taking the measured adsorption and desorption rates into consideration. For both proteins (BSA and γ -globulin), resulting values were in the range of 30-50 $\mu\text{g}/\text{cm}^2$, which is less than the calculated protein monolayer.

Protein adsorption on hydrophobic membrane surfaces (e.g., CN membranes) depends on the composition of the formulation: For formulations containing a non-ionic surfactant (PS80) in a concentration above the CMC, protein adsorption was found to be reversible and comparable with adsorption on hydrophilic membrane surfaces. For surfactant free formulations or formulations with a surfactant content below CMC, significantly stronger adsorption was observed, which was partly irreversible, resulting in a protein layer much thicker than a monolayer. It was observed that repeated adsorption and desorption cycles with surfactant-free protein formulations on hydrophobic CN membranes lead to conditioning of the membrane surface. The first protein layer cannot be removed completely by the rinsing buffer and turns the surface hydrophilic. Afterwards reversible adsorption can be observed.

According to these results, protein adsorption must always be discussed in relation to the composition of the formulation and the presence of surfactants. A low degree of protein adsorption can be expected for filtration of stabilized protein drug formulations independent of the membrane filter used. Membrane filters with a hydrophilic surface should be used for filtration of non-stabilized protein formulations and destabilizing process conditions.

4. The scalability of filter devices from lab scale to process was studied for protein filtration by means of a new flow rate and resistance-based up-scaling approach.

The up-scaling approach is based on the modeling of filtration curves using a resistance-in-series model based on the Darcy equation. Basic requirements are the knowledge of the active membrane area and the device resistance. These parameters and the scale-up factor can be determined by pressure-dependent water flow rate measurements of lab scale and process scale filter products. With these data, target process filtration curves can be modeled on the basis of the resistance vs. throughput curves of small-scale filtration trials. The necessary equations are described for constant flow and constant pressure filtration processes. The up-scaling approach was validated by filtration of a particulate test solution through lab-scale and process scale products with excellent agreement between calculated and experimental data.

To use the approach for up-scaling studies for the filtration of protein formulations (test solutions according to item 1), experimental work procedures and setups (pumping, tubing, tube angles and valves) had to be defined to produce and handle metastable protein formulations in process scale, to conduct filtration trials and to evaluate filtration results. Filtration trials were performed in constant flow mode. The flow rate had to be adjusted according to the active filter area as determined by water flow measurements, which can be distinctly smaller than the embedded filter areas, which are documented in the product specification.

Scalability could be demonstrated for filtration of BSA formulations through a large number of pleated and stacked sterile filter devices containing PES, Hydrosart and PVDF_{hyd} membranes (all with 0.2 µm nominal pore size) with filter areas between 4.5 cm² and 6 000 cm². Contrary to this, significant differences in the fouling behavior of small-scale and process scale filter devices were observed for the filtration of the γ-globulin formulation through stacked filter devices. Beside the membrane related filter-fouling, additional fouling processes were observed, probably caused by an unsuitable fluid design or inappropriate housing material of the process filters.

5. Protein formulations are challenging concerning bacteria retention, due to their complex formulation containing salts and excipients, e.g., surfactants, sugar and lipid molecules. Salts and further excipients have an impact on bacteria retention. It could be demonstrated that the breakthrough bubble point of PES membranes shows an increase of ca. 0.2 bar in presence of salts or surfactants, regardless of type and concentration. According to these results membrane filters with a narrower pore size distribution should be selected for protein filtration.

6. Furthermore, the filterability of liposomal formulations through various sterile filter membranes has been studied. Filtration trials were performed with two liposomal solutions, both with a particle size distribution of ca. 100 nm.

According to the obtained results, filterability of liposomal solutions can be very different in dependence on the chemical nature of the lipids used for formulation and the filtration process conditions.

Liposomal solutions should be filtered preferably by constant pressure filtration at differential pressure larger than 1.5 bar or constant flow filtration. With constant flow filtration, the necessary filtration flow rate depends on the membrane material. Usually, hydrophilic Hydrosart membranes performed better than hydrophobic PES membranes.

The rigidity of the liposome vesicles is an important factor for filterability of the formulation, which is defined by the lipid composition but can be influenced by filtration temperature. Filterability is improved above the transition temperature of the respective liposomes.

The degree of filter fouling was generally high, as indicated by high initial resistances, often much larger than the membrane resistance. SEM images of membrane surface after filtration show the formation of closed fouling layers rather than the deposition of individual liposome vesicles. The strong fouling tendency can be explained by the chemical nature of liposomes and their surface activity rather than surface charge effects. Liposome vesicles are formed by aggregation of lipid molecules, which can reorganize after contact with the membrane surface, when passing the membrane pores during filtration. Fouling can occur by deposition of entire liposomes or lipid molecules or both. Small pores or pores with unfortunate turns get clogged right at the beginning of the filtration process and do not contribute to the filtration process any more.

7 Literature

- [1] H.A.D. Lagassé, A. Alexaki, V.L. Simhadri, N.H. Katagiri, W. Jankowski, Z.E. Sauna, C. Kimchi-Sarfaty, Recent advances in (therapeutic protein) drug development [version 1; referees: 2 approved], *F1000 Res.* 6 (2017) 1–17. doi:10.12688/f1000research.9970.1.
- [2] B. Leader, Q.J. Baca, D.E. Golan, Protein therapeutics: A summary and pharmacological classification, *Nat. Rev. Drug Discov.* 7 (2008) 21–39. doi:10.1038/nrd2399.
- [3] P.S. Sarangapani, S.D. Hudson, K.B. Migler, J.A. Pathak, The limitations of an exclusively colloidal view of protein solution hydrodynamics and rheology, *Biophys. J.* 105 (2013) 2418–2426. doi:10.1016/j.bpj.2013.10.012.
- [4] E. Rosenberg, Aggregation of Therapeutic Antibodies in the Course of Downstream Processing, (2010) 1–255.
- [5] M.C. Manning, D.K. Chou, B.M. Murphy, R.W. Payne, D.S. Katayama, Stability of protein pharmaceuticals: An update, *Pharm. Res.* 27 (2010) 544–575. doi:10.1007/s11095-009-0045-6.
- [6] J.M. Berg, J.L. Tymoczko, L. Stryer, *Biochemistry*, Int. ed., W.H. Freeman and Company, New York, 2012.
- [7] Z. Elgundi, M. Reslan, E. Cruz, V. Sifniotis, V. Kayser, The state-of-play and future of antibody therapeutics, *Adv. Drug Deliv. Rev.* 122 (2017) 2–19.
- [8] H.-I. Chang, M.-Y. Cheng, M.-K. Yeh, Clinically-Proven Liposome-Based Drug Delivery: Formulation, Characterization and Therapeutic Efficacy, *Sci Rep.* 1 (2012) 1–8. <https://www.omicsonline.org/scientific-reports/2155-983X-SR195.pdf>.
- [9] S.L. Nail, M.J. Akers, eds., *Development and Manufacture of Protein Pharmaceuticals*, Springer US, Boston, MA, 2002. doi:10.1007/978-1-4615-0549-5.
- [10] PDA Technical Report No. 26: Sterilizing Filtration of Liquids Final Draft, Parenter. Drug Assoc. (1997) 1–51.
- [11] Parenteral Drug Association, Points to Consider For Aseptic Processing, *PDA J. Pharm. Sci. Technol.* 57 (2003) 1–72.
- [12] S. Kandula, S. Babu, M. Jin, A.A. Shukla, Design of a filter train for precipitate removal in monoclonal antibody downstream processing, *Biotechnol. Appl. Biochem.* 54 (2009) 149–155. doi:10.1042/BA20090181.
- [13] L.J. Harris, S.B. Larson, K.W. Hasel, A. McPherson, Refined structure of an intact IdG2a monoclonal antibody, *Biochemistry.* 36 (1997) 1581–1597.
- [14] H.M. Berman, J. Westbrook, Z. Feng, G. Gilliland, T.N. Bhat, H. Weissig, I.N. Shindyalov, P.E. Bourne, The Protein Data Bank, *Nucleic Acids Res.* 28 (2000) 235–242.
- [15] A.S. Rose, A.R. Bradley, Y. Valasatava, J.M. Duarte, A. Prlić, P.W. Rose, NGL viewer: web-based molecular graphics for large complexes, *Bioinformatics.* 34 (2018) 3755–3758. doi:10.1093/bioinformatics/bty419.
- [16] F. Fang, I. Szleifer, Kinetics and thermodynamics of protein adsorption: A generalized molecular theoretical approach, *Biophys. J.* 80 (2001) 2568–2589. doi:10.1016/S0006-3495(01)76228-5.
- [17] H.-C. Mahler, W. Friess, U. Grauschopf, S. Kiese, Protein Aggregation: Pathways, Induction Factors and Analysis, *J. Pharm. Sci.* 98 (2009) 2909–2934.

- [18] G. Ben-Nissan, M. Sharon, Capturing protein structural kinetics by mass spectrometry, *Chem. Soc. Rev.* 40 (2011) 3627–3637. doi:10.1039/c1cs15052a.
- [19] Y. Moskovitz, S. Srebnik, Conformational changes of globular proteins upon adsorption on a hydrophobic surface, *Phys. Chem. Chem. Phys.* 16 (2014) 11698–11707. doi:10.1039/c4cp00354c.
- [20] M. Rabe, D. Verdes, S. Seeger, Understanding protein adsorption phenomena at solid surfaces, *Adv. Colloid Interfac.* 162 (2011) 87–106.
- [21] E.Y. Chi, S. Krishnan, T.W. Randolph, J.F. Carpenter, Physical stability of proteins in aqueous solution: Mechanism and driving forces in nonnative protein aggregation, *Pharm. Res.* 20 (2003) 1325–1336. doi:10.1023/A:1025771421906.
- [22] D. Sek, Breaking old habits: Moving away from commonly used buffers in pharmaceuticals, *Eur. Pharm. Rev.* (2012).
- [23] L. Jorgensen, S. Hostrup, E.H. Moeller, H. Grohganz, Recent trends in stabilising peptides and proteins in pharmaceutical formulation – considerations in the choice of excipients, *Expert Opin. Drug Deliv.* 6 (2009) 1219–1230. doi:10.1517/17425240903199143.
- [24] S. Uchiyama, Liquid formulation for antibody drugs, *Biochim. Biophys. Acta.* 1844 (2014) 2041–2052. doi:10.1016/j.bbapap.2014.07.016.
- [25] N.K. Jain, I. Roy, Effect of trehalose on protein structure, *Protein Sci.* 18 (2009) 24–36. doi:10.1002/pro.3.
- [26] E.Y. Chi, Excipients and their Effects on the Quality of Biologics, *Aaps.* 1 (2012) 1–12.
- [27] B.S. Chang, S. Hershenson, Practical approaches to protein formulation development., *Ration. Des. Stable Protein Formul. Pract.* (2002) 1–25. doi:10.1007/978-1-4615-0557-0_1.
- [28] H.J. Lee, A. McAuley, K.F. Schilke, J. McGuire, Molecular origins of surfactant-mediated stabilization of protein drugs, *Adv. Drug Deliv. Rev.* 63 (2011) 1160–1171. doi:10.1016/j.addr.2011.06.015.
- [29] B. Chen, R. Bautista, K. Yu, G.A. Zapata, M.G. Mulkerrin, S.M. Chamow, Influence of Histidine on the Stability and Physical Properties of a Fully Human Antibody in Aqueous and Solid Forms, *Pharm. Res.* 20 (2003) 1952–1960. doi:10.1023/B:PHAM.0000008042.15988.c0.
- [30] H. Hamada, T. Arakawa, K. Shiraki, Effect of Additives on Protein Aggregation, *Curr. Pharm. Biotechnol.* 10 (2009) 400–407. doi:10.2174/138920109788488941.
- [31] N. Inoue, E. Takai, T. Arakawa, K. Shiraki, Specific decrease in solution viscosity of antibodies by arginine for therapeutic formulations, *Mol. Pharm.* 11 (2014) 1889–1896. doi:10.1021/mp5000218.
- [32] R.L. Hutchings, S.M. Singh, J. Cabello-Villegas, K.M.G. Mallela, Effect of antimicrobial preservatives on partial protein unfolding and aggregation, *J. Pharm. Sci.* 102 (2013) 365–376.
- [33] M.S. Neergaard, D.S. Kalonia, H. Parshad, A.D. Nielsen, E.H. Møller, M. Van De Weert, Viscosity of high concentration protein formulations of monoclonal antibodies of the IgG1 and IgG4 subclass - Prediction of viscosity through protein-protein interaction measurements, *Eur. J. Pharm. Sci.* 49 (2013) 400–410. doi:10.1016/j.ejps.2013.04.019.
- [34] The Immunisation Advisory Centre, Vaccine ingredients, Fact Sheet. (2017) 1–9. <http://www.immune.org.nz/sites/default/files/resources/WrittenResources/ConcernVaccineIngredients20170825V01Final.pdf> (accessed September 24, 2018).

- [35] G.L. Morefield, A rational, systematic approach for the development of vaccine formulations., *AAPS J.* 13 (2011) 191–200. doi:10.1208/s12248-011-9261-1.
- [36] W. Wang, M. Singh, Selection of Adjuvants for Enhanced Vaccine Potency, *World J. Vaccines.* 01 (2011) 33–78. doi:10.4236/wjv.2011.12007.
- [37] R.J. Hunter, *Foundations of Colloid Science*, 2nd ed., Oxford University Press, 2001.
- [38] S.R. McGuffee, A.H. Elcock, Atomically detailed simulations of concentrated protein solutions: The effects of salt, pH, point mutations, and protein concentration in simulations of 1000-molecule systems, *J. Am. Chem. Soc.* 128 (2006) 12098–12110. doi:10.1021/ja0614058.
- [39] J. Jezek, M. Rides, B. Derham, J. Moore, E. Cerasoli, R. Simler, B. Perez-Ramirez, Viscosity of concentrated therapeutic protein compositions, *Adv. Drug Deliv. Rev.* 63 (2011) 1107–1117. doi:10.1016/j.addr.2011.09.008.
- [40] A. Saluja, A. V Badkar, D.L. Zeng, S. Nema, D.S. Kalonia, Ultrasonic storage modulus as a novel parameter for analyzing protein-protein interactions in high protein concentration solutions: correlation with static and dynamic light scattering measurements., *Biophys. J.* 92 (2007) 234–44. doi:10.1529/biophysj.106.095174.
- [41] A. Allmendinger, S. Fischer, J. Huwyler, H.-C. Mahler, E. Schwarb, I.E. Zarraga, R. Mueller, Rheological characterization and injection forces of concentrated protein formulations: An alternative predictive model for non-Newtonian solutions, *Eur. J. Pharm. Biopharm.* 87 (2014) 318–328. doi:10.1016/j.ejpb.2014.01.009.
- [42] N. Rathore, R.S. Rajan, Current perspectives on stability of protein drug products during formulation, fill and finish operations, *Biotechnol. Prog.* 24 (2008) 504–514. doi:10.1021/bp070462h.
- [43] J. Atkins, Peter W., de Paula, *Physikalische Chemie*, 4th ed., Wiley-VCH-Verlag GmbH & Co KGaA, Weinheim, 2006.
- [44] R.J. Kortschot, A.P. Philipse, B.H. Ern e, Debye Length Dependence of the Anomalous Dynamics of Ionic Double Layers in a Parallel Plate Capacitor, *J. Phys. Chem. C.* 118 (2014) 11584–11592. doi:10.1021/jp5025476.
- [45] A.A. Malmberg, C.G., Maryott, Dielectric Constant of Water from 0° to 100° C, *J. Res. Natl. Bur. Stand.* (1934). 56 (1956) 1–8.
- [46] Y. Zhang, P.S. Cremer, Interactions between macromolecules and ions: the Hofmeister series, *Curr. Opin. Chem. Biol.* 10 (2006) 658–663. doi:10.1016/j.cbpa.2006.09.020.
- [47] R.P. Sear, Nucleation: theory and applications to protein solutions and colloidal suspensions, *J. Phys. Condens. Matter.* 19 (2007) 033101. doi:10.1088/0953-8984/19/3/033101.
- [48] J.S. Bee, M. Davis, E. Freund, J.F. Carpenter, T.W. Randolph, Aggregation of a monoclonal antibody induced by adsorption to stainless steel, *Biotechnol. Bioeng.* 105 (2010) 121–129. doi:10.1002/bit.22525.
- [49] A. Hagedorf, N. Lill, *Formulierungen f ur Insulin - Von der Spritze zum k nstlichen Pankreas*, *Pharmakon.* 1 (2013) 128–138. doi:10.1691/pn.20130015.
- [50] A.M. Morris, M.A. Watzky, R.G. Finke, Protein aggregation kinetics, mechanism, and curve-fitting: a review of the literature., *Biochim. Biophys. Acta.* 1794 (2009) 375–97. doi:10.1016/j.bbapap.2008.10.016.
- [51] W. Wang, Instability, stabilization, and formulation of liquid protein pharmaceuticals, *Int. J. Pharm.* 185 (1999) 129–188. doi:10.1016/S0378-5173(99)00152-0.

- [52] K.D. Ratanji, J.P. Derrick, R.J. Dearman, I. Kimber, Immunogenicity of therapeutic proteins: Influence of aggregation, *J. Immunotoxicol.* 11 (2014) 99–109. doi:10.3109/1547691X.2013.821564.
- [53] K.M. Hosseini, M. Ghasemzadeh, Implementation of Plasma Fractionation in Biological Medicines Production, *Iran. J. Biotechnol.* 14 (2016) 213–220.
- [54] R.S. Tirumalai, K.C. Chan, D.A. Prieto, H.J. Issaq, T.P. Conrads, T.D. Veenstra, Characterization of the Low Molecular Weight Human Serum Proteome, *Mol. Cell. Proteomics.* 2 (2003) 1096–1103. doi:10.1074/mcp.M300031-MCP200.
- [55] B. Jachimska, K. Tokarczyk, M. Łapczyńska, A. Puciul-Malinowska, S. Zapotoczny, Structure of bovine serum albumin adsorbed on silica investigated by quartz crystal microbalance, *Colloids Surfaces A Physicochem. Eng. Asp.* 489 (2016) 163–172.
- [56] W. Liao, F. Wei, M.X. Qian, X.S. Zhao, Characterization of protein immobilization on alkyl monolayer modified silicon (1 1 1) surface, *Sens. Actuator B. Chem.* 101 (2004) 361–367. doi:10.1016/j.snb.2004.04.006.
- [57] K.A. Majorek, P.J. Porebski, A. Dayal, M.D. Zimmerman, K. Jablonska, A.J. Stewart, M. Chruszcz, W. Minor, Structural and immunologic characterization of bovine, horse, and rabbit serum albumins, *Mol. Immunol.* 52 (2012) 174–182. doi:10.1016/j.molimm.2012.05.011.
- [58] Carl Roth, Technical Info Bovine Serum Albumins (BSA), (2016). https://www.carlroth.com/downloads/allgemein/en/Info_Brochure_Albumins_EN.pdf (accessed November 5, 2018).
- [59] W. Wang, S. Singh, D.L. Zeng, K. King, S. Nema, Antibody structure, instability, and formulation, *J. Pharm. Sci.* 96 (2007) 1–26. doi:10.1002/jps.20727.
- [60] T. Boenisch, M.S. Revised, H. Winther, S. Steen, J. Ms, *Immunohistochemical Staining Methods Chapter 1: Antibodies*, 5th ed., Carpinteria, 2009.
- [61] A. Hawe, W.L. Hulse, W. Jiskoot, R.T. Forbes, Taylor Dispersion Analysis Compared to Dynamic Light Scattering for the Size Analysis of Therapeutic Peptides and Proteins and Their Aggregates, *Pharm. Res.* 28 (2011) 2302–2310. doi:10.1007/s11095-011-0460-3.
- [62] Y.N. Wang, C.Y. Tang, Protein fouling of nanofiltration, reverse osmosis, and ultrafiltration membranes-The role of hydrodynamic conditions, solution chemistry, and membrane properties, *J. Membr. Sci.* 376 (2011) 275–282. doi:10.1016/j.memsci.2011.04.036.
- [63] K. Nakanishi, T. Sakiyama, K. Imamura, On the adsorption of proteins on solid surfaces, a common but very complicated phenomenon, *Biosci. Bioeng.* 91 (2001) 233–244. doi:10.1263/Jbb.91.233.
- [64] R. Wang, M.G. Brattain, The maximal size of protein to diffuse through the nuclear pore is larger than 60 kDa, *FEBS Lett.* 581 (2007) 3164–3170. doi:10.1016/j.febslet.2007.05.082.
- [65] C.M. Gruian, C. Rickert, S.C.T. Nicklisch, E. Vanea, H.-J. Steinhoff, S. Simon, Conformational Changes and Competitive Adsorption between Serum Albumin and Hemoglobin on Bioceramic Substrates, *Chem. Phys. Chem.* 18 (2017) 634–642. doi:10.1002/cphc.201600886.
- [66] A.A. Shukla, J. Thömmes, Recent advances in large-scale production of monoclonal antibodies and related proteins, *Trends Biotechnol.* 28 (2010) 253–261. doi:10.1016/j.tibtech.2010.02.001.

- [67] D. Pedrites, C. Siletti, J. Jimenez, P. Psathas, Y. Mannion, Optimizing the design and operation of fill-finish facilities using process simulation and scheduling tools, *Pharm. Eng.* 31 (2011) 1–10. <https://pdfs.semanticscholar.org/860a/63d15c38c0ab60c97d2033f270909c85be9f.pdf>.
- [68] D. Low, R. O’Leary, N.S. Pujar, Future of antibody purification, *J. Chromatogr. B Anal. Technol. Biomed. Life Sci.* 848 (2007) 48–63. doi:10.1016/j.jchromb.2006.10.033.
- [69] CMC Biotech Working Group, A-Mab: a Case Study in Bioprocess Development, *Prod. Dev. Realis. Case Study A-Mab.* (2009).
- [70] A.S. Rathore, A. Shirke, Recent developments in membrane-based separations in biotechnology processes: Review, *Prep. Biochem. Biotechnol.* 41 (2011) 398–421. doi:10.1080/10826068.2011.613976.
- [71] U.S. Department of Health and Human Services - Food and Drug Administration, Sterile Drug Products Produced by Aseptic Processing - Current Good Manufacturing Practice, (2004) 1–63. <http://www.fda.gov/downloads/Drugs/GuidanceComplianceRegulatoryInformation/Guidances/ucm070342.pdf>.
- [72] R. van Reis, A. Zydney, Bioprocess membrane technology, *J. Membr. Sci.* 297 (2007) 16–50. doi:10.1016/j.memsci.2007.02.045.
- [73] S. Aldington, J. Bonnerjea, Scale-up of monoclonal antibody purification processes, *J. Chromatogr. B Anal. Technol. Biomed. Life Sci.* 848 (2007) 64–78. doi:10.1016/j.jchromb.2006.11.032.
- [74] R. Van Reis, A. Zydney, Membrane separations in biotechnology, *Curr. Opin. Biotechnol.* 12 (2001) 208–211. doi:10.1016/S0958-1669(00)00201-9.
- [75] L. Besnard, V. Fabre, M. Fettig, E. Gousseinov, Y. Kawakami, N. Laroudie, C. Scanlan, P. Pattnaik, Clarification of vaccines: An overview of filter based technology trends and best practices, *Biotechnol. Adv.* 34 (2016) 1–13. doi:10.1016/j.biotechadv.2015.11.005.
- [76] ASTM International, Standard Test Method for Determining Bacterial Retention of Membrane Filters Utilized for Liquid Filtration, F838. 05 (2013) 1–6. doi:10.1520/F0838-05R13.2.
- [77] M.D. Isacciaci, A.Q. Uarteroni, Navier-Stokes/Darcy Coupling : Modeling , Analysis , and Numerical Approximation, *Rev. Mat. Complut.* 22 (2009) 315–426.
- [78] J.L. Novais, M. Hoare, Economic Comparison Between Conventional and Disposables-Based Technology for the Production of Biopharmaceuticals, *Biotechnol. Bioeng.* 75 (2001).
- [79] Sartorius Stedim Biotech GmbH, Sartopore® 2 0.2 µm, *Prod. Inf. SPK2167-e1* (2017) 1–4.
- [80] Sartorius Stedim Biotech GmbH, MaxiCaps® MR Unique Large Scale Single-Use Filter Device, *Prod. Inf. SPK2172-e1* (2017) 1–3.
- [81] Sartorius Stedim Biotech GmbH, Sartopore® 2 XLI Cartridges, MaxiCaps® & MidiCaps® 0.2 µm, *Valid. Guid. SPK5768-e1* (2013) 1–76.
- [82] Sartorius Stedim Biotech GmbH, Filtration Technology Overview for the Biopharmaceutical Industry, *Prod. Inf. S--0033-e1* (2013) 1–20.
- [83] S. Guillaume, Untersuchungen zur Sterilfiltration von hochkonzentrierten pharmazeutischen Proteinlösungen, PhD Thesis, Univ. Hann. (2016).
- [84] A. Ley, P. Altschuh, V. Thom, M. Selzer, B. Nestler, P. Vana, Characterization of a macro porous polymer membrane at micron-scale by Confocal-Laser-Scanning Microscopy and 3D image analysis, *J. Membr. Sci.* 564 (2018) 543–551. doi:10.1016/j.memsci.2018.07.062.

- [85] Verein Deutscher Ingenieure, VDI-Gesellschaft Verfahrenstechnik und Chemieingenieurwesen (GVC), eds., VDI-Wärmeatlas, 10th ed., Springer-Verlag Berlin Heidelberg New York, 2006.
- [86] A.M. Pitt, The nonspecific protein binding of polymeric microporous membranes, *J. Parenter. Sci. Technol.* 41 (1987) 110–113. <https://www.scopus.com/inward/record.uri?eid=2-s2.0-0023634224&partnerID=40&md5=a7c1f2ab1c877089c788fc829cf9c10e>.
- [87] A. Belgaid, B. Benaji, N. Aadil, S. Moussamih, Y. Khayati, S. Taoudi Benchekroune, M. El Guezzar, Sterilisation of aseptic drug by sterile filtration: Microbiology validation by microbiology challenge test, *J. Chem. Pharm. Res.* 6 (2014) 760–770.
- [88] H.F. Liu, J. Ma, C. Winter, R. Bayer, Recovery and purification process development for monoclonal antibody production, *MAbs.* 2 (2010) 480–499. doi:10.4161/mabs.2.5.12645.
- [89] C. Herrero, P. Prádanos, J.I. Calvo, F. Tejerina, A. Hernández, Flux decline in protein microfiltration: Influence of operative parameters, *J. Colloid Interface Sci.* 187 (1997) 344–351. doi:10.1006/jcis.1996.4662.
- [90] A.M. Allmendinger, Rheological investigation of manufacturability and injectability of highly concentrated monoclonal antibody formulations, (2014).
- [91] L. McBurnie, B. Bardo, Validation of sterile filtration, *Pharm. Technol.* (2004) 13–23. <http://www.pharmtech.com/pharmtech/data/articlestandard/pharmtech/432004/128855/article.pdf>.
- [92] B.S. Chang, B. Yeung, Physical Stability of Protein Pharmaceuticals, *Formul. Process Dev. Strateg. Manuf. Biopharm.* (2010) 69–104. doi:10.1002/9780470595886.ch3.
- [93] C.C. Ho, A.L. Zydney, Transmembrane pressure profiles during constant flux microfiltration of bovine serum albumin, *J. Membr. Sci.* 209 (2002) 363–377. doi:10.1016/S0376-7388(02)00282-X.
- [94] D.M. Kanani, X. Sun, R. Ghosh, Reversible and irreversible membrane fouling during in-line microfiltration of concentrated protein solutions, *J. Membr. Sci.* 315 (2008) 1–10. doi:10.1016/j.memsci.2008.01.053.
- [95] M.E. Laska, R.P. Brooks, M. Gayton, N.S. Pujar, Robust scale-up of dead end filtration: Impact of filter fouling mechanisms and flow distribution, *Biotechnol. Bioeng.* 92 (2005) 308–320. doi:10.1002/bit.20587.
- [96] H.-C. Mahler, F. Huber, R.S.K. Kishore, J. Reindl, P. Rückert, R. Müller, Adsorption Behavior of a Surfactant and a Monoclonal Antibody to Sterilizing-Grade Filters, *J. Pharm. Sci.* 99 (2009) 2620–2627.
- [97] A. Allmendinger, R. Mueller, J. Huwyler, H.-C. Mahler, S. Fischer, Sterile Filtration of Highly Concentrated Protein Formulations: Impact of Protein Concentration, Formulation Composition, and Filter Material, *J. Pharm. Sci.* 104 (2015) 3319–3329. doi:10.1002/jps.24561.
- [98] Sartorius Stedim Biotech GmbH, Interner Bericht, 2018. https://projects.portal.sartorius.com/sites/RD_FiltrationPlatform/_layouts/15/WopiFrame.aspx?sourcedoc=%7B93579A3C-EE38-4F51-AA1D-8DB290CD0319%7D&file=Overview_Filtration_Processes_Reiche.xlsx&action=default.
- [99] Robert Bosch Packaging Technology GmbH, Filtrationsanlagen, (n.d.). <https://www.boschpackaging.com/de/pa/produkte/branchen/pd/product-detail/filtrationsanlagen-19456.php?ind=1675&pt=3686&mt=15327> (accessed January 9, 2019).

- [100] Robert Bosch Packaging Technology GmbH, FLC 3000, (n.d.).
<https://www.boschpackaging.com/de/pa/produkte/branchen/pd/product-detail/flc-3000-4608.php?ind=1675&pt=3686&tg=17600> (accessed January 9, 2019).
- [101] Snowbell Machines, Sterile Injectable Filling - Vial Liquid Line, (2018).
<https://www.youtube.com/watch?v=Z3Noh9r9--Q> (accessed December 20, 2018).
- [102] Snowbell Machines, Filling and closing machines for VIALS, (n.d.).
<https://www.snowbellmachines.com/pdf/Filling & Closing Mc for Vials.pdf> (accessed January 9, 2019).
- [103] C.A. Challener, Filtration technologies advance to meet bioprocessing needs, *BioPharm Int.* (2015).
- [104] S. Giglia, G. Straeffer, Combined mechanism fouling model and method for optimization of series microfiltration performance, *J. Membr. Sci.* 417–418 (2012) 144–153.
 doi:10.1016/j.memsci.2012.06.026.
- [105] X. Sun, D.M. Kanani, R. Ghosh, Characterization and theoretical analysis of protein fouling of cellulose acetate membrane during constant flux dead-end microfiltration, *J. Membr. Sci.* 320 (2008) 372–380. doi:10.1016/j.memsci.2008.04.017.
- [106] EMD Millipore Corporation, Vmax™ Constant Pressure Test, Protocol. (2014).
http://www.merckmillipore.com/INTERSHOP/web/WFS/Merck-ID-Site/id_ID/-/SGD/ShowDocument-File?ProductSKU=MM_NF-C9146&DocumentId=201508.062.ProNet&DocumentUID=30073479&DocumentType=UG&Language=EN&Country=NF&Origin=PDP.
- [107] Sartorius Stedim Biotech GmbH, SartoScale 25, *Prod. Inf.* SPK2145-e1 (2016) 1–4.
- [108] Pall Corporation, Supor® EKV-Membran in Mini Kleenpak™ 20-Kapsulen, (2016).
<http://www.pall.de/main/biopharmaceuticals/product.page?lid=gri78lfw> (accessed December 19, 2018).
- [109] S. Giglia, Scale-up of High Area Filters for Microfiltration of Biological Fluids Points to consider for reliable scale-up, Presentation. (2017). <https://de.slideshare.net/MilliporeSigma/scaleup-of-high-area-filters-for-microfiltration-of-biological-fluids-points-to-consider-for-reliable-scaleup> (accessed May 23, 2019).
- [110] P. Rajniak, S.C. Tsinontides, D. Pham, W.A. Hunke, S.D. Reynolds, R.T. Chern, Sterilizing filtration-Principles and practice for successful scale-up to manufacturing, *J. Membr. Sci.* 325 (2008) 223–237. doi:10.1016/j.memsci.2008.07.049.
- [111] H. Lutz, Rationally defined safety factors for filter sizing, *J. Membr. Sci.* 341 (2009) 268–278. doi:10.1016/j.memsci.2009.06.015.
- [112] A. Kumar, J. Martin, R. Kuriyel, Scale-up of Sterilizing-grade Membrane Filters from Discs to Pleated Cartridges: Effects of Operating Parameters and Solution Properties., *PDA J. Pharm. Sci. Technol.* 69 (2015) 74–87. doi:10.5731/pdajpst.2015.01006.
- [113] E. Iritani, N. Katagiri, Developments of blocking filtration model in membrane filtration, *KONA Powder Part. J.* 33 (2016) 179–202. doi:10.14356/kona.2016024.
- [114] A. Saluja, D.S. Kalonia, Nature and consequences of protein-protein interactions in high protein concentration solutions, *Int. J. Pharm.* 358 (2008) 1–15. doi:10.1016/j.ijpharm.2008.03.041.
- [115] S. Giglia, D. Yavorsky, Scaling from Discs to Pleated Devices, *PDA J. Pharm. Sci. Technol.* 61 (2007) 314–323.

- [116] G. Bolton, D. LaCasse, R. Kuriyel, Combined models of membrane fouling: Development and application to microfiltration and ultrafiltration of biological fluids, *J. Membr. Sci.* 277 (2006) 75–84. doi:10.1016/j.memsci.2004.12.053.
- [117] C.C. Ho, A.L. Zydney, A combined pore blockage and cake filtration model for protein fouling during microfiltration, *J. Colloid Interface Sci.* 232 (2000) 389–399. doi:10.1006/jcis.2000.7231.
- [118] Merck KGaA, Vmax™ Constant Pressure Test Protocol, PR1326EN00 Rev A. (2014) 1–16.
- [119] S. Giglia, K. Rautio, G. Kazan, K. Backes, M. Blanchard, J. Caulmare, Improving the accuracy of scaling from discs to cartridges for dead end microfiltration of biological fluids, *J. Membr. Sci.* 365 (2010) 347–355. doi:10.1016/j.memsci.2010.09.032.
- [120] S. Giglia, G. Straeffer, Model and Method for Optimal Sizing of Serial Microfiltration Systems, *Bioprocess. J.* 12 (2013) 31–39. doi:10.12665/J123.Giglia.
- [121] M.W. Jornitz, Integrity testing, *Adv. Biochem. Eng. Biotechnol.* 98 (2006) 143–180. doi:10.1007/b104248.
- [122] M.W. Mittelman, M.W. Jornitz, T.H. Meltzer, Bacteria Cell Size and Surface Charge Characteristics Relevant to Filter Validation Studies, *PDA J. Pharm. Sci. Technol.* 52 (1998) 37–42.
- [123] Sartorius Stedim Biotech GmbH, Interner Bericht, (2017).
- [124] I. Lundström, Models of protein adsorption on solid surfaces, *Progr. Colloid Polym. Sci.* 70 (1985) 76–82. doi:10.1007/BFb0114308.
- [125] R.A. Latour, The Langmuir isotherm: A commonly applied but misleading approach for the analysis of protein adsorption behavior, *J. Biomed. Mater. Res. A.* 103 (2015) 949–958. doi:10.1002/jbm.a.35235.
- [126] T. Bialopiotrowicz, P. Blanpain, F. René, M. Lalande, An Adsorption of Bovine Serum Albumin on Carbon/Zirconium Oxide Microfiltration Membranes at Different pH's as Determined from Breakthrough Curves, *Ars Separatoria Acta.* 1 (2002) 111–137.
- [127] H. Ye, L. Huang, W. Li, Y. Zhang, L. Zhao, Q. Xin, S. Wang, L. Lin, X. Ding, Protein adsorption and desorption behavior of a pH-responsive membrane based on ethylene vinyl alcohol copolymer, *RSC Adv.* 7 (2017) 21398–21405. doi:10.1039/C7RA03206D.
- [128] K. Nakamura, K. Matsumoto, Protein adsorption properties on a microfiltration membrane: A comparison between static and dynamic adsorption methods, *J. Memb. Sci.* 285 (2006) 126–136. doi:10.1016/j.memsci.2006.08.012.
- [129] J.D. Andrade, V. Hlady, Protein adsorption and materials biocompatibility: A tutorial review and suggested hypotheses, *Adv. Polym. Sci.* 79 (1986) 1–63. doi:10.1007/3-540-16422-7_6.
- [130] I. Kiesel, In situ Untersuchung von Proteinen an Grenzflächen mit oberflächensensitiven Röntgenstreuungsmethoden, (2014) 115. doi:10.17877/DE290R-11750.
- [131] P. Schaaf, J. Talbot, Surface exclusion effects in adsorption processes, *J. Chem. Phys.* 91 (1989) 4401–4409.
- [132] Y.P. Patil, S. Jadhav, Novel methods for liposome preparation, *Chem. Phys. Lipids.* 177 (2014) 8–18. doi:10.1016/j.chemphyslip.2013.10.011.
- [133] D.D. Lasic, The mechanism of vesicle formation, *Biochem. J.* 256 (1988) 1–11.
- [134] Food and Drug Administration, Liposome Drug Products - Guidance for Industry, Pharm. Qual. Revision 1 (2015) 1–13.

- [135] V.N. Raibhole, S.N. Sapali, Simulation of medium purity gaseous oxygen cryogenic plant for biomass gasification by Aspen plus, *Int. Rev. Mech. Eng.* 6 (2012) 1339–1344. doi:10.4172/scientificreports.
- [136] R. Segura, C. Javierre, M.A. Lizarraga, E. Ros, Other relevant components of nuts: Phytosterols, folate and minerals, *Br. J. Nut.* 96 (2006) 36–44. doi:10.1017/BJN20061862.
- [137] K.M.G. Taylor, R.M. Morris, Thermal analysis of phase transition behaviour in liposomes, *Thermochim. Acta.* 248 (1995) 289–301. doi:10.1016/0040-6031(94)01884-J.
- [138] M.-R. Toh, G.N.C. Chiu, Liposomes as sterile preparations and limitations of sterilisation techniques in liposomal manufacturing, *Asian J. Pharm.* 8 (2013) 88–95. doi:10.1016/j.ajps.2013.07.011.
- [139] M.O. Eze, Phase Transitions in Phospholipid Bilayers: Lateral Phase Separations Play Vital Roles in Biomembranes, *Biochem. Educ.* 19 (1991) 204–208.
- [140] A.R. Mohammed, V.W. Bramwell, A.G.A. Coombes, Y. Perrie, Lyophilisation and sterilisation of liposomal vaccines to produce stable and sterile products, *Methods.* 40 (2006) 30–38. doi:10.1016/j.ymeth.2006.05.025.
- [141] J. Endruschat, K. Henschke, Bench scale manufacture of multilamellar liposomes using a newly developed multistage pressure filtration device, *Int. J. Pharm.* 196 (2000) 151–153. doi:10.1016/S0378-5173(99)00410-X.
- [142] S. Vemuri, C.T. Rhodes, Preparation and characterization of liposomes as therapeutic systems: a review, *Pharm. Acta Helv.* 70 (1995) 95–111.
- [143] A. Wagner, K. Vorauer-Uhl, Liposome Technology for Industrial Purposes, *Drug Deliv.* 2011 (2011) 1–9. doi:10.1155/2011/591325.
- [144] Z. Drulis-Kawa, A. Dorotkiewicz-Jach, Liposomes as delivery systems for antibiotics, *Int. J. Pharm.* 387 (2010) 187–198. doi:10.1016/j.ijpharm.2009.11.033.
- [145] U. Bulbake, S. Doppalapudi, N. Kommineni, W. Khan, Liposomal formulations in clinical use: An updated review, *Pharmaceutics.* 9 (2017) 1–33. doi:10.3390/pharmaceutics9020012.
- [146] Y. Fan, Q. Zhang, Development of liposomal formulations: From concept to clinical investigations, *Asian J. Pharm. Sci.* 8 (2013) 79–90. doi:10.1016/j.ajps.2013.07.010.
- [147] Sartorius Stedim Biotech GmbH, Rezeptur 1, Zusammensetzung und Herstellung einer BSA-Lösung ohne Glycerin, SAP-Dok.-Nr. 2461916. (2019).
- [148] Sartorius Stedim Biotech GmbH, Rezeptur 2, BSA mit variabler Viskosität, SAP-Dok.-Nr. 2461918. (2019).
- [149] Sartorius Stedim Biotech GmbH, Rezeptur 3, Zusammensetzung und Herstellung einer γ -Globulin-Lösung ohne Glycerin, SAP-Dok.-Nr. 2461920. (2019).
- [150] Sartorius Stedim Biotech GmbH, Bestimmung der Filterstandzeit mit Caro-Ovomaltine an 142 mm Filterronden, SAP-Dok.-Nr. 2274143. (2018).
- [151] Sartorius Stedim Biotech GmbH, Bestimmung der Konzentration einer BSA-Lösung in Phosphatpuffer mittels SoloVPE, SAP-Dok.-Nr. 2461651. (2019).
- [152] Sartorius Stedim Biotech GmbH, Bestimmung der Viskosität einer Proteinformulierung von 1-50 cP, SAP-Dok.-Nr. 2461649. (2019).

- [153] Sartorius Stedim Biotech GmbH, Bestimmung der Partikelgrößenverteilung einer BSA-Lösung in Phosphatpuffer und einer γ -Globulinlösung in Histidinpuffer mittels DLS, SAP-Dok.-Nr. 2461631. (2019).
- [154] Sartorius Stedim Biotech GmbH, Präparation und Einbettung von Membranen in Epoxidharz, MAI (in Prep.). (2019).
- [155] V. Spratte, B. Schneider, MATLAB - Inner Membrane Structure Toolbox, Version 3.0, 2019.
- [156] Sartorius Stedim Biotech GmbH, Filtrationsuntersuchungen mit standardisierten Lösungen aus Caro-Ovomaltine, SAP-Dok.-Nr. 2462507. (2019).
- [157] Sartorius Stedim Biotech GmbH, Filtrationsuntersuchungen mit standardisierten Protein-Lösungen, SAP-Dok.-Nr. 2461652. (2019).
- [158] S. Pagel, Characterization of ion-exchange chromatography membranes by application of fluorescence microscopy, (2017).
- [159] Sartorius Stedim Biotech GmbH, Herstellung von Standardisierten Protein-Lösungen und deren Charakterisierung für Filtrationsuntersuchungen, SAP-Dok.-Nr. 2461655. (2019).
- [160] VISCO JET® Rührsysteme GmbH, VISCO JET® Rührtechnik, (2014). <http://www.viscojet.com/wp-viscojet/wp-content/uploads/2014/03/rührwerke-wirkung-diagramm.png> (accessed November 23, 2018).
- [161] Sartorius Stedim Biotech GmbH, MaxiCaps_S-O_Massblatt, P2D 1000009374. (2014).
- [162] Sartorius Stedim Biotech GmbH, Kappe O, komplett, P2D Maxicaps_olive_neu. (2014).
- [163] Sartorius Stedim Biotech GmbH, MaxiCaps_F-F_Massblatt, P2D 1000009376. (2014).
- [164] Sartorius Stedim Biotech GmbH, Stufenolive, P2D 85117-042-40. (2014).
- [165] Sartorius Stedim Biotech GmbH, Sartopore® 2 γ -Irradiatable or Autoclavable T-Style MaxiCaps® 0.1 & 0.2 μm , Valid. Guid. SPK5784-e1 (2013) 1–55.
- [166] S. Haindl, J. Stark, J. Dippel, S. Handt, A. Reiche, Scale-up of microfiltration processes, CIT. submitted (2019).
- [167] B.A. Kerwin, Polysorbates 20 and 80 Used in the Formulation of Protein Biotherapeutics: Structure and Degradation Pathways, *J. Pharm. Sci.* 97 (2008) 2924–2935. doi:10.1002/jps.
- [168] A. Huntress, Are Proteins Adsorbing to Your Labware?, (n.d.). <https://bitesizebio.com/32181/proteins-adsorbing-labware/> (accessed July 10, 2019).
- [169] A.M. Brendzel, I.F. Miller, Effects of lipid-soluble substances on the thermotropic properties of liposome filtration, *Biochim. Biophys. Acta.* 601 (1980) 260–270.

Wissenschaftliche Publikationen und Tagungsbeiträge

Liste wissenschaftlicher Publikationen

S. Haindl, O. Doppleb, L. Förster, S. van der Kruijs, N. Gehrman, A. Reiche, Protein adsorption in microfiltration processes (submitted).

S. Haindl, J. Stark, J. Dippel, S. Handt, A. Reiche, Scale-up of microfiltration processes, CIT. (accepted).

A. Peschel, A. Langhoff, E. Uhl, A. Dathathreyan, S. Haindl, D. Johannsmann, I. Reviakine, Lipid phase behavior studied with a quartz crystal microbalance: A technique for biophysical studies with applications in screening, *J. Chem. Phys.* 145 (2016), 204904.

S. Haindl, J. Xu, T. Freese, E. G. Hübner, A. Schmidt, The intersection of allenylidenes and mesomeric betaines. 1-Methylpyridinium-2-acetylide and its palladium complexes, *Tetrahedron*. 72 (2016) 7906-7911.

Konferenzbeiträge

S. Haindl, S. van der Kruijs, A. Reiche, Protein adsorption in microfiltration processes, Engineering with membranes conference (2019), Båstad, presentation.

S. Haindl, A. Reiche, Protein-membrane-interactions during sterile filtration in biopharmaceutical production, Thermodynamics and energetics of soft matter systems (2018), Grenoble, poster.

S. Haindl, A. Reiche, Up-scaling dead-end microfiltration processes (2018), València, poster.

S. Haindl, A. Reiche, Sterile Filtration in Biopharmaceutical Industry, Network Young Membranes conference (2018), València, presentation.

S. Haindl, A. Reiche, Up-scaling dead-end microfiltration processes, Jahrestreffen der Process-Net-Fachgruppen Fluidverfahrentchnik, Membrantechnik und Mischvorgänge (2018), München, poster.

S. Haindl, A resistance-based approach to scale-up of membrane filtration, International Conference on Membrane Science and Technology (2017), Paris, poster; published in: *J. Membr. Sci. Technol.* 7 (2017) 50.

Betreute Abschlussarbeiten

O. Doppleb, Untersuchung der Proteinadsorption in Verbindung mit Mikrofiltrationsprozessen, Masterarbeit (2018), TU Clausthal.

J. Starke, Untersuchung des Verblockungsverhaltens von Proteinlösungen bei Sterilfiltration, Masterarbeit (2017), Hochschule Anhalt.

Danksagung

Die vorliegende Arbeit entstand im Rahmen meiner Tätigkeit als wissenschaftlicher Mitarbeiter bei Sartorius Stedim Biotech GmbH in der Membranentwicklung nach dem Verdunstungsverfahren in Zusammenarbeit mit der Leibniz Universität Hannover. An dieser Stelle möchte ich mich bei allen bedanken, die bei der Durchführung und Erstellung der Arbeit geholfen haben.

An erster Stelle möchte ich Frau Dr. Annette Reiche und Prof. Dr. Thomas Scheper für die Aufgabenstellung und die Unterstützung während des Projekts danken.

Ein Danke geht auch an alle Praktikanten, Johannes Starke, Jan-Luca Wichmann und Olivia Doppleb, für die vielen durchgeführten Messungen die Bestandteil dieser Arbeit geworden sind.

Bei Tim Schormann, Sophia Wraage und Franziska Bätke möchte ich ebenfalls für zahlreiche Messungen Danke sagen.

A huge thank you to our colleagues in Bangalore for the BCT-measurements: Dinesh Raveendrarajuh, Prasanna Kirthi and Swathi Bhaskara.

Für die gute Zusammenarbeit mit der Deviceabteilung im Rahmen der Skalierungsversuche möchte ich mich speziell bei Jannik Dippel bedanken.

Bei allen Kollegen der Abteilung SMVE möchte ich mich für das gute Arbeitsklima und zahlreiche Diskussionen bedanken. Insbesondere bei Isabelle Masselin für die Heranführung an Filtration und Sandra van der Kruijs für die Unterstützung bei den Adsorptionsmessungen.

Außerdem möchte ich mich bei allen bedanken, die diese Arbeit Korrektur gelesen haben.

Lebenslauf

1. Persönliche Daten

Name: M.Sc. Susanne Maria Hilda Haidl

Geburtsdatum: 15.01.1992

Geburtsort: München

Staatsangehörigkeit: Deutsch

2. Schulbildung

9/98 – 7/02 Grundschule in Markt Schwaben

8/02 – 5/11 Gymnasium in Markt Schwaben

5/11 Abitur

3. Studium

4/11 – 9/11 Sondereinschreibung an der Ludwig-Maximilians-Universität München

10/11 – 9/14 Studium der Chemie (Bachelor of Science), Technische Universität Clausthal

7/14 – 9/14 Bachelorarbeit, „Punicinderivate als organische Liganden“, Institut für Organische Chemie, Technische Universität Clausthal bei apl. Prof. Dr. rer. nat. habil. Andreas Schmidt

10/14 – 6/16 Studium der Chemie (Master of Science), Vertiefung in Organischen Materialien und Spezieller Physikalischer Chemie, Technische Universität Clausthal

1/16 – 6/16 Masterarbeit, „Komplexchemie mit Ethinylpyridinen“, Institut für Organische Chemie, Technische Universität Clausthal bei apl. Prof. Dr. rer. nat. habil. Andreas Schmidt

Seit Juli 2016 Forschungsarbeit bei der Sartorius Stedim Biotech GmbH als Promotionsstudentin der Leibniz Universität Hannover

Seit März 2019 Junior Scientist bei der Sartorius Stedim Biotech GmbH, Abteilung Membranentwicklung nach dem Verdunstungsverfahren